

VOLCANOGENIC MINERALISATION IN THE LIMESTONE
LAKE AREA, SASKATCHEWAN, CANADA.

by

DAVID WILLIAM ADAMSON

Thesis submitted for the degree of

Doctor of Philosophy

at the

University of Aston in Birmingham

February, 1988

The copy of the thesis has been supplied on condition that anyone who consults it is understood to recognise that its copyright rests with its author and that no quotation from the thesis and no information derived from it may be published without the author's prior, written consent.

ACKNOWLEDGMENTS

Thanks are extended to Dr. J.W. Gaskarth, who initiated and supervised the project. Logistical support in Canada was provided by Dr. G.R. Parslow, and Saskatchewan Energy and Mines, and is gratefully acknowledged. Unlimited access to drill core was kindly provided by Granges Exploration Ltd. Mark Kretscmar and Mike Jerema are thanked in particular for their help at the drill site. Thanks are extended to Kevin Cole for his work as field assistant during the summer of 1984. Financial support for the project was provided by a University of Aston studentship, and is gratefully acknowledged.

Thanks are due to the technical staff in the department of geology at Aston for their assistance throughout the course of study. The thesis benefitted through long discussions with various postgraduates and members of staff in the department; particular thanks are extended to Jon Naden.

Many of the microprobe analyses reported in the thesis were carried out in the department of Geology, at the University of Leicester, by kind permission of Rob Wilson. Dr T. Hopkins, and David Plant of the Department of Geology at Manchester University are thanked for their assistance with

microprobe analyses.

Finally, sincere thanks are extended to my parents for their support, and especially to my wife, Peggy, for her patience and understanding throughout the course of the thesis.

VOLCANOGENIC MINERALISATION IN THE LIMESTONE LAKE AREA,
SASKATCHEWAN, CANADA ©

by

DAVID WILLIAM ADAMSON

Submitted for the degree of

Doctor of Philosophy

February, 1988

Summary

This thesis describes the geology, geochemistry and mineralogy of a Lower Proterozoic, metamorphosed volcanogenic Cu-Zn deposit, situated at the western end of the Flin Flon greenstone belt.

Stratabound copper mineralisation occurs in silicified and chloritoid-bearing alteration assemblages within felsic tuffs and is mantled by thin (<3m) high-grade sphalerite layers. Mineralisation is underlain by garnet-hornblende bearing Lower Iron Formation (LIF), and overlain by garnet-grunerite bearing Upper Iron Formation (UIF).

Distinctive trace element trends, involving Ti and Zr, in mineralised and footwall felsic tuffs are interpreted to have formed by fractionation associated with a high-level magma chamber in a caldera-type environment. Discrimination diagrams for basaltic rocks are interpreted to indicate their formation in an environment similar to that of recent, primitive, tholeiitic island arcs.

Microprobe studies of key mineral phases demonstrate large and small scale chemical variations in silicate phases related to primary lithological, rather than metamorphic, controls. LIF is characterised by aluminiferous-tschermakite and relatively Mn-poor, Ca-rich garnets, whereas UIF contains manganese grunerite and Mn-rich garnets. Metamorphic mineral reactions are considered and possible precursor assemblages identified for garnet-, and chloritoid-bearing rocks. Chloritoid-bearing rocks are interpreted as the metamorphosed equivalents of iron-rich feeder zones formed near the surface. The iron-formations are thought to represent iron-rich sediments formed on the sea floor from the venting of the ore fluids. Consideration of various mineral assemblages leads to an estimate for peak metamorphic conditions of 450-500°C and >4Kb total pressure.

Comparisons with other volcanogenic deposits indicate affinities with deposits of 'Matabi-type' from the Archean of Ontario. An extrapolation of the main conclusions of the thesis to adjacent areas points to the presence of a number of geologically similar localities with potential for mineralisation.

Keywords volcanogenic, Cu-Zn mineralisation, iron-formation, Proterozoic, mineralogy.

CONTENTS

	<u>Page No.</u>
Title Page	1
Acknowledgements	2
Summary	4
Contents	5

CHAPTER 1: INTRODUCTION AND GENERAL GEOLOGY.

1.1 Introduction	15
1.2 Regional geology	19
1.2.1 The Hanson Lake Block	20
1.2.2 Geology of the North Limestone Area (NLA)	20

CHAPTER 2: STRATIGRAPHY AND PETROLOGY OF THE BIGSTONE DEPOSIT SEQUENCE.

2.1 General Introduction	24
2.2 Detailed Deposit Stratigraphy	25
2.2.1 The Footwall Sequence	26
2.2.2 The Mineralised Horizon	35
2.2.3 High grade zinc mineralisation	47
2.2.4 Iron Formation	49
2.2.5 The Hanging Wall Sequence	60
2.3 Deposit structure	63
2.4 Interpretations and Summary	70
2.5 Conclusions	76

CHAPTER 3: WHOLE ROCK GEOCHEMISTRY

	<u>Page No</u>
3.1 Introduction	78
3.2 Sample Details and Analytical Techniques	78
3.3 Sample Classification	79
3.4 Geochemical Plots	82
3.4.1 Mafic Rocks	82
3.4.2 Evolved Rocks	86
3.4.3 Iron-Formation	90
3.5 Interpretation	92
3.6 Discussion and Conclusions	100

CHAPTER 4: MINERAL CHEMISTRY AND METAMORPHISM

4.1 Introduction	102
4.2 Mineral Chemistry	105
4.2.1 Analytical Techniques	105
4.2.2 Iron-Formation	105
4.2.3 Summary of Iron Formation Mineral Chemistry	119
4.2.4 The Chloritoid Zone	119
4.3 Metamorphic Reactions	123
4.3.1 Iron-Formation	123
4.3.2 Chloritoid Zone	126
4.4 An Assessment of Peak Metamorphic Conditions	128

CHAPTER 5: DISCUSSION AND CONCLUSIONS

5.1 Classification of Mineral Deposits	130
5.2 Model for Bigstone Mineralisation	136

	<u>Page No</u>
5.3 Implications for Exploration in the Flin Flon Belt	145
5.4 Summary of Conclusions.	148
REFERENCES	150
Appendix 1 Sample location details.	163
Appendix 2 Whole rock data.	166
Appendix 2.1 Analytical techniques.	166
Appendix 2.2 Whole rock data tables.	170
Appendix 2.3 Zr-Y-Nb-Ti regression data.	188
Appendix 3 Microprobe data.	189
Appendix 3.1 Analytical techniques.	189
Appendix 3.2 Microprobe data tables.	190
Appendix 3.3 Fe-Zn zoning in gahnite	237
Appendix 3.4 Trace element contents in plagioclase	238

LIST OF FIGURES

	<u>Page No.</u>
Figure 1.1 General geology and lithotectonic subdivisions of the Churchill Province.	16
Figure 1.2 Location of sampled drill holes from the Bigstone deposit.	17
Figure 1.3 Sketch map of the geology of the North Limestone area (NLA)	22
Figure 2.1 General stratigraphy of the Bigstone deposit.	27
Figure 2.2 Interpretative isometric projection to show major lithological variations in the deposit sequence.	28
Figure 2.3 Isometric projection to show the relationship between copper and zinc mineralisation.	29
Figure 2.4 Schematic diagram of the 1700N section.	38
Figure 2.5 Fence diagram of the Mineralised Horizon.	66
Figure 3.1 TiO_2 vs Zr for Bigstone mafic rocks.	83
Figure 3.2 MORB-normalised plots for the Bigstone, NLA, Hanson Lake and Amisk Lake areas.	83

	<u>Page No.</u>
Figure 3.3 Ti-Zr-Y plot for Bigstone and NLA mafic rocks.	84
Figure 3.4 Y vs Cr for Bigstone and NLA mafic rocks.	85
Figure 3.5 Nb/Y vs Ti/Y for Bigstone mafic rocks.	85
Figure 3.6 AFM plot for a subset of Bigstone samples.	87
Figure 3.7 TiO ₂ vs Zr for Bigstone volcanic rocks.	87
Figure 3.8 Zr vs V plot for various rock types from the deposit sequence.	89
Figure 3.9 SiO ₂ vs Zr for Footwall mafic to felsic rocks, and felsic rocks of the Mineralised Horizon.	89
Figure 3.10 TiO ₂ vs Zr for TIF and Mineralised Horizon felsic rocks.	91
Figure 3.11 TiO ₂ vs Zr for Bigstone and NLA volcanics.	97
Figure 4.1 Mn vs Fe+Mn/Fe+Mn+Mg in Fe-Mg amphiboles.	106
Figure 4.2 Actinolite-tremolite and tschermakite-ferro- tschermakite substitutions in Fe-Mg amphiboles.	106
Figure 4.3 Classification of calcic amphiboles.	109

Figure 4.4 Range of tschermakite substitutions in calcic amphiboles.	110
Figure 4.5 Range of glaucophane-riebeckite substitutions in calcic amphiboles.	112
Figure 4.6 Pargasite and glaucophane substitutions in calcic amphiboles.	115
Figure 4.7 Mg ratio vs $Fe^{3+}/Fe^{3+}+Al^{3+}$ for calcic amphiboles.	115
Figure 4.8 Ternary diagram of atomic % Fe, Mn and Ca in LIF and UIF garnets.	116
Figure 4.9 Ternary diagram of atomic % Fe, Mn and Ca in garnetites.	116
Figure 4.10 Profiles of atomic % Fe, Mn, Ca, Mg and weight % Zn+Cu in LIF from DDH BS-35.	118
Figure 4.11 Tourmaline compositions.	122
Figure 4.12 Feldspar compositions.	122
Figure 5.1 (a to d) Proposed evolutionary model for the Bigstone deposit.	138
Appendix figure A3.1 Zoning of Fe and Zn in gahnite.	237

LIST OF PLATES

		<u>Page No.</u>
Plate 1.1	Well preserved pillow lavas from the NLA.	23
Plate 1.2	Primary pillow breccias from the NLA.	23
Plate 2.1	Relatively undeformed quartz-eyes from the Footwall quartz-eye Porphyry.	32
Plate 2.2	Coalesced quartz-eyes in the Footwall quartz-eye porphyry.	32
Plate 2.3	Euhedral plagioclase with oscillatory zoning in a meta-arenitic matrix from the Footwall feldspar crystal tuffs.	34
Plate 2.4	Broken feldspar from the Footwall feldspar crystal tuffs showing well preserved oscillatory zoning.	34
Plate 2.5	Plagioclase phenocryst from the Footwall feldspar crystal tuffs replaced by quartz and biotite.	34
Plate 2.6	Photograph from drill core of intermediate lapilli tuffs showing dark fiamme-like structures and lighter felsic fragments.	36
Plate 2.7	Feldspar-phyric lithic fragment in intermediate lapilli tuffs showing the development of sub-trachytic texture.	36
Plate 2.8	Heavily silicified rock from the Mineralised Horizon representing the near total destruction of primary igneous textures in MH tuffs.	41
Plate 2.9	Pyrite replaced by pyrrhotite in heavily mineralised rocks.	41
Plate 2.10	Primary ilmenite adjacent to chalcopyrite in heavily mineralised rocks.	41
Plate 2.11	Development of chloritoid and sulphides within heavily altered plagioclase feldspar.	43
Plate 2.12	Development of retrograde chlorite in rocks of the Chloritoid Zone	43

Plate 2.13	Anomalously green luminescence of plagioclase in rocks of the Mineralised Horizon.	46
Plate 2.14	Development of 'birds-eye' textures in mineralised rocks.	46
Plate 2.15	Radial intergrowth of garnet (dominant phase) with chloritoid in TIF.	46
Plate 2.16	Euhedral gahnite containing concentric inclusions of silicates, ilmenite, chalcopyrite and pyrrhotite.	48
Plate 2.17	Development of groundmass apatite (white to yellow) in mineralised rocks.	48
Plate 2.18	Blue-green zoned tourmalines intergrown with sphalerite and quartz from high-grade zinc ore.	50
Plate 2.19	Etched sample of high-grade sphalerite mineralisation showing the development of an annealed texture.	50
Plate 2.20	Iron formation in DDH BS-37, showing major variations in the abundance of garnet.	52
Plate 2.21	Pull-apart garnet with retrograde chlorite plus quartz.	52
Plate 2.22	Spessartine and almandine in mineralised UIF.	54
Plate 2.23	High grade ore from BS-119 showing well developed durchbewegung texture.	54
Plate 2.24	Development of typical bladed grunerite associated with magnetite in UIF.	56
Plate 2.25	Development of acicular and felted grunerite associated with quartz, garnet, minor chlorite and biotite.	56
Plate 2.26	Fine-grained radial intergrowth between garnet and grunerite in UIF.	57

Plate 2.27	Non-luminescent Fe-carbonate rhombs associated with bladed grunerite, being replaced by orange calcite or dolomite.	57
Plate 2.28	Relict tuffaceous texture in TIF rocks.	59
Plate 2.29	Intergrowth of garnet-sphalerite-pyrrhotite and blue-green ferro-alumino-tschermakite in quartz from LIF rocks.	59
Plate 2.30	Primary bladed hematite replaced by magnetite in LIF.	61
Plate 2.31	Intergrowth between garnet and magnetite after bladed hematite.	61
Plate 2.32	Mineralised clast of quartz+plagioclase+sulphides containing a large brown tourmaline in fine-grained host Graphitic Schist.	62
Plate 2.33	Rounded detrital grain of yellow-brown tourmaline in Graphitic Schist.	62
Plate 2.34	Scour structures in fine-grained Hanging Wall tuffs in BS-119.	64
Plate 2.35	Large embayed quartz phenocryst in poorly bedded Hanging Wall crystal lithic tuffs.	65
Plate 2.36	Lithic clast in Hanging Wall crystal lithic tuffs.	71

LIST OF TABLES

		<u>Page</u>
Table 2.1	Chloritoid Zone mineralogy.	39
Table 3.1	Total numbers of rock types from the main deposit units.	80
Table 3.2	Average contents of selected elements for major rock types from the NLA and Bigstone sequences.	81
Table 4.1	Summary statistics of Fe-Mg amphiboles.	109
Table 4.2	Summary statistics of calcic amphiboles.	113
Table 4.3	Summary statistics of garnet divalent cations.	117

CHAPTER 1. INTRODUCTION AND REGIONAL GEOLOGY

1.1 INTRODUCTION

The Bigstone Lake Cu-Zn deposit occurs beneath 50m of Palaeozoic cover (the Ordovician Winnipeg Formation) within a sub-vertical basement sequence of metamorphosed felsic and mafic volcanic rocks, which form part of the Hanson Lake Block at the western end of the Lower Proterozoic Flin Flon greenstone belt (Figure 1.1a and b). It is one of only two known base metal deposits within the Block, the other being the now worked-out Pb-Zn deposit of the Hanson Lake Mine (Fox, 1977).

The deposit was discovered in 1983 by Granges Exploration Ltd. following diamond drilling of a lens-shaped electro-magnetic anomaly located at the southern end of Limestone Lake but is referred to as the Bigstone Lake deposit because it occurs within the larger Bigstone claim block. The anomaly trends NNE over a strike length of 200m and attains a maximum width of 50m (Figure 1.2). Subsequent diamond drilling, at a general grid spacing of 25m, has outlined the presence of 3,950,000 tons of reserves grading 1.8%Cu and 1.1%Zn which includes 1,600,000 tons of 2.9%Cu and 340,000 tons of 11.2%Zn (Northern Miner, 1987). Precious metal reserves have not been published, but data available to the author indicate average grades of 0.5ppm Au and 12.5ppm Ag over a true width of 22m in copper-rich rocks, and 0.36ppm Au and 8.5ppm Ag over 4.4m in zinc-rich rocks. Surface exposures of basement rocks to the deposit crop out approximately 12.5 km along strike to the northeast within an area (Figure 1.3) herein referred to as the North Limestone Area (NLA). Field work was done during the summer (May to September) of 1984. Three weeks were spent sampling the North Limestone Area (see Figure 1.3 for traverse locations and Appendix 1 for sample details. The remainder of the time was used for working on, and sampling, Bigstone drill core at the

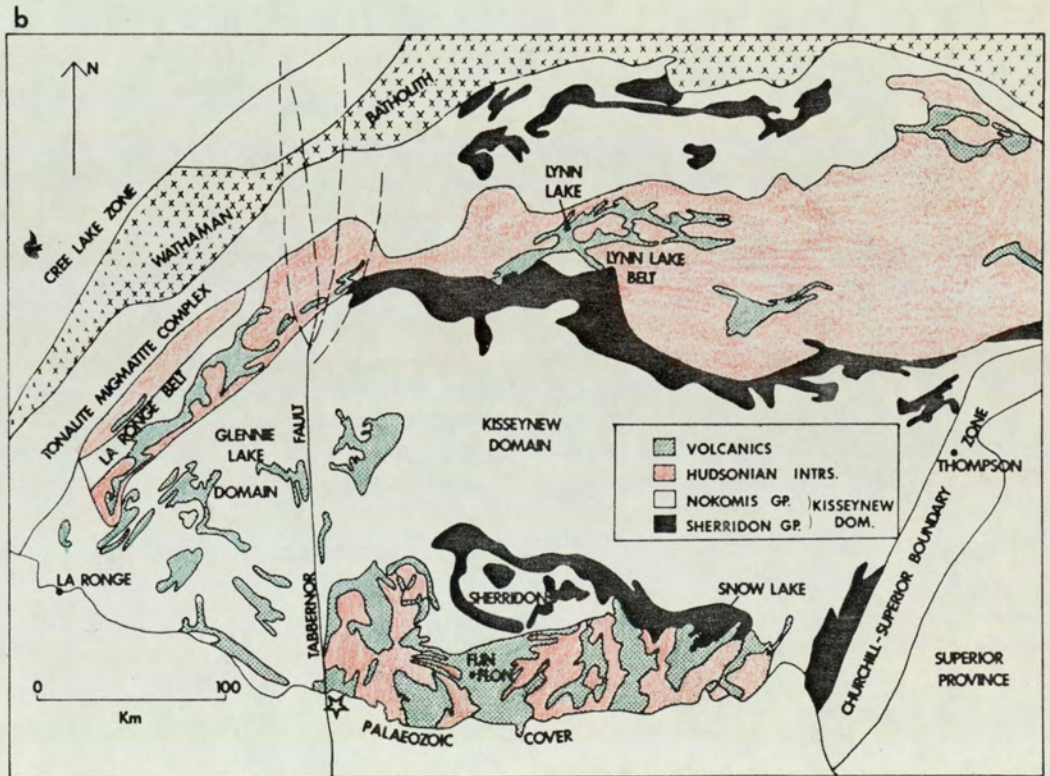
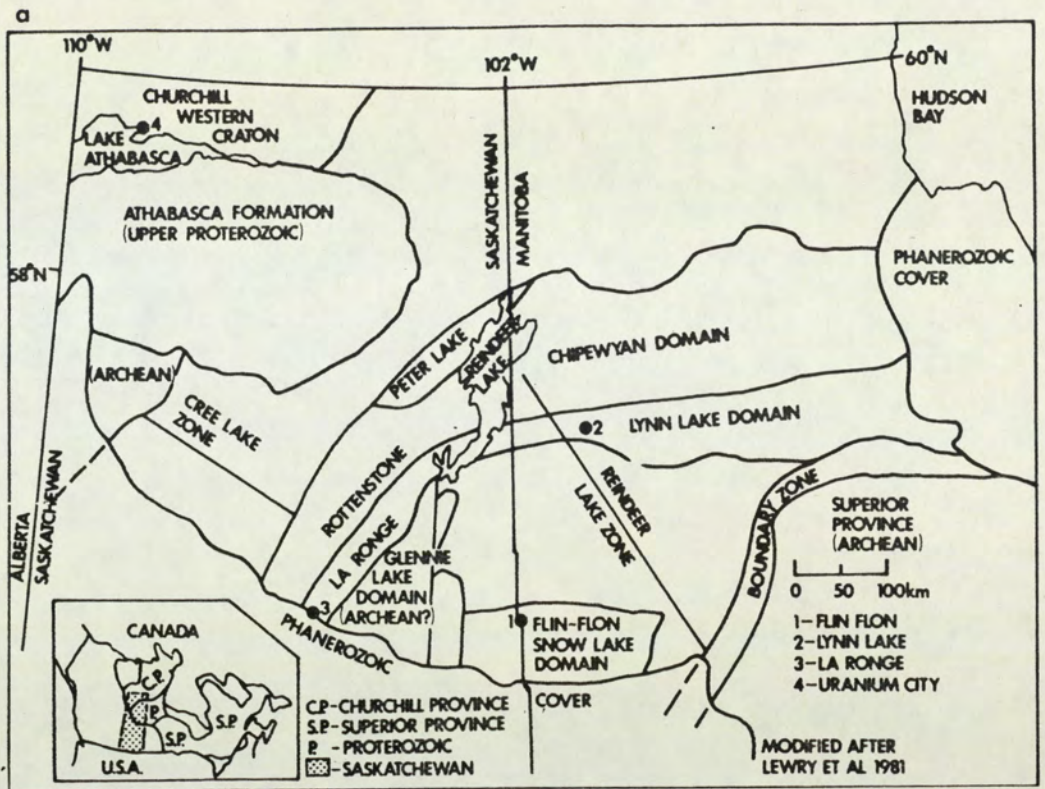


Figure 1.1 a) Major litho-tectonic subdivisions after Lewry et. al. 1981 and b) general geology of the Churchill Province in Saskatchewan and Manitoba after Gaskarth and Parslow (1987). Star symbol corresponds to the location of the Bigstone Lake deposit.

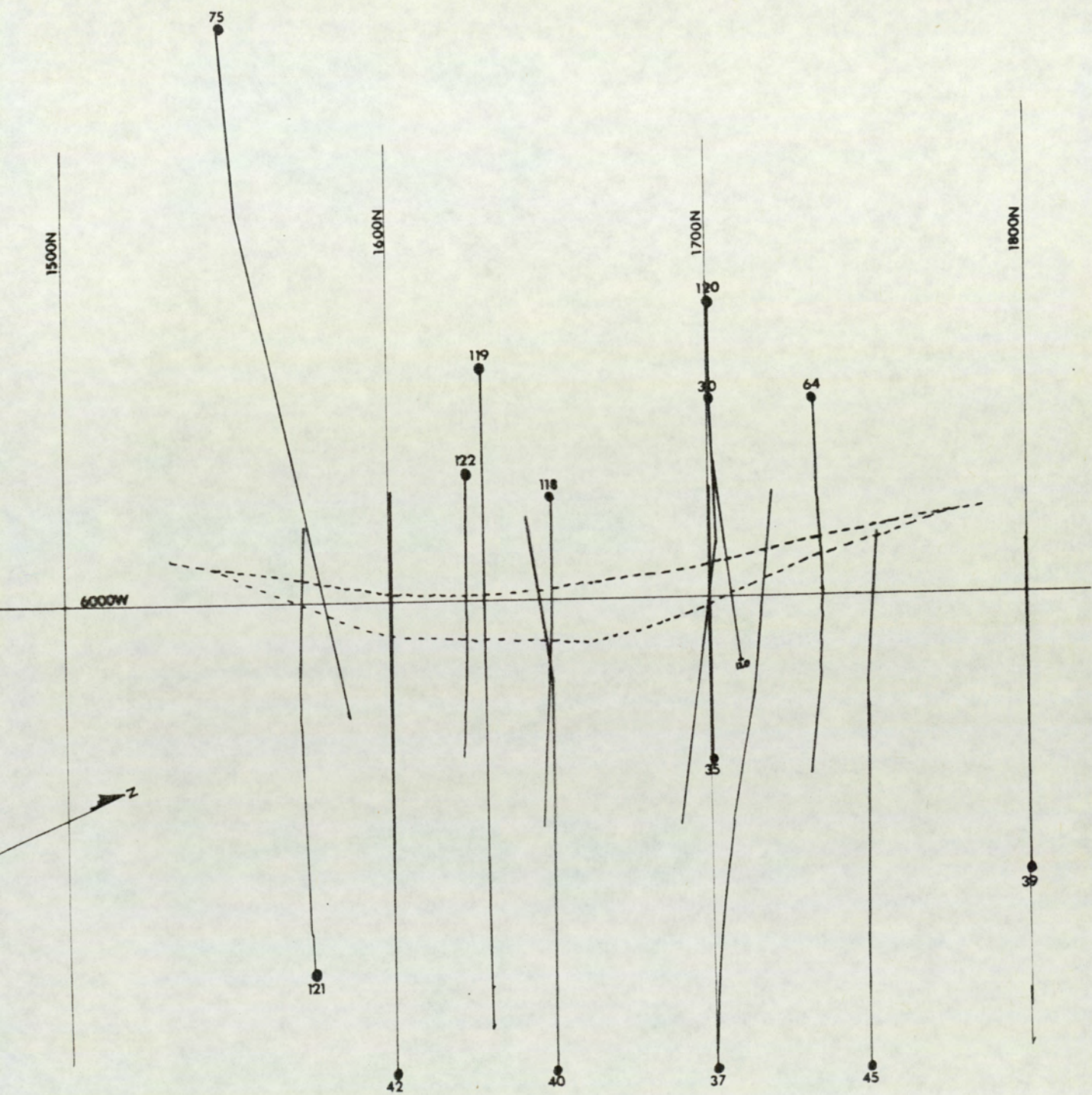


Figure 1.2 Map showing the location of sampled drill holes. Dotted line outlines the electromagnetic anomaly associated with deposit. Grid lines are in metres.

drill site (see Appendix 1 for details of sample locations). The thesis describes the geology and geochemistry of the Bigstone Lake deposit and demonstrates the presence of chemically and mineralogically distinctive lithologies associated with mineralisation which have important differences to known deposits of the area. The plan of the thesis is as follows:

The regional geological setting of the deposit is summarised in Chapter 1. The stratigraphy and petrology of the deposit sequence (Chapter 2) are described and mineralogically distinctive units associated with mineralisation are identified. The geochemistry of these distinctive units is detailed in Chapter 3. Distinctive trace element patterns in felsic tuffs associated with, and underlying, mineralisation are demonstrated and assessed in terms of their importance in primary igneous and alteration processes.

The compositions of key mineral phases in units associated with mineralisation are investigated (Chapter 4). Chemical differences between minerals from similar rock types from different parts of the sequence are demonstrated, and are assessed in terms of the relative importance of primary bulk rock controls and metamorphic effects. Various metamorphic mineral reactions are considered and an estimate made of peak metamorphic conditions for the deposit with a re-construction of possible precursor assemblages. The main features of the deposit are summarised in Chapter 5, and a comparison made with other deposits from the Flin Flon belt and elsewhere. A general model for the evolution of the deposit sequence is proposed. The main conclusions of the study are used to identify a number of places in adjacent areas which appear to have mineralisation potential.

1.2 REGIONAL GEOLOGY

The Lower Proterozoic Flin Flon greenstone belt (Figure 1.1) is part of the Southwestern Complex of the Trans-Hudson orogen in Saskatchewan and Manitoba (Lewry and Sibbald, 1977; 1980; Lewry, 1981, Lewry et.al, 1985). In the area around the town of Flin Flon, rocks of the belt have been subdivided into the Amisk Group consisting of abundant, mafic, pillowed and massive flows, andesitic breccias and 'quartz-porphyry', and the Missi Group, comprising coarse-grained metasediments, which disconformably overlies the Amisk Group (Byers and Dahlstrom, 1954). The belt is bounded to the south by overlying Phanerozoic rocks, eastwards by the Thompson Shear Zone at the Churchill-Superior boundary, westwards by the Tabbernor Shear Zone and northwards by an extensive belt of ortho-, and para-gneisses known as the Kisseynew Domain (Figure 1.1b, Bailes and McRitchie, 1978).

At least three successive phases of deformation have affected Amisk and Missi Group rocks (Sibbald, 1986), resulting in 1) east-trending tight folds, 2) north-trending tight folds accompanied by a penetrative foliation, and 3) northwest-trending shear and drag folds. The intense deformation has hampered attempts to extrapolate the volcanic stratigraphy to the east and west from the area of excellent exposure around Flin Flon, and the term "Amisk-type" is used to refer to volcanic rocks elsewhere in the greenstone belt. The general grade of metamorphism ranges from greenschist to amphibolite, increasing towards the Kisseynew domain (Figure 1.1b).

The Amisk-type volcanics are tholeiitic and have been interpreted from studies of major element chemistry to have formed in a relatively immature island-arc (Stauffer et.al., 1975). More comprehensive trace

element studies have indicated the presence of oceanic-, and arc-type basalts possibly formed in a back arc environment (Gaskarth and Parslow, 1987). Rocks of the Kisseynew Domain are considered to represent the metamorphosed equivalents of an extensive volcano-sedimentary basin derived from neighbouring arc systems (Bailes and McRitchie, 1978), though the possibility that they underlie the Amisk Group has been suggested (Parslow and Gaskarth, 1985).

1.2.1 The Hanson Lake Block

The Hanson Lake Block comprises a domain of Lower Proterozoic volcano-sedimentary rocks (Sibbald, 1986) containing older (Archean) granitoid intrusives (MacQuarrie, *in* Sibbald, 1986). It has been interpreted as an exotic block incorporated into the Flin Flon belt during the development of the Flin Flon arc (Lewry, 1981), or as a deeper structural level of the belt which exposes older basement rocks (Parslow and Gaskarth, 1984).

In the type area of Hanson Lake (Gaskarth, 1967), mafic intrusives and flow rocks of Amisk-type are overlain by abundant dacitic to rhyolitic flows, tuffs and minor intrusives. These igneous rocks are in turn overlain by a series of meta-greywackes which may be equivalent to Missi Group rocks in the type area around Flin Flon. Preliminary geochemical data for volcanic rocks of the Hanson Lake area (Parslow and Gaskarth, 1986) are interpreted as being consistent with generation in a subduction-related environment. As a whole, the Hanson Lake Block contains a considerably larger proportion of felsic rocks than the Flin Flon area.

1.2.2 Geology of the North Limestone Area (NLA)

The North Limestone Area (Figure 1.2) forms a small part of the

larger Deschambault Lake Area mapped by Padgham (1968). It is characterised by the presence of a highly tectonised group of mafic volcanics and intrusives, with minor intermediate to felsic lithologies, preserved between splay faults associated with the Tabbernor Shear Zone (Figure 1.1b), and intruded by late-, to syn-kinematic granitoids. Despite the combined effects of amphibolite-facies metamorphism and intense deformation, primary pillow, pillow-breccia and amygdaloidal textures, are preserved in some rocks (Plates 1.1 and 1.2) which attest to their submarine origin.

84 samples of mafic to felsic volcanic rocks were collected from the NLA in order to: a) investigate the geochemistry of the area, and b) to provide a 'control group' of analyses of unmineralised rocks against which analyses of similar rocks from the Bigstone deposit sequence could be compared and contrasted (for sample locations, see Appendix 1).

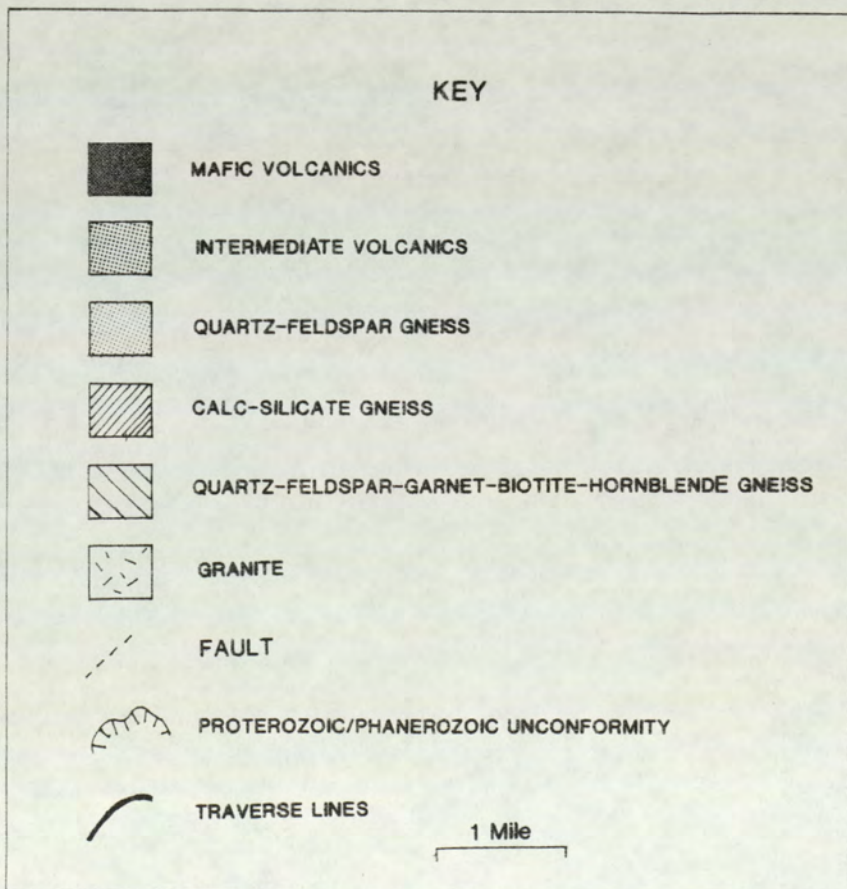
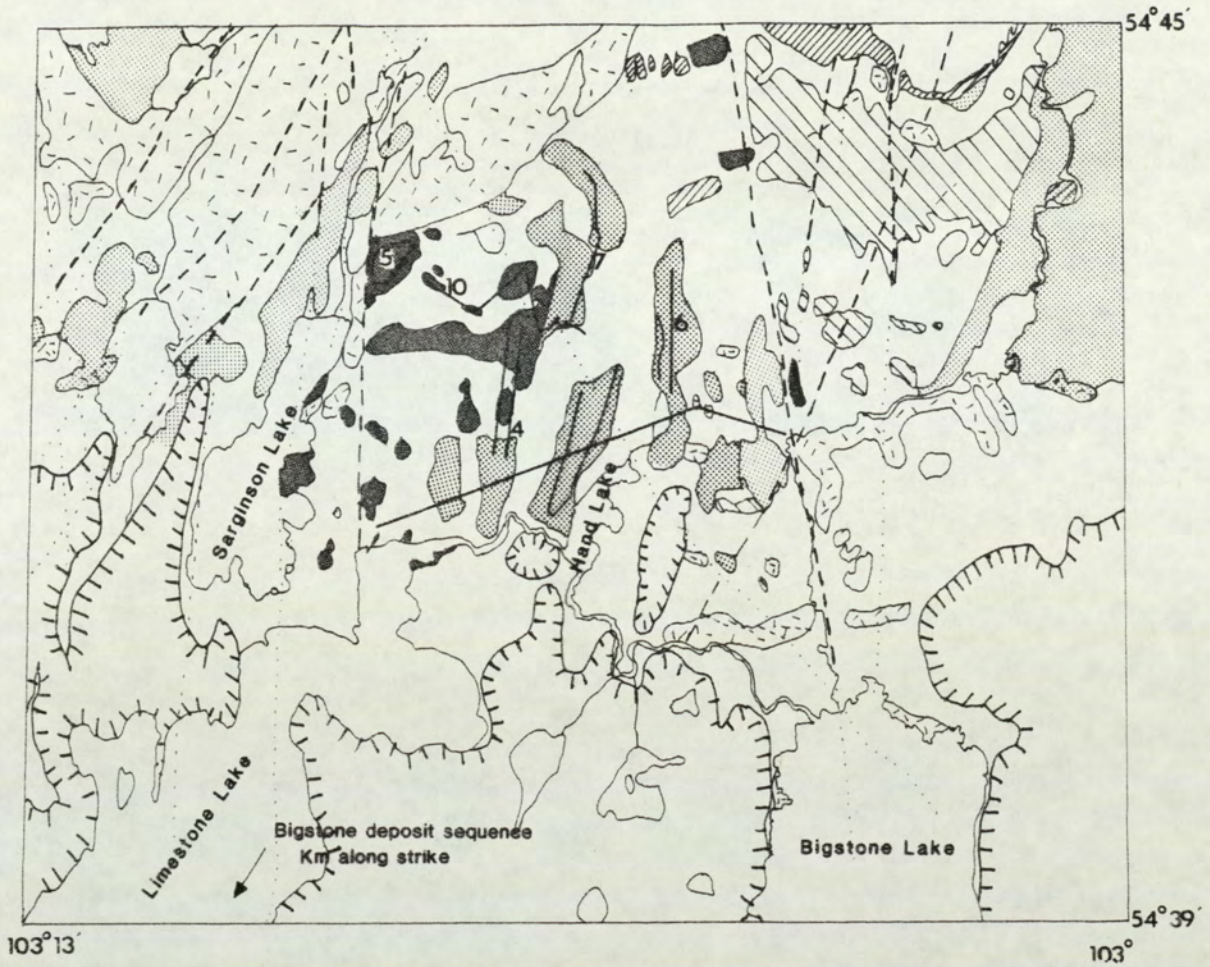


Figure 1.3 General geology of the North Limestone Area simplified from Padgham (1968)

Samples used in this study are from numbered traverses only, and are listed in Appendix 1



Plate 1.1

Well preserved pillow lavas in basalts from the North Limestone Area.

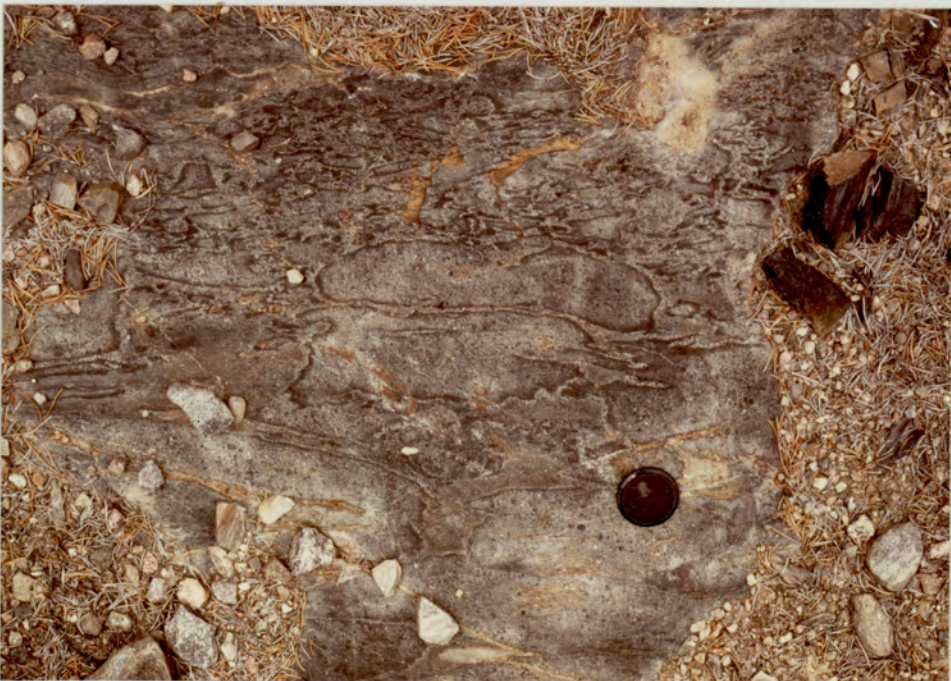


Plate 1.2

Pillows and brecciated pillows in basalts from the North Limestone Area.

CHAPTER TWO

STRATIGRAPHY AND PETROLOGY OF THE BIGSTONE DEPOSIT SEQUENCE.

2.1 GENERAL INTRODUCTION

This chapter describes the general characteristics and petrography of the deposit sequence, going from the Footwall, through the Mineralised Horizon and into the Hanging Wall as determined from borehole logs. The following points outline the main features of sequence:

1. The deposit is extensively deformed. Most units have a strong NNE-trending foliation which is either vertical, or dips steeply ($>80^{\circ}$) to the west. The foliation is parallel to observed lithological contacts and is therefore assumed to be generally parallel to bedding. A mineral lineation, defined by an alignment of biotite knots in the plane of the foliation, is developed in pelitic units, and plunges south at 80° . Diamond drill hole BS-74, located at the southern end of the deposit, intersects highly sheared and disrupted rocks along its entire length supporting the interpretation that the deposit is fault-bounded along its southern margin.

2. Metamorphism has produced amphibole in mafic rocks, biotite in siliceous rocks, and garnet in restricted Fe- and Al- rich pelites (iron-formation) associated with mineralisation. These (assumed prograde) phases are cut by extensive late chlorite and magnetite-bearing shears which crosscut the foliation.

3. Primary depositional features (scour structures, graded bedding and growth faults) are preserved in some fine-grained tuffs of the Hanging Wall which indicate way up to the north west. In the Footwall,

although primary igneous textures and fine-scale compositional layering are present, felsic rocks have generally undergone widespread alteration (mainly silicification). Minor stringer sulphide (chalcopyrite, pyrite, arsenopyrite) veins are sporadically developed in the Footwall, but are absent from Hanging Wall rocks. The alteration is considered to be spatially related to a zone of major copper mineralisation (described below) which was developed within, or above, the QFP.

4. Copper mineralisation (contained within the 'Copper Body') comprises 'blebs' and segregations of chalcopyrite in a stratabound zone within a) characteristically bleached and silicified rocks (the Silicified Zone), which grade up-dip into b) heavily altered, green pyrrhotite dominated lithologies (later designated as the Chloritoid Zone from thin section studies). The latter occur up-dip of the Silicified Zone and most commonly contain lower grade copper ore. Zinc grades in the Copper Body range up to 3%Zn, and show a systematic decrease towards the Silicified Zone.

5. High-grade zinc mineralisation is confined to sphalerite-rich, chalcopyrite-poor layers, (<3m) at both margins of the Copper Body. It is mostly within thinly layered (<10m), quartz-rich, lithologies ('mineralised rhyolites' of Granges' logs) which, in hand specimen, are similar to those of the Copper Body. These rocks occur in contact with, and parrallel to, distinctive garnet-magnetite-chlorite units which are up to 30m thick.

2.2 DETAILED DEPOSIT STRATIGRAPHY

Examination of available drill core, drill logs and 306 thin and polished thin sections identified of a number of rock types comprising

the deposit sequence which is here shown as a simple stratigraphic succession from Footwall through to Hanging Wall (Figure 2.1). The locations of major mineralisation, and gross lithological variations both within, and between, various sections are shown in the interpretive isometric projections of Figures 2.2 and 2.3. High-grade zinc mineralisation occurs in thin layers, at the upper and lower margins of the Copper Body, which extend up-dip beyond copper-bearing rocks. Major lateral lithological variations within a particular section correlate with the change from copper-rich to zinc-rich mineralisation. The occurrence of iron formation and zinc-rich mineralisation above and below rocks of the Copper Body (Figures 2.2 and 2.3) may result from either stratigraphic or structural repetition. The detailed interpretation of this repetition is considered below in section 2.3. The overall sequence is here subdivided into three component parts for descriptive purposes: Footwall, Mineralised Horizon and Hanging Wall sequences.

2.2.1 The Footwall Sequence

Two major units are recognised:

- (i) Footwall Mafic Unit (FMU) and
- (ii) Quartz-Feldspar Porphyry (QFP), subdivided into the following sub-units:
 - a) Quartz-eye porphyry
 - b) Feldspar crystal tuffs
 - c) Intermediate lapilli tuffs

The Footwall Mafic Unit is developed within the Quartz Feldspar Porphyry (Figures 2.1 and 2.2) and attains a maximum thickness of 50m in the NNE and SSW of the deposit. The Quartz Feldspar Porphyry has major variations in thickness both down-dip and along strike. In contrast to rocks of the Hanging Wall, Footwall rocks have undergone widespread alteration which, because of its spatially restricted nature, is thought to

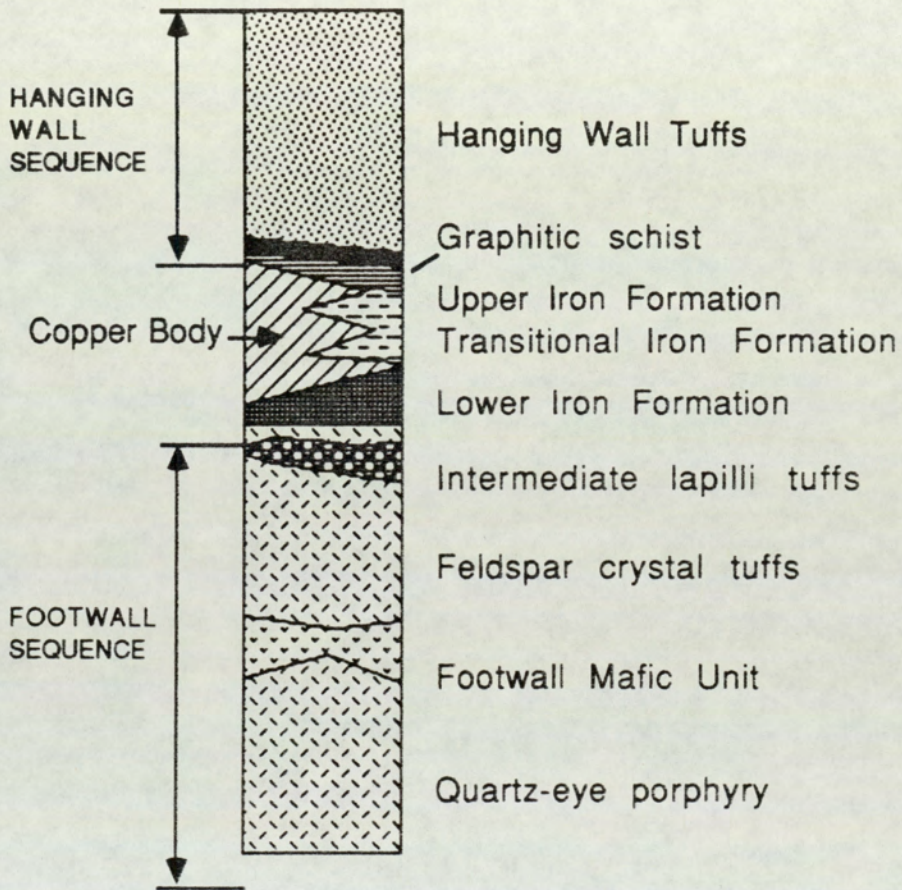


Figure 2.1 General stratigraphy of the Bigstone deposit.

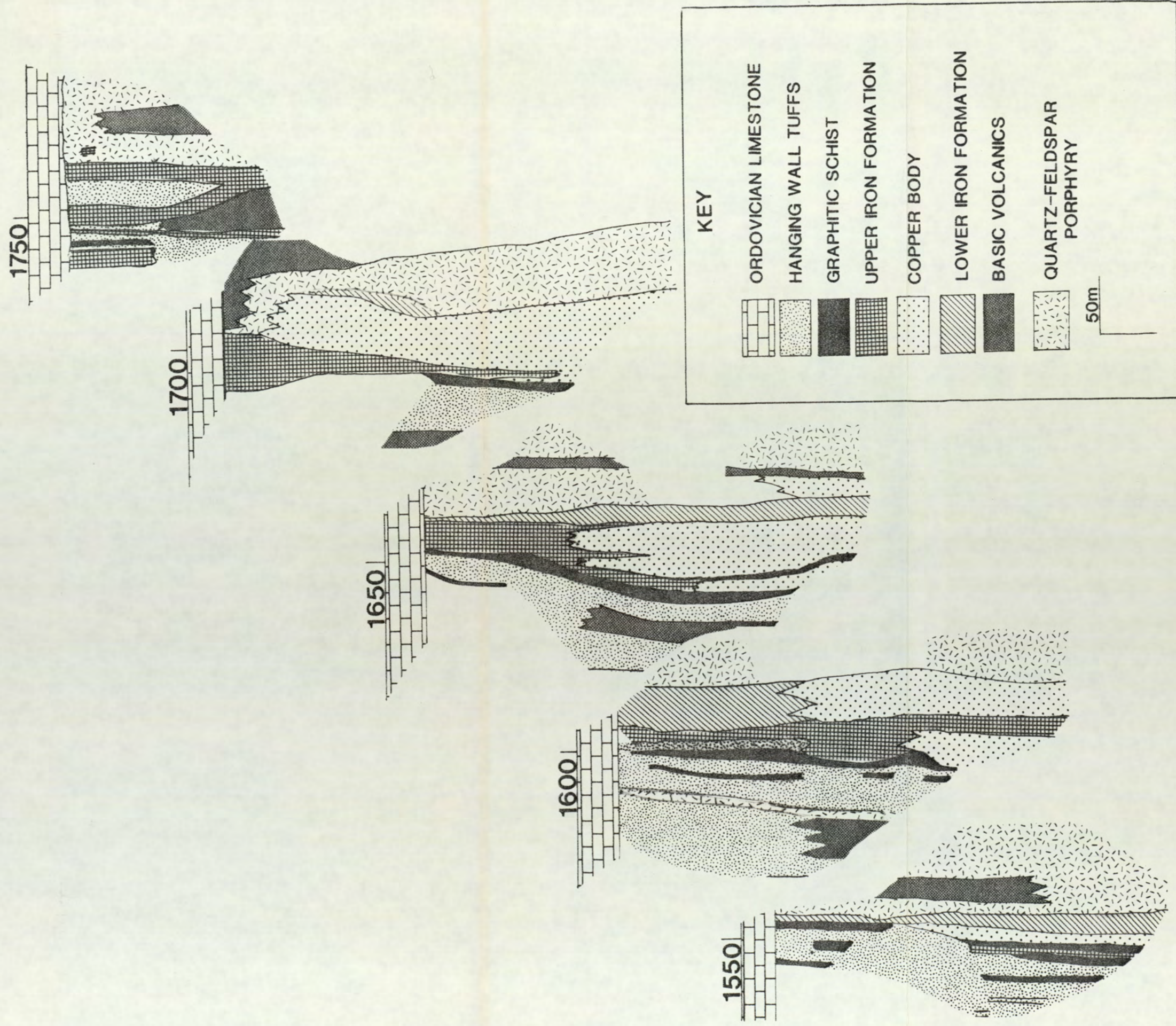


Figure 2.2 Isometric projection of the Bigstone deposit sequence

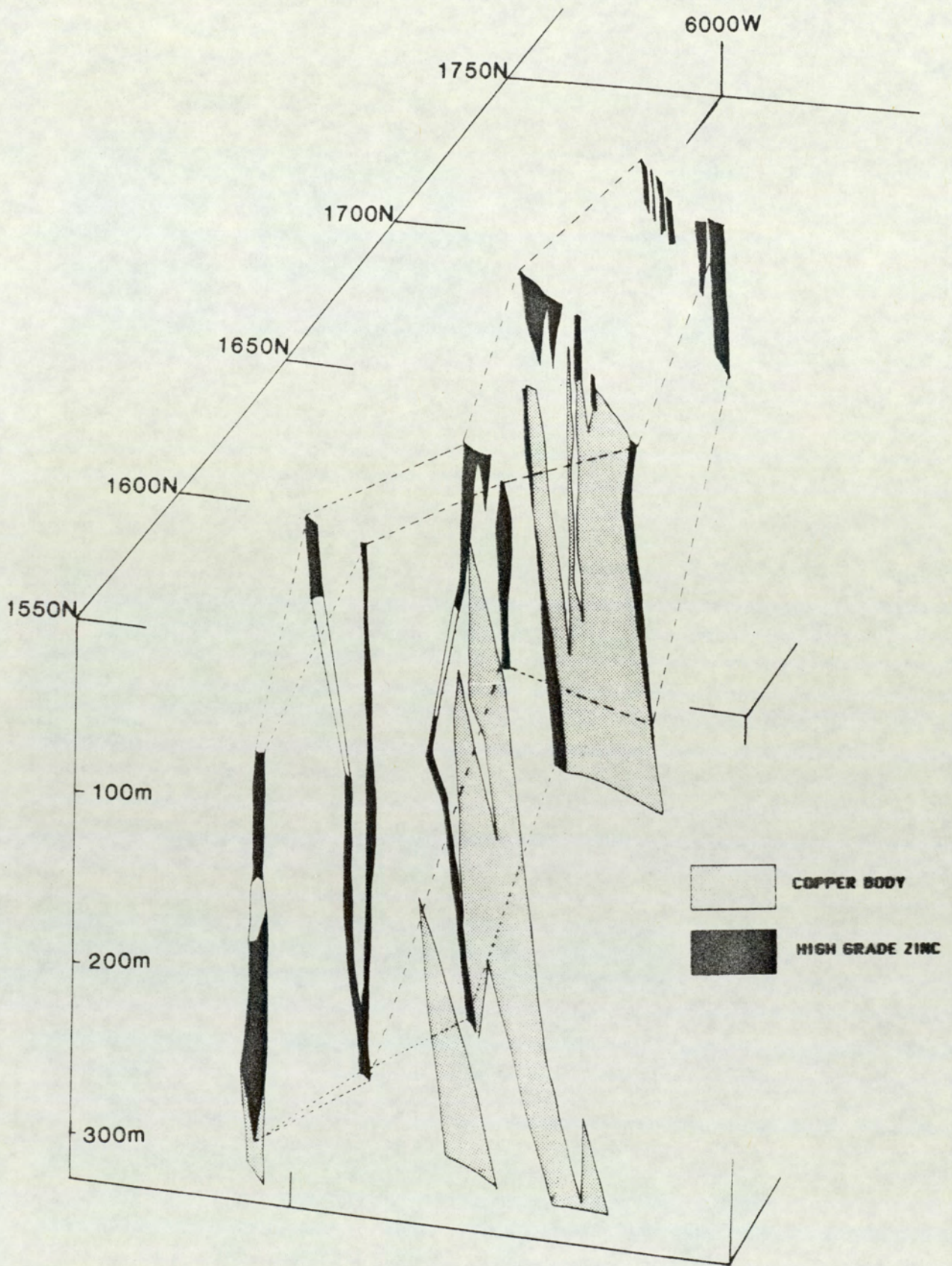


Figure 2.3 Isometric projection showing the relationship between copper and zinc mineralisation.

have occurred prior to metamorphism. In the QFP plagioclase crystals are pseudomorphed by silica, and there is the sporadic development of stringer sulphide mineralisation. In the Footwall Mafic Unit patchy pale green alteration containing carbonate and epidote, within which primary igneous plagioclase is largely destroyed, is developed within less altered rock which is dark green and within which plagioclase outlines are well preserved. Both units are described in more detail below.

(a) The Footwall Mafic Unit.

In hand specimen, rocks of this unit are characteristically light to medium green and coarse-grained consisting of amphibole (80%) and up to 20% euhedral plagioclase which is largely replaced by epidote, zoisite and carbonate. Large masses of amphibole (up to 1cm across) comprise a mosaic of smaller crystals of actinolite which contain fracture-parallel patches and rims of blue-green hornblende. Some preserve twin patterns and habits suggestive of former pyroxenes and contain relict ortho-, and clinopyroxene. Magnetite, ilmenite and sphene are present as accessory phases.

(b) The Quartz Feldspar Porphyry

Porphyritic felsic rocks, containing variable proportions of quartz and plagioclase phenocrysts, are the dominant Footwall rocks. The unit is a complex sequence of interbedded tuffs (possibly with minor flow material) and thin sedimentary layers. Contacts between the various units are gradational and all three sub-units may not necessarily be present within any given drill core. In the upper parts of the sequence, intermediate lapilli tuffs are intermittently developed and contain a minor component (<10%) of interlayered feldspar crystal tuffs. In general, all units are heavily altered and primary textures occur in only a

minority of samples. The sub-units are described in more detail below:

1) Quartz-eye porphyry

This sub-unit is characterised in hand specimen by the presence of blue opalescent quartz eyes (up to 4 x 3mm) slightly flattened in the Plate 2.1 + 2.2 in the plane of a poorly defined foliation. In thin section, a complete range of quartz-eye textures are seen, ranging from single, subhedral phenocrysts to heavily deformed coalesced quartz eyes (Plates 2.1 and 2.2). The matrix to the quartz is extensively recrystallised, and comprises fine-grained quartz and minor sodic plagioclase (<5%). Biotite, with associated allanite, is commonly present in stringers located along minor fracture planes.

b) Feldspar crystal tuffs

The quartz eye porphyry grades upwards into plagioclase-rich rocks containing up to 40% oligoclase to andesine phenocrysts (5 x 2mm) and minor lithic fragments. The Plagioclase occurs as clusters of broken and single crystals of various sizes (0.2 to 20mm long) in a fine-grained siliceous matrix (Plate 2.3). Most of the feldspars are heavily altered (see below), but some retain primary simple twinning and oscillatory zoning (Plate 2.4). In general, there is an increase in the abundance of feldspar upwards in the sequence. Quartz is present as quartz-eyes (<5%) and as the major component of the matrix. Biotite occurs in stringers along with minor chlorite and carbonate.

Upwards in the sequence, primary textures are generally less readily recognised. In hand specimen, the core has a bleached appearance, and most feldspar phenocrysts are replaced by silica. In thin section, all stages in the replacement of feldspars are seen; in less altered rocks the

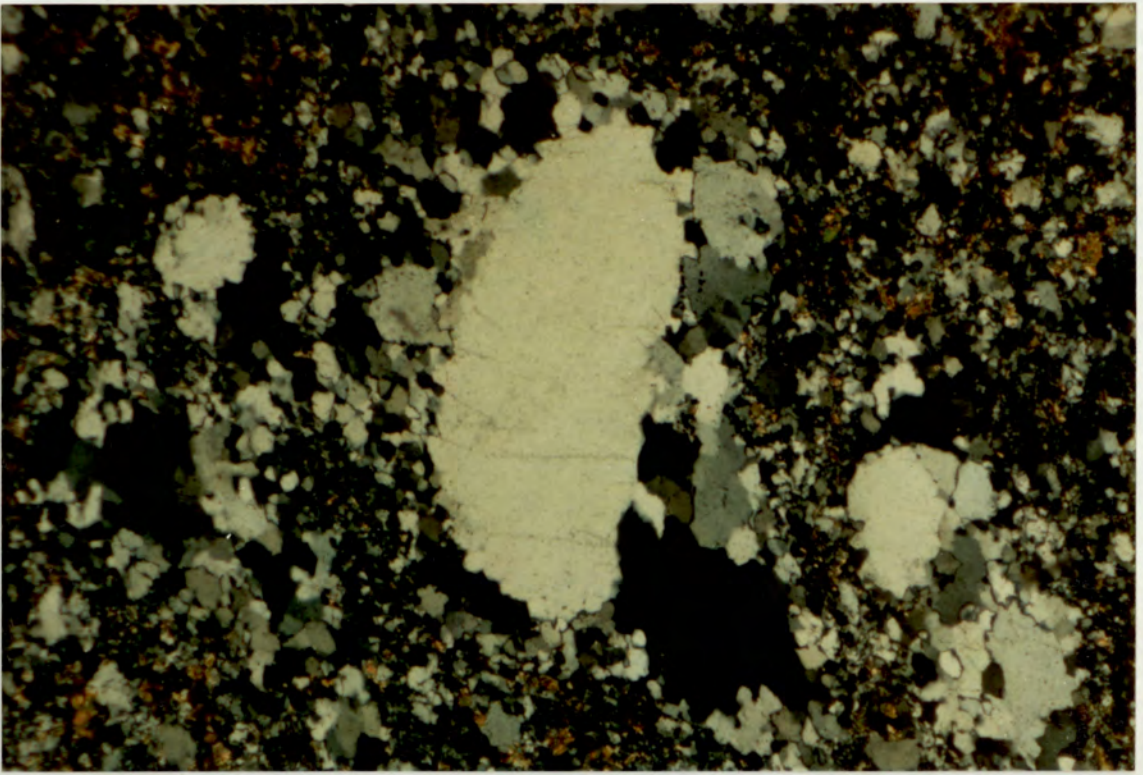


Plate 2.1

Relatively undeformed quartz-eyes from the Footwall Quartz-eye Porphyry. Sample No. 89, field of view 3.4mm, XPL

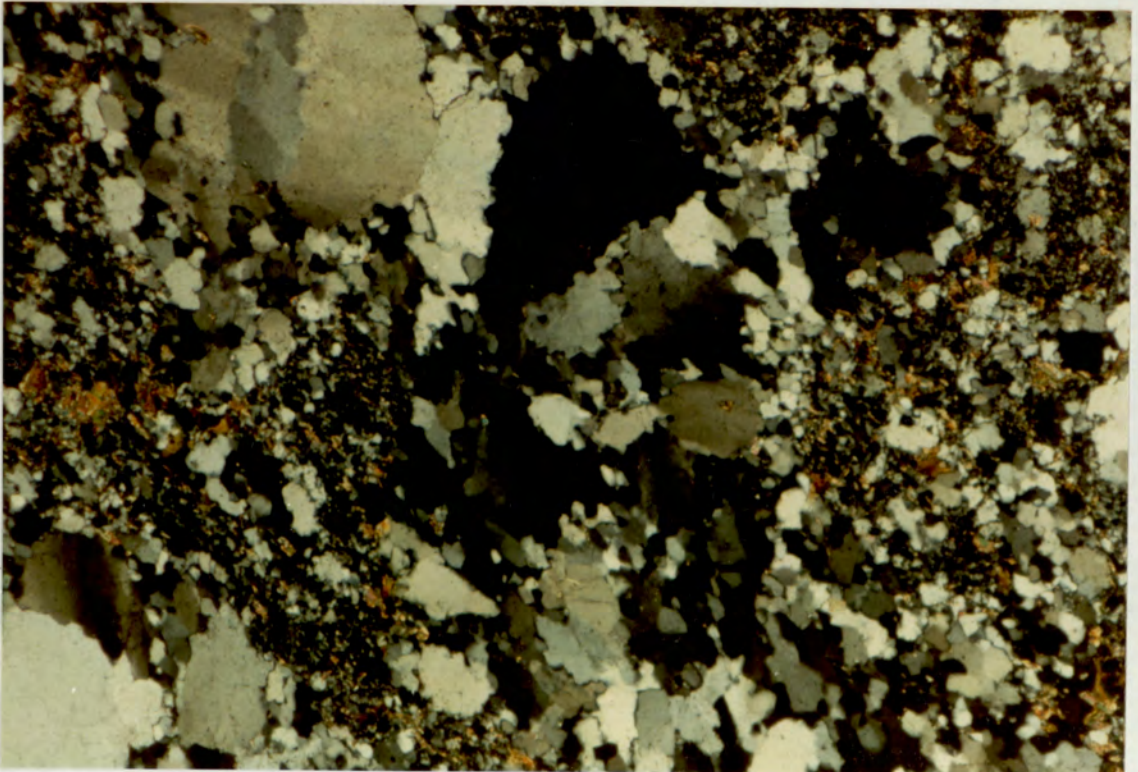


Plate 2.2

Coalesced quartz-eyes in the footwall Quartz-eye Porphyry. Sample No. 89, field of view 3.4mm, XPL.

Plate 2.3

Euhedral plagioclase phenocryst, with oscillatory zoning in a quartz-rich, meta-arenitic matrix in Footwall feldspar crystal tuffs.

Sample No. 280, field of view 2.7mm, XPL.

Plate 2.4

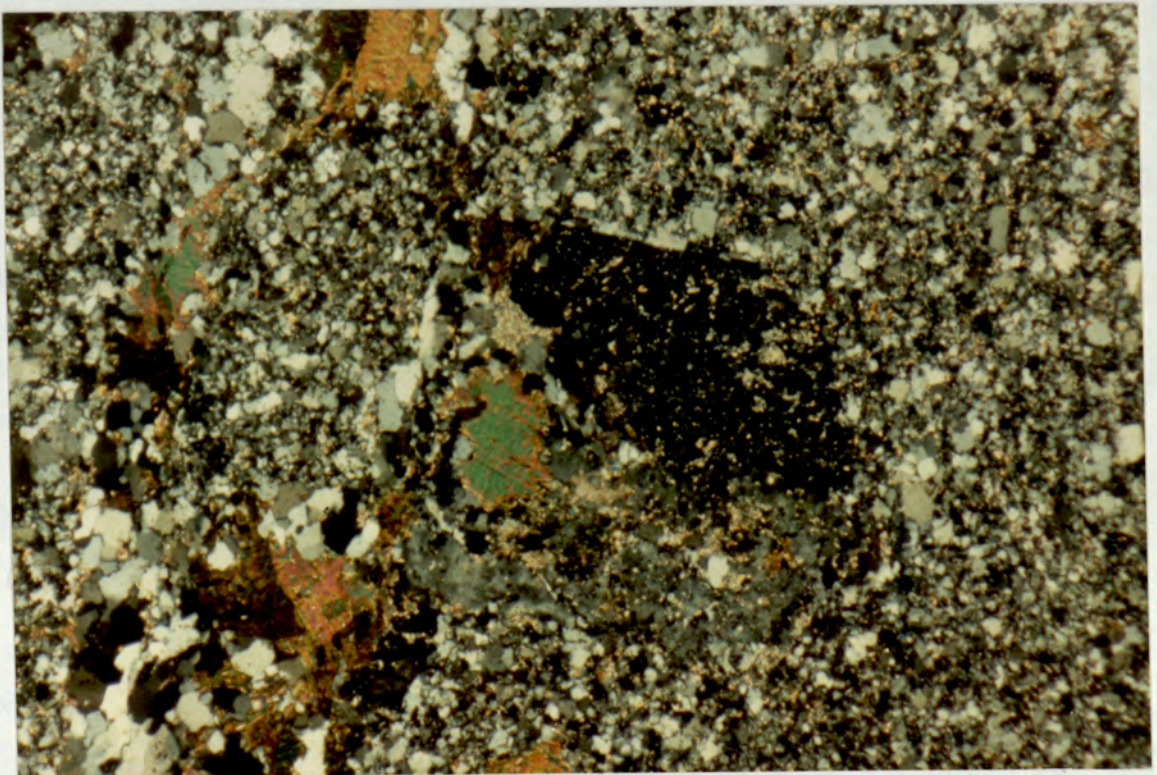
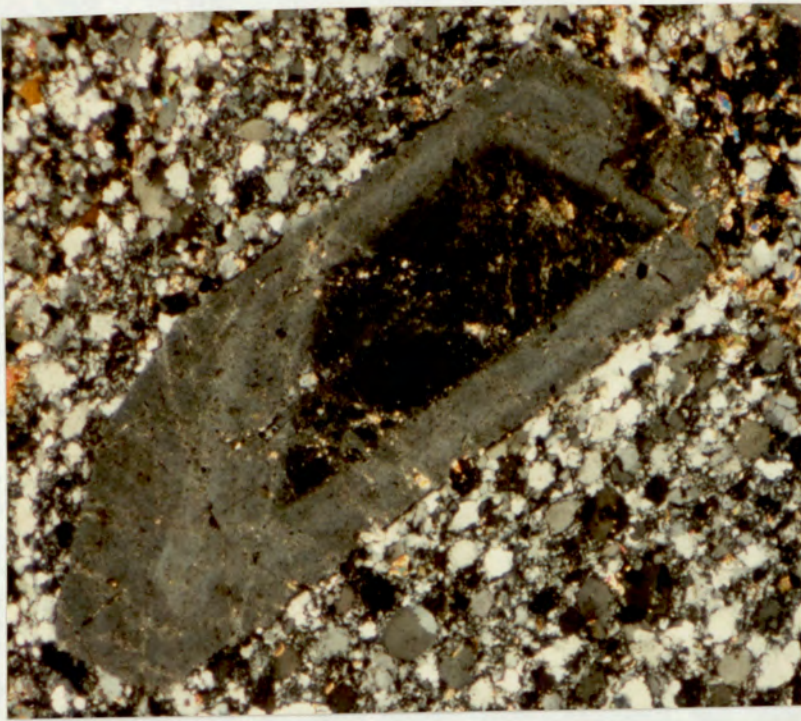
Broken plagioclase phenocryst with well preserved oscillatory zoning in the Footwall feldspar crystal tuffs.

Sample No. 200, field of view 2.7mm, XPL

Plate 2.5

Plagioclase phenocryst replaced by quartz and veined by abundant biotite in the Footwall feldspar crystal tuffs.

Sample No. 279, field of view 3.4mm, XPL.



feldspars are incipiently replaced by sericite and/or chlorite, and, in more altered examples, feldspars are cut by quartz and biotite stringers. The final stage of alteration involves the complete replacement of the feldspar by quartz (Plate 2.5). This general increase in alteration is accompanied by the development of numerous biotite stringers with epidote, carbonate and allanite. In some heavily altered rocks, silicate alteration minerals are accompanied by stringer sulphide mineralisation, comprising chalcopyrite, arsenopyrite and pyrrhotite, along with the development of veins containing blue-green tourmaline.

c) Intermediate lapilli tuffs.

Down-dip (in deeper drill holes within any section), the stringer mineralisation, described above, grades directly into the Copper Body. Less commonly, it is separated from the ore zone by a sub-unit of intermediate lapilli tuffs, which vary in thickness between 5 and 30m. They are characterised by the presence of dark-green, lapilli-sized fiammé, and white, felsic, lithic fragments, comprising up to 50% of the rock (Plate 2.6).

The fiammé are seen in thin section to consist of radiating mosaics containing hornblende with minor interstitial quartz. Surrounding these lensoid areas are well preserved anhedral and broken plagioclase crystals and subordinate felsic lithic fragments. All are in a fine-grained siliceous matrix. Examination of the lithic fragments using cathodo-luminescence (CL) techniques reveals the presence of igneous flow textures exhibited by blue-luminescent plagioclase microlites (Plate 2.7).

2.2.2 The Mineralised Horizon (M.H)

In general, the following units are progressively intersected up-dip



Plate 2.6

Drill core of the Footwall intermediate lapilli tuff from BS-37 showing the development of dark, fiamme-like structures and lighter felsic lithic fragments. Photograph supplied by J.W. Gaskarth.

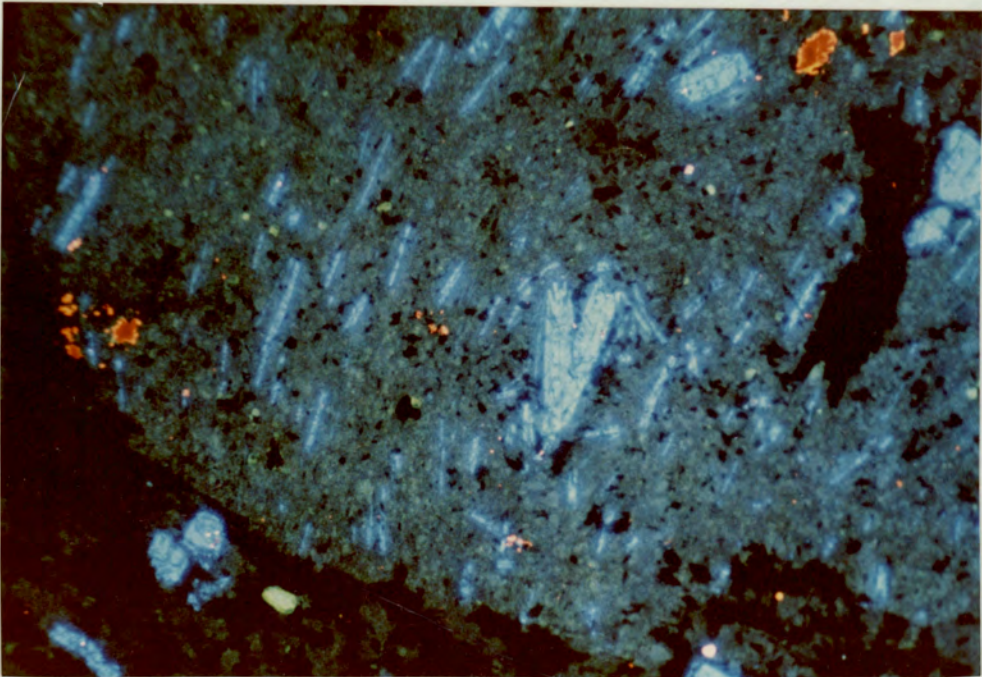


Plate 2.7

C.L. photograph of a feldspar-phyric lithic fragment with the development of a sub-trachytic texture displayed by blue-luminescent plagioclase crystals. Sample No. 750, taken from the footwall Intermediate Lapilli Tuffs, field of view 2.5mm.

within any particular section of the deposit: (Figure 2.4):

(i) The Copper Body divided into the Silicified Zone and the Chloritoid Zone (Figure 2.4) on the basis of their distinctive alteration mineralogies.

ii) The high-grade zinc zone is best developed as thin, sphalerite-rich, layers at the margins, and up-dip, of the Chloritoid Zone (Figure 2.3).

iii) Iron-Formation subdivided into Upper Iron Formation (UIF), Transitional Iron Formation (TIF) and Lower Iron Formation (LIF).

The various units are described in more detail below:

The Copper Body.

Down-dip, in any particular section, up to 15% chalcopyrite occurs as 'blebs' and segregations within characteristically bleached-white rocks of the Silicified Zone. This zone narrows up-dip grading into dark-green and pyrrhotite-dominated lithologies of the Chloritoid Zone. The narrowing of the Copper Body is accompanied by a general decrease in the ratio $Cu/Cu+Zn$ (Figure 2.4).

a) The Silicified Zone.

Rocks of this zone are dominated by quartz (~80%), muscovite (~10-20%), and variable amounts of chalcopyrite and pyrite, with subordinate pyrrhotite and magnetite. Thin sections reveal heavily altered and silicified plagioclase crystals and the near total destruction of pre-existing primary textures (Plate 2.8). Chalcopyrite occurs in anhedral patches up to several centimeters across. It is closely associated with pyrrhotite which forms rims around, and replaces, earlier pyrite (Plate 2.9), and contains minor

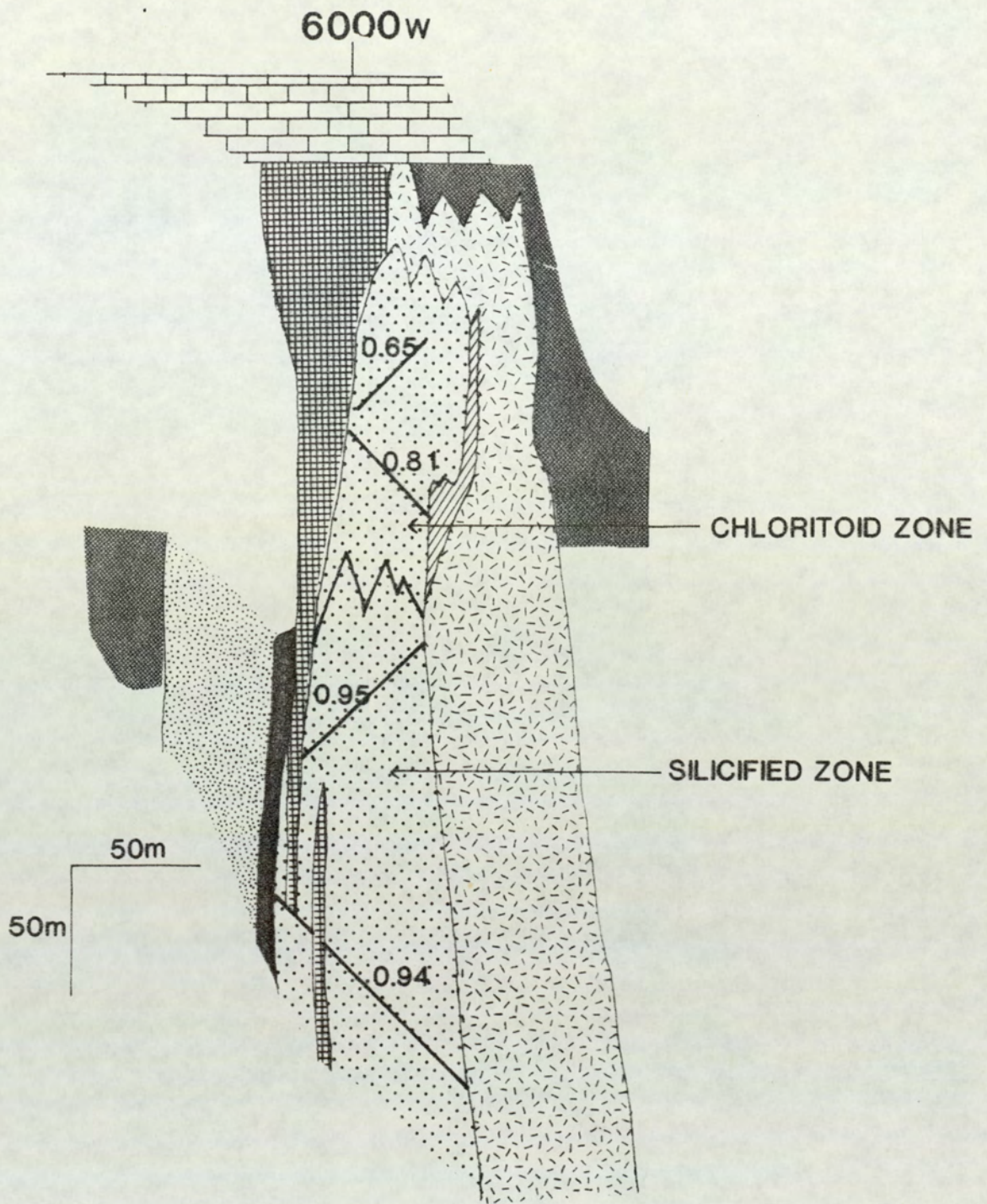


Figure 2.4 Schematic diagram of the 1700N section. Numbers correspond to the ratio $Cu/Cu Zn$. Key as in Figure 2.2.

euohedral magnetite. Arsenopyrite is present in some samples as 1-2mm long euohedral blades cut by later pyrrhotite and chalcopyrite. Sphalerite occurs in minor and variable amounts (<5%), associated with chalcopyrite. Ilmenite is ubiquitous as an accessory phase within silicates, although in some specimens it is also present adjacent to, and within, sulphide phases (Plate 2.10).

b). The Chloritoid Zone

These rocks are characterised by an extensive alteration mineralogy dominated by highly variable quantities of chloritoid, pyrrhotite and magnetite which are developed in the narrow up-dip portion of the Copper Body (Figure 2.4). The transition between the Silicified Zone and the Chloritoid Zone is defined by the first occurrence of minor chloritoid veinlets in silicified rocks. The complete mineralogy of the Chloritoid Zone (Table 2.1) is not seen in

TABLE 2.1 Chloritoid Zone Mineralogy

<u>MAJOR MINERALS</u>	<u>MINOR MINERALS</u>
Plagioclase ¹	Ilmenite ¹
Quartz	Sphalerite
Chloritoid	Gahnite
Muscovite	Tourmaline
Pyrrhotite	Apatite
Pyrite	Margarite
Magnetite	Fluorite
Chalcopyrite	Garnet
Chlorite ²	

¹ denotes relict mineral

² denotes retrograde mineral

single thin sections and the absolute abundance of any particular

Plate 2.8

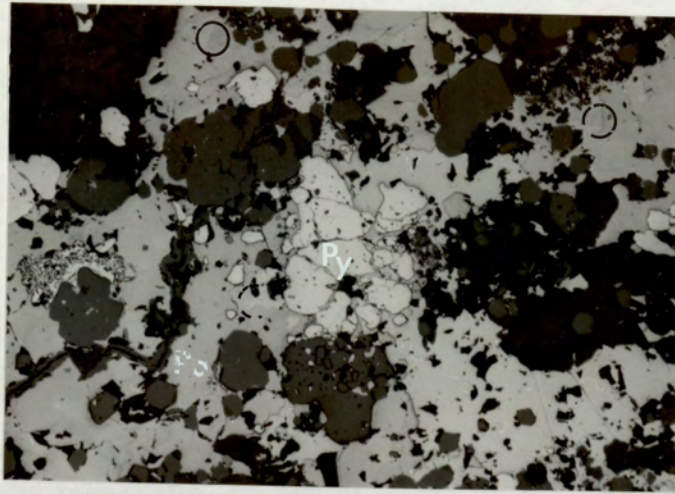
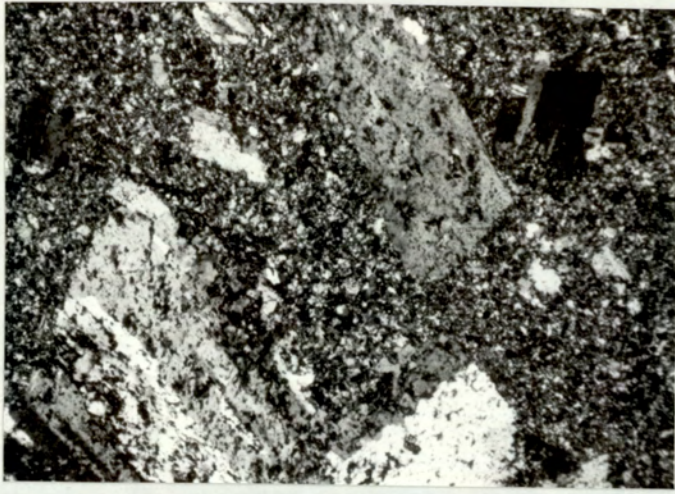
Heavily silicified rock from the Mineralised Horizon representing the near total destruction of primary igneous textures. Sample No. 588, field of view 3.4mm XPL.

Plate 2.9

Pyrite (Py) replaced by pyrrhotite (Po) in heavily mineralised rocks. Dark grey is gahnite (gn) also partly replaced by pyrrhotite. Just visible within individual pyrrhotite grains are sub-grains (circled) with sutured boundaries interpreted to represent unmixing of hexagonal and monoclinic pyrrhotite during cooling. 'Birds-eye' texture involving the late stage replacement of pyrrhotite by pyrite and marcasite is developed around a large gahnite grain at the left hand side of the photograph. Sample No. 234, photograph taken under partly crossed nicols, field of view 1.4mm.

Plate 2.10

Primary ilmenite laths (circled) preserved adjacent to sulphides in heavily mineralised rocks. Sample No. 588, field of view 1.4mm, PPL.



mineral phase is highly variable. Important mineralogical and textural associations are detailed below.

Chloritoid forms monomineralic cross-cutting veinlets in weakly mineralised rocks. In heavily mineralised samples idioblastic chloritoid crystals comprise up to 50% of the rock as a matrix to pyrrhotite-rich areas. In the latter case, it is typically associated with heavily altered plagioclase feldspar (Plate 2.11). Although largely developed in feldspar-bearing rocks, chloritoid is also present in some which are composed almost entirely of quartz plus sulphides. Most samples contain chlorite as a minor or accessory phase though some have significant quantities which is inferred to have formed largely by the replacement of chloritoid (Plate 2.12).

Large, anhedral plagioclases (up to 1cm across) are untwinned and lack the pervasive silicification seen in the adjacent rocks of the Silicified Zone. They are heavily altered with replacement by fine-grained micaceous (?) minerals, and some are totally replaced by patches of chloritoid and opaques. Inclusions of sulphide minerals are surrounded by zones of recrystallised feldspar which are out of optical continuity with the host phase. Under cathodo-luminescence (C.L.), the plagioclase feldspars display anomalous green luminescence (Plate 2.13), in marked contrast to the normal blue-luminescence of those in unmineralised rocks (Plate 2.7). The intensity of green alteration appears directly related to the degree of feldspar alteration.

Quartz is ubiquitous and occurs as highly strained, ovoid crystals (~.2mm long), which lie in the foliation plane. Under C.L., it has a dull red-brown luminescence colour at accelerated voltages some 11 or 12 Kv below those normally required to cause luminescence in quartz.

Muscovite is developed as either the sole phyllo-silicate, or in

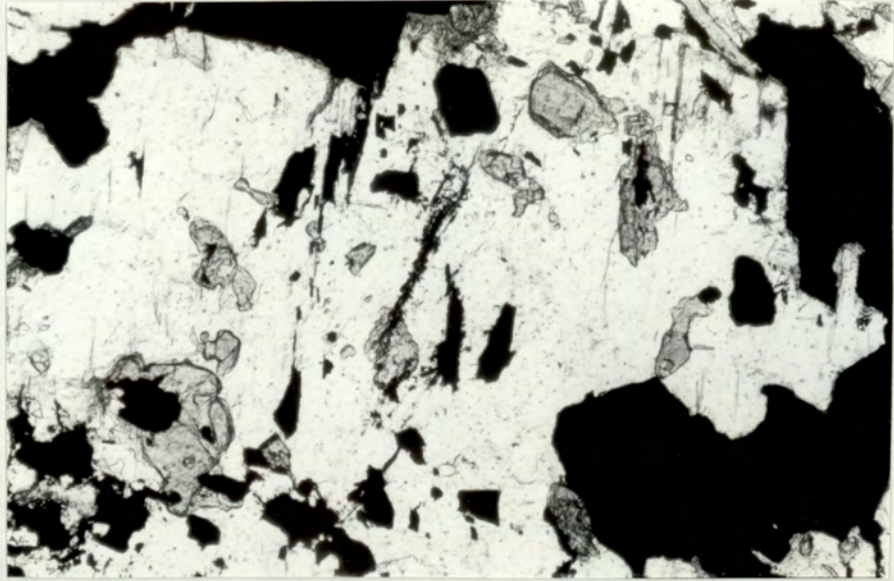


Plate 2.11

Development of chloritoid (dark grey) and sulphides within heavily altered plagioclase feldspar. Sample No. 840, field of view 0.89mm, PPL.

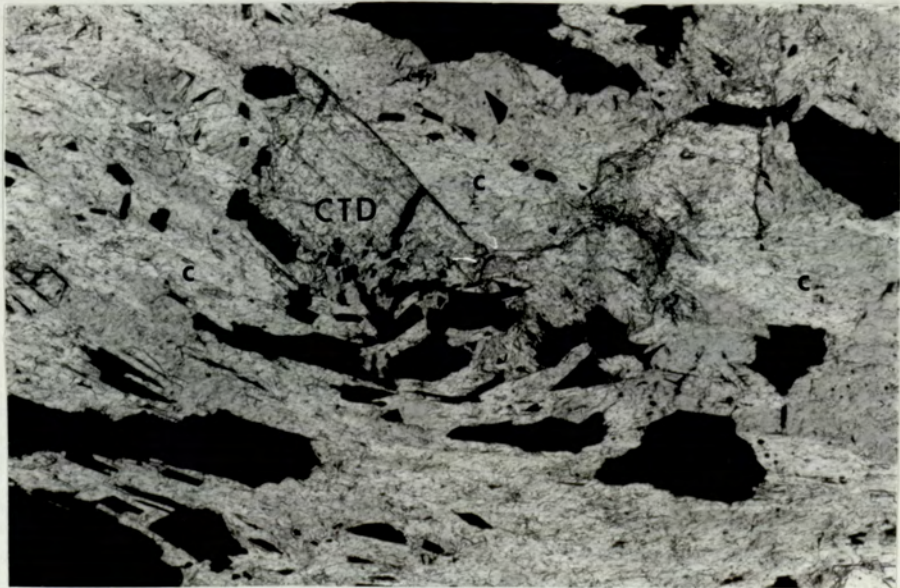


Plate 2.12

Development of retrograde chlorite (c) from chloritoid (CTD) in rocks of the Chloritoid Zone. Sample No. 835, field of view 3.4mm, PPL.

close association with chloritoid and feldspar. The brittle mica, margarite is also present in some muscovite bearing samples.

Pyrrhotite and magnetite are the dominant opaque phases along with lesser quantities of pyrite, chalcopyrite, sphalerite, ilmenite and arsenopyrite. Pyrrhotite forms veins across, and rims around, earlier pyrite, and randomly orientated polygonal segregations containing small (100 μ m), relict pyrite grains. Magnetite occurs as disseminated idiomorphs within pyrrhotite and pyrite; as coalescing grain aggregates at the margins of polygonal, annealed pyrrhotites; or as the sole iron-bearing opaque mineral. Chalcopyrite, with subordinate sphalerite, occurs in the matrix in association with pyrrhotite, and less commonly with magnetite and gahnite. Ilmenite occurs within silicate gangue minerals, as inclusions within gahnite, and less commonly within pyrrhotite.

"Birds-eye" textures, involving late stage replacement of pyrrhotite by magnetite, pyrite and marcasite, are present in some specimens (Plate 2.14).

Up to 10% anhedral garnets are present in some samples associated with chloritoid, plagioclase and quartz. The chloritoid typically occurs as euhedral blades forming the matrix to poorly defined masses of garnet. Less commonly, the two minerals occur together as radial intergrowths indicating co-crystallisation (Plate 2.15).

Gahnite (ZnAl_2O_4) generally comprises <5% of Chloritoid Zone rocks, but in some it is spectacularly developed as up to 60% of individual thin sections. It is most common in those samples containing major quantities of Al-bearing silicates (chloritoid, muscovite and garnet) in association with sphalerite. It occurs as euhedral cubes and octahedra which coalesce in some specimens to

Plate 2.13

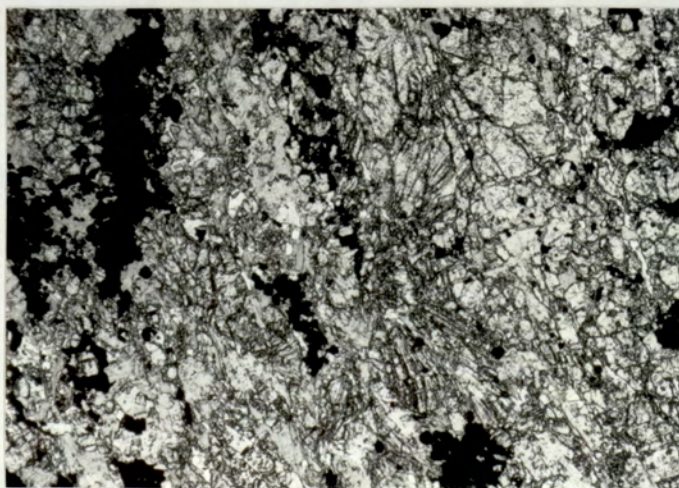
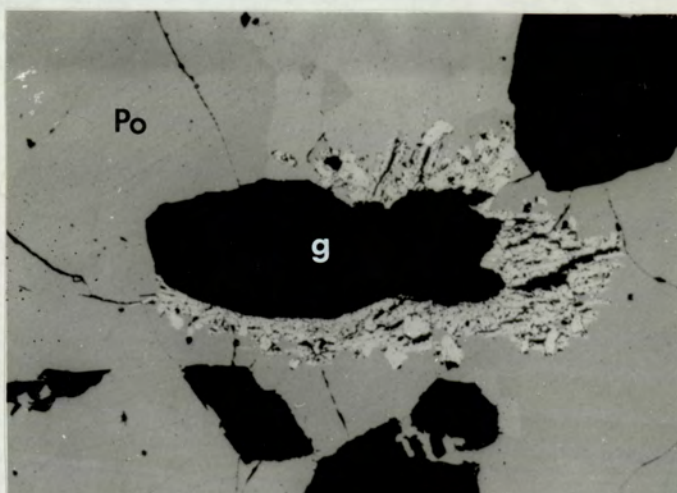
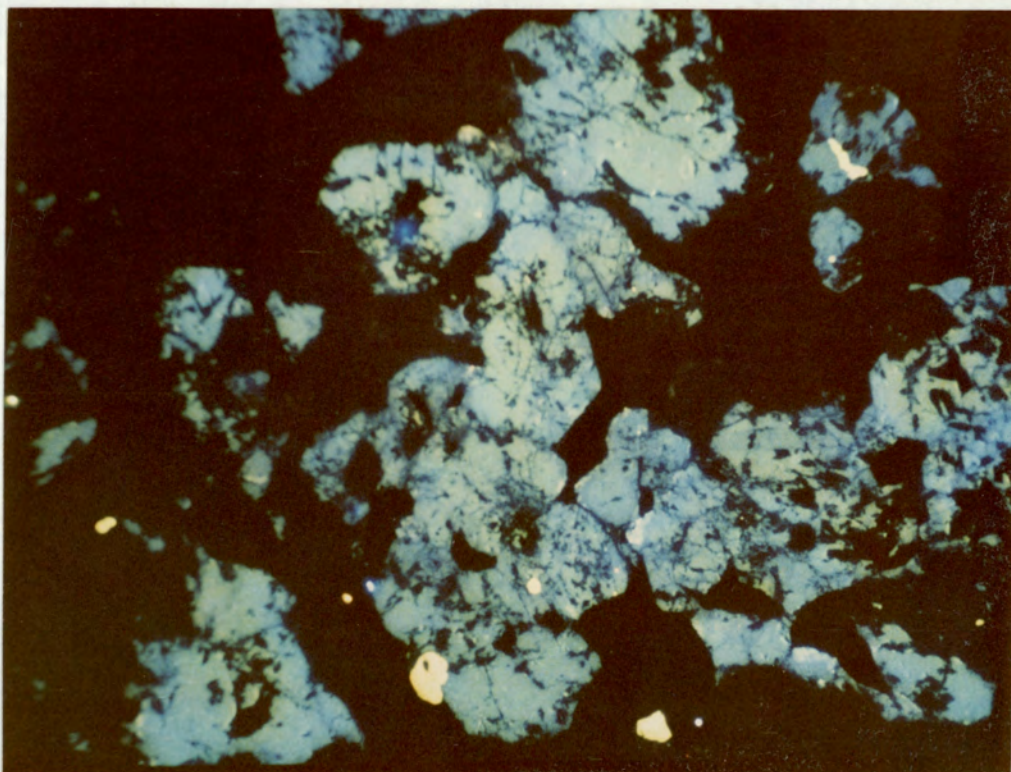
Anomalous green luminescence of plagioclase in rocks of the Mineralised Horizon. The intensity of green luminescence is related to the degree of alteration of the feldspar. Pale blue luminescence corresponds to less altered feldspar. Cores of individual feldspars in some cases have been completely replaced. The dark blue luminescent phase in the upper part is fluorite. The bright yellow luminescence is that of apatite. Sample No. 5, field of view 2.5mm.

Plate 2.14

Development of 'Birds eye' texture around silicate gangue (g) in pyrrhotite (Po). Pyrrhotite is replaced by a late-stage fine-grained intergrowth of pyrite and marcasite. Sample No. 5, field of view 1.8mm, photograph taken in reflected light under partially crossed nicols

Plate 2.15

Radial intergrowths of garnet (dominant phase) with chloritoid in TIF. Opaque mineral is magnetite. Sample No. 1441, field of view 3.4mm, PPL.



form gahnite-rich patches, distinguished from garnet by a faint blue colouration. Most gahnite-bearing rocks are rich in sulphides, commonly pyrrhotite, with lesser sphalerite, pyrite and magnetite. Gahnite contains poorly orientated inclusions of sphalerite, ilmenite, chalcopyrite and pyrrhotite (Plate 2.16). Where developed in sulphide-free or sulphide-poor rocks, it is commonly full of minute magnetite inclusions and appears almost opaque. Blue-green, zoned tourmaline is a common (~2%), accessory phase occurring both as single, euhedral crystals 0.2mm long, and intergrown with pyrrhotite, sphalerite, chloritoid and gahnite.

Apatite is an accessory in most specimens, but in some may form 10% of the matrix (Plate 2.17). It occurs as small (50 μm) zoned, euhedral crystals in replacive, sulphide-rich portions of the rock.

Fluorite is a minor component of the groundmass of heavily mineralised rocks. It also forms veins and patches within altered silicate minerals or small crystals within the cores of heavily altered plagioclase feldspars (Plate 2.13).

2.2.3 High Grade Zinc Mineralisation

Most high-grade zinc ore occurs at the margins of the Chloritoid Zone of the Copper Body; however, individual layers, commonly less than 5m thick, extend down-dip for distances of up to 400m, and are adjacent to rocks of the Silicified Zone. Thus, high-grade zinc layers form a mantle to the Copper Body, which extends up-dip, beyond the zone of copper-bearing rocks (Figure 2.3).

The mineralised rock consists of a fine-grained intergrowth of sphalerite and pyrrhotite along with quartz, untwinned plagioclase, and muscovite. In a typical intersection, sphalerite increases from a

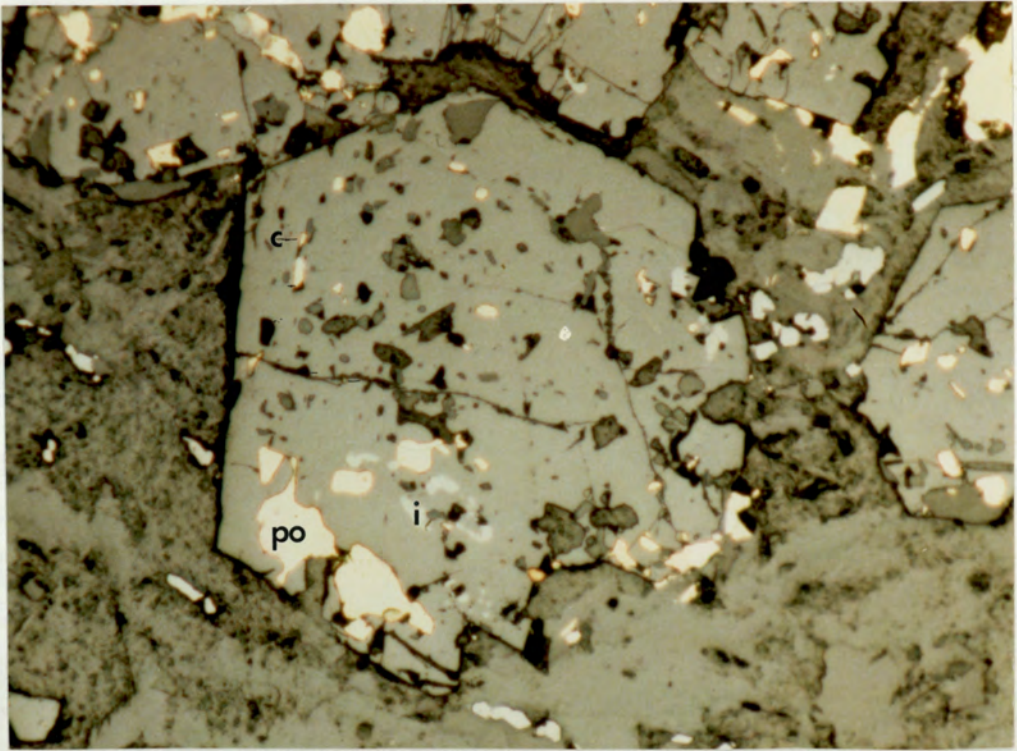


Plate 2.16

Euhedral gahnite containing concentric inclusions of silicates (medium grey), ilmenite (i), chalcopyrite (c) and pyrrhotite (po). Ilmenite and pyrrhotite are also present in the groundmass. Sample No. 235, field of view 1.1mm, reflected light, PPL.

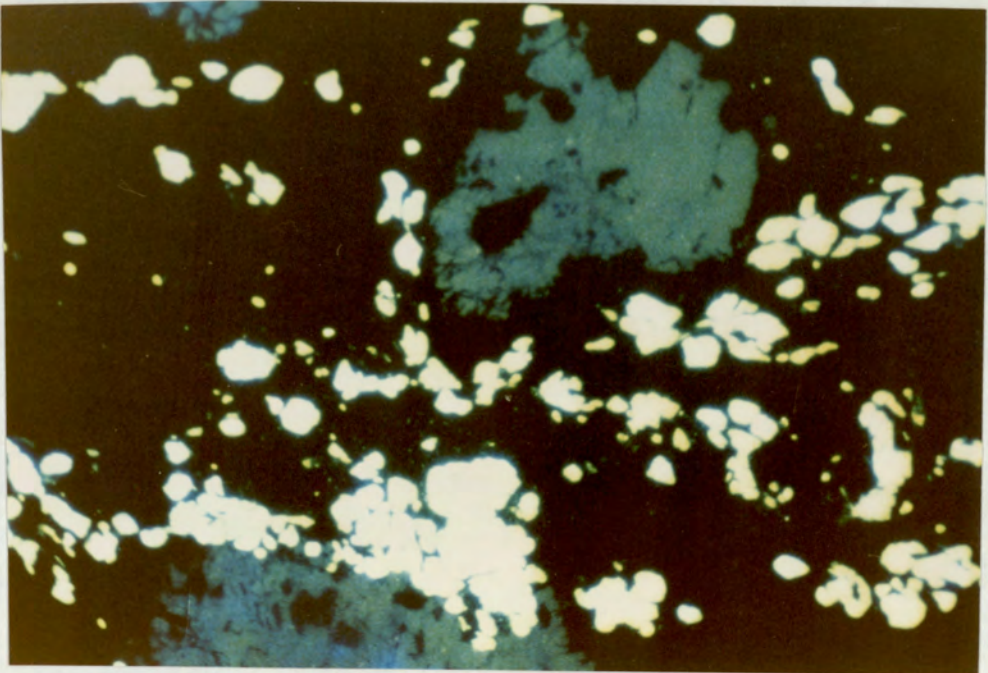


Plate 2.17

Development of groundmass apatite (white/yellow) in mineralised rocks. Altered plagioclase is dominantly green luminescent, with relict less-altered blue patches. Sample no. 242, field of view 2.5mm.

few percent at the margins of mineralisation, up to essentially monomineralic layers <0.5m across. In lower grade ore, the sulphides are either disseminated, or form discontinuous laminations within siliceous host rocks parallel to foliation /bedding.

Quartz comprises >60% of most samples, with muscovite and plagioclase comprising the remainder in approximately equal amounts. Plagioclase is anhedral and unzoned and, in the least deformed samples, it occurs within, and adjacent to, sphalerite-rich laminations. It is heavily altered and replaced, in part, by a mass of fine-grained alteration minerals. Brown-green alteration patches contain relict fragments of a slate-blue to green coloured amphibole (later identified as ferro-tschermakite). Accessory gahnite, along with sphalerite and pyrrhotite, forms rims around, and patches within, individual muscovite laths. It also occurs as isolated euhedra within quartz. Zoned blue-green tourmaline is intergrown with, or entirely enclosed within, sphalerite (Plate 2.18).

High-grade sphalerite, when etched, displays annealing twins, distinguished by their parallel habit and relatively even spacing (Plate 2.19). The sphalerite is devoid of the 'chalcopyrite disease' commonly described from other volcanogenic massive sulphide deposits, and exsolved grains of chalcopyrite are largely absent from grain boundaries. Thus, high-grade sphalerite mineralisation is copper-poor, even though it is commonly immediately adjacent to ore-grade copper mineralisation.

2.2.4 Iron-formation

Quartz-rich, sphalerite-bearing, rocks of the high-grade zinc zone are closely associated with a distinctive group of garnet-chlorite-magnetite rocks. In some drill cores (eg. BS-64,

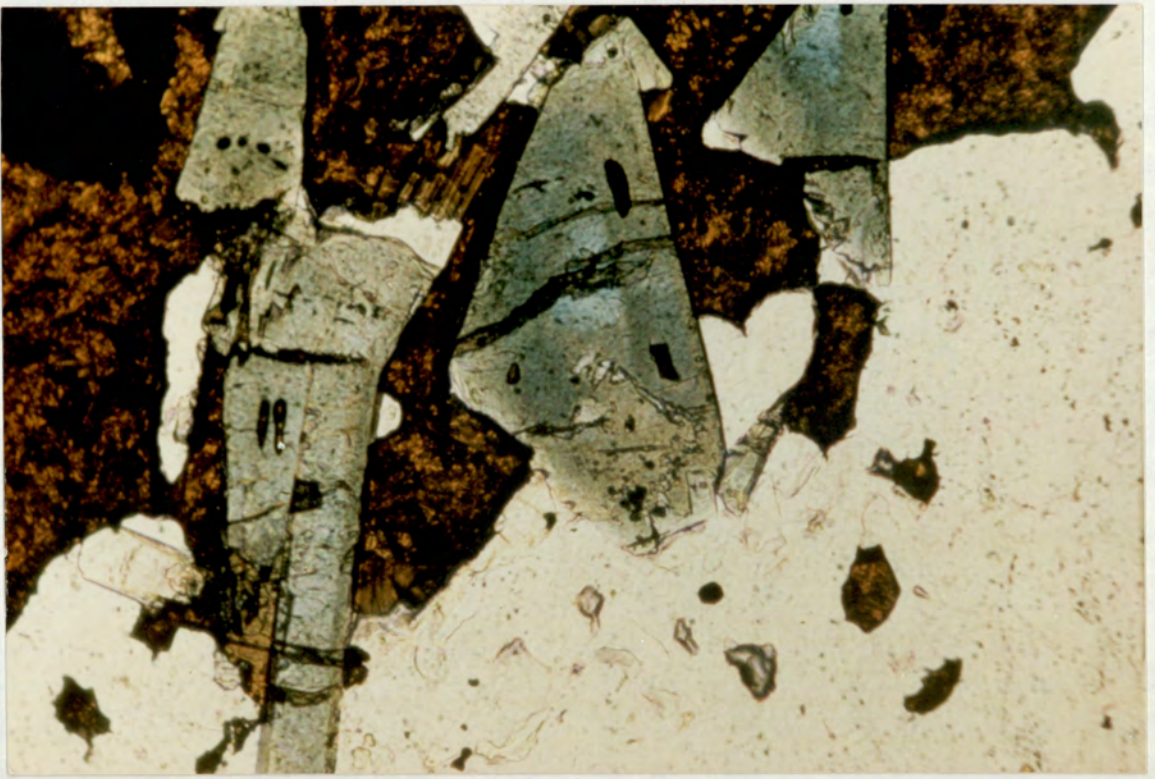


Plate 2.18

Zoned blue-green tourmalines associated with sphalerite and quartz in the high-grade zinc zone. Sample No. 56, field of view 2.2mm, PPL.



Plate 2.19

Etched sample of high grade sphalerite mineralisation showing the development of an annealed texture. Note the absence of chalcopyrite within sphalerite and at triple point boundaries. Sample No. 3, field of view 0.9mm, reflected light XPL. Sample etched by a 7 second exposure to 40% HF fumes.

1750N) siliceous and garnetiferous rocks comprise beds a few metres thick, interlayered over 150m. In other cores, garnetiferous rocks occur above and/or below the Mineralised Horizon. Less commonly, high-grade mineralisation is entirely within garnet-rich rocks where sphalerite ore is separated from the host rock by an approximately 20cm thick layer of almost monomineralic pyrrhotite.

Spatial relationships between siliceous, garnetiferous and zinciferous units are thus complex within, and between, individual drill holes. It is emphasized however that garnet-bearing rocks are entirely confined to the Mineralised Horizon and therefore serve as approximate stratigraphic markers.

The garnets vary in size from a few mm up to 4cm across, and in abundance from a few percent up to almost monomineralic 'garnetite' layers (Plate 2.20). These variations impart a centimetre-scale layering to the units parallel to lithological contacts, thought to represent primary compositional variations in the precursor lithology.

Recognition of primary mineral assemblages and textures is hampered by the widespread effects of a major retrogressive metamorphic event which has produced replacement of prograde amphiboles, and partial replacement of garnet by dark green chlorite and magnetite. (Plate 2.21).

Three mineralogically distinct types of iron-formation have been identified, these are:

a). Upper Iron Formation (UIF), comprising assemblages of garnet, grunerite, magnetite, quartz and minor amounts of arsenopyrite, and carbonate

b). Transitional Iron Formation (TIF), comprising assemblages of garnet, hornblende, magnetite, ilmenite, quartz, plagioclase, gahnite, tourmaline, apatite and up to 5% base metal sulphides.



Plate 2.20

Photograph from DDH BS-37 of LIF, showing development of garnetite. Photograph supplied by J.W.Gaskarth

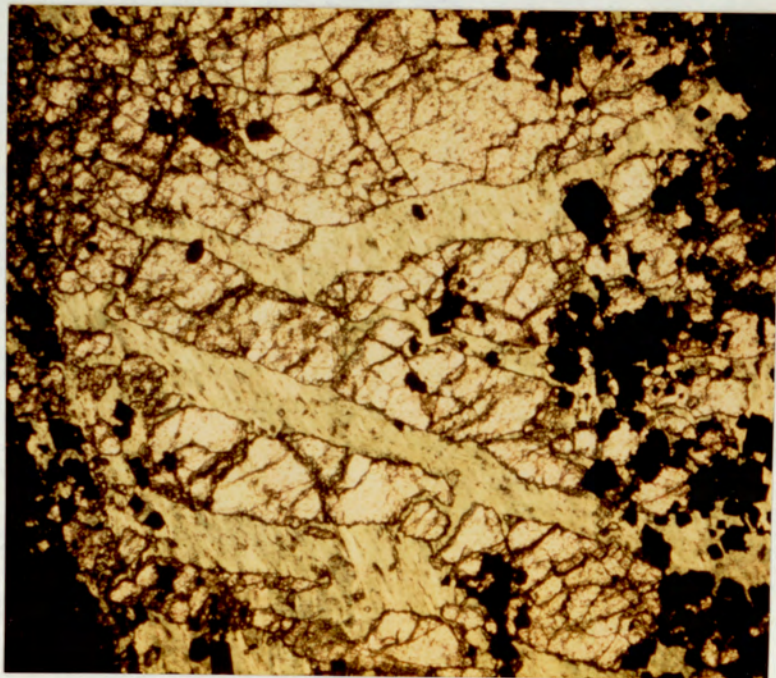


Plate 2.21

Pull apart garnet, infilled with retrograde chlorite plus quartz. Sample No. 223, field of view 3.4mm, PPL.

c). Lower Iron Formation (LIF) made up of garnet, hornblende, magnetite, ilmenite, and gahnite, along with minor quartz, grunerite and base metal sulphides.

The major difference between UIF and LIF is the presence of widespread grunerite in the former, and hornblende in the latter. Both UIF and TIF are devoid of abundant quartz, plagioclase feldspar, gahnite and chloritoid and are thus easily distinguished from TIF. The three types of iron-formation are described in more detail below:

Upper Iron Formation

This unit forms a continuous marker horizon (approximately 8m thick) overlying rocks of the Chloritoid Zone and parts of the Silicified Zone. Garnet is by far the most abundant mineral in UIF, and generally comprises >40% of the rock. Garnet size is variable, even on the scale of a single thin section, but is generally in the range 0.2mm to 10mm. Some sections of drill core comprise >80% masses of anhedral garnetite, which poikiloblastically enclose quartz and grunerite. In thin section, the majority of the garnets are colourless (almandine), but some contain zones or patches of a brown-orange variety corresponding to spessartine-rich compositions (Plate 2.22). The spessartine has no apparent relationship to crystal habit on the scale of a thin section. The centimetre-scale layering visible in hand specimens is present on a finer scale in thin section. Subidioblastic to idioblastic garnet-rich layers (up to 1mm thick) are separated by layers (5mm-10mm thick), dominated by grunerite, within which garnet is either less abundant or absent.

In mineralised samples, sphalerite and pyrrhotite generally form the matrix to individual garnets, and in some clearly replace them. Where replacement has occurred, individual veins of sulphides are

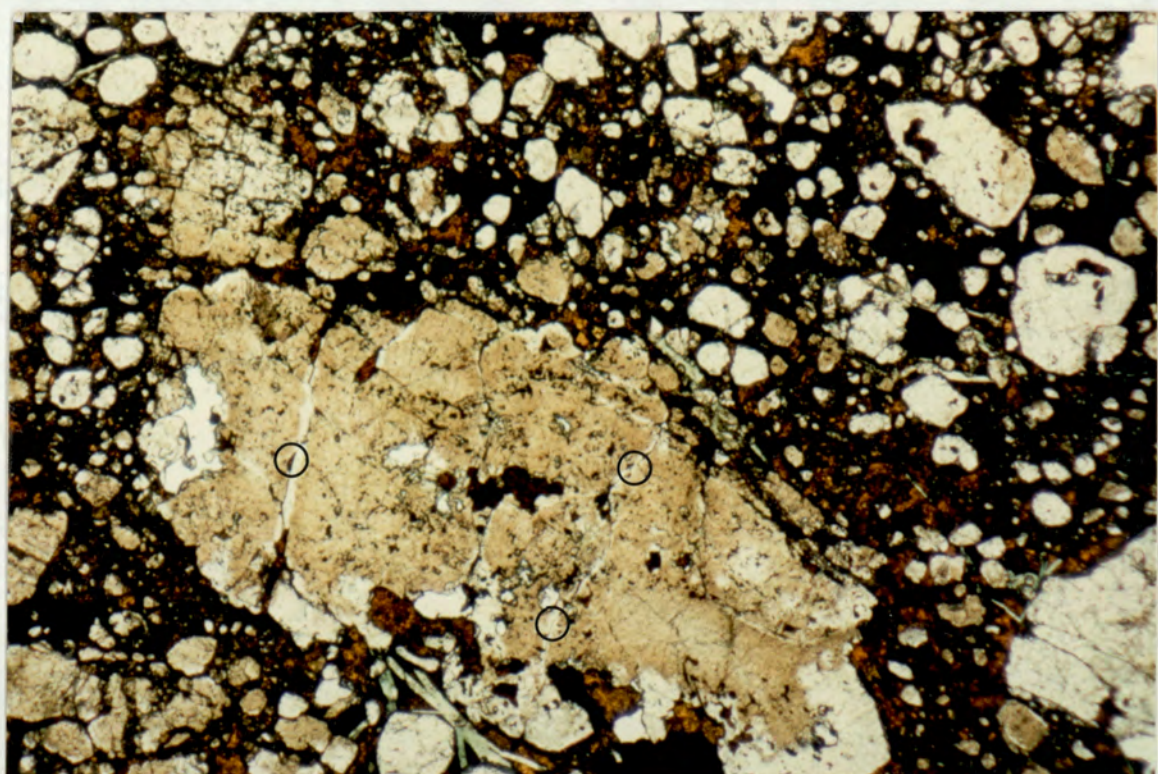


Plate 2.22

Brown (spessartine-rich) and colourless (almandine) in mineralised UIF in a pyrrhotite-sphalerite matrix.

Note the thin almandine reaction zones in spessartine, adjacent to late sulphide veinlets (circled).

Sample no. 1459, field of view 3.4mm, PPL.



Plate 2.23

Photograph of high grade ore from BS-119, showing well-developed durchbewegung texture of sphalerite and pyrrhotite flowing around dislocated fragments of UIF. Note the reaction halo of pyrrhotite (po) adjacent to the continuous bed of iron-formation (colourless). Long axis of photo is 8cm.

surrounded by a 50 μ m-wide reaction zone of colourless garnet (Plate 2.22). High-grade sphalerite layers commonly display classical 'durchbewegung' textures, with sphalerite and pyrrhotite 'flowing' around rotated fragments of grunerite-bearing beds. (Plate 2.23).

Grunerite occurs in a variety of textural associations, most commonly as equant, bladed (up to 2 mm long) crystals associated with garnet and magnetite (Plate 2.24). It also occurs as very fine-grained brown-coloured patches and needle-like crystals intergrown with quartz (Plates 2.25).

In some specimens, garnet occurs in delicate radial intergrowths with fine-grained quartz and biotite, or, less commonly, with grunerite (Plate 2.26).

About one-third of grunerite-bearing specimens have carbonate as part of the assemblage. Two carbonate minerals are present, one is iron-poor (calcite or dolomite), the other iron-rich (siderite or ankerite). Both carbonates occur as patches within, and between, grunerite blades (Plate 2.27) and as late veinlets which crosscut prograde silicates.

Ilmenite forms small laths, up to 40 μ m long which define straight inclusion trails or, less commonly, cusps preserved at the margins of coalesced garnets.

Transitional Iron Formation (TIF)

T.I.F occurs as thin discontinuous layers developed within, and lateral to, rocks of the Chloritoid Zone. It is characterised by complex and variable assemblages within which garnet comprises 5-40% of the rock, and both garnetite layers and grunerite are absent. The matrix surrounding the garnets is generally schistose and chlorite-rich, though variations in garnet abundance impart a layered appearance to the rock. Some garnet porphyroblasts preserve radial

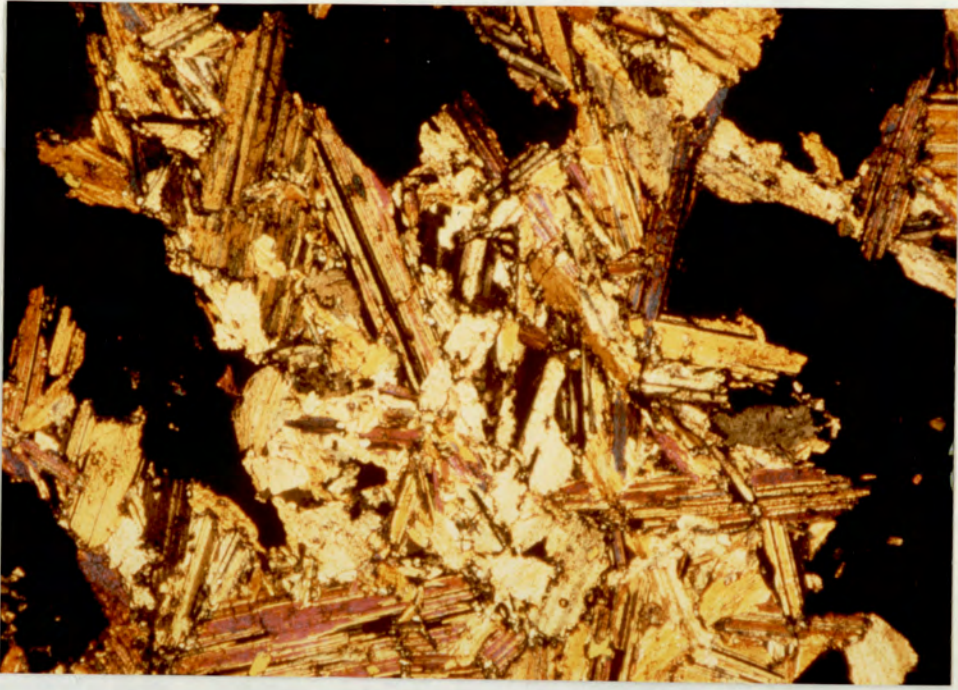


Plate 2.24

Development of typical bladed grunerite associated with magnetite in UIF. Sample No. 263, field of view 3.4mm, XPL.

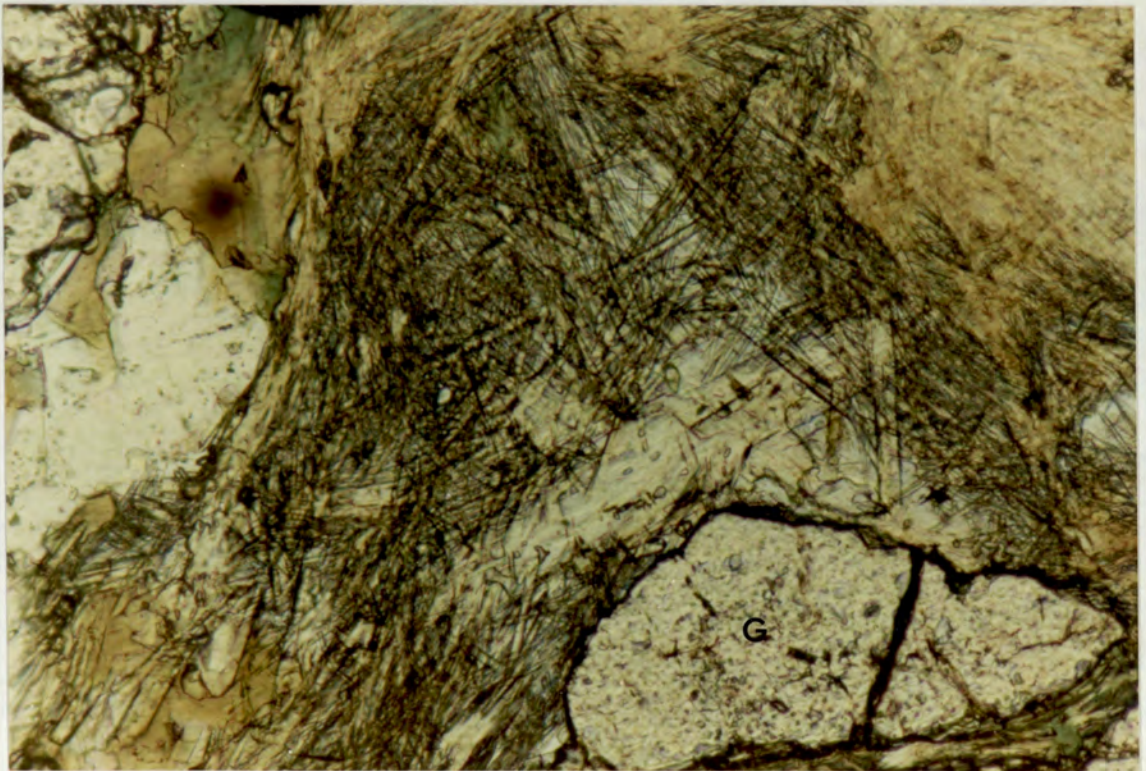


Plate 2.25

Development of acicular (centre) and felted (top right) grunerite, associated with quartz, garnet (G), minor chlorite and bitoite (top left). Sample No. 262, field of view 1mm. PPL.

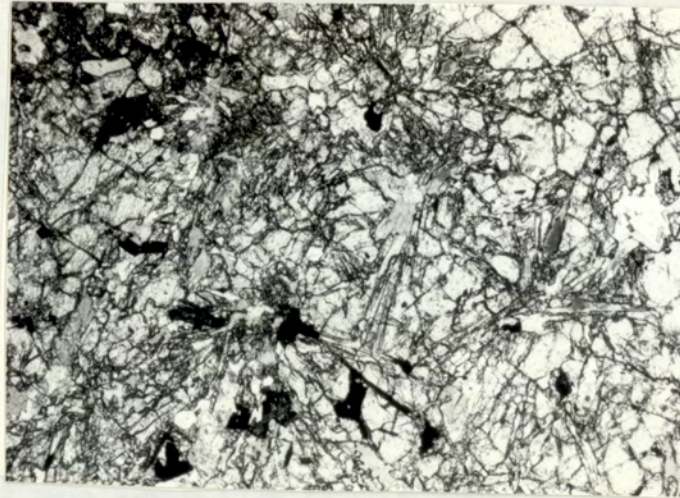


Plate 2.26

Fine-grained radial intergrowth between grunerite and garnet in UIF. Sample No. 627, field of view 3.4 mm, PPL.

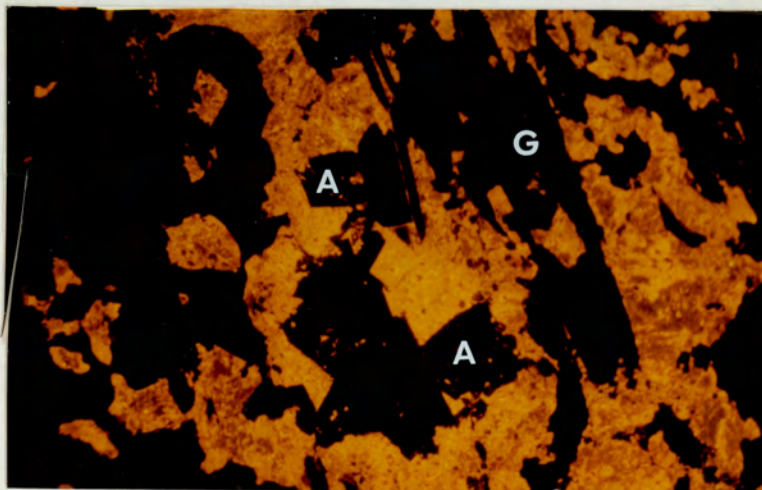


Plate 2.27

Non-luminescent Fe-carbonate rhombs (A) associated with bladed grunerite (G), replaced by orange calcite or dolomite. Sample of high grade ore from BS-119, field of view 2.5mm.

textures similar to those described from the UIF, and in a few samples, hornblende is a major matrix mineral.

Quartz comprises >30% of the rock and in some specimens is associated with up to 10% relict plagioclase feldspar in textures similar to those in feldspathic tuffs (Plate 2.28).

Magnetite is the most abundant opaque phase, and is accompanied by minor quantities of ilmenite, sphalerite and pyrrhotite. Chloritoid forms idioblastic crystals, up to 4mm long, as a matrix to anhedral garnets. Gahnite is the most common accessory mineral and is typically impure with >50% magnetite inclusions. In a few samples, it is closely associated with small, blue-green, euhedral tourmalines. Apatite commonly forms <2% of the rock, though in some millimetre-wide layers it is present in quantities up to 30 %.

Lower Iron Formation (LIF)

LIF forms a continuous layer underlying, and partly lateral to, rocks of the Chloritoid Zone. It is characterised by assemblages containing garnet and/or hornblende along with minor amounts of magnetite, ilmenite, sphalerite, pyrrhotite, quartz and allanite. Biotite and chlorite are commonly developed as retrograde minerals formed from the breakdown of hornblende.

LIF contains a spectrum of rock types, ranging from thin (<1m) hornblendite horizons, through assemblages containing both garnet and hornblende, to garnetite horizons up to 15m thick. The hornblende is characterised by its unusual slate-blue to blue-green pleochroic scheme. It occurs either in radial textures intergrown with garnet, or as idiomorphic crystals aligned within the plane of foliation, within a matrix to large garnet porphyroblasts. Where present in the LIF, sphalerite and pyrrhotite occur intergrown with hornblende (Plate



Plate 2.28

Relict tuffaceous texture in TIF rocks. Sample no. 154, field of view 3.4mm.

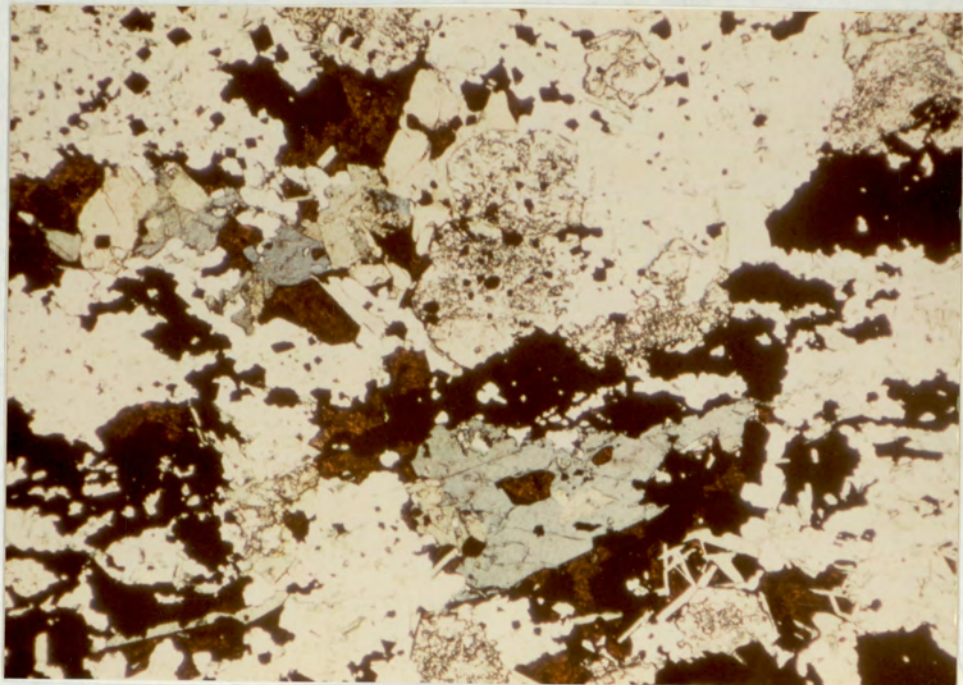


Plate 2.29

Intergrowth of garnet-sphalerite (orange-brown)-pyrrhotite (black) and blue-green ferro-aluminotschermakite in quartz (colourless) in LIF rocks. Sample No. 756, field of view 3.4mm, PPL.

2.29).

In general LIF rocks are grunerite-free, however in two specimens grunerite is present intergrown with (or possibly exsolved from) hornblende.

Magnetite occurs as disseminated (10 μ m to 200 μ m) octahedra, and as pseudomorphs after large (5mm long), bedded, rhombohedral hematites (Plate 2.30). Magnetite pseudomorphs after bladed hematite are also delicately intergrown with, and in places partially replaced by, poikiloblastic garnet (Plate 2.31).

2.2.5 The Hanging Wall Sequence

The following two major lithologies are recognised:

- a) Graphitic schist, and
- b) Crystal-lithic tuffs.

Graphitic schist

The Mineralised Horizon is overlain by thin (<5m), well foliated graphite-bearing schists which are good stratigraphic marker horizons ('graphitic rhyolites' of Granges' logs). In thin section, they are fine-grained, and have a poorly defined layering of lighter and darker patches, caused by varying quantities of fine-grained magnetite, ilmenite laths, pyrrhotite and ubiquitous fine-grained (<10 μ m) graphite. The lighter-coloured areas contain 5% lithic clasts containing plagioclase, muscovite and quartz up to 1cm across (Plate 2.32) and minor, brown, euhedral tourmaline associated with chalcopyrite, pyrrhotite and sphalerite mineralisation. Less commonly, brown tourmaline is present as round, detrital grains in the groundmass (Plate 2.33).

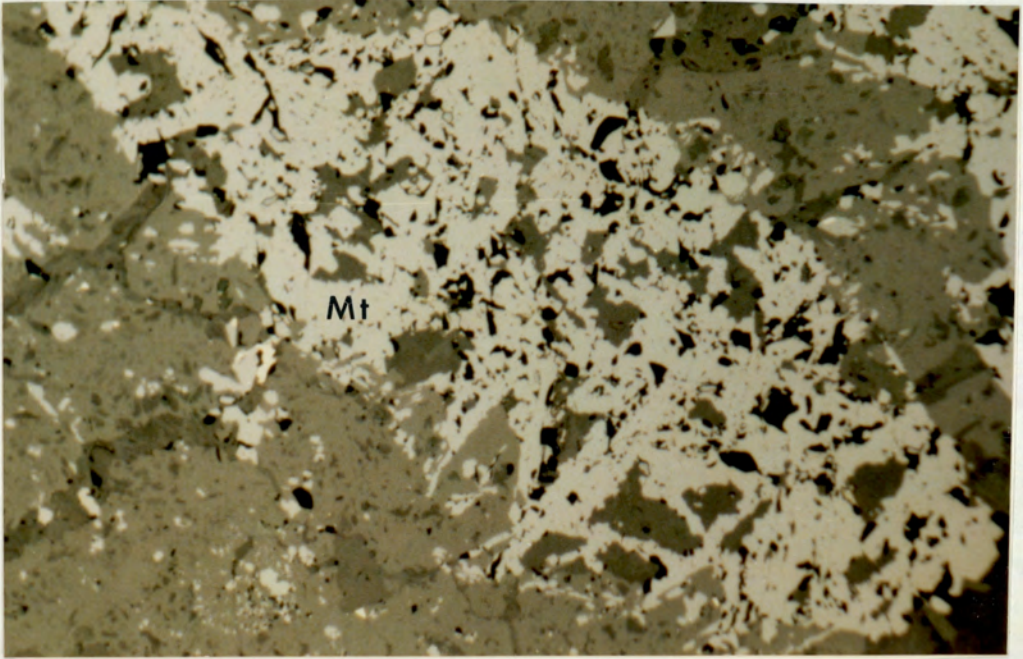


Plate 2.30

Reflected light photograph of primary bladed hematite replaced by magnetite (Mt) in LIF. Sample No. 764, field of view 1.1mm, PPL.

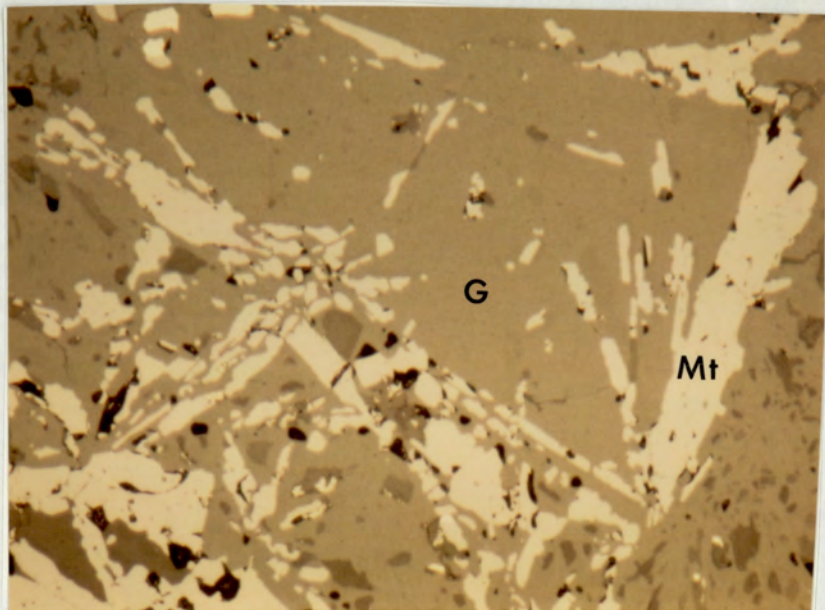


Plate 2.31

Intergrowth between garnet (G) and magnetite (Mt) after bladed hematite (Mt). Sample No. 764, field of view 1.8mm PPL.

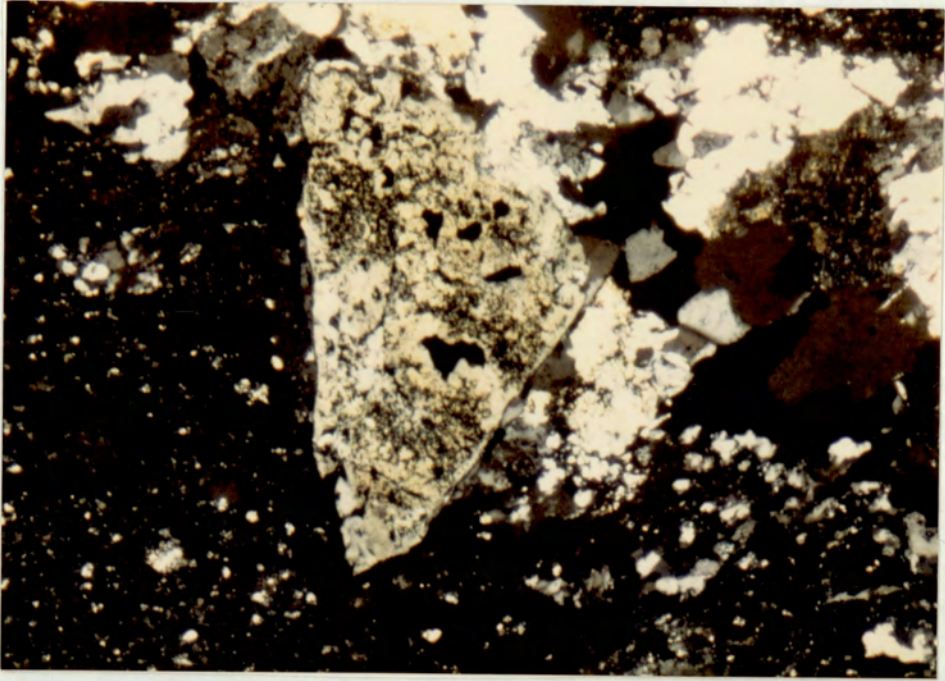


Plate 2.32

Mineralised clast (top third of the photo) of quartz+plagioclase+sulphides containing a large brown tourmaline in fine-grained host Graphitic Schist. Sample No. 858, field of view 0.9mm, PPL.



Plate 2.33

Rounded detrital grain of brown-yellow tourmaline in Graphitic Schist. Sample No. 858, field of view 0.7mm, PPL.

Crystal-lithic tuffs.

Felsic, fine-grained tuffs of the Hanging Wall contain well-preserved sedimentary structures (graded bedding, syn-sedimentary faults and scour structures) on a hand specimen scale (Plate 2.34). Mafic rock types comprise <10% of the hanging wall sequence. Tuffaceous textures in felsic rocks have abundant, poorly sorted euhedral and broken plagioclase and quartz phenocrysts (Plate 2.35) and lapilli-sized sub-angular lithic fragments (Plate 2.36) set in a poorly bedded matrix of biotite, muscovite, fine-grained quartz and carbonate.

2.3 DEPOSIT STRUCTURE

The purpose of this section is to show how the previously described lithologies are related within, and between, various sections of the deposit. Seven drill holes detailing the geology of the Mineralised Horizon have been re-interpreted in the light of the petrological observations, and are shown in an isometric fence diagram (Figure 2.5).

The petrologically distinct horizons and zones described above are correlated between drill holes. (Figures 2.2, 2.3 2.4 and 2.5). There is some evidence for the repetition of Graphitic Schist in DDH BS-122, and of Lapilli Tuffs in DDH BS-119 (Figures 2.2 and 2.5.) In addition, notwithstanding differences in mineralogy, iron formation, and high-grade zinc mineralisation occur both above and beneath the Copper body (Figures 2.2, 2.3, 2.4 and 2.5), which could be interpreted to indicate the presence of a large fold structure rather than a simple stratigraphic sequence.

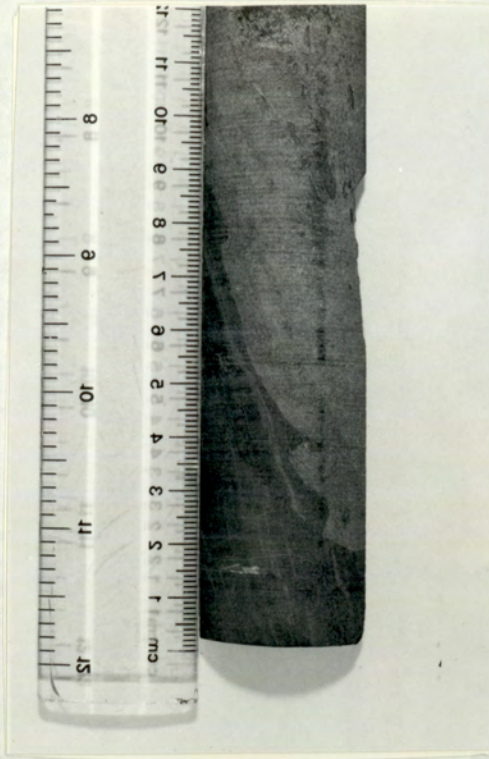


Plate 2.34

Syn-depositional scour structures in fine-grained Hanging Wall tuffs from BS-119.



Plate 2.35

Large, embayed, quartz phenocryst in poorly bedded Hanging Wall crystal-lithic tuffs. Sample No. 1025, field of view 3.4mm, XPL.

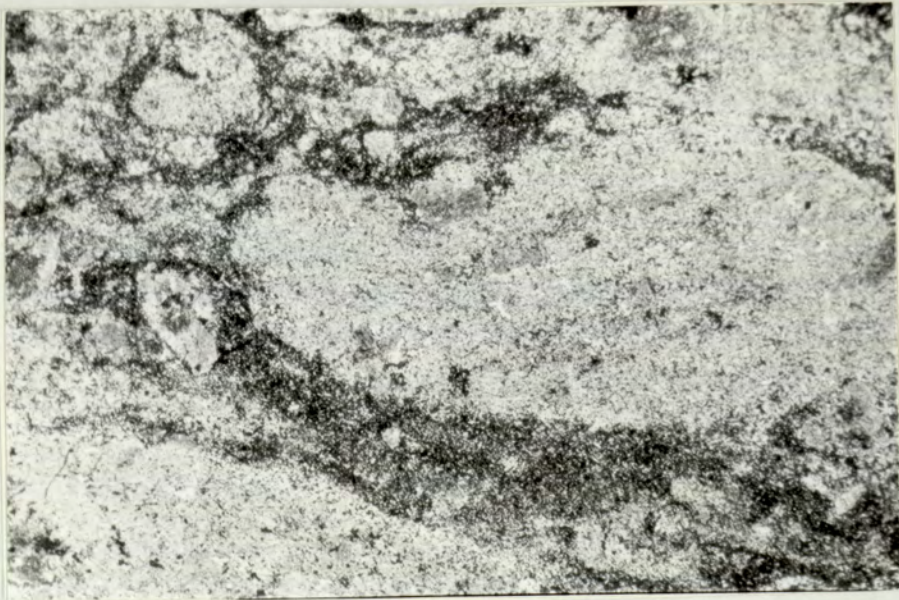


Plate 2.36

Lithic clast in Hanging Wall crystal lithic tuffs. Sample No. 1038, field of view 8.3mm. PPL.

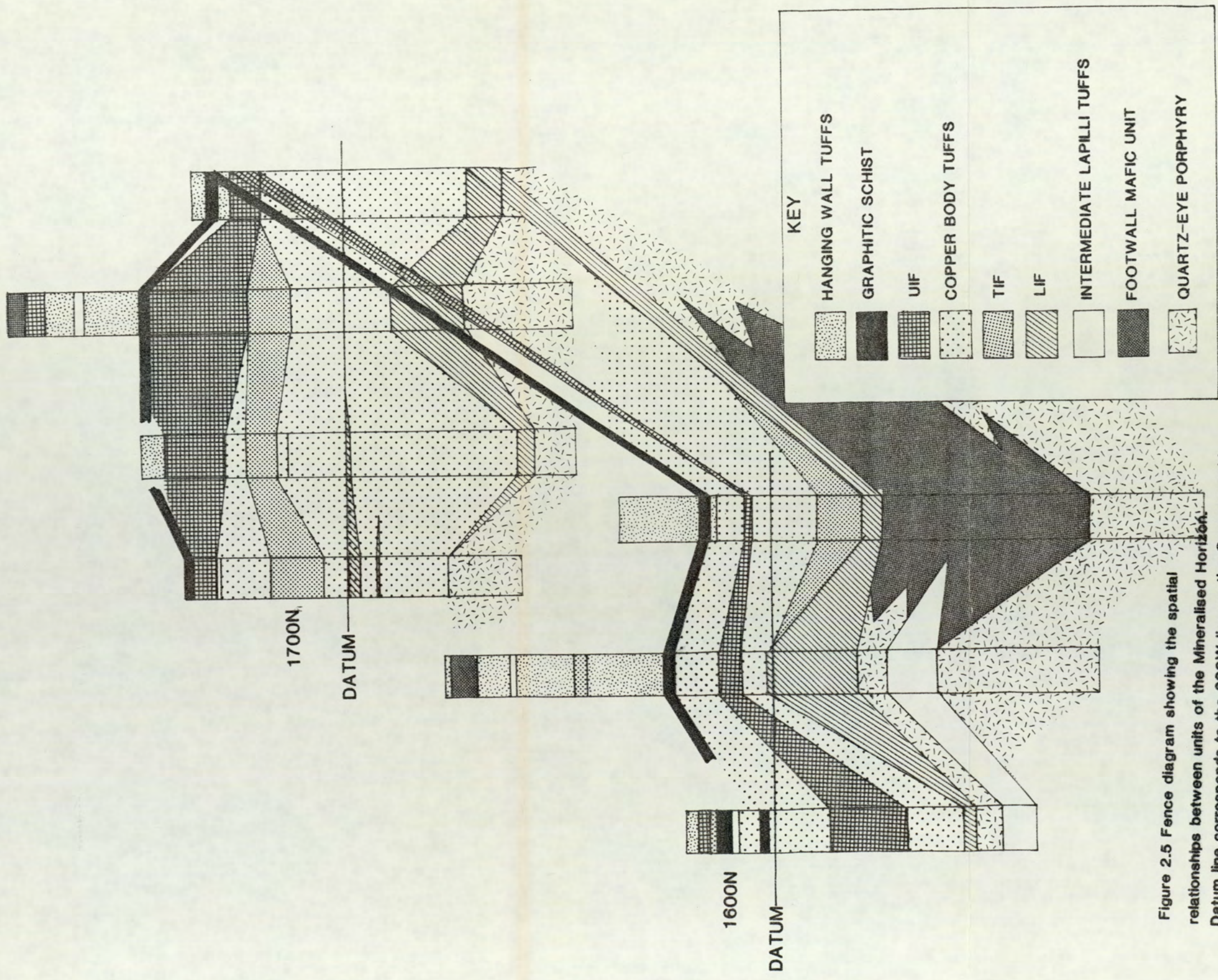


Figure 2.5 Fence diagram showing the spatial relationships between units of the Mineralised Horizon. Datum line corresponds to the 600W line on the Granges grid. The diagram has been rotated parallel to the paleo-horizontal

Three general models could account for the observed sequence, these are:

1) The entire sequence represents a large isoclinal fold, the core of which comprises the Copper Body. Prior to deformation, the stratigraphy therefore would have been:

TOP Tuffaceous rocks containing lateral facies variations.

Discontinuous graphite-bearing rocks

Laterally zoned iron-formation

Continuous high grade zinc mineralisation

BASE Mineralised rocks comprising the Copper Body

These features can be explained by considering lateral facies variations in tuffaceous rocks, from coarse-grained, proximal, to fine-grained, distal types, corresponding to the present Footwall Quartz Feldspar Porphyry (QFP) and tuffs in the Hanging Wall, respectively. Iron-formation contained facies variations which, upon metamorphism, were converted to hornblende-bearing and grunerite-bearing types. The non-occurrence of graphitic rocks in the Footwall could be explained either by their non-deposition over what is now hornblende-bearing iron-formation, or differential erosion shortly following deposition. An alternative explanation is that the graphitic rocks were sheared out along one limb of the fold during deformation.

2). Rocks of the Mineralised Horizon may represent an intrafolial fold developed adjacent to relatively competent rocks of the Footwall and Hanging Wall sequences. In this model, both Footwall and Hanging Wall rocks are the right way up, and thus mineralisation is underlain



by coarse-grained pyroclastic rocks of the QFP, and overlain by fine-grained tuffaceous rocks. The Copper Body (and overlying high-grade zinc and iron-formation), which was originally developed within the QFP, has been detached and rotated during deformation (cf. Sangster and Scott, 1976). Like model 1 (above) this also requires that the iron formation represents two different facies (which are now two mineralogical types), and that graphite-bearing rocks were either preferentially developed above rocks that are now grunerite-bearing iron-formation or they were sheared out adjacent to hornblende-bearing iron-formation in the Footwall.

3) The sequence is fining upwards, with no major fold structures and is a simple stratigraphic sequence. This model requires that copper-bearing rocks of the Mineralised Horizon comprise a separate unit of tuffs overlying altered and partially mineralised rocks of the Footwall sequence. It also requires the development of two separate units of iron formation and two separate layers of high-grade zinc mineralisation. Graphite bearing rocks would comprise a continuous layer overlying mineralised rocks deposited prior to fine-grained bedded tuffs of the Hanging Wall (Figure 2.1). The local repetition of graphite-bearing rocks in the Hanging Wall (Figures 2.2 and 2.5) would be by repeated deposition of graphitic rocks in quiescent conditions following explosive pyroclastic activity and mineralisation.

The use of models 1 and 2 to account for the repetition of units must account for:-

a) the apparent absence of coarse-grained pyroclastics in the Hanging Wall, and the absence of fine-grained tuffs in the Footwall (Figure 2.2).

b) the presence of extensive silicification, and minor stringer sulphide and tourmaline veins in Footwall rocks, which has overprinted many primary igneous features, in contrast to the well preserved igneous textures, and lack of alteration in rocks of the Hanging Wall.

c) the mineralogical differences between Upper and Lower Iron Formation.

d) the non-occurrence of Graphitic Schist in the Footwall.

From the three models presented above, the first is considered unlikely because it requires altered and partially veined, chalcopyrite-bearing rocks of the QFP to overlie rocks of the Mineralised Horizon. The metallogenic zonation of the deposit in this model would have an enrichment of copper upwards in the sequence. This zonation is the reverse of that described from all other described volcanogenic mineral deposits (Franklin and Thorpe, 1982), and that predicted from experimental studies of sulphide mineral stabilities (Franklin et.al, 1981).

It is recognised that, using only drill core and without underground exposures, it is difficult to rule out the other two models, and that models 2 and 3 are not mutually exclusive. It is possible to test the viability of models 2 and 3 by investigating the geochemistry of tuffaceous rocks from the Mineralised Horizon. If the Copper Body represents a detached part of the underlying unit (model 2) then its major and trace element characteristics (excluding the effects of alteration associated with mineralisation) should be

identical to those of the present Footwall rocks. If there are differences in chemistry between rocks of the Copper Body, and the underlying tuffs, then the tuffs of the former are thought more likely to represent a distinctive stratigraphic unit, lending support to the simple stratigraphic model. This geochemical test is discussed in Chapter 3.

2.4 INTERPRETATIONS AND SUMMARY

Footwall Tuffs and the Footwall Mafic Unit

The Footwall sequence is dominated by crystal-rich felsic rocks with subordinate mafic flow material (the Footwall Mafic Unit). The following points are interpreted to suggest that the felsic rocks represent the metamorphosed and altered equivalents of crystal, and crystal-lithic tuffs of dacitic to rhyolitic composition which may have originated as pyroclastic ash flow deposits:

1) Broken plagioclase feldspar crystals are present in all felsic Footwall units.

2) Volcanic fragments occur as a major component of the intermediate lapilli tuffs, and as a minor component of the underlying units. Lensoid mafic segregations in the intermediate lapilli tuffs are interpreted as having close similarities with fiammé structures described in association with other volcanogenic deposits (Deptuck, *et.al*, 1982).

All rocks of the Footwall sequence have been both altered and metamorphosed. Alteration in the Footwall rocks increases in intensity upwards in the sequence, and culminates in the mineralisation of the Copper Body. The products of alteration are now seen as cross-cutting veinlets and replacements comprising

metamorphic minerals, (biotite, white mica, chloritoid, and pyrrhotite) derived from lower grade assemblages. Alteration is thus considered to have preceded regional metamorphism of the deposit sequence. Alteration within the Mineralised Horizon is more pervasive and intense than in the underlying rocks, and coincides with a decrease in the ratio $Cu/Cu+Zn$ (Figure 2.4). Silicified rocks are copper-rich, whereas Chloritoid Zone rocks contain copper along with minor zinc.

MacGeehan and MacLean (1980) described mineralogical (and chemical) effects of syn-volcanic spilitisation, on tholeiitic basalts from beneath massive sulphide deposits from the Matagami region of Quebec, where the alteration products resemble dacites and rhyolites with apparent calc-alkaline affinities. However, in those rocks, relict basaltic textures are preserved, along with abundant actinolite, chlorite and sphene plus rutile, derived from the breakdown of mafic minerals. At Bigstone, no primary basaltic textures, or textures similar to those now present within the Footwall Mafic Unit, have been recognised in the Footwall felsic units, and mafic minerals (other than biotite and minor epidote) are absent. Furthermore, textures in the Footwall rocks are similar to those described from a number of metamorphosed and mineralised felsic volcanic and volcanoclastic sequences (Vernon, 1986). It is thus considered unlikely that any of the Footwall felsic rocks at Bigstone were derived from basaltic precursors.

The Mineralised Horizon Tuffs.

The following points are interpreted to indicate that sulphide-bearing rocks of the Mineralised Horizon represent the heavily mineralised

equivalents of altered and weakly mineralised rocks of the Footwall sequence:

a) The mineralisation, although largely stratabound, is replacive on both a macro-, and micro-scale. The original rock contained a high proportion of plagioclase feldspar.

b) In a few specimens, relict textures are found similar to those of the Footwall tuffs (Plate 2.18).

c) Primary ilmenite is a consistent feature of both Mineralised Horizon and Footwall rocks (Plates 2.10 and 2.16).

The restricted occurrence of gahnite, as part of an inferred equilibrium assemblage with aluminium-rich silicates, suggests that zinc-, and aluminium-rich lithologies were locally developed within altered tuffs prior to metamorphism. In addition, the presence of inclusions of ilmenite, chalcopyrite and pyrrhotite within gahnite (Plate 2.16), trapped during prograde growth, indicates that copper was also present in the rocks. It is thus suggested that most of the presently observed zinc and copper (and presumably iron) was in situ prior to metamorphism. The laterally persistent, gahnite-bearing, layers of high-grade sphalerite mineralisation, which occur both at the margins and up-dip of the Copper Body, are similarly interpreted as being primary features of the deposit. It is considered highly unlikely that the presently observed zonation of base metals could have been produced as a result of the metamorphic diffusion of zinc (but not copper) to the margins of the Copper Body. The metallogenic and mineralogical zonations within the Mineralised Horizon are consistent with similar zonations described from a large number of volcanogenic massive sulphide deposits (Franklin and Thorpe, 1982;

Sangster and Scott, 1976). An unusual feature at Bigstone however, is that zonation occurs laterally along lithological layering (Figure 2.4). Mineralisation is confined within a particular stratigraphic horizon of felsic volcanoclastic rocks and does not have the form of the layered pyritic or pyrrhotitic massive sulphides of 'typical' deposits. It is worth noting that, apart from minor discontinuous zones in the Chloritoid Zone, total sulphide (by volume) is >50% only in the 0.5 to 1m-wide layers of high-grade zinc mineralisation. The deposit is thus not strictly a massive sulphide body and might therefore be expected to show other differences to the 'type' massive sulphide deposits.

Iron-Formation

UIF and LIF have mineral assemblages which are diagnostic of metamorphosed Algoma-type, or Al-rich, Superior-type, iron formations from many parts of the world (Klein, 1982; Floran and Papike, 1978; Haase, 1982a; Stanton, 1976; Vaughan and Stanton, 1986; Nilsen, 1978). Many studies have detailed the textural and mineralogical effects of metamorphism on iron formations (eg., Klein, 1982; Floran and Papike, 1978). In addition, primary textural (and chemical) features have been recognised in a number of garnet-rich iron formations associated with massive sulphide deposits (Stanton and Williams, 1978; Laajoki and Saikkonen, 1977) some of which have been metamorphosed up to upper amphibolite grades of metamorphism (Stanton, 1976). Upper and Lower Iron Formation at Bigstone probably formed in a similar way to these 'type' deposits, ie. as chemical precipitates on the sea (or lake) floor. When viewed in conjunction with the preservation of volcanoclastic textures in Footwall and Hanging Wall rocks, along with growth faults and scour structures in Hanging Wall tuffs, it is not unreasonable to expect that

some primary textures should also have been preserved within the chemical sediments at Bigstone. The following features are similar to those of the 'type' iron formations, and are hence interpreted as being primary (ie. early metamorphic, or possibly late diagenetic) in origin:

1) The millimetre-scale alternation of garnet-rich and garnet-poor beds in UIF is thought to be related to variations in bulk rock composition (mainly Al) in the precursor lithology. The overall high abundance of garnet within the iron-formation, and the common occurrence of garnetite layers in LIF suggests that, to a first approximation, the chemistry of the precursor rocks must have been close to that of garnet.

2) The contrast between grunerite-bearing UIF and hornblende-bearing LIF is tentatively interpreted to indicate that the two units may have formed from different precursor lithologies.

3) Magnetite pseudomorphs after hematite (Plates 2.30 and 2.31) are strikingly similar to those described by Frater (1985) from the Golden Grove deposit in Australia where they are interpreted to indicate that hematite was developed as part of an early-formed assemblage.

4) Delicate intergrowths between garnet and magnetite after hematite (Plate 2.31) show that only limited interaction occurred between early iron oxides and the enclosing silicate minerals during metamorphism.

5) Many of the intergrowths between garnet and grunerite, and fine-grained grunerite and quartz (Plates 2.25 and 2.26), are

texturally similar to those described between minnesotaite and quartz in low-grade (lower greenschist facies and below) iron-formation of the Gunflint range (Floran and Papike 1978; Klein, 1982).

Radial intergrowths between garnet and amphibole (Plate 2.26) are interpreted to indicate co-crystallisation during metamorphism, rather than the pseudomorphing of pre-existing phyllosilicate structures, as suggested for similar textures in the Pegmont Pb-Zn deposit in Australia (Vaughan and Stanton, 1986). Radially textured garnets occur in regionally metamorphosed graphite-bearing pelites in Norway (Burton, 1986). There, the presence of graphite is considered to have reduced silica solubility during metamorphism, causing both quartz and graphite to be included within garnets in a texture analogous to that of inclusions within chiastolite. It is interesting to note that, the radially textured garnets from Pegmont (Vaughan and Stanton 1986) contain quartz, iron oxide and graphite inclusions, and are almost identical to those described by Burton (1986). The absence of analogous textures at Bigstone is taken to indicate that graphite was never developed within the iron-formation. This assumption is supported by the suggestion that hematite was a primary iron-formation component.

T.I.F is interpreted as a hybrid rock containing variable proportions of the following components:

- 1) Quartz and relict igneous plagioclase; representing a tuffaceous component.
- 2) Chloritoid, gahnite and tourmaline; representing an alteration and mineralisation component.
- 3) Garnet and hornblende; representing an iron-formation component.

T.I.F. grades up-dip into LIF or UIF, and is considered to mark the transition from a clastic-dominated to a chemical-dominated system.

Although both UIF and LIF contain high-grade sphalerite mineralisation, much of the mineralisation is replacive, and clearly post-dates the formation of the garnet, grunerite and hornblende. A few specimens contain intergrowths of sphalerite with prograde silicates (Plate 2.30), which indicates that sphalerite was originally present as a component of iron-formation. The general absence of sphalerite, and gahnite in most of the iron-formations is, however, taken to indicate that base metals were not originally present in major quantities. Copper-bearing minerals are absent from all samples of UIF and LIF, and are uncommon within the T.I.F. This observation is consistent with the general metallogenic zonation of Cu/Cu+Zn described for the Copper Body (Figure 2.4).

2.5 CONCLUSIONS

The following general features are associated with mineralisation at Bigstone:.

- 1) Replacive, epigenetic, copper-rich mineralisation of the Copper Body occurs within altered felsic tuffs.
- 2) Stratiform, high-grade, zinc-rich mineralisation is at the margins of the Copper Body.
- 3) Garnet-, and hornblende-bearing LIF underlie the Copper Body.
- 4) Garnet-, and grunerite-bearing UIF overlie the Copper Body.
- 5) The Footwall sequence is dominated by felsic pyroclastic rocks and contains minor mafic flows of the Footwall Mafic Unit.

The sharp juxtaposition of copper-rich and zinc-rich mineralisation, and the intimate association between the mineralisation and chemical sediments (iron-formation), points to an over-riding influence of primary, pre-metamorphic controls on the deposit stratigraphy. The development of distinctive mineralogies in LIF, UIF, and Copper Body rocks, may thus be related to variations in the compositions of precursor lithologies.

CHAPTER 3:

WHOLE ROCK GEOCHEMISTRY

3.1 INTRODUCTION

The purpose of this chapter is to investigate the chemical compositions of a representative suite of rocks from the deposit sequence and the North Limestone Area (NLA) in order to:

1) Determine the chemical compositions of the major lithological units around the mineral deposit.

2) Determine the environment of formation of volcanic rocks associated with the mineralisation.

3) Compare and contrast the chemistry of the rocks of the mineral deposit with those of the adjacent NLA, and other parts of the greenstone belt.

4) Compare and contrast the chemistries between rocks of the Footwall and Mineralised Horizon (MH) and assess the relative importance of alteration and primary igneous processes.

3.2 SAMPLE DETAILS AND ANALYTICAL TECHNIQUES

225 samples (85 are surface samples from the NLA, and 140 are samples of drill core from the deposit sequence), were analysed by X-ray fluorescence (XRF) for a range of trace elements (see Appendix 2.1 for details of sample sources, preparation techniques and estimates of precision and accuracy). A selected group of unmineralised rocks (n=42) were analysed for major elements using standard fused disc techniques. Because of difficulties encountered in producing fused discs for sulphide-bearing rocks using standard techniques, major element XRF analyses on the remaining, generally mineralised, rocks were done semi-quantitatively using pressed powder pellets (see Appendix 2.1 for details). Particular attention was paid to the determination of TiO_2 , and

SiO₂, because of their potential use as geochemical discriminants. Analyses for both oxides using this method have relative accuracies (compared to fused disc values) of better than 5% of the 'true' amount (Appendix 2.1). These errors do not affect the positions and patterns of plotted points on discriminant diagrams, and therefore do not impede interpretation of the data.

In this, and subsequent chapters, use is made of correlation coefficients between two or more chemical variables. The quoted correlations are statistically significant at the >99.99% level unless stated otherwise.

3.3 SAMPLE CLASSIFICATION

Samples of the major rock types from the deposit sequence and the adjacent North Limestone Area (NLA) were subdivided into five groups (basalt to rhyolite) based on their SiO₂ contents. The relative abundances of these rock types within the major stratigraphic groups (Table 3.1) shows that, both the Footwall Quartz-Feldspar Porphyry (QFP) and tuffs of the Mineralised Horizon are dominantly dacitic to rhyolitic in composition whereas the Footwall Mafic Unit (FMU) is dominantly basaltic. It is noted that there is only one analysis available for felsic tuffs from the Hanging Wall.

	BASALT	BASALTIC ANDESITE	ANDESITE	DACITE	RHYOLITE
FMU	34	6	4	2	-
FOOTWALL QFP	3	1	6	9	27
HW	4	1	-	1	-
MINERALISED HORIZON	5	-	1	4	25

Table 3.1 Total number of rock types from the main units of the deposit sequence.

Average contents of selected elements from major lithological units (Table 3.2, complete data tables in Appendix 2.2) show that NLA basalts are less evolved (ie. they contain lower average SiO_2 , Nb and Zr, and higher Cr, Ni, V, Cu) than basalts from the Footwall Mafic Unit (FMU). When data for both basalts and basaltic andesites are combined however, averages of trace and major elements are similar in both areas, with the exceptions of both Cu and Ni, which are depleted in the FMU relative to NLA rocks. Y and Zr are depleted, and V, Cu and Zn are enriched, in MH relative to QFP rhyolites (Table 3.2). Immobile element contents of felsic rocks from both the MH and QFP are consistent with those of similar rock types from tholeiitic arc sequences (Ewart, 1979; Bokhari and Kramers, 1981).

Multiple regressions of Ti, Zr, Nb and Y in NLA and FMU mafic rocks, QFP and MH felsic rocks (Appendix 2.3) show that all four elements are well correlated in mafic rocks, and can thus be considered to have remained relatively immobile during alteration and metamorphism (Pearce, 1982). In the QFP Ti, Zr and Nb are generally well correlated and have thus probably remained immobile, whereas low correlations involving Y indicate its mobility during alteration and/or metamorphism. In MH felsic rocks, Ti and Zr are well correlated ($r = 0.91$), whereas Nb and Y are not, and have probably been mobile. The elements Nb and Y thus show increasing degrees of mobility (lower correlation coefficients) going from mafic to felsic rocks, and from Footwall to Mineralised Horizon evolved rocks.

It is assumed here that, if other trace or major elements show consistently high degrees of correlation with both Ti and Zr, they may also be considered to have remained relatively immobile during metamorphism and alteration.

	NORTH LIMESTONE AREA					F.M.U					Q.F.P. AND M.H				
	1	2	3	4	5	6	7	8	9	10	11	12	13	14	
SiO ₂	40.33	54.5	58.0	65.7	70.4	49.2	54.2	58.4	62.3	47.6	65.04	66.5	76.3	71.9	
TiO ₂	0.68	0.94	0.73	0.48	0.3	0.76	0.82	0.75	0.72	0.84	0.33	0.37	0.34	0.29	
Rb	8	27	29.9	30.6	37.7	22.4	24.0	21.3	20	12.8		31.0		25.9	
Sr	327	452	529	388	280	369	345	501	478	195		212	115	119	
Y	10	23	22	25	32	14	15	19	19	16	14	33	14	30	
Zr	30	90	73	99	114	45	52	78	72	49	56	112	57	96	
Nb	3	7	7	8	9	5	6	7	5	6		8	6	7	
Zn	103	109	105	99	87	92	81	72	54	2231	>10 ⁴	63	>10 ⁴	56	
Cu	98	138	132	49	35	28	67	14	145	161	2453	41	2498	283	
Cu*	67	134	126	45	13	6	59	8		48	1106	3	199	8	
Ni	104	25	8	8	3	38	27	11	9	52	9	2	4	3	
Cr	309	46	11	21	6	136	97	12	6	138	20	10	13	8	
V	408	222	119	49	18	343	291	193	223	294	84	12	83	8	
n	29	14	24	16	7	34	6	4	2	5	4	9	25	27	

TABLE 3.2 Average values of selected elements from a number of rocktypes. Numbers at the top of each column correspond to the following rocktypes: 1=NLA basalt, 2=NLA Basaltic andesite 3=NLA Andesite, 4=NLA Dacite, 5=NLA rhyolite, 6=FMU Basalt, 7=FMU Basaltic Andesite 8=FMU Andesite, 9=FMU Dacite, 10=MH Basalt, 11=MH Dacite, 12=QFP Dacite, 13=MH Rhyolite, 14=QFP Rhyolite. Rocktypes are based on subdivision according to silica content (see Appendix 4.1). Where standard deviations are large median data are reported (denoted by asterisk).

3.4 GEOCHEMICAL PLOTS

3.4.1. Mafic rocks

Analyses of mafic rocks (basalts to basaltic andesites) from the Footwall Mafic Unit, Mineralised Horizon and Hanging Wall plotted on a TiO_2 -Zr diagram (Figure 3.1) have all but three points above the line separating basic from more evolved rocks in the overlapping MORB-ARC field. This is taken to indicate that silica-depleted evolved rocks (for example, chloritised felsic volcanics) have not been included in the plots. Alumina contents (fused disc samples) of mafic rocks average ($15.31\% \pm 0.97$); thus feldspar crystal accumulation was probably not an important process in their formation.

Values for selected elements (normalised to average MORB) for the average mafic rock from the deposit sequence (Figure 3.2) show enrichments, relative to MORB, in the large-ion lithophile elements (Sr to Ba). These elements are thought to be relatively mobile during alteration and metamorphism (Pearce, 1982), and so their abundances must be judged carefully. The relatively immobile high field strength (HFS) elements, Nb to Y show weak enrichments in Nb and P, and depletions in Zr, Ti and Y, and thus have signatures similar to those for recent primitive island arc sequences (Pearce 1982). Rock types from the NLA (this study), the average Hanson Lake basalt (Parslow and Gaskarth, 1986), and the average low-Ti basalt from the east Amisk area, near Flin Flon (Parslow and Gaskarth, 1986) show similar patterns (Figure 3.2), and hence probably formed in similar environments.

The majority of Bigstone and NLA samples lie in the overlapping MORB and ARC fields on a Ti-Zr-Y diagram (Figure 3.3), with some scatter into the fields of high-K tholeiites and within-plate basalts. A Y-Cr plot (Figure 3.4), shows that the Bigstone and NLA rocks fall within, or below, the field of island arc tholeiites (IAT), and that the samples

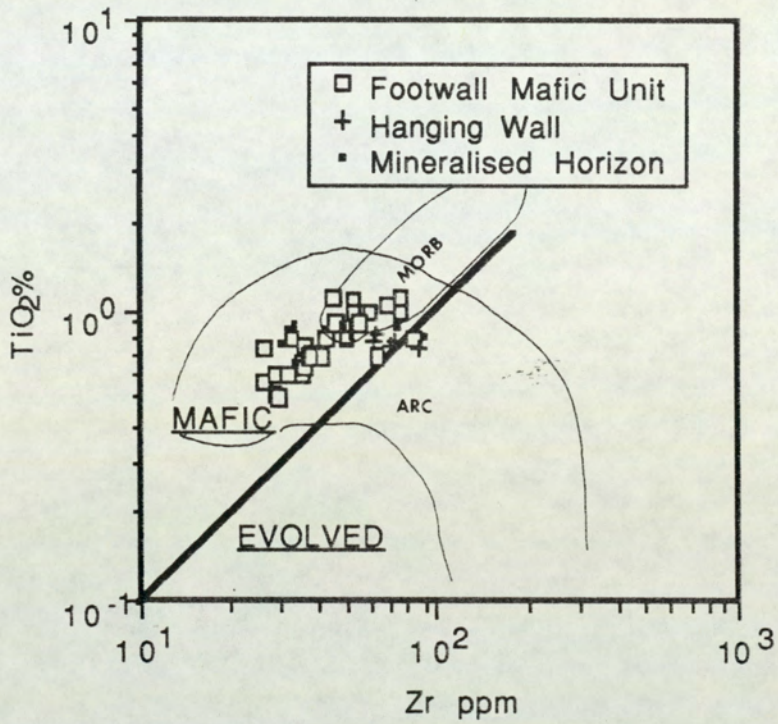


Figure 3.1 TiO_2 vs Zr for mafic rocks from the Bigstone deposit sequence. Line separating evolved from basic rocks, and field boundaries are from Pearce (1982).

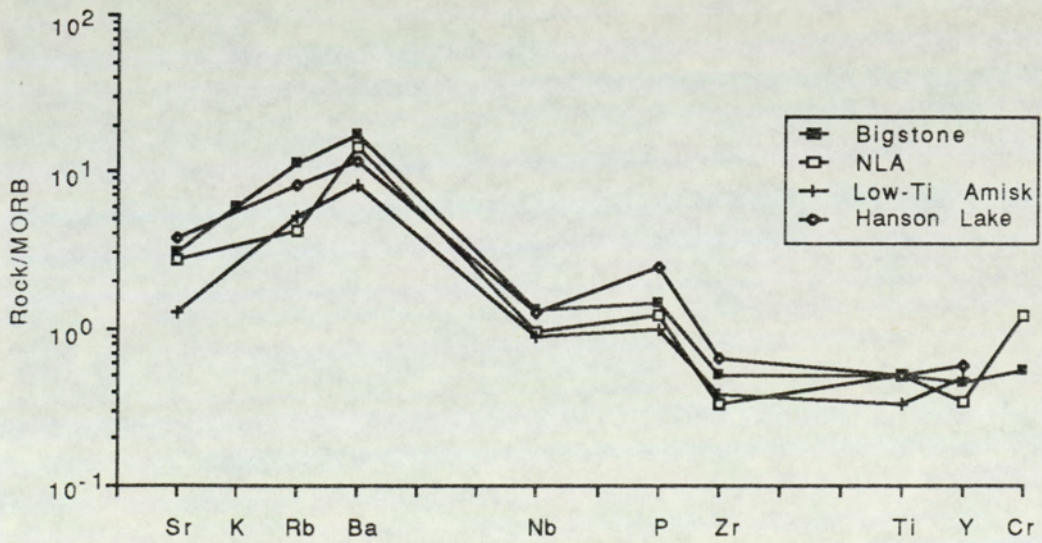


Figure 3.2 Abridged MORB normalised plots for Bigstone, NLA, Amisk and Hanson Lake areas (see text for data sources). Normalising values for MORB taken from Pearce (1983).

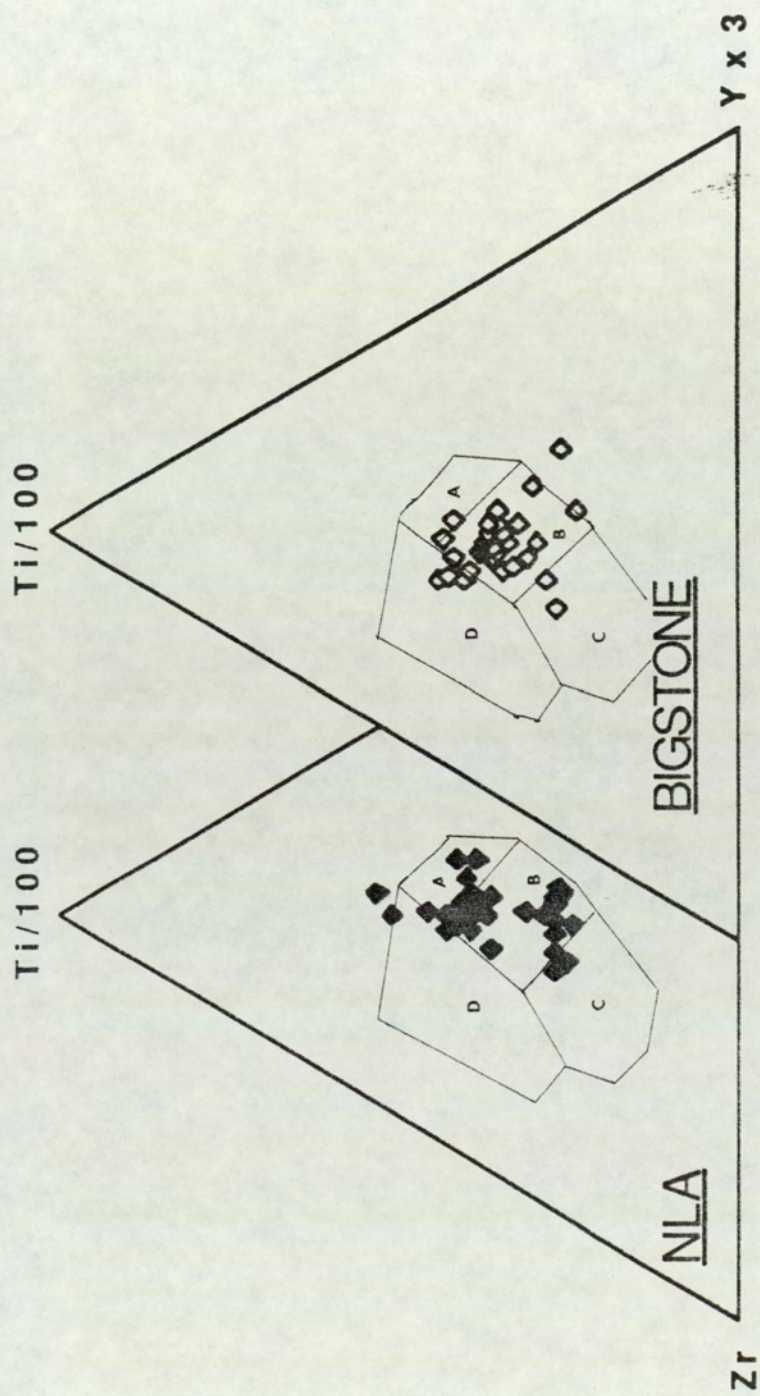


Figure 3.3 Ternary Ti-100 - Zr - Y x 3 diagrams for the NLA and Bigstone areas. Classification fields are taken from Pearce and Cann (1973).

A = High K tholeiites

B = MORB tholeiites

C = Low K tholeiites

D = Alkalic (within plate) basalts

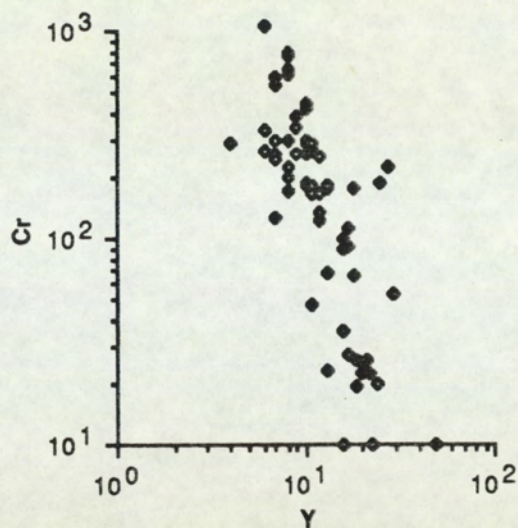


Figure 3.4 Y vs Cr for basic rocks from the Bigstone deposit sequence (open symbol) and the NLA (filled symbol). Fields are taken from Pearce (1982) and correspond as follows: IAT=Island Arc Tholeiites CAB=Continental Arc Basalts, MORB=Mid Ocean Ridge Basalt WPB= Within Plate Basalts, VAB= Volcanic Arc Basalts

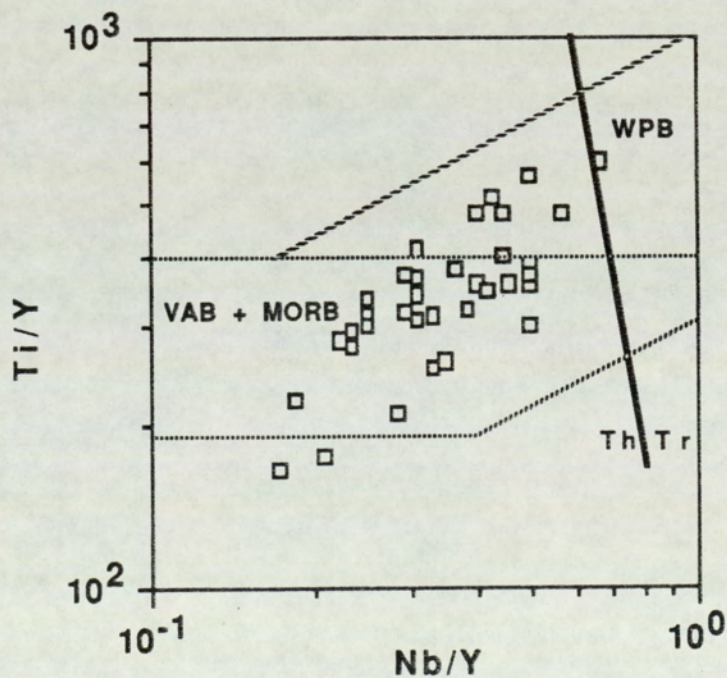


Figure 3.5 Nb/Y vs Ti/Y (values in ppm) plot for basaltic rocks from the Bigstone sequence. Compositional fields from Pearce (1982) are Th = tholeiitic, Tr = transitional, MORB = mid ocean ridge basalt, VAB = volcanic arc basalt, WPB = within plate basalt.

define a primitive, chrome-spinel or olivine and/or clinopyroxene dominated, fractionation trend parallel to the Cr axis, (cf. Pearce and Norry, 1979). A plot of Nb/Y-Ti/Y (Figure 3.5) for the FMU confirms the tholeiitic character of the mafic rocks, with most samples falling within the overlapping MORB and volcanic arc basalt (VAB) fields, and a minority extending into the field of within plate basalts (WPB). An AFM plot (Figure 3.6) also shows a strong tholeiitic trend, and is interpreted to indicate that the components of the diagram (FeO, MgO and total alkalis) have remained relatively immobile during alteration and/or metamorphism.

These data are consistent with an origin for the Bigstone and NLA mafic rocks as island arc tholeiites.

3.4.2 Evolved rocks.

A TiO_2 -Zr plot (Figure 3.7) for all Bigstone rock types, has the following major features:

- 1) Samples with SiO_2 contents $>56\%$ all lie within the evolved field in terms of their TiO_2 and Zr contents. This is considered to indicate that SiO_2 is effective as a discriminant between evolved and basic rock types. No sample with $>56\%$ SiO_2 plots within the basic field, which confirms the absence of silicified basalts, as suggested earlier on petrographic evidence (Chapter 2).

- 2) Increasing fractionation, (ie. decreasing whole rock TiO_2) correlates with decreasing Zr in evolved rocks.

- 3) Evolved rocks define two distinctive, separate and sub-parallel trends which form 'higher' and 'lower' Zr groups (for TiO_2 vs. Zr, $r=0.89$ and 0.91 , respectively). The 'higher' group comprises samples from the

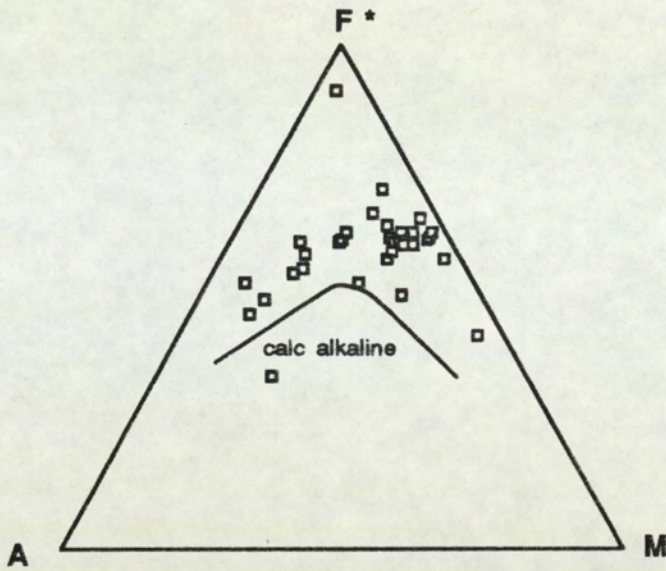


Figure 3.6 AFM plot of selected samples from the Bigstone sequence. See Appendix 4.1a for sample sources. Line dividing tholeiitic and calc-alkaline fields is from Irvine and Barager (1971) F* is total iron as FeO.

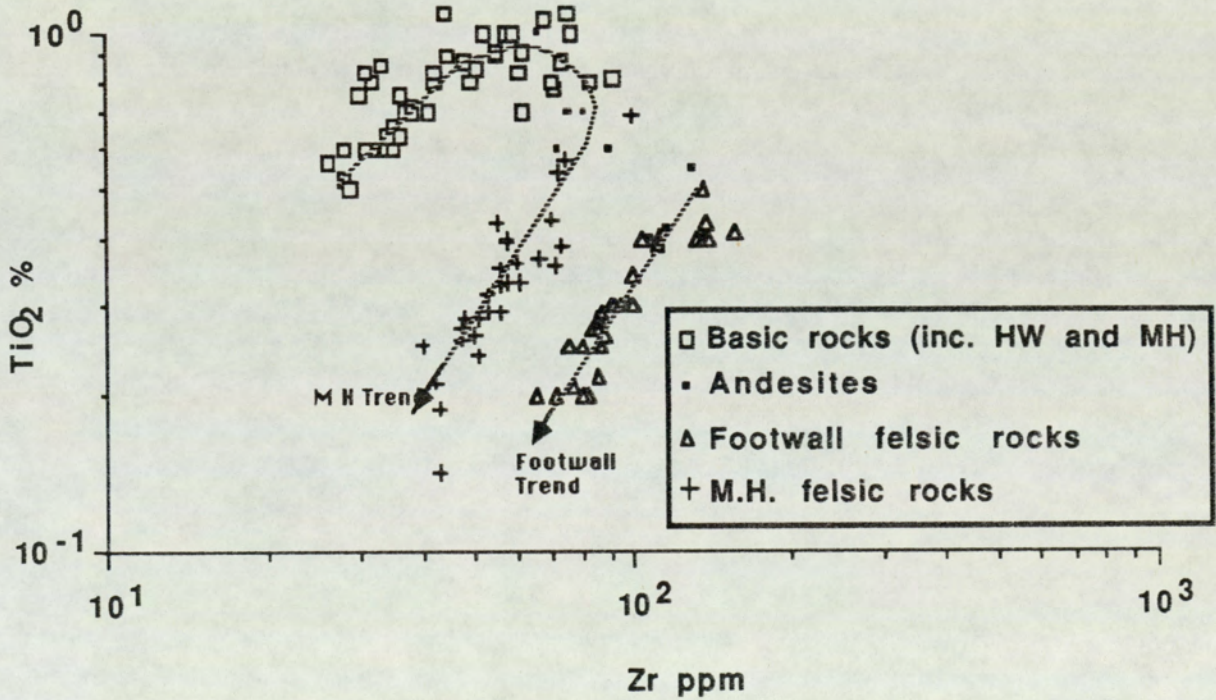


Figure 3.7 A plot of TiO_2 vs Zr for all rock types from the Bigstone deposit

QFP, whereas the 'lower' trend comprises tuffs from the Mineralised Horizon. The plot achieves 100% separation between the two stratigraphic groups.

4) A poorly defined continuum of points (dotted line of Figure 3.7), exists from basic rocks, through minor intermediate compositions, to evolved rocks of the Mineralised Horizon (ie low Zr) trend. This continuum is seen more clearly in a plot of Zr-V (Figure 3.8) which also illustrates the enrichment of V in MH rocks relative to those of the Footwall QFP (see also Table 3.2).

A plot of SiO_2 vs. Zr (Figure 3.9), shows that, for the SiO_2 range 40%-65% (FMU), Zr shows normal incompatible behavior, and increases with increasing silica content. However, for SiO_2 contents >65%, Zr contents in Footwall rocks decrease, and Zr appears to behave as a compatible element. A minority of points define a continuation of the trend of increasing TiO_2 and Zr. Mineralised Horizon tuffs have a considerable degree of scatter on the diagram possibly due to the influence of alteration processes.

In QFP rocks with >68% SiO_2 (rhyolites) Zr, in addition to showing strong correlations with Nb and TiO_2 , also correlates strongly with Sr ($r=0.74$), Na_2O ($r=0.78$), CaO ($r=0.71$), and, to a lesser extent, V ($r=0.54$; statistically significant at the 98.5% level). In addition, Zr is negatively correlated with SiO_2 and positively correlated with Al_2O_3 (correlation coefficients not reported because both elements contain more than one trend when plotted against Zr). Both Zr and TiO_2 are not correlated with Y, Rb, Zn, Cu, Ni, Cr, P_2O_5 and MnO. High correlation coefficients between the immobile elements Ti and Zr were previously inferred to indicate that they had both remained relatively immobile in

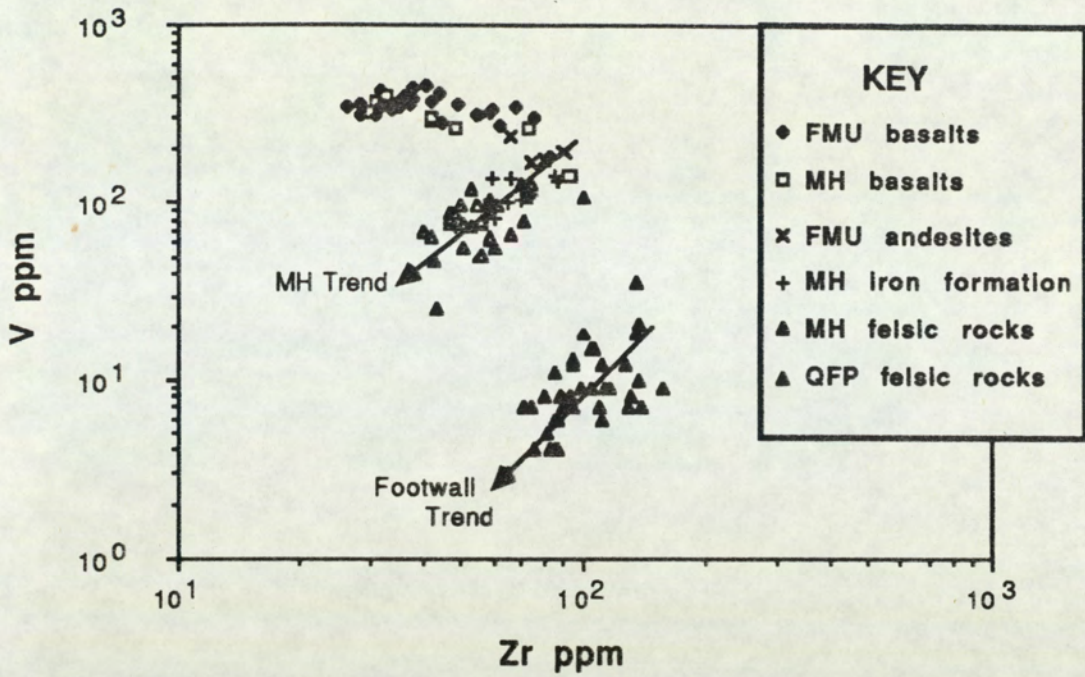


Figure 3.8 Zr vs V for various rock types from the Bigstone sequence, showing the continuum of data points from mafic rocks through to felsic rocks of the MH trend, and the marked separation of MH and Footwall trends.

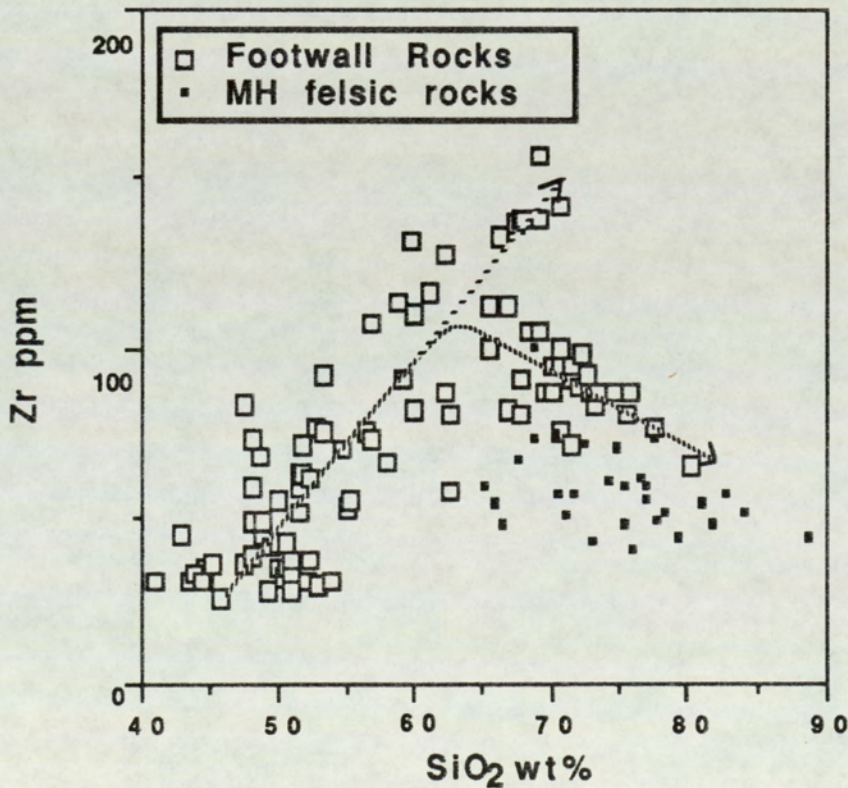


Figure 3.9 SiO_2 vs Zr for all Footwall rocks and felsic rocks from the Mineralised Horizon. Dotted lines correspond to trends involving Footwall rocks.

felsic rocks during alteration and/or metamorphism. It follows that high degrees of correlation between Ti and Zr and the elements Sr, Ca, Na, Si, Al, described above, allow a similar interpretation. In QFP rocks (which dominantly comprise plagioclase and quartz), the elements Na, Ca, Sr, Al are likely to be contained almost entirely within the plagioclase feldspar component. Thus, increasing Zr and TiO_2 in QFP rocks correlates with increasing plagioclase content. The tendency for Ti and Zr to increase with increasing plagioclase content is interpreted to indicate that dilution due to crystal fractionation during tuff emplacement (Walker, 1972), which would have the effect of causing Ti and Zr to decrease with increasing plagioclase content, has not occurred.

In the MH, many elements that are well correlated in QFP rocks, show no correlation with either Ti or Zr; however, Zr still correlates with Ti ($r=0.91$), Al_2O_3 ($r=0.78$), and V ($r=0.73$). This is interpreted to indicate that the plagioclase components other than Al_2O_3 , ie. Ca, Na and Sr have been mobile during alteration and/or metamorphism of the MH. This interpretation is compatible with petrographic observations in MH rocks, where feldspars are commonly replaced by silicates (chloritoid, chlorite, muscovite), which contain little or no Ca or Na.

3.4.3 Iron-formation

In the MH, felsic tuffs with minor intercalated mafic material are interbedded with three types of iron-formation (UIF, LIF and TIF). Bulk geochemical analysis has been carried out on only one sample of UIF, and none of LIF. This is because of the large grain size and heterogeneity of these units which would render the results statistically meaningless. It was thus considered more important to investigate the mineral chemistry of the iron-formations (Chapter 4). However, analyses of 15

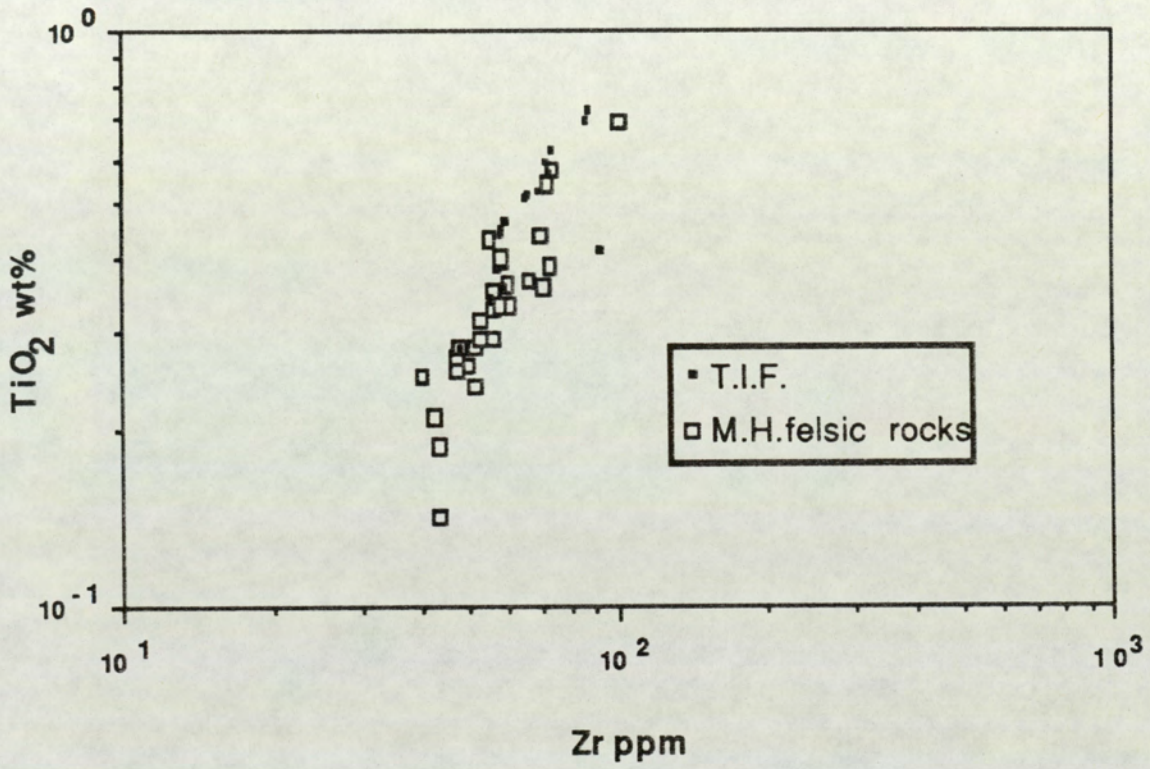


Figure 3.10 TiO₂ vs Zr for TIF and MH felsic rocks.

samples of TIF, show that, in terms of SiO_2 contents, 8 samples are ultramafic, 4 basaltic, 2 basaltic andesite and 1 dacitic. The preponderance of 'ultramafic' compositions reflects the low SiO_2 contents (and high Fe_2O_3) inherent in iron formations (Klein 1982). In addition, the samples have MnO contents up to 6.1% (27 times average Bigstone mafic rocks). The TIF samples thus have chemical characteristics, in terms of the elements Mn, Fe and Si, compatible with those of typical iron formations.

In terms of TiO_2 and Zr (Figure 3.10), iron-formation samples plot at the upper end of the trend defined by Mineralised Horizon rocks i.e. they contain both elements in the same proportions (but higher absolute abundances) as the tuffaceous and evolved rocks with which they are interbedded. These data confirm petrological evidence, and point to the presence of both a chemical, and a tuffaceous component in the T.I.F.

3.5 INTERPRETATION

The observed trends and abundances of trace elements in mafic and felsic rocks from the Bigstone sequence may be explained in two ways:

1) The decreasing Ti and Zr trends in felsic rocks may occur as a result of dilution (by addition of SiO_2) associated with a volume increase during the alteration process (Finlow-Bates and Stumpfl, 1981).

2) Ti-Zr trends (and other correlated elements) may record evidence of some primary igneous control.

These two hypotheses are reviewed below:

Dilution during alteration

The work of MacGeehan and MacLean (1980) on spilitisation of tholeiitic basalts beneath massive sulphide bodies showed that these rocks suffered major adjustments in both their major and trace element chemistries but that they retain relict basaltic textures. At Bigstone, QFP and MH siliceous rocks have no textures resembling those of basaltic rocks, or textures similar to those now present within the FMU. Furthermore, their mineralogies and textures are similar to those described from other metamorphosed felsic volcanoclastic sequences (Vernon, 1986). Thus, if some metasomatic process has altered the trace element contents in QFP and MH rocks, then that process must have acted upon felsic precursors.

Both trends in Figure 3.7 could be generated by considering the progressive dilution of rocks which originally contained relatively high levels of Ti and Zr (ie. contents of Ti and Zr similar to rocks which plot at the top of the respective trends). However, because increased plagioclase content correlates with increasing Ti and Zr, another source for dilution must be found. It could be suggested that increasing silicification associated with a volume increase has caused this dilution. However this would be faced with the following problems:

a) Quartz-rich rocks (the Quartz-eye Porphyry) are most abundant at the base of the sequence, furthest away from mineralisation and, presumably, the most intense alteration.

b) Where silicification of plagioclase has been observed in thin section, pseudomorphic textures are interpreted to indicate that little or no volume change occurred during the alteration process. Where quartz veining is seen, the amount of volume adjustment is generally <10%, and is considered too small to account for observed reduction in Ti and Zr contents. An estimate of the volume increase required to generate the

two trends has been generated following the method of Gresens (1967). Application of the Gresens method requires knowledge of the initial and final compositions of a given chemical component (in this case TiO_2), and of initial and final rock densities. In the calculation, it has been assumed that the dilution process is one of silicification of dacitic rocks, this yields density estimates of approximately 2.9 for dacites, and 2.6 for the end product 'rhyolites'. Calculations indicate that volume increases of >275% are required in order to produce the low TiO_2 (and Zr) rocks which plot at the lower end of the two trends. Changing initial and final density estimates does not significantly affect the volume estimate. If initial rock compositions containing intermediate levels of TiO_2 (0.4%) were chosen, then the rocks would have to have undergone volume changes of up to 200% . Furthermore, changes would have to be positive (dilution) to produce the lower whole rock TiO_2 values at the base of the trend, and negative (concentration by leaching) to produce higher levels of TiO_2 . Such large volume changes are incompatible with the petrological evidence and are thus rejected as the major cause for the trends (Figure 3.7).

c) Mafic rocks from the FMU and MH have immobile element contents and ratios similar to those of mafic rocks from the unmineralised NLA, and modern primitive arc sequences (Pearce 1982). It is difficult to envisage a process affecting the deposit sequence which causes a 50% reduction of trace element contents in some felsic rocks but which leaves mafic rocks entirely unaffected, even where they contain appreciable amounts of Cu and/or Zn mineralisation.

The Ti-Zr trends (Figure 3.7) could also be explained by considering the dissolution of accessory phases (involving negligible volume change)

during the alteration process. This is considered unlikely because petrographic observations indicate that ilmenite (which presumably constitutes most of the whole rock Ti budget) is stable in both MH and QFP rocks. Also, such removal is unlikely to preserve Ti/Zr ratios in altered rocks.

The trend defined by MH rocks in Figure 3.7 could be produced by removal of approximately 50% Zr from QFP rocks. Such a process would presumably involve dissolution of highly resistant zircon whilst leaving ilmenite unaffected. Finlow-Bates and Stumpfl (1981) report that depletion of Zr has not occurred within the Footwall sequences of six volcanogenic deposits studied. Moreover, it would be expected that, if dissolution of zircon had occurred in QFP rocks, at least some analyses from that unit would plot either off the QFP trend, or on the MH trend. However, even where QFP rocks contain stringer sulphide mineralisation and abundant tourmaline veins analyses plot on the QFP trend (Figure 3.7) along with other, less altered, rocks.

The two TiO_2 -Zr trends in the MH and QFP rocks thus appear to reflect a stratigraphic discontinuity between the two units which is preserved despite the combined effects of alteration and subsequent metamorphism.

It is thus concluded that dilution and dissolution processes do not adequately account for the observed trends and abundances within mafic and felsic rocks of the Bigstone sequence. Similar conclusions have been reached concerning Ti/Zr ratios from heavily altered and mineralised rocks from the Pecos greenstone belt, New Mexico (Peterson, 1983), altered rocks from the Buchans deposit in Newfoundland (Thurlow and Swanson, 1975), and for Ti/Zr in footwall rocks of the United Verde massive sulphide deposit, Jerome, Arizona (Kelly-Vance and Condie, 1987).

Primary igneous controls

If primary igneous processes are invoked to explain the observed trends and abundances of TiO_2 and Zr, then they must account for:

a) The apparent reversal of 'normal' fractionation trends of Ti, Zr and V in evolved rocks (Figures 3.7, 3.8, and 3.9).

b) The relatively wide range of trace element contents and, to a lesser extent, SiO_2 in both Footwall and Mineralised Horizon rocks.

c) The complete discrimination on Ti-Zr plots between Footwall and Mineralised Horizon evolved rocks.

d) The essentially bimodal (basalt-rhyolite) nature of the rocks.

These points are addressed in more detail below:

a) The reversal of normal fractionation trends.

The TiO_2 -Zr plot (Figure 3.11) shows a visually estimated, best-fit line through all data points for the NLA and Bigstone sequences. In both sequences, the elements Ti, Zr, Y and Nb behave incompatibly in basic rocks. In evolved rocks from geologically recent tholeiitic and most calc-alkaline sequences, such as those of the Tongan and South Sandwich arcs the elements Zr, Nb, and Y increase with decreasing TiO_2 due to the crystallisation of Ti-bearing oxide phases (Pearce and Norry, 1979). Evolved rocks from the NLA display this normal trend whereas in evolved rocks from the deposit sequence, Zr decreases with increasing fractionation (ie. decreasing TiO_2).

In some Andean-type suites, eg. Ecuador and Mexico (Pearce and Norry 1979) and Mesozoic volcanic and plutonic rocks from the Antarctic

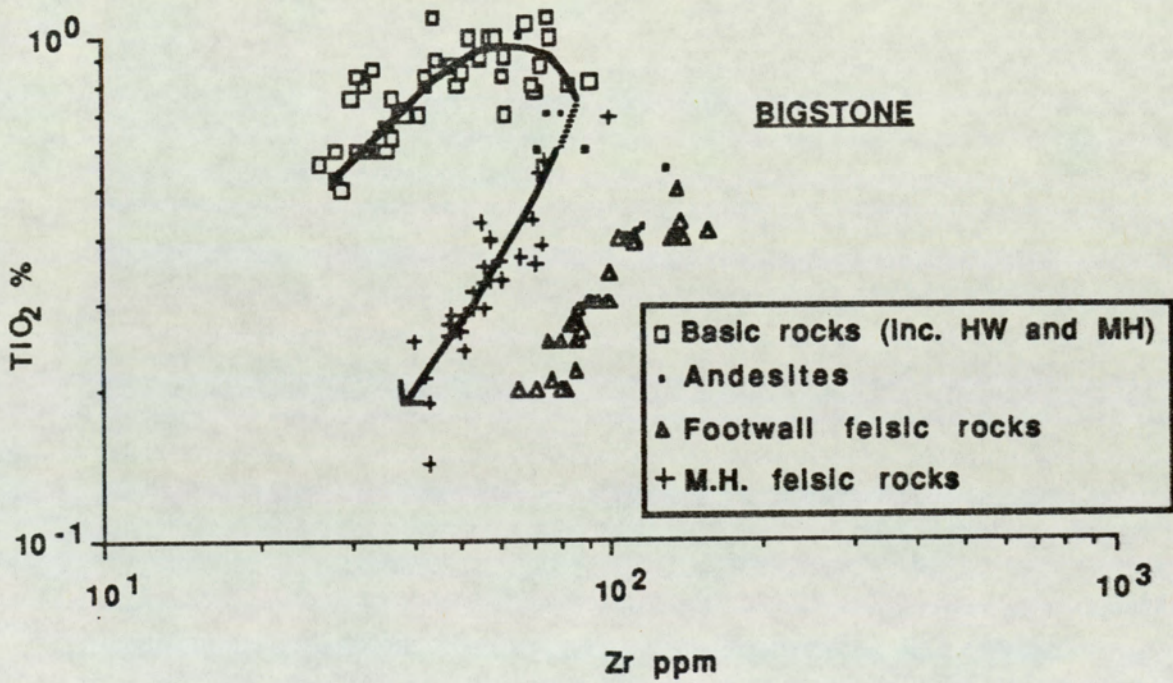
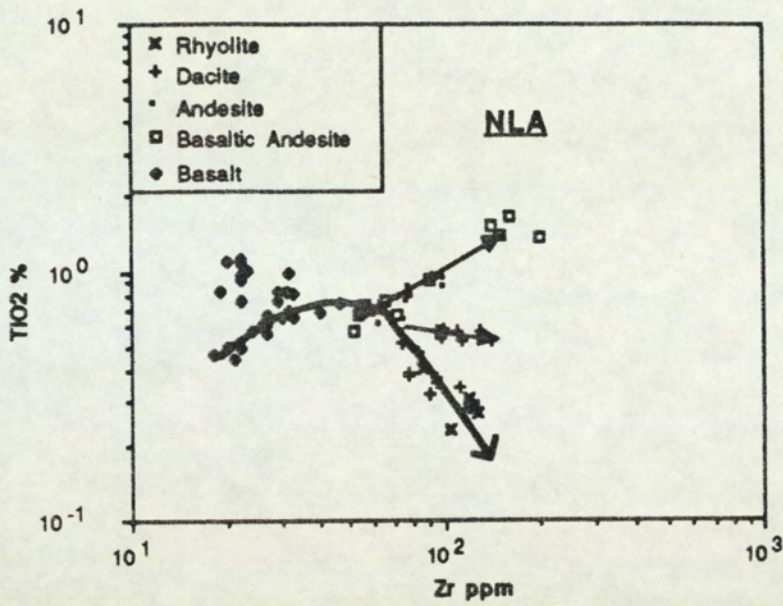


Figure 3.11 TiO_2 vs Zr for all rock types from the Bigstone deposit sequence (excluding iron-formation) and NLA, showing visually-estimated fractionation trends (heavy lines)

Peninsular and South Shetland islands (Saunders et.al., 1980), Y, Zr and Nb decrease in rocks of acidic composition. This can be achieved by considering biotite and/or zircon as either crystallising phases in a source magma or as residual phases in a zone of partial melting. Although the 'Andean-type' examples contain generally higher absolute concentrations of HFS elements, a similar process might be invoked for evolved rocks, in the Bigstone sequence. In addition, the published examples are all calc-alkaline, with the exception of the basalt-rhyolite volcanism of the South Shetland Islands, which is transitional between IAT and calc-alkaline (Tarney et.al., 1982). Thus, although South Shetland is a reasonable analogy, no identical trends have been described in young IAT sequences. Notwithstanding the absence of good analogies from modern terrains, fractionation of zircon and/or biotite remains a viable mechanism to account for the well-correlated negative trends observed here.

b) The wide range of trace element contents.

The relatively wide range in trace element contents shown in the two different TiO_2 trends (Figure 3.7) may occur because Footwall and Mineralised Horizon tuffs represent separate and parallel fractionation sequences each generated by a similar zircon (and/or biotite) controlled fractionation mechanism. It is considered unlikely that the two sequences represent separate flows or their hypabyssal equivalents, because samples of such would plot as distinct clusters rather than evolutionary trends on the various plots. This observation, combined with petrographic data (Chapter 2), is interpreted to indicate that the Footwall and Mineralised Horizon rocks represent separate, chemically zoned pyroclastic units derived from a source (or sources) undergoing fractionation of zircon and/or biotite.

Chemically zoned rhyolitic to andesitic tuffs are known from a

number of currently active, and older areas (eg. the Bishop Tuff, Hildreth, 1981; La Primavera tuff, Mahood, 1981). Furthermore, Hildreth (1981) suggested that no pyroclastic eruption $>1\text{km}^3$ is compositionally homogenous and that the products of such eruptions commonly have relatively small major element variations, but extensive variations in trace elements.

TiO₂-Zr discrimination between Mineralised Horizon and Footwall evolved rocks

Ash-flow tuffs are an inverted record of a magma chamber at a single point in time (Hildreth 1981). The earliest erupted tuffs are typically the most evolved (highest Zr, Y, Nb, lowest TiO₂) and are crystal-poor. Later ones are more primitive and crystal-rich. In addition, in most zoned eruptions, there is a sharp compositional interface, or narrow transition zone, between the earliest and latest eruptive products which is an inherited feature of the source magma body (Hildreth 1981).

At Bigstone, the observed trends amongst HFS elements, and the stratigraphically-controlled differences between the more evolved Footwall tuffs, and the less evolved tuffs of the Mineralised Horizon, are compatible with an origin as compositionally-zoned products of a single magma chamber undergoing zircon and/or biotite fractionation.

Bimodal volcanism

Bimodal volcanism is commonly associated with regions of crustal tension, and occurs in a variety of tectonic environments, but is apparently unknown from modern day primitive oceanic island arcs. Bimodal volcanic sequences showing strong IAT characteristics have been described from the Flin Flon area (Gaskarth and Parslow 1987),

where they are associated with important Cu-Zn-(Pb) massive sulphide bodies. The Bigstone sequence has IAT affinities, and is bimodal (basalt-rhyolite) with only minor andesitic rocks. Basaltic flow material is interbedded with consanguineous pyroclastic dacitic to rhyolitic rocks. Such a feature is relatively common in small-scale caldera systems, where mafic magma from deeper levels of a magma chamber may be mixed with dacitic magma during eruption (Smith 1979).

3.6 DISCUSSION AND CONCLUSIONS

The major conclusions drawn from geochemical studies of the deposit sequence are:

1) Presently observed trace element abundances, and ratios, within felsic and mafic rocks are probably primary igneous features, and are not due to alteration and/or metamorphic processes.

2) The presence of two distinctive Ti-Zr trends in Mineralised Horizon and Footwall rocks is not compatible with the hypothesis that Mineralised Horizon rocks represent a folded and detached part of the footwall sequence. Copper Body mineralisation occurs within chemically distinctive felsic rocks which form the upper (more primitive) part of a larger, compositionally zoned, sequence of tuffs. The apparent fractionation trends of Ti and Zr in felsic rocks probably are the result of biotite and/or zircon fractionation in a source magma of presumed intermediate composition.

Many massive sulphide deposits in volcano-sedimentary sequences are concentrated along specific stratigraphic horizons (Franklin and Thorpe, 1982; Thurlow and Swanson, 1975). Thus, the recognition of a distinctive chemical break between mineralised and unmineralised tuffs may have potential exploration applications at Bigstone.

3) Widespread alteration of plagioclase feldspar in MH rocks during

the mineralisation process resulted in the breakdown of correlations involving the elements Ca, Na and Sr

4) Volcanism is bimodal basalt-rhyolite and has strong island arc tholeiite (IAT) characteristics. As such, it is similar to the ore-bearing bimodal sequences of the Flin Flon area (Gaskarth and Parslow, 1987), and differs from modern oceanic arc sequences. Mafic rocks of FMU are notably depleted in copper relative to MORB and Island Arc Tholeiites (Pearce, 1983; Pearce and Gale, 1977).

5) Volcanism and mineralisation may have occurred within a caldera-type environment. The presence of a high level magma chamber within such an environment would provide an ideal source of heat (and possibly fluids and metals) to drive ore-forming hydrothermal systems (Scott, 1982; Urabe et.al., 1983). Similar fractionation trends within felsic rocks from adjacent areas might therefore indicate the presence of other high level magma bodies, and point to areas of increased mineral potential.

CHAPTER 4: MINERAL CHEMISTRY AND METAMORPHISM

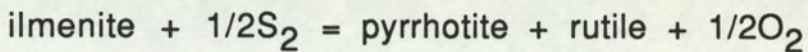
4.1 INTRODUCTION

The preservation of primary textural (Chapter 2) and chemical (Chapter 3) features within Footwall and Mineralised Horizon (MH) rocks raises the possibility that the compositions of the mineral phases themselves may be related to primary ore-forming processes. The purpose of this chapter is to investigate the chemical compositions of major silicate phases in MH rocks, and to examine whether systematic differences exist between similar minerals in different rock units. Particular attention is paid to the investigation of amphibole and garnet which are common in both LIF and UIF. The data are interpreted in terms of primary lithological controls, and metamorphic processes.

Several studies of metamorphosed ore deposits have documented distinct variations in oxide-sulphide-silicate assemblages and of the compositions of ferromagnesian silicates in and around ore as a direct result of reactions occurring during metamorphism (Froese, 1969; Bachinski, 1976; Nesbitt and Kelly, 1982; Nesbitt, 1982; Nesbitt, 1986a, 1986b). In the study of metamorphosed deposits, any application of mineral assemblages and their chemistries in terms of original processes must take into account the possible effects of metamorphism. Thus, prior to considering details of the chemistry of mineral phases at Bigstone, it is essential to review some of the predicted and observed effects of metamorphism from other deposits, based mainly on the observations and calculations of Nesbitt (1982, 1986a and 1986b) and Nesbitt and Kelly (1982).

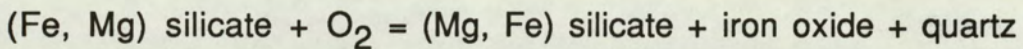
In many metamorphosed deposits eg the cupriferous deposits of Notre Dame Bay, Newfoundland (Bachinski, 1976), and at Ducktown, Tennessee (Nesbitt and Kelly, 1980) there are distinct variations in oxide-sulphide-graphite mineralogy which are attributed to gradually increasing fS_2 and fO_2 due to the proximity of mineralisation. At

Ducktown, as ore is approached, graphite is oxidised, and ilmenite breaks down to rutile according to the reaction:

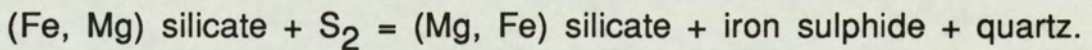


Pyrrhotite is variably sulphidised and oxidised to form pyrite + magnetite.

These changes in oxide-sulphide-graphite mineralogy occur in parallel with changes in the compositions of co-existing ferro-magnesian minerals, during conditions of elevated $f\text{O}_2$ or $f\text{S}_2$, by the following general reactions:



and,



Such reactions have been calibrated experimentally by Popp *et.al.* (1977) for Fe-Mg amphiboles, and for biotite by Tso *et.al.* (1979). In a simple case, progressively increased levels of $f\text{O}_2$ and/or $f\text{S}_2$ cause a progressive decrease in the X_{Fe} (Fe/Fe+Mg) of Fe-Mg silicates (Froese, 1969, Bachinski, 1976, Nesbitt, 1982, Nesbitt, 1986a and 1986b). Manganese is the main cation which substitutes for Fe in garnet, and so the calculated X_{Fe} is Fe/Fe+Mg+Ca+Mn. Theoretical calculations (Nesbitt, 1986a, 1986b) show that phases which are relatively intolerant of large amounts of Mg in their structure (eg. garnet and staurolite) give way, under conditions of increasing $f\text{O}_2$ and/or $f\text{S}_2$, to more Mg-rich minerals (eg. cordierite, chlorite and biotite).

If the fugacities of vapour phases are externally imposed during metamorphism (due to the diffusion of O_2 and S_2 away from mineralised rocks), then the compositions of ferro-magnesian minerals within a single rock sample should define a narrow range in terms of the ratio Mg/Mg+Fe (Frost, 1982). Alternatively, if the Mg/Mg+Fe ratios are

variable within, and between various samples, then the fugacities of O_2 and S_2 are controlled by mineral reactions on a small scale (Frost, 1982).

The following preliminary comparisons between Bigstone and 'type' metamorphic deposits are made:

1) Petrographic studies at Bigstone indicate that graphite is stable in graphitic schists of the Hanging Wall at distances of $< 5\text{m}$ from ore (compared to 90m at Ducktown).

2) Ilmenite appears to have been stable in all units throughout metamorphism, and is unaltered even adjacent to sulphides and/or oxides in the Mineralised Horizon (Plate 2.10). Whole rock geochemical data (Chapter 3) support the suggestion that Ti has remained immobile throughout metamorphism.

3) Chloritoid is generally intolerant of high Mg contents (Deer et.al., 1986), and would therefore not be expected in environments with high fO_2 and/or fS_2 . At Bigstone, it is present in large quantities as an integral part of the Copper Body.

The above points are tentatively interpreted to indicate that widespread diffusion of S_2 and/or O_2 may not have occurred, and that mineral assemblages in various units may therefore have buffered the fugacities of vapour phases during metamorphism. Nevertheless, the presence of gahnite, which is thought to form as a desulphidation product of sphalerite during metamorphism (Spry and Scott, 1986), indicates that sulfidation and/or oxidation may have been important, at least locally, in mineralised rocks.

4.2 MINERAL CHEMISTRY

4.2.1 Analytical techniques

The compositions of various mineral phases were determined by microprobe analysis using both Energy Dispersive Systems (EDS) and Wavelength Dispersive Systems (WDS) at the Universities of Leicester, Manchester and Aston. Details of analytical techniques and operating conditions are reported in Appendix 3.1.

4.2.2 Iron Formation

a) Fe-Mg amphiboles

Compositions of analysed amphiboles span the range from cummingtonite ($\text{Mg}/\text{Mg}+\text{Fe} >0.3$) to grunerite ($\text{Mg}/\text{Mg}+\text{Fe} \leq 0.3$) and contain Mn as an important minor component. The major chemical components of cummingtonite-grunerite analyses are summarised in Table 4.1 (complete lists of all analyses are contained in Appendix 3.2)

A plot of Mn vs $\text{Fe}+\text{Mn}/\text{Fe}+\text{Mn}+\text{Mg}$ (Figure 4.1) shows the complete range of analyses subdivided according to sample number and iron formation type (LIF or UIF). All cummingtonite-grunerites from the UIF contain >0.25 atoms Mn per unit formula (23 oxygens) and should be prefixed by the term 'manganoan' (Leake 1978). Cummingtonite-grunerites from the hornblende-bearing LIF are characterised by markedly lower Mn contents. The data set as a whole defines a wide range of $\text{Fe}+\text{Mn}/\text{Fe}+\text{Mn}+\text{Mg}$ values (0.575-0.775) within which analysed amphiboles from individual samples define groups with generally overlapping values.

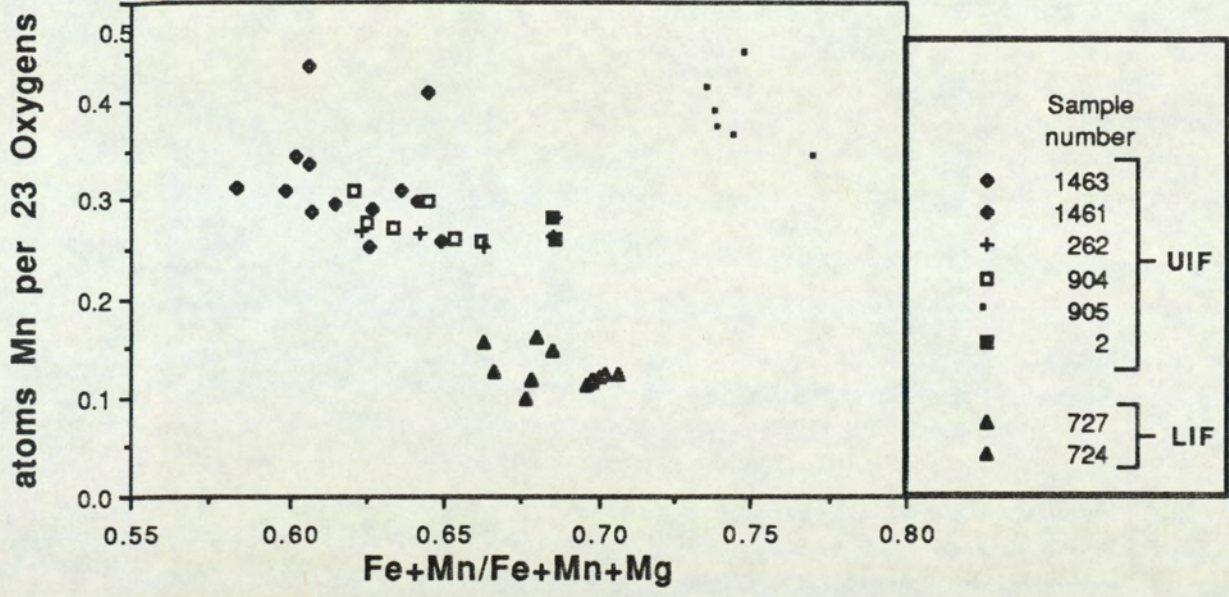


Figure 4.1 Plot of the number of atoms of Mn (per 23 oxygens) vs. the ratio $Fe+Mn/Fe+Mn+Mg$ (atoms) in Bigstone Fe-Mg amphiboles, subdivided according to sample number and iron formation type. UIF = Upper Iron Formation, LIF = Lower Iron Formation.

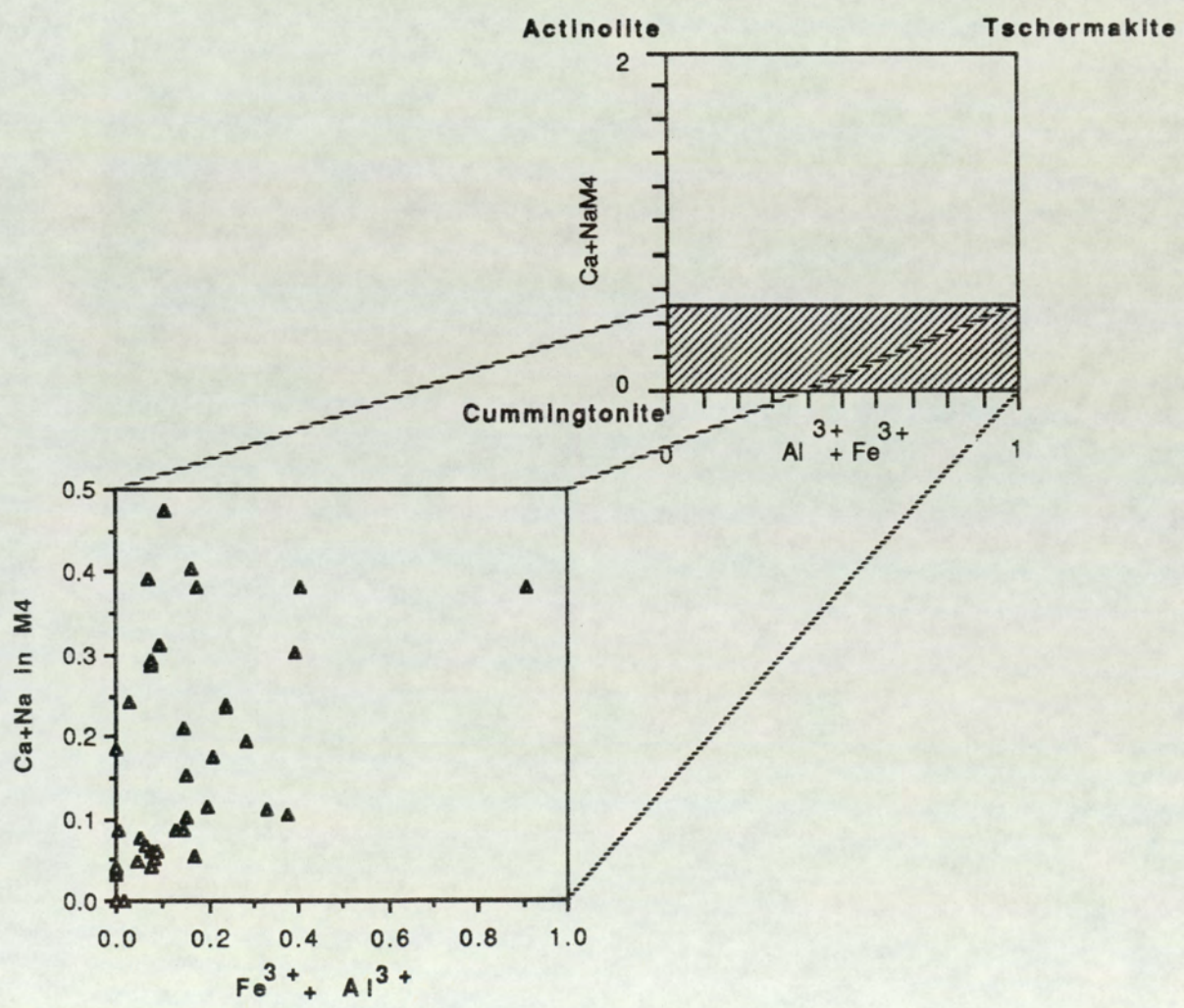


Figure 4.2 Plot showing the extent of actinolite-tremolite and tschermakite—ferro-tschermakite substitutions in Bigstone Fe-Mg amphiboles.

<u>component</u>	<u>min</u>	<u>max</u>	<u>mean</u>	<u>s.d</u>
Si	7.34	8.21	7.84	0.19
Al total	0.00	0.81	0.23	0.20
Fe ²⁺	3.42	4.77	4.17	0.33
Mg ²⁺	1.52	2.90	2.26	0.35
Mn ²⁺	0.10	0.45	0.26	0.10
Mg/Mg+Fe	0.24	0.44	0.35	0.05
Fe+Mn/Fe+Mn+Mg	0.58	0.77	0.66	0.05
Fe ³⁺ /Fe ³⁺ + Fe ²⁺ *	0.00	0.21	0.02	0.04
% non quadrilateral **	1.85	34.75	10.95	7.74
(Ca+Na)M4	0.04	0.47	0.17	0.11
(Ca/Ca+Na)M4	0.32	1.00	0.92	0.20

Table 4.1 Summary statistics of major Fe-Mg amphibole analyses

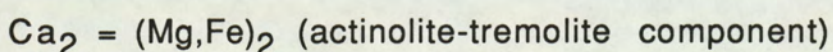
* Calculated summing total cations to 15 using the computer program of Rock (1987)

** Calculated using the method of Papike et.al. (1974)

Table based on a total of 46 analyses.

The total variation of Fe+Mn/Fe+Mn+Mg within samples varies from small, eg #724 (range ~ 0.66-0.68) to large, eg #262 (range ~0.625-0.68).

On average, the cummingtonite-grunerites contain a moderate and variable (high s.d.) non-quadrilateral component (Table 4.1). A plot of Fe³⁺+ Al³⁺ vs. Ca+Na in the M4 site (Figure 4.2) shows that substitution takes place according to:



and

(Mg,Fe), Si = Al^{vi}, Al^{iv} (tschermakite, ferro-tschermakite component).

The following points summarise the main details of the occurrence and chemistry of cummingtonite-grunerite at Bigstone:

1). Manganoan cummingtonite-grunerites occur in the Upper Iron Formation unit, along with garnet + magnetite + quartz.

2). Relatively Mn-poor cummingtonite-grunerites occur in minor quantities along with hornblende + garnet + magnetite in Lower Iron Formation rocks.

3). There is a relatively wide range of Mg/Mg+Fe ratios in analysed amphiboles both within, and, to a lesser extent, between various samples which is apparently unrelated to the proximity or abundance of oxide and/or sulphide minerals.

4). Fe-Mg amphiboles contain moderate and variable amounts of ferro-tschermakite and tremolite components.

b) Calcic Amphiboles.

All analyses of calcic amphiboles contain <6.25 Si atoms per unit formula, and have Mg/Mg+Fe <0.5 (Table 4.2, complete lists of all analyses contained in Appendix 3.2). Using the classification scheme proposed by Leake (1978), most analyses fall into the compositional field of ferro-tschermakite, with a minority plotting as ferro-pargasite or ferroan pargasite (Figure 4.3). All these amphiboles are characterised by high contents of Fe, Ca and Al, moderate Mg and minor Na and K. They are the most aluminous described from any iron formation to date.

A plot of Mg ratio (Mg/Mg+Fe) vs. $Fe^{3+}/Fe^{3+} + Al^{3+}$ (Figure 4.4) shows the range of substitutions shown by Bigstone calcic amphiboles

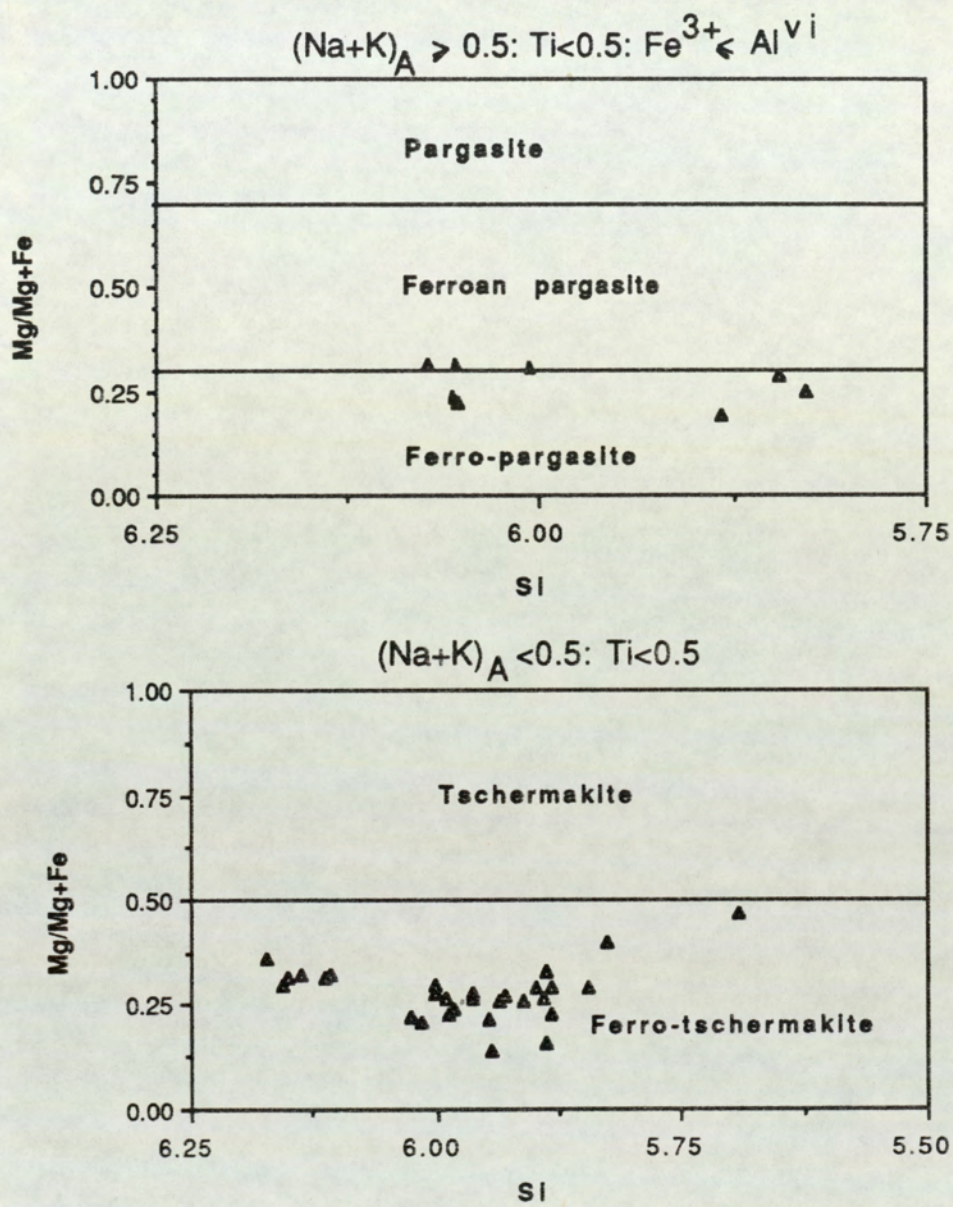


Figure 4.3 Classification of calcic amphiboles after Leake (1978).

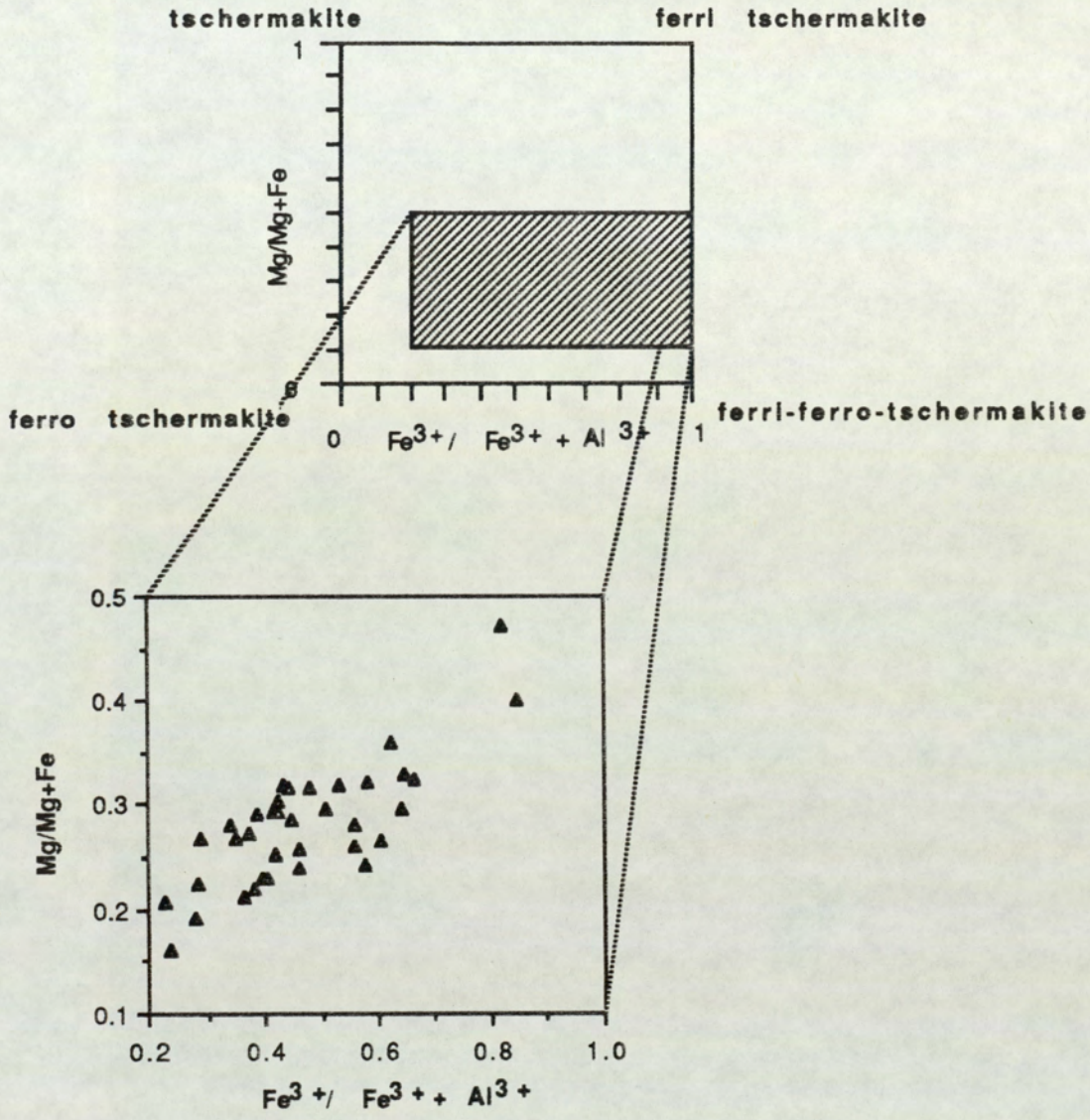
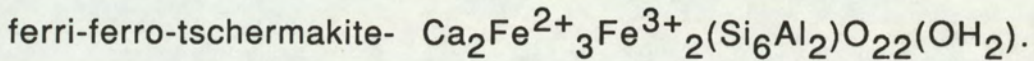
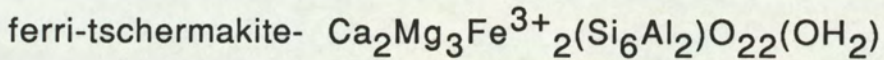
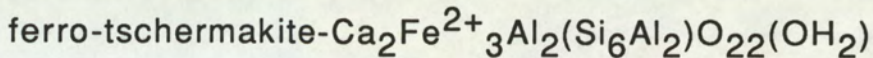
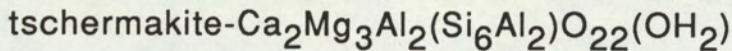


Figure 4.4 Plot showing the range of tschermakite compositions within the area of the shaded quadrilateral.

within the quadrilateral:



<u>component</u>	<u>min</u>	<u>max</u>	<u>mean</u>	<u>s.d.</u>
Si	5.69	6.17	5.98	0.11
Al ^{vi}	0.33	1.40	0.95	0.24
Al ^{iv}	1.83	2.31	2.02	0.11
Fe ³⁺ *	0.38	2.25	0.90	0.07
Fe ²⁺	1.17	3.06	2.26	0.34
Mg ²⁺	0.50	1.15	0.86	0.18
Mg/Mg+Fe ²⁺	0.14	0.47	0.28	0.06
Fe ³⁺ /Fe ³⁺ + Fe ²⁺	0.13	0.66	0.28	0.12
(Ca/Ca+Na)M4	0.78	1.0	0.93	0.05
(Na+K) ^A	0.21	0.63	0.44	0.10
Total Fe/Total Fe + Mg	0.73	0.86	0.79	0.04

Table 4.2 Summary statistics of major calcic amphibole components

* Fe³⁺ estimated from crystal chemical limits, by summing total cations to 13 exclusive of K, Na, Ca using the computer program of Rock (1987). Table based on a total of 38 analyses.

The trend away from the ferro-tschermakitic apex towards the ferri-tschermakite apex in the figure involves the stabilisation of increasingly magnesian amphibole compositions. A plot of Ca/Ca+Na in the M4 site vs. Mg ratio (Figure 4.5) shows that the ferri-tschermakite substitution (ie increasing Mg ratio) is coupled with substitution of a minor amount of Mg-riebeckite component (Na into the M4 site) into the amphibole structure. A plot of Na+K in the A site vs. Ca/Ca+Na in the M4 site (Figure 4.6) shows the antipathetic relationship between the pargasite (Na+K in A) and the Mg-riebeckite (Na in M4) substitutions.

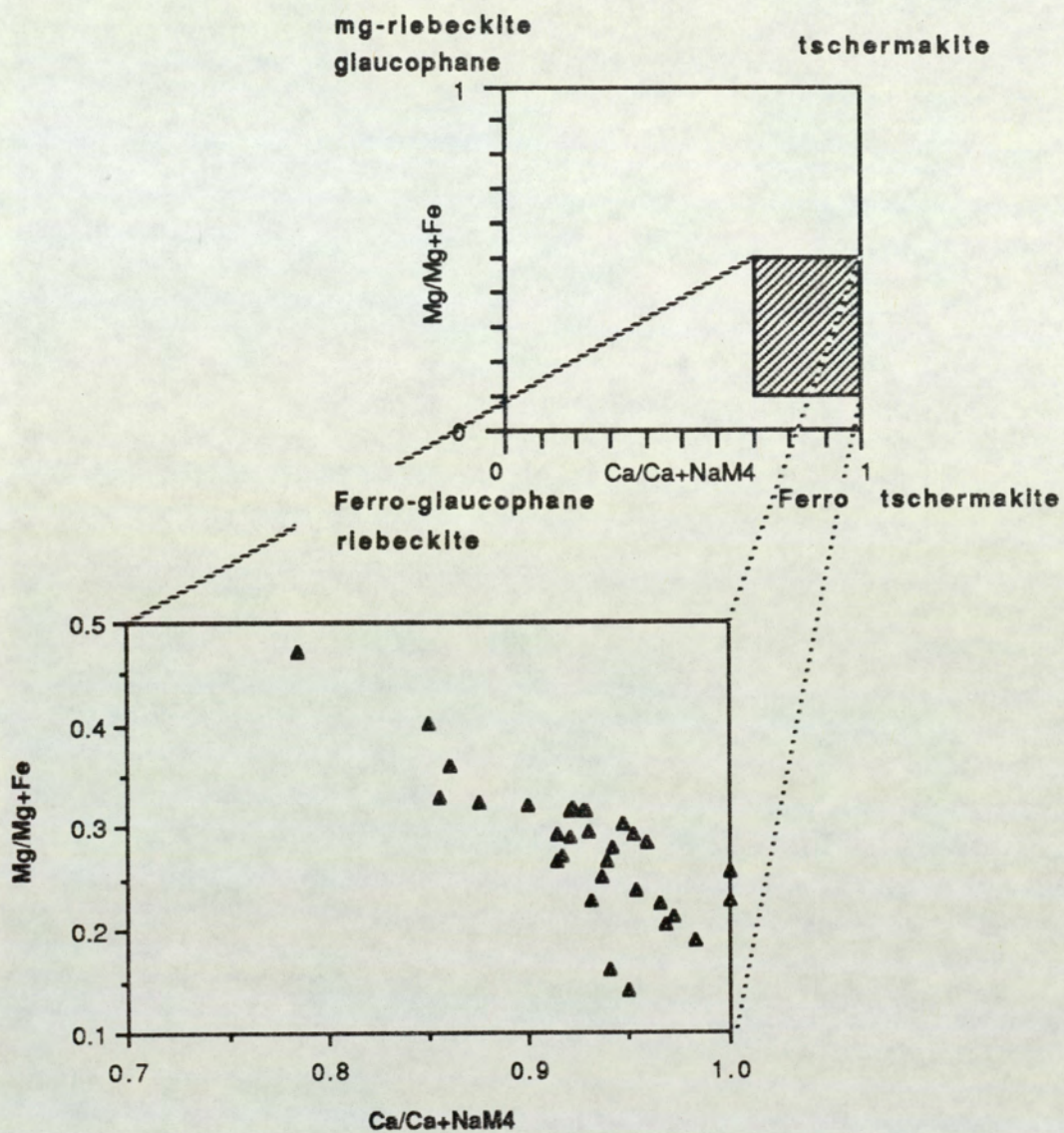


Figure 4.5 Plot showing the extent of the glaucophane-Mg-riebeckite substitution in calcic amphiboles.

Thus, the trend away from ferro-tschermakite involves the stabilisation of increasingly magnesian amphibole compositions up to a maximum Mg/Mg+Fe of 0.5, and also involves uptake of Na into the M4 site as a riebeckite – Mg-riebeckite component. A plot of $Fe^{3+}/(Fe^{3+}+Fe^{2+})$ vs Mg/Mg+Fe for the entire data set, (Figure 4.7) shows that, whilst some samples define relatively small variations in both components (Samples 227, 236, 237), others show variations in oxidation ratio and hence Mg/Mg+Fe (Samples 928, 764, 724). The largest range occurs in sample 724 in which hornblende coexists with cummingtonite with a restricted Fe+Mn/Fe+Mg+Mn of 0.66 to 0.68 (Figure 4.1). The presence or absence of garnet from the assemblage has no discernable effect on Mg/Mg+Fe ratios.

The wide range in Mg/Mg+Fe ratios within the data set as a whole and within separate amphiboles from individual samples is interpreted to indicate that fluid compositions were internally buffered over small distances (<1mm) during metamorphism.

In conclusion, the following points summarise the main details of calcic amphiboles at Bigstone:

- 1). Calcic amphiboles are confined to the Lower Iron Formation.

- 2). Compositions range from (alumino)-ferro-tschermakite to ferri-tschermakite and contain ferro-pargasite and minor Mg-riebeckite - riebeckite components.

- 3). The wide variation in Mg/Mg+Fe within and between individual samples is interpreted to indicate that O_2 and S_2 were internally buffered during metamorphism, and that presently observed variations in amphibole chemistry reflect local variations in precursor bulk rock chemistry.

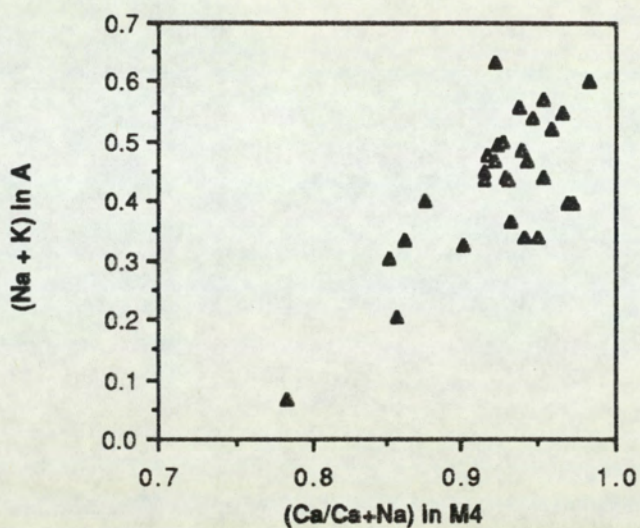


Figure 4.6 Plot showing the antipathetic relationship between pargasite (Na+K in A) and glaucophane- Mg-riebeckite (Ca/Ca+Na in M4) substitutions in calcic amphiboles

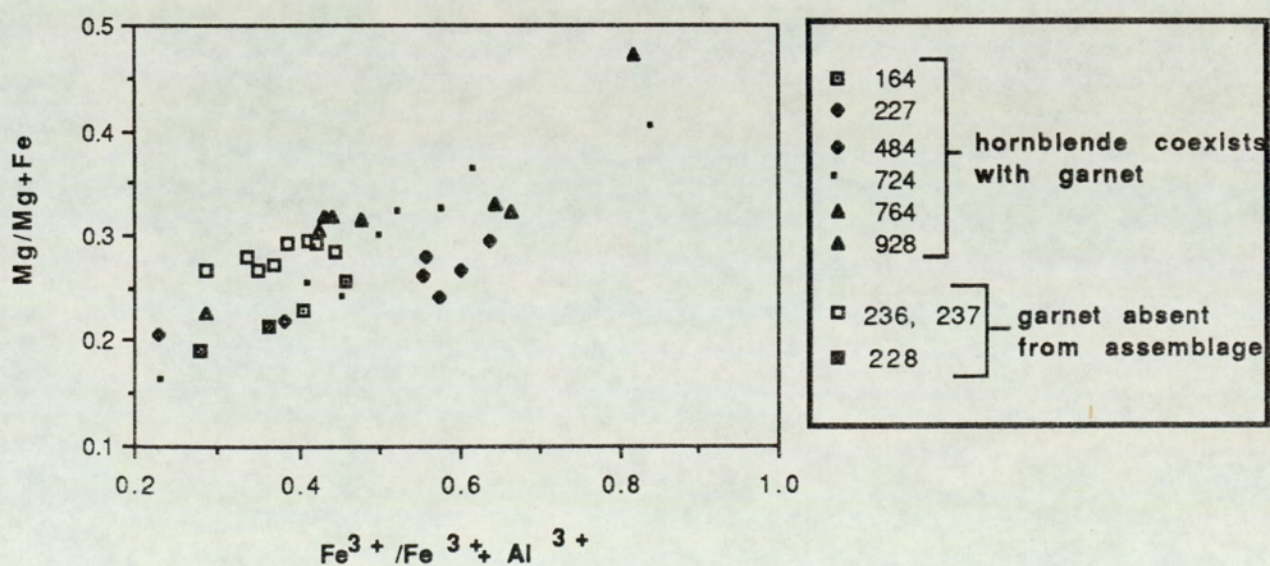


Figure 4.7 Plot of Mg ratio vs $Fe^{3+}/Fe^{3+} + Al^{3+}$ of calcic amphiboles subdivided according to sample number.

c) Garnet.

Garnet is ubiquitous (generally >50%) in both LIF and UIF, and has largely escaped the effects of widespread retrogression. It has been studied in detail in order to furnish details of spatial variations in composition.

Taken as a whole, the data set has wide variations in content of the divalent cations of Fe, Mn, Ca and Mg. Iron and manganese are dominant; calcium is a minor component; and magnesium is uniformly low in

	Min	Max	Mean	s.d.
FeO%	14.2	40.8	31.0	4.4
MnO%	1.2	22.5	7.9	3.9
CaO%	0.0	7.4	2.4	1.2
MgO%	0.0	7.5	1.0	0.6

Table 4.3. Summary statistics of divalent cations in garnets.

abundance (Table 4.3, complete list of analyses in Appendix 3.2). Occupancy of the Y site in garnet is generally >98%, which is taken to indicate that ferric iron is not an important component, and that Ca is present in the grossular, rather than the andradite, molecule.

A ternary plot of atomic percent Fe, Mn and Ca (Figure 4.8), for those garnets co-existing with either hornblende (LIF) or cummingtonite (UIF), shows that garnets from hornblende-bearing samples of the LIF are markedly depleted in Mn, enriched in Fe and, to a lesser extent, Ca compared to those from the UIF.

Garnets from garnetite (>80% garnet) from LIF immediately below low-grade copper mineralisation of the Chloritoid Zone (DDH BS-35), were analysed (16 samples). A plot of atomic percent Fe, Mn and Ca, for the garnetite samples (Figure 4.9), superimposed on the fields of garnet

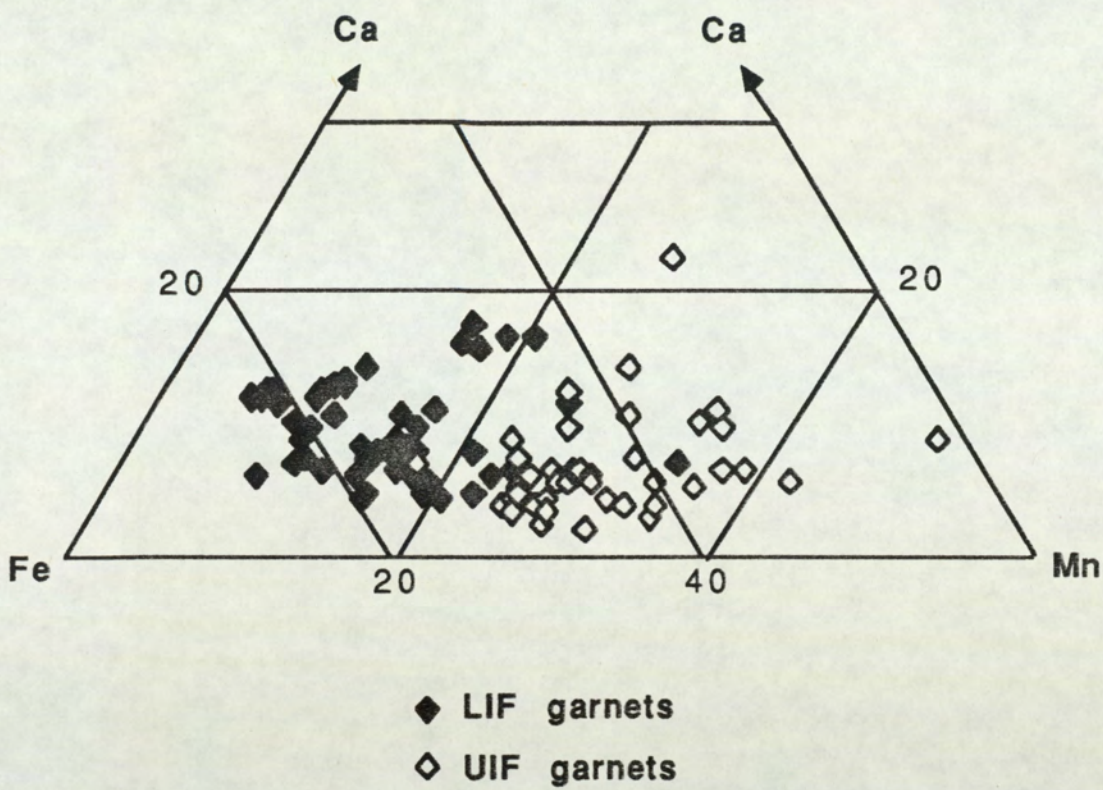


Figure 4.8 Ternary diagram of atomic % Fe, Mn and Ca in LIF and UIF garnets.

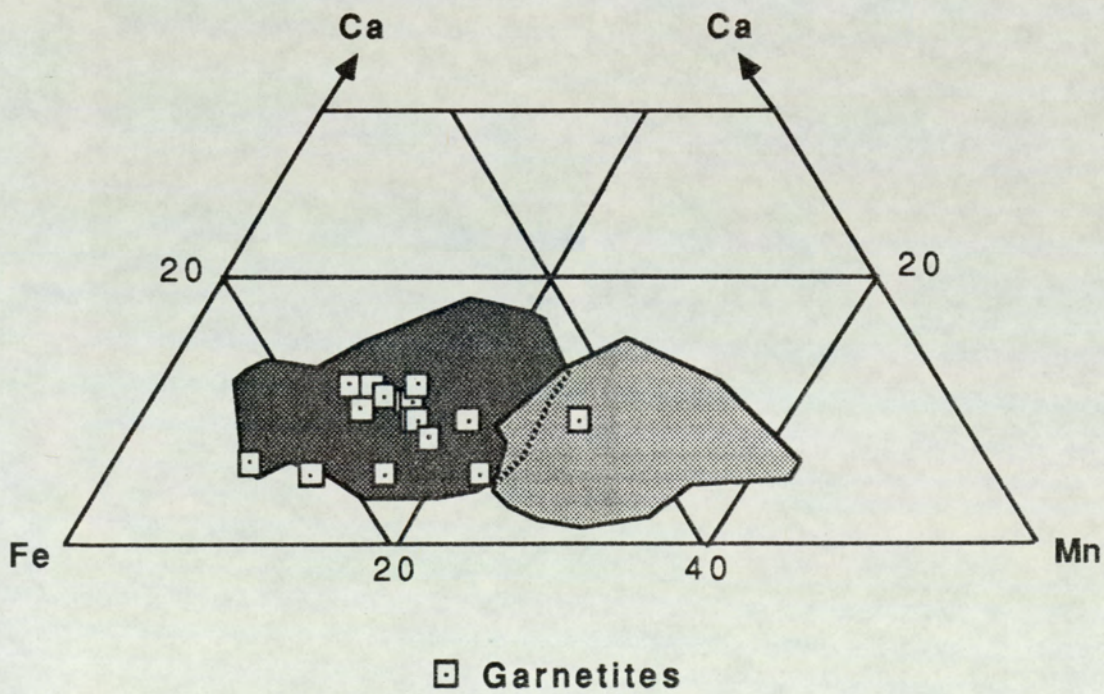


Figure 4.9 Ternary diagram of atomic % Fe, Mn and Ca in garnetites. Fields correspond to hornblende- (dark shading) and grunerite- (light shading) bearing assemblages of Figure 4.8

composition from Figure 4.8, shows that Fe, Mn and Ca contents are similar to those of hornblende-bearing LIF. Thus, all LIF garnets (with or without hornblende) are chemically different to those of the UIF.

Profiles of mean atomic percent Fe, Mn, Mg and Ca in LIF garnets from DDH BS-35 (Figure 4.10) show that:

1). Calcium and Mg vary systematically and sympathetically across the LIF unit. Both elements are present as minor components at the upper and lower margins of the unit and increase in the central portions to give a dome-shaped profile. Second order polynomial regressions on Mg, Ca and Mg+Ca vs depth (m) give correlation coefficients of 0.79, 0.91, and 0.94, respectively.

2). Mineralisation occurs at 75m, 87m, and is present at low levels (<0.25%) at all points in between. The proximity of mineralisation has no systematic effect on any of the iron-formation components. Mg and Ca are seemingly unaffected by the presence of mineralisation (although Mg shows a slight increase at 75m. Mn is unaffected by the 75m mineralisation and decreases at the 87m mineralisation whereas Fe is largely unaffected by the pattern of mineralisation over most of the interval, though it shows a sympathetic variation with mineralisation grades in the interval 85-90m. The largest increase in the almandine component (X_{Fe}) occurs within mineralised rocks at 87m. This increase is exactly the opposite of the effect of elevated fS_2 and/or fO_2 levels on garnet compositions predicted to occur as a result of metamorphic processes (Nesbitt, 1982).

3). Because most of the garnets analysed are from garnetites, garnet chemistry should serve as a reasonable estimate of bulk rock composition. It follows, therefore, that the sympathetic variation of Mg

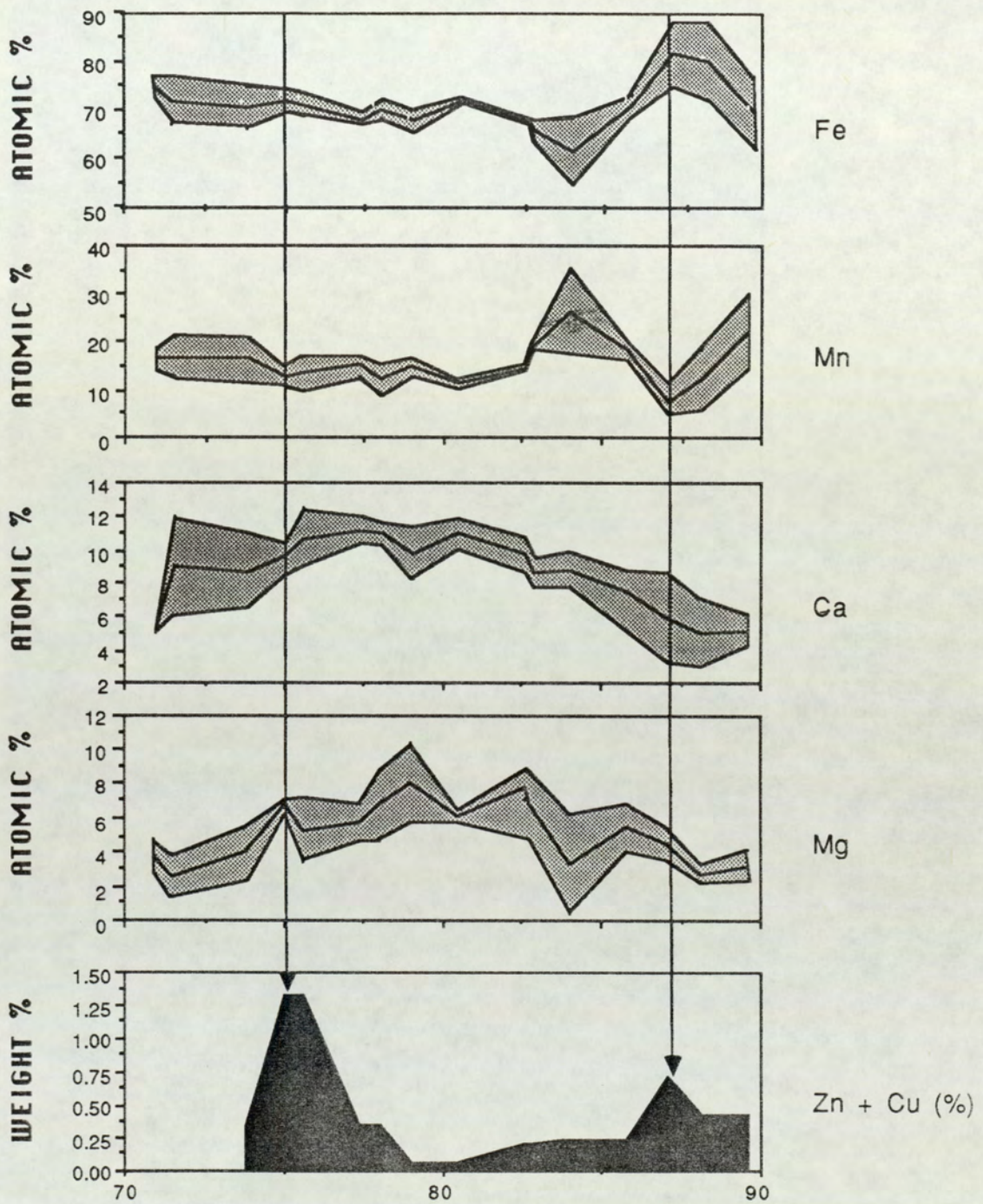


Figure 4.10 Profiles of mean atomic % Fe, Mn, Ca and Mg in garnet, and weight% Zn+Cu (whole rock) for an intersection of LIF from DDH BS35. Shaded area of garnet profiles corresponds to one standard deviation of the mean (medial line). Arrowed lines mark the location of mineralisation at 75m and 87m.

and Ca across LIF, which is unrelated to variations of Fe and Mn, and the proximity of mineralisation, is due to variations in precursor bulk rock chemistry and mineralogy.

4.2.3 Summary of iron-formation mineral chemistry

1) Garnet compositions in garnet-rich rocks (garnetites) are related to variations in bulk rock chemistry. UIF garnets have high Mn, and low Fe and Ca, relative to LIF garnets.

2) Manganoan cummingtonite-grunerites from the UIF are similarly enriched in Mn relative to LIF cummingtonite-grunerites.

3) Because UIF rocks dominantly comprise garnet plus grunerite, UIF bulk compositions are likely to be Mn-rich. This is supported by available whole rock compositional data (Chapter 4).

4) Although depleted in Mn relative to UIF, LIF garnets still have an important Mn component (c.15At%) indicating that they are enriched in Mn relative to all other rock types at Bigstone other than the UIF.

It is concluded that precursor bulk rock chemistry has an over-riding control on the compositions and compositional variations shown by major silicate minerals in LIF and UIF and that the fugacities of O_2 and S_2 may have been buffered by the mineral assemblages during metamorphism.

4.2.4 Chloritoid Zone

The minerals chloritoid, garnet, tourmaline, gahnite and feldspar from the Chloritoid Zone, along with tourmaline from the Hanging Wall Graphitic Schist, and feldspar from the QFP, have been analysed (Appendix 3.2) and furnish the following details:

1) Chloritoid

The average chloritoid contains:

At%Fe 88.60 ± 2.94

At%Mg 8.05 ± 2.18

At%Mn 3.37 ± 0.98

n=21

Chloritoid is thus iron-rich, with a minor and variable component of both Mg and Mn. Where it coexists with garnet it has lower magnesium (mean Fe/Mg = 15.9) and manganese (mean atom% Mn = 2.8) than when garnet is absent from the assemblage (mean Fe/Mg = 8.5, atom% Mn = 4.2).

2). Garnet

Compositions are highly variable, and many more analyses would be needed to provide reliable coverage of the zone. Nevertheless, it is noted that the most iron-rich garnets encountered in the entire deposit sequence occur within heavily mineralised rocks of the Chloritoid Zone.

3). Tourmaline

Blue-green tourmalines from the Chloritoid Zone (Figure 4.11) are relatively Fe-rich (schorl) compared to both brown, Mg-rich (dravite) tourmalines from the Hanging Wall Graphitic Schist, and those reported from other massive sulphide deposits (data from Slack, 1980).

4) Gahnite

This mineral has a relatively consistent composition with an average ZnAl_2O_4 component of 80.67% (± 0.71) in solid solution with hercynite (FeAl_2O_4). The magnesium end member (MgAl_2O_4 , spinel s.s.), is not present at Bigstone, thus the presence of an Mg-rich environment (Spry and Scott, 1986), is not indicated. Zoned gahnites have a slight core to rim enrichment in the hercynite component (Appendix 3.3). Such a zoning

pattern is analogous to increases in Fe from core to rim in zoned metamorphic garnets (Spry, 1987), and forms by crystallisation during a prograde event.

5). Plagioclase

Feldspar compositions from the immediate footwall and the Mineralised Horizon (Figure 4.12) span a relatively wide range, with a clustering of oligoclase-andesine compositions. Individual samples may also show a wide range in composition eg. sample no. 200 contains separate feldspars which range from oligoclase through to labradorite in composition. Both normal and reverse zoning patterns occur within the same section. These features are taken to indicate a lack of equilibration during metamorphism, and lend support to the hypothesis that the rocks were originally tuffaceous.

As was noted earlier (Chapter 2), feldspars (and quartz) from the Mineralised Horizon have anomalous luminescence (green) relative to those of the footwall (blue). Trace element contents were investigated to see if the green luminescence was related to any compositional differences between the two groups. Many more data are needed to fully characterise the trace element contents of the two groups, but available data (see Appendix 3.4 for analytical details and representative analyses) indicate that whereas feldspars in the Footwall rocks contain variable quantities of Fe (from 180 to 7980 ppm) and Zn, Cu and Mn are all below detection levels (500, 400 and 175 ppm respectively), Mineralised Horizon feldspars contain Fe from 540 to 19850 ppm, Cu from < 400 to 1750 ppm, Zn from < 500 to 1380 ppm and Mn from < 175 to 770 ppm. It is tentatively concluded that anomalous green luminescence in plagioclase indicates the presence of anomalous quantities of base metals, and thus may have potential as an exploration guide. It is interesting in this respect to note the descriptions of anomalously yellow luminescent, copper-bearing, feldspars described from Zambian Copper-belt rocks by Sweeney (1985).

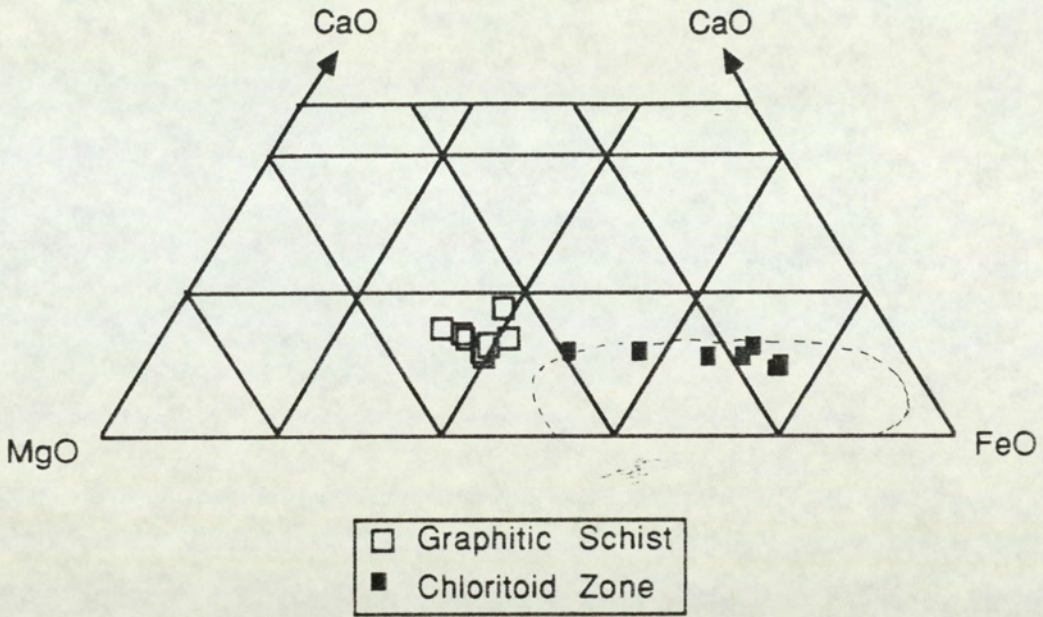


Figure 4.11 Tourmaline from the Bigstone sequence compared with the field of massive sulphide-associated tourmalines (from Slack, 1982)

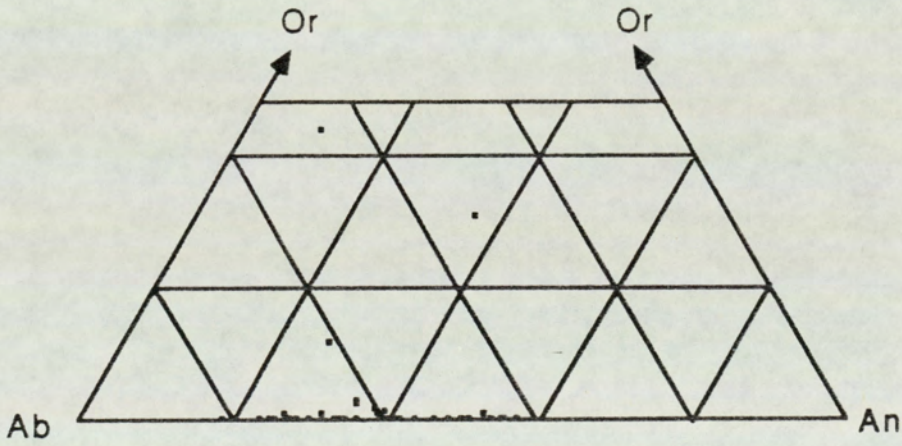


Figure 4.12 Feldspar compositions from Footwall and Mineralised Horizon rocks. Total number of plotted points is 38; total number of samples is 10.

4.3 METAMORPHIC REACTIONS.

The purpose of this section is to describe possible reactions for the observed mineral assemblages in the Bigstone deposit, and to interpret these assemblages in terms of the general conditions of peak metamorphism.

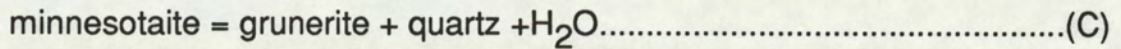
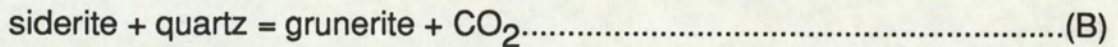
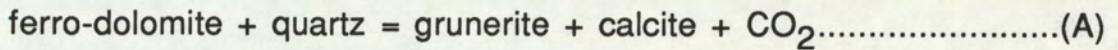
4.3.1 Iron Formation

A large number of researchers have described the effects of progressive metamorphism upon Superior-type iron formation, (Klein, 1966, 1973, 1978, 1982; Miyano, 1978; Frost, 1979, 1982; French, 1968; Floran and Papike, 1978,). Reactions leading to the formation of many mineral assemblages, particularly those of low metamorphic grades, are reasonably well established. Garnet-, and hornblende-bearing iron formation of the Superior-type has been described by Floran and Papike (1978), Immegea and Klein (1976), Klein (1976) and Haase (1982b). However Superior-type iron-formation is not commonly Al-rich, and as a result the various reactions involving Al-rich phases (garnet and hornblende) are less well understood. Smaller scale iron formations of the Algoma-type are typically associated with massive sulphide deposits and are closely associated with volcanism (Stanton, 1976; Vaughan and Stanton, 1986). Such iron formations have some important differences with the larger Superior-type, most notably in their elevated contents of Al_2O_3 , MnO, P_2O_5 , and base metals (Stanton, 1976; Vaughan and Stanton, 1986).

Possible reactions, derived from the above works, which can be directly applied to the Bigstone deposit, are discussed in detail below.

1) Formation of grunerite in UIF

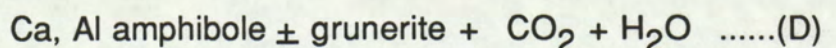
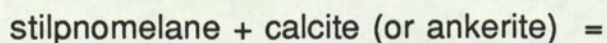
The following reactions are considered important in the generation of grunerite (Klein, 1982):



At Bigstone, grunerite occurs in a wide variety of textural associations, from fine-grained felted masses, through acicular varieties, to large bladed crystals (Chapter 2). This is taken to indicate that it may have formed from more than one precursor phase. Intergrowths of needle-like grunerite with quartz are similar to those described between minnesotaite and quartz (Floran and Papike, 1978) and may indicate operation of the reaction C (cf. Floran and Papike, 1978), whereas bladed grunerite associated with carbonate may indicate the operation of the reactions A and/or B.

2) Formation of hornblende in LIF.

Petrographic observations from a number of iron formations (French, 1968; Floran and Papike, 1978, Haase, 1982) have demonstrated that stilpnomelane is the low-grade precursor mineral to hornblende. This is the most common low-grade iron formation silicate (Klein, 1982), and is the only low-grade phase to carry substantial amounts of K and Na. Floran and Papike (1978) suggested the following reaction (amongst others) involving stilpnomelane:



Floran and Papike (1978) noted that addition of Fe-chlorite (ripidolite) to the reaction (reaction 13 of Haase, 1979) would lead to the formation of increasingly aluminous amphiboles. Such a reaction is proposed for hornblendes of the present study.

3) Formation of garnet in LIF and UIF.

Hornblende- and grunerite-bearing rocks contain large quantities of garnet and thus additional reactions need to be considered in addition to those listed above. Common precursor minerals to garnet are ripidolite (Haase, 1979) and/or chamosite (Stanton, 1976). Stanton (1976) demonstrated that conversion of chamosite to garnet is an essentially isochemical process. At Bigstone, the widespread occurrence of millimetre-wide layers composed of >80% garnet and the preservation of delicate intergrowths between garnet and early hematite (Plate 2.31) were earlier interpreted (Chapter 2) to indicate that precursor compositions were close to those of garnet, and that only limited chemical interaction (reduction) occurred between the precursor phases and adjacent oxide minerals. These observations are consistent with the direct derivation of garnet from a chamosite (or ripidolite) precursor phase.

It is suggested that iron formation at Bigstone was probably derived from a ripidolite- and/or chamosite-rich precursor containing important components of carbonate, oxides, stilpnomelane and, locally, sulphides. The most important difference between LIF and UIF was probably the presence of stilpnomelane and calcite in the former, leading to widespread hornblende-bearing assemblages, and the presence of manganoan precursor iron carbonates and/or silicates in the latter.

4.3.2 Chloritoid zone.

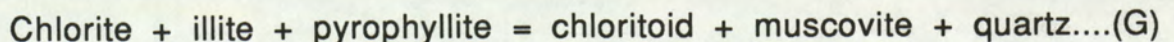
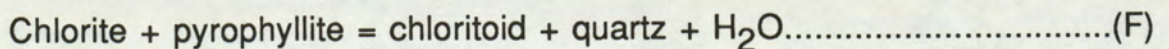
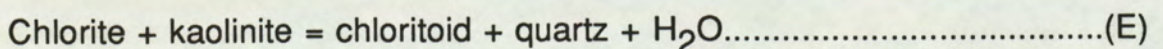
The diagnostic assemblage developed within the Chloritoid Zone is:

Chloritoid + muscovite + quartz ± garnet + sulphides + oxides

Halferdahl (1961), considered the paragenesis of chloritoid, and subdivided its occurrence into five associations, one of which was its presence in hydrothermally altered rocks. More recently, chloritoid has been described as an important phase in the footwall alteration (feeder) zones of a number of volcanogenic ore deposits. Amongst these the Helen siderite deposit in the Michipicoten belt of Ontario is the most striking example (Morton and Nebel, 1984). Other examples include the Matabi deposit, Ontario (Franklin *et.al.* 1975) and the Teutonic Bore deposit in Australia (Hallberg and Thompson, 1985). One factor common to all of these deposits is their location within felsic-rich pyroclastic sequences.

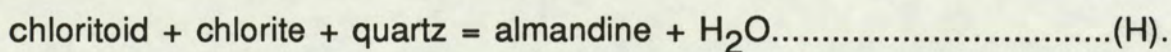
At Bigstone, the stratigraphically restricted occurrence of chloritoid to narrow portions of the Copper Body (Figure 2.4), and adjacent to exhalative sediments (LIF and UIF) has been interpreted to indicate that Chloritoid Zone rocks represent narrow feeder zone lithologies developed at, or near the sea floor (Chapter 2).

Chloritoid is considered to form from reactions involving chlorite and aluminium silicates in rocks with high Fe/Fe+Mg and low alkali contents (Winkler, 1979). The following reactions are considered possible at Bigstone:



Reactions E and F (Hoschek, 1969) were considered by Siedel and

Okrusch (1975) less likely to occur than reactions involving minerals of the mica/illite group. Reaction G (Chouder *in* Deer *et.al.*, 1986), has a lateritic ferruginous clay as the precursor rock type. A similar bulk composition might be envisaged for heavily altered footwall rocks of the present study. Assemblages containing almandine and chloritoid are typical of regionally metamorphosed pelites from the 'garnet zone' (Winkler, 1979) and indicate the following reaction, (Thompson and Norton, 1968):

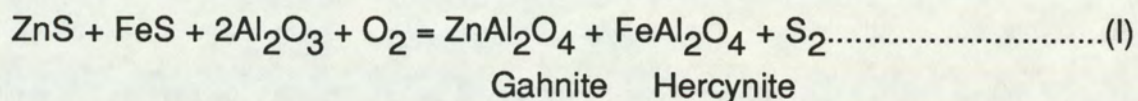


This reaction requires both a low $f\text{H}_2\text{O}$ and the presence of chlorite in excess of that required to form chloritoid. The sporadic occurrence of garnet-bearing assemblages at Bigstone, suggests these two conditions may have been achieved only locally within the Chloritoid Zone.

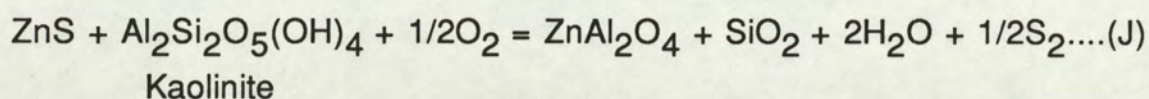
It is concluded that, prior to metamorphism, altered rocks of the Mineralised Horizon were characterised by the presence of abundant Fe- and Al- rich silicates, along with Fe-oxide and Fe-sulphide minerals, and that chloritoid was derived from reactions between the silicates. This hypothesis fits well with the petrographic evidence, which indicates that chloritoid is preferentially developed in feldspar-bearing rocks. In some specimens it appears to have nucleated within plagioclase crystals (Plate 2.11), from which it is concluded that Al-bearing and/or Fe-bearing precursor minerals were present within feldspar prior to metamorphism. Feldspars of the Mineralised Horizon may thus have undergone acid hydrolysis during mineralisation leading to the development of Al-rich minerals which later reacted during metamorphism to form chloritoid. The presence of both feldspar, and the metamorphosed products of its alteration (chloritoid, mica) within the Chloritoid Zone, is interpreted to suggest that the process of hydrolysis never went to completion.

Gahnite has a close spatial relationship with assemblages containing appreciable quantities of sphalerite and Al-bearing silicates (Chapter 2).

It may form as a product of desulphuration during metamorphism (Wall and England, 1979; Spry and Scott, 1986). Spry and Scott(1986) described a number of gahnite-forming reactions, including:



and,



The common development of both gahnite and chloritoid in rocks of the Chloritoid Zone indicates that reactions G and J may have operated simultaneously in zinc-rich parts of the Chloritoid Zone.

4.4 AN ASSESSMENT OF PEAK METAMORPHIC CONDITIONS

Assemblages containing chloritoid ± garnet, cummingtonite + garnet; hornblende + garnet; and hornblende + actinolite (in footwall rocks) are consistent with conditions in the garnet zone of the greenschist facies (Winkler, 1979; Klein,1982; Robinson et.al., 1982). The presence of the **assemblage margarite + quartz** in some rocks of the Chloritoid Zone indicates pressures >4kb at temperatures around 500⁰C (Winkler,1979). Equilibrium assemblages containing pyrite, pyrrhotite and sphalerite are generally not developed at Bigstone, it has not therefore been possible to use the sphalerite geobarometer (Scott,1973). Measurements of sphalerite co-existing with ferro-tschemakite in one sample (No. 764), indicate average mole %FeS compositions of 13.86 ± 0.86. Such compositions give pressure estimates, using the equation of Hutchinson and Scott, (1980) which vary between 6.5kb and 4.8kb within the one sample. This is taken to imply that a_{FeS} has not been buffered during metamorphism. Application of the garnet-hornblende geothermometer of

Graham and Powell (1984) produces unreliable estimates probably because most analysed garnets contain >10 At% Mn.

From the above considerations, peak metamorphic conditions at Bigstone are suggested to have been within the range 450⁰-500⁰C and > 4kb.

CHAPTER 5: DISCUSSION AND CONCLUSIONS

5.1 CLASSIFICATION OF MINERAL DEPOSITS

The purpose of this section is to review various classification schemes for Precambrian base metal sulphide deposits, and to summarise the main features associated with the Bigstone deposit, leading to the generation of a general model for its evolution. The conclusions are then applied to other parts of the Hanson Lake Block in a re-examination of known rock types and mineral showings.

A wide variety of schemes have been developed in an attempt to classify Precambrian volcanogenic deposits (Sangster, 1972; Hutchinson, 1973; Franklin *et al.*, 1981; Lydon, 1984). Recently, Franklin (1986) has delineated the following three types of deposit:

1a) A Copper-Zinc (Cu-Zn) group, which includes deposits formed in mafic-dominated sequences eg. Cyprus-type deposits, Besshi-type deposits, and Noranda-type deposits.

1b) A subgroup of type 1a), containing a minor lead component eg. the Mattabi and Kidd Creek deposits (Franklin and Thorpe, 1982), and termed the Cu-Zn (Pb) group.

2) A Zinc-Lead-Copper (Zn-Pb-Cu) group, developed in felsic-dominated sequences, and typified by Kuroko-type deposits. Other examples include those of the Iberian Pyrite Belt, the Bathurst deposits of New Brunswick, and Paleozoic deposits of the Tasman geosyncline.

Many deposits in the Flin Flon belt are developed within mafic-dominated sequences, and are of Cu-Zn-(Pb) type (Franklin and

Thorpe, 1982). The Bigstone deposit is extremely impoverished in Pb (no galena has been found in any studied section or core), and, would be classified as of Copper-Zinc type. However, it contains a number of features which contrast with those occurring in the Flin Flon area. The most notable of these are:

1) Mineralised rocks at Bigstone have a conspicuous association with silicate facies (former silicate-carbonate-oxide facies) iron formation. According to Franklin and Thorpe (1982), one characteristic feature of deposits of the Flin Flon belt is their lack of association with iron formations. The iron-formation developed at Bigstone is similar to those described from a large number of deposits around the world, including the iron ore deposits of the Helen Mine, Michipicoten, Ontario (Goodwin, 1964, Goodwin et.al, 1985); the Pegmont Zn-Pb deposit, Australia (Vaughan and Stanton, 1986); the Aggeneys-Gamsberg Pb-Zn deposits, South Africa (Rozendal, 1978). These iron formations are probably the metamorphic equivalents of iron carbonate and iron silicate strata similar to those forming in hydrothermally active areas at the present day (Pottorf and Barnes, 1983). Their apparent scarcity in the Flin Flon belt is thus considered somewhat anomalous.

2) Mineralisation at Bigstone occurs within a series of felsic pyroclastic flow deposits which contain primary, lapilli-size, pyroclastic fragments and subordinate mafic flows and/or sills. The deposit sequence is overlain by a sequence of generally unaltered crystal-lithic tuffs. Typical deposits in the Flin Flon area are developed within mafic-dominated sequences (Koo and Mossman, 1975; Price, 1977; Franklin and Thorpe, 1982), although some, eg, the Anderson Lake Mine in

the Snow Lake area (Walford and Franklin, 1982), have felsic-dominated footwall sequences. Many of the massive sulphides are finely layered pyrite-, or pyrrhotite-rich bodies zoned upwards from a copper-rich base to a zinc-rich top eg. Flin Flon, (Koo and Mossman, 1975). Such bodies are thought to have formed as chemical precipitates from brine pools on the ancient sea floor (Sangster, 1972). At Bigstone, except for the presence of thin (<0.5m) high-grade sphalerite layers, massive sulphides sensu stricto are essentially absent from the sequence, and mineralisation is inferred to have taken place largely within a series of felsic pyroclastic rocks. Where hydrothermal fluids reached the surface at Bigstone, they deposited carbonate-silicate iron formation (LIF) largely devoid of base metals.

3) The alteration systems typically occurring in deposits of the Flin Flon area are Mg chlorite-rich, copper-bearing pipes developed below the massive sulphide horizon (Franklin and Thorpe, 1982). In this respect, they show close affinities with alteration developed beneath Archean Noranda-type deposits of the Superior Province (Sangster, 1972; Franklin and Thorpe, 1982). At Bigstone, alteration is developed on the same stratigraphic level as mineralisation, and is zoned with a copper-rich Silicified Zone, similar in many respects to 'keiko' ore of Kuroko-type deposits (Eldridge, et.al., 1983), and a lateral Fe-rich, chloritoid bearing zone. The chloritoid is thought to have developed during metamorphism from reactions involving hydrous aluminium silicates and iron-rich chlorite (Chapter 4). The mineralogy and composition of the alteration zone at Bigstone is strikingly similar to a growing number of descriptions of mineral deposits, including the Helen Mine (Morton and

Nebel, 1984), the Mattabi deposit (Franklin et.al, 1975), and the Teutonic Bore deposit in Australia (Hallberg and Thompson, 1985).

Recently, Morton and Franklin (1987) proposed a two-fold classification for Archean massive sulphide deposits into Noranda-type and Mattabi-type. The two types display fundamental differences in terms of the type of volcanism and the style of alteration associated with mineralisation.

1. Noranda-type deposits

Deposits of the this type commonly formed at water depths >500m, within sequences containing >50% mafic material. Both mafic and felsic volcanic rocks have only a small component of fragmental lithologies. Alteration pipes associated with these deposits commonly extend several hundred metres into the footwall and are distinctly zoned from chlorite + quartz cores, to sericite plus quartz margins (Urabe et.al, 1983). The chlorite is typically Mg-rich, and is thought to have formed from extensive interaction between Mg-poor hydrothermal fluid, and Mg-rich seawater (Urabe et.al, 1983, Franklin, 1986; Morton and Franklin 1987). At high metamorphic grades (amphibolite facies), the Noranda-type alteration assemblage is characterised by the development of cordierite-anthophyllite rocks, eg. at the Coronation mine in the Flin Flon belt (Froese, 1969). In a few examples, alteration pipes extend downwards to lower semi-conformable alteration zones which are up to thousands of metres thick and several kilometres long (MacGeehan and MacLean, 1980; Gibson et.al, 1983; Franklin, 1986; Morton and Franklin 1987). These zones may have been the reservoir units for metal-rich hydrothermal fluid (Morton and Franklin, 1987).

Notwithstanding differences in age, many deposits in the Proterozoic Flin Flon belt are considered to have close similarities to the Archean Noranda -type deposits.

2. Mattabi-type deposits

Mattabi-type deposits occur within sequences dominated by felsic fragmental rock types, including hydro-volcanic tuffs, massive and bedded pyroclastic flows, dome and flow breccias, welded ash flows and epiclastic rocks. Subordinate mafic rocks comprise pillowed and non-pillowed flows, hyaloclastites and mafic tuffs. Detailed studies of volcanic stratigraphy in well-preserved sequences (Morton and Nebel, 1983) have been interpreted to indicate that volcanism took place at shallow (<500m) water depths. Alteration pipes beneath Mattabi-type deposits are poorly defined. They are generally wider, and less distinctly zoned, than those of the Noranda-type. Alteration assemblages comprise iron chlorite, iron carbonate, sericite and quartz. Chloritoid (up to 75% of the rock) is a major constituent of metamorphosed deposits of this class and the presence of excess alumina during metamorphism may have led to the development of large quantities of aluminosilicate minerals (kyanite, sillimanite). The iron-rich nature of the alteration has been interpreted to suggest that there was only limited interaction between the ascendant hydrothermal fluid and sea water (Urabe et.al., 1983; Franklin, 1986; Morton and Franklin 1987). Various mechanisms have been suggested to account for the lack of interaction, these include; the sealing of hydrothermal systems by silicification, preventing prolonged interaction with Mg-rich seawater (Urabe et.al., 1983); the absence of Mg-rich water in the vicinity of the hydrothermal system (Urabe, et.al.,

1983); and the less marked effect of the drawdown of Mg-rich seawater in shallow water (Franklin, 1986). Lower, semi-conformable, alteration zones are developed at higher stratigraphic levels than those of the Noranda-type (Morton and Franklin, 1987), and may occur on the same stratigraphic level as the mineralisation itself (Franklin, 1986). Alteration minerals are similar to those occurring within the alteration pipes, but ankerite is present rather than siderite (Morton and Franklin, 1987). According to Franklin (1986), carbonatisation of footwall strata may be related to the segregation of a low-density CO₂-rich fluid from a high density metalliferous brine. The reaction between this CO₂-rich phase and cold seawater would cause the precipitation of a blanket of carbonate at or near the surface, preceding the main mineralisation event (Franklin, 1986). The carbonate layer is later metasomatised by the passage of the mineralising fluid to form iron carbonates (Franklin, 1986).

The Bigstone deposit sequence shows a close affinity to deposits of the Mattabi-type but differs mainly in that, carbonate is generally absent from feeder zone rocks, and is only sporadically developed in footwall rocks. Carbonate rocks are inferred to have been present (or are still present) within iron-formation units. The Lower Iron Formation (LIF) forms a continuous blanket beneath mineralised rocks and is interpreted as the high-level equivalent of the lower, semi-conformable, carbonate-rich alteration zone which may occur along the same stratigraphic horizon as mineralisation itself (Franklin 1986). The absence of carbonate minerals in the presumed feeder zone at Bigstone, is interpreted to indicate that Eh, pH conditions (acid and/or reduced) were outside the stability range of carbonate minerals. Thus, it is

suggested that CO₂-rich fluids were highly focalised within the feeder zone, and that carbonate deposition occurred only upon interaction with cold seawater.

The general absence of carbonates from feeder zone and footwall rocks at Bigstone could also be explained by considering reactions between early formed carbonates and plagioclase feldspars during metamorphism to produce the more Ca-rich plagioclases characteristic of low to medium metamorphic grades (Winkler, 1979).

5.2 A MODEL FOR BIGSTONE MINERALISATION

Consideration of the main features of Mattabi-type deposits, along with those of the Bigstone deposit has led to the generation of a tentative evolutionary model for the deposit (Figure 5.1a,b,c,d). The actual development of mineralisation is envisaged as a continuous process developed over a short period of time, however, it is convenient to subdivide the process into a number of stages:

STAGE 1

The first stage (Figure 5.1a) involves emplacement of a series of felsic pyroclastic flows, with subordinate mafic flows and/or sills. Hydrothermal circulatory systems are initiated at some unspecified depth. A CO₂-rich phase may have separated from a metalliferous brine (cf Franklin, 1986) producing deposition of the LIF as layers of silicates and carbonates blanketing the footwall rocks.

STAGE 2

Following deposition of LIF, volcanic activity produced large

quantities of tuffs (of the Mineralised Horizon) which swamped the hydrothermal system (Figure 5.1b). The hydrothermal regime then begins to re-establish itself as the more dense metalliferous hydrothermal brine is channelled towards the surface.

STAGE 3

Stage 3 represents the main mineralising event (Figure 5.1c). Rather than venting to the sea floor, the ascendant dense mineralising fluids encountered porous and permeable feldspathic tuffs of the Mineralised Horizon. Reactions proceeded between the fluid and the host rocks being most intense in the fluid source region. Alteration via acid hydrolysis and silicification produced the quartz-sericite assemblage of the Silicified Zone. An increase in the pH of the fluid and a decline in temperature initiated deposition of chalcopyrite along with minor zinc and iron sulphides. The residual fluid moved outwards along the unit and became enriched in Zn, Fe, Mn (and the feldspar components, Ca, Na, Sr). Further increases in pH and declining T initiated deposition of zinc and iron sulphides and iron silicates in the Chloritoid Zone. Petrographic and mineralogical evidence (Chapters 2 and 4) suggests that this zone represents an area of arrested hydrolysis. Relict plagioclase was heavily altered, probably to kaolinite \pm chlorite, which was later to react during metamorphism to form the abundant chloritoid and gahnite. Reactions between the metalliferous fluid and the feldspars caused Fe and Cu (plus minor Zn and Mn) to be incorporated within the feldspar lattice, perhaps accounting for the anomalous blue luminescence of mineralised feldspars. Temperature gradients at the margins of the Mineralised Horizon tuffs are inferred to have been large, leading to the effective separation

Figure 5.1a

STAGE 1

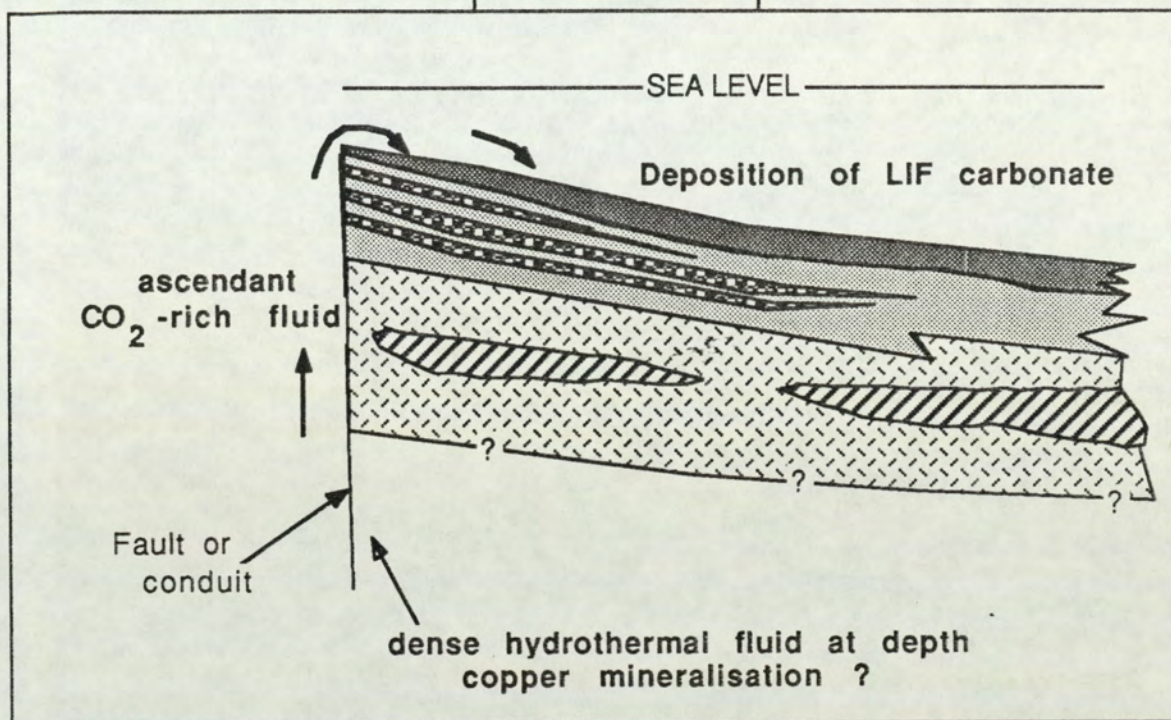


Figure 5.1b

STAGE 2

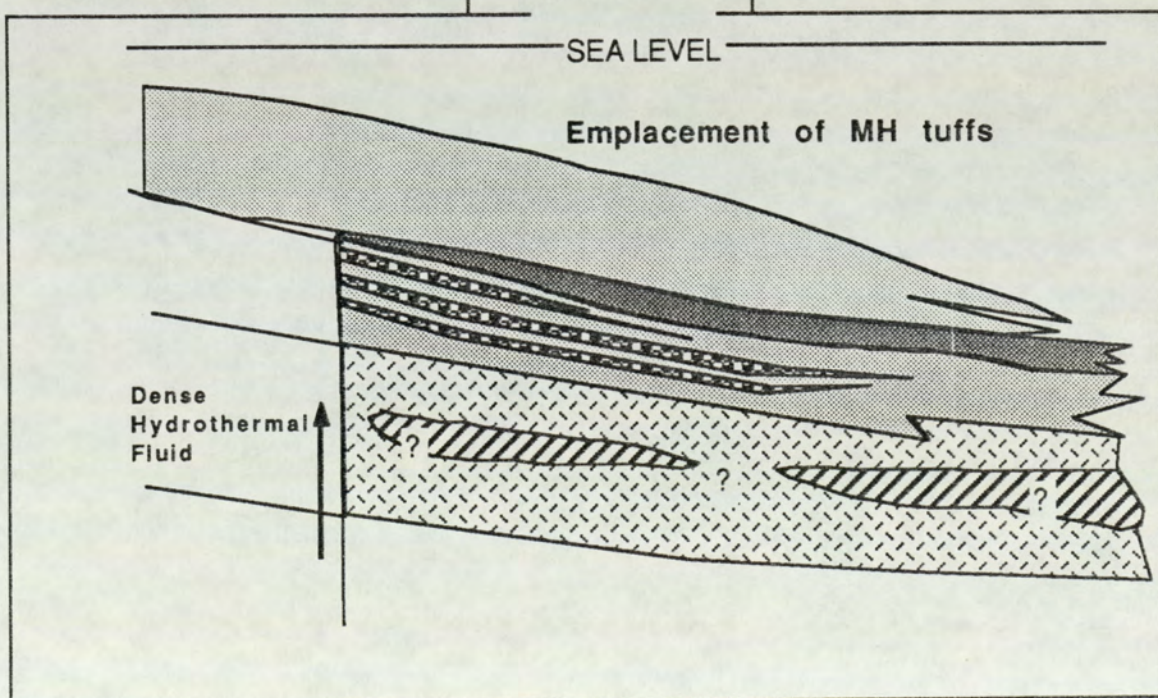


Figure 5.1c

STAGE 3

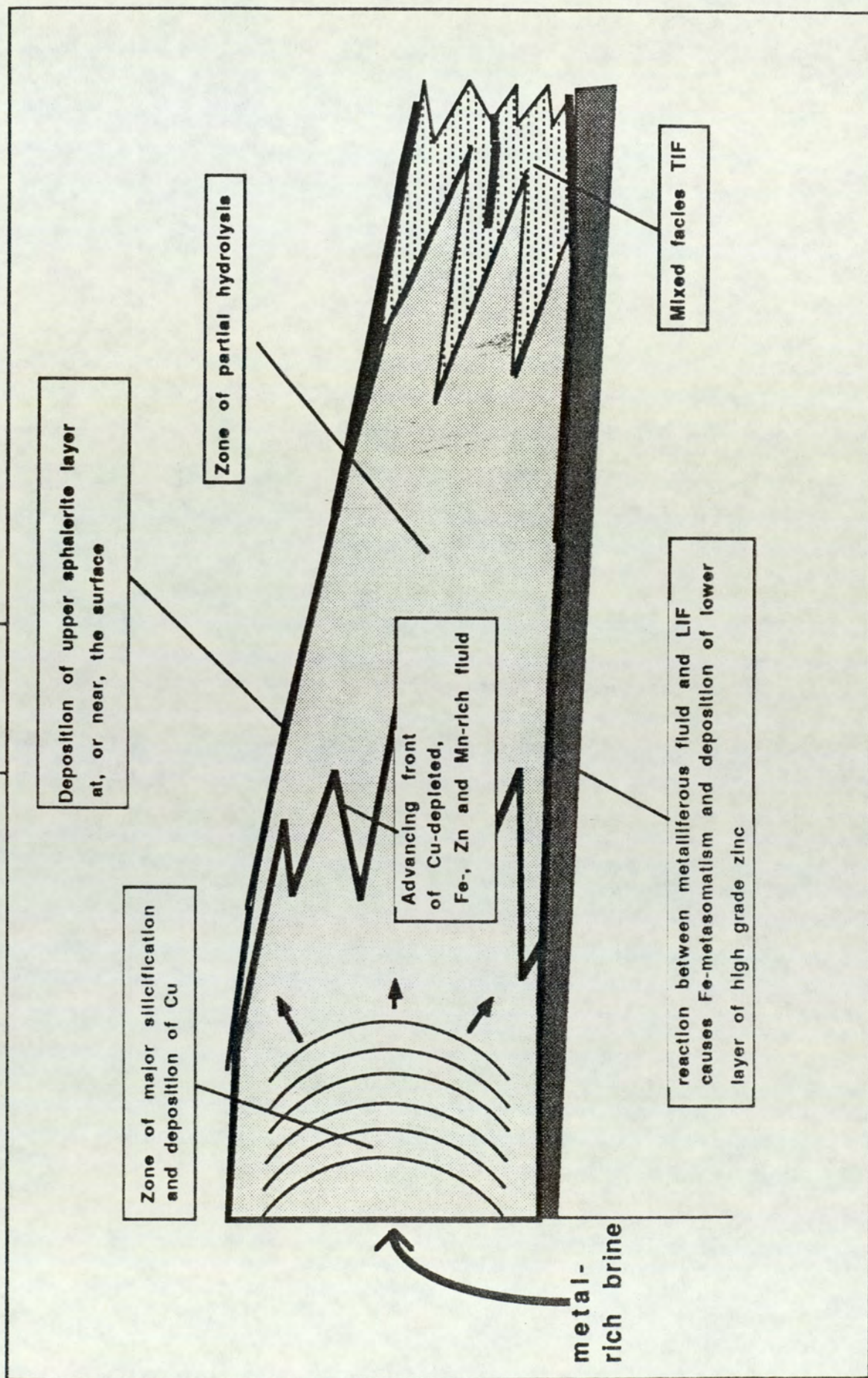
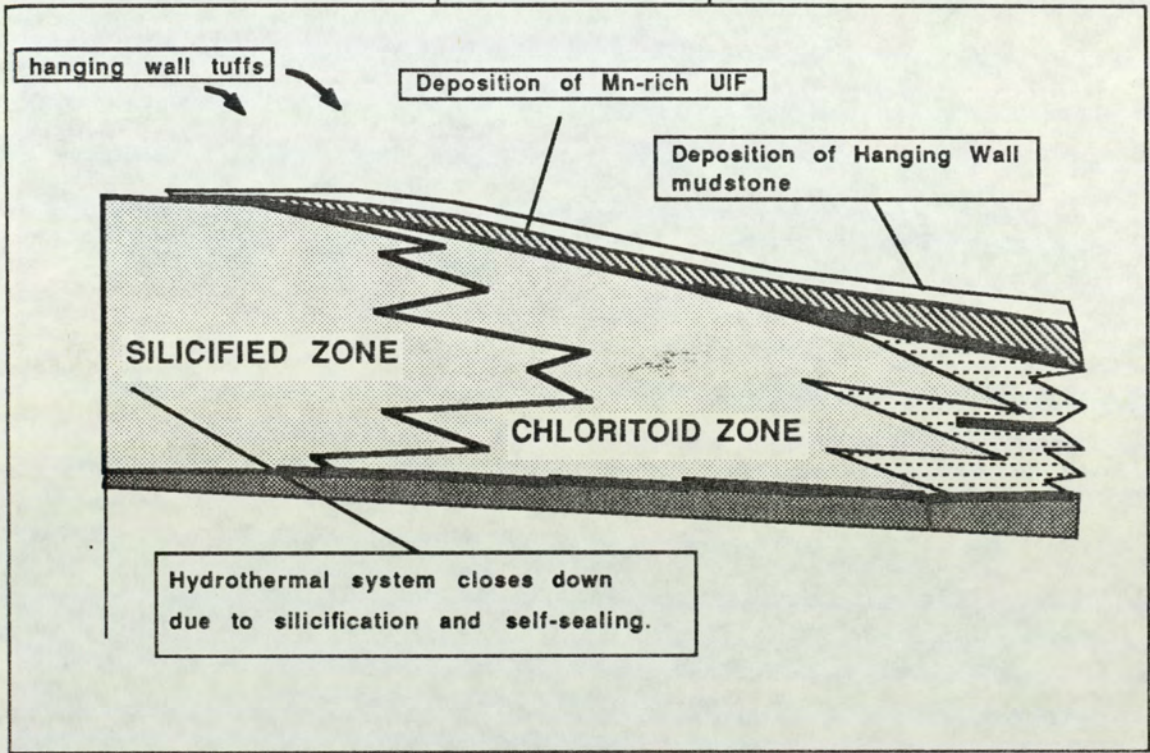


Figure 5.1d

STAGE 4



KEY

- | | | | |
|---|-----------------------------|---|---------------------------------|
|  | QUARTZ-EYE PORPHYRY |  | LOWER IRON FORMATION |
|  | FOOTWALL MAFIC UNIT |  | SPHALERITE MINERALISATION |
|  | MINERALISED HORIZON TUFFS |  | UPPER IRON FORMATION |
|  | INTERMEDIATE LAPILLI TUFFS |  | HANGING WALL GRAPHITIC MUDSTONE |
|  | TRANSITIONAL IRON FORMATION |  | FELDSPAR-CRYSTAL TUFFS |

Figure 5.1a to d Proposed evolutionary sequence for the Bigstone deposit.

of Zn from Cu, and causing the deposition of thin, marginal sphalerite layers, similar to the encrustations of sphalerite described from the Detour Cu-Zn deposit (Deptuck, et.al. 1982). At the lower margin of the unit, metalliferous fluid may have reacted with LIF to form an Fe-rich, carbonate-silicate assemblage and a lower layer of high-grade sphalerite mineralisation. An alternative, less favoured, interpretation is that the lower sphalerite layer was formed during deposition of the LIF, prior to emplacement of the tuffs of the Mineralised Horizon This alternative is rejected because coeval copper mineralisation and feeder zone lithologies in the underlying QFP, and manganese-rich iron-formation overlying the lower sphalerite layer are absent.

Lateral to the MH unit, the mineralising fluid was deposited in a mixed facies rock (TIF) representing the transition from clastic-dominated to chemical-dominated environments, which contains a detrital feldspathic component, a base metal component, and an iron formation component (Chapter 2).

STAGE 4

The stage (Figure 5.1d) represents the waning of the mineralisation event. Manganese-rich iron formation (UIF), deposited on top of the Mineralised Horizon tuffs, and is considered to be similar to the Mn-rich units which overlie many other types of deposit eg, the Mn shales overlying deposits of the Iberian Pyrite Belt (Schermerhorn, 1970), the umbers of Cyprus-type deposits (Robertson and Hudson, 1973), and chemical sediments of presently active hydrothermal areas (Pottorf and Barnes, 1983).

A period of quiescence followed, during which graphitic mudstone (later to become the Graphitic Schist) was deposited as a cap to the

deposit. The mudstone contains clasts of mineralised rocks containing Mg-tourmaline, derived from the erosion of nearby (?) mineralisation(s). The entire sequence was then covered by a sequence of felsic tuffs containing minor mafic material.

General environment of deposit formation

Geochemical data are interpreted to indicate that pyroclastic rocks of the Footwall and Mineralised Horizon were developed in a caldera environment associated with a high-level magma chamber (Chapter 3). Such environments are characterised by bimodal (basalt-rhyolite) volcanism and the extensive development of silicic ignimbrites. The ignimbrite-forming eruptions are generally associated with major structural changes associated with caldera collapse. Caldera collapse occurs during, or after eruption around a circular ring fracture formed above the depleted magma chamber. The central parts of the caldera may then undergo doming associated with a resurgent stage of magma emplacement. Smith and Bailey (1968) identified seven stages in caldera development based on studies of the Valles caldera, New Mexico:

- a) generation of ring fractures
- b) ignimbrite eruption
- c) caldera collapse
- d) pre-resurgence ring volcanism and intra-caldera sedimentation
- e) resurgent doming
- f) major ring fracture volcanism
- g) terminal fumarolic activity

Within ignimbrite sequences, there may exist a complex variety of

lithologies. Stratigraphic relationships are also likely to be complex, as each eruption fills an erosional surface cut into the older succession (Cas and Wright, 1987). Crystal-rich silicic ignimbrites in such environments may indicate near-vent emplacement from a high level magma chamber (Cas and Wright, 1987).

Submarine resurgent calderas have been proposed as the principal site for the generation of Kuroko-type massive sulphide deposits (Sillitoe, 1980; Hodgson and Lydon, 1977) where the presence of highly permeable rocks, ring structures and high level plutons leads to the establishment of convective hydrothermal systems.

Spence and De Rosen-Spence (1975) recognised that many Archean massive sulphide deposits were emplaced above rhyolite flows within a caldera structure. Similar associations have been noted for deposits in Fiji, Bathurst, New Brunswick, Buchans, Newfoundland, New South Wales and in the Roseberry area of Tasmania (Sillitoe, 1980).

At Bigstone, mineralisation is associated with bimodal volcanism, and crystal rich tuffs developed in the Footwall. In addition, co-linear trends involving Ti and Zr in rocks of the QFP and Mineralised Horizon indicate that both were derived from a single magma chamber undergoing fractionation of zircon. The high degree of correlation between Ti and Zr in both units is interpreted to indicate that contamination from coeval pyroclastic rocks has been minimal. The tuffs are therefore thought to have been erupted near to their source, possibly within the caldera structure. Such a location would serve as an effective barrier from onlapping pyroclastic rocks, and allow the development of a post-eruptive environment conducive to mineral deposit formation.

It is concluded that the deposit was formed within a shallow level

(<500m ?) caldera environment developed within an island arc having geochemical affinities with primitive arcs of the present day.

Source of Metals

It is not possible, with presently available data, to constrain the source of metals for the Bigstone deposit. However, the following speculations are made:

1) Footwall Mafic Unit rocks are heavily depleted in copper (see Chapter 3), and it is possible that this metal may have been leached from it and incorporated into the ore fluid.

2) The lead poor nature of the deposit may indicate that:

either a) Suitable lead-rich rocks were not present within the zone of hydrothermal leaching, or, if a magmatic origin for ore metals is considered, Pb was not present in a primary magmatic ore fluid. Lead-rich deposits are less likely to form within a primitive arc environment due to the absence of an appreciable (Pb-rich) crustal component.

or b) Lead may have been originally present in the ore fluid, and may have separated from the rest of the fluid, and deposited (or lost) elsewhere, in a manner analogous to the separation of Zn from Cu. This allows the possibility that distal lead-rich deposits, similar to those of the iron formation-associated deposits of the Pegmont area in Australia (Vaughan and Stanton, 1986), may be developed along the same stratigraphic horizon.

5.3 IMPLICATIONS FOR EXPLORATION IN THE FLIN FLON BELT

Consideration of the main features of the Bigstone deposit, and others of the related Mattabi-type (Morton and Franklin, 1987), leads to the identification of the following features which may indicate the proximity of similar mineralisation elsewhere in the Flin Flon belt:

1) The presence of felsic-rich pyroclastic sequences, with the local development of patchy carbonate-rich and/ or Fe-silicate alteration. Linear depletions of Ti and Zr (Chapter 3) within felsic rocks, whether caused by hydrothermal activity, or by primary igneous processes, may indicate the proximity of favourable ore-forming environments.

2) Mineralised rocks are associated with the metamorphosed equivalents of iron-rich strata. At the grades of metamorphism present within the belt (upper greenschist to amphibolite), such lithologies are likely to contain minerals such as garnet, grunerite, iron-rich pyroxene, and possibly olivine, along with abundant iron oxides and carbonates. Iron- and calcium-rich units ie. the equivalents of the lower, semi-conformable, zones of Mattabi-type deposits may be present as extensive calc-silicate horizons containing abundant hornblende and garnet along with varying proportions of other iron-rich silicates, oxides and carbonates

3) Alteration (feeder) zones associated with mineralisation may be conformable, and composed of iron rich silicates \pm carbonates. At upper greenschist grades, the local development of large quantities of chloritoid associated with a distinctive accessory mineralogy including tourmaline (Fe-, or Mg-rich), fluorite, apatite and gahnite, is considered to be a strong indication of the proximity of mineralisation. At higher metamorphic grades, chloritoid is replaced by staurolite, and thus the

restricted occurrence of staurolite-bearing rocks, particularly when associated with iron-rich units, may be equivalent to the feeder zone assemblages developed within the Chloritoid Zone at Bigstone.

The above criteria have been applied to a re-examination of various known rock types, and associated mineralisation, in the western part of the Flin Flon belt (the Hanson Lake and Deschambault Lake areas).

The eastern part of the Hanson Lake area contains a N-S trending belt of metasomatised felsic rocks (Gaskarth, 1967) termed the Agnew Bay-Bluebird Island zone by Smith (1970). Metasomatism was defined by the presence of shearing, abundant garnet and segregations of pale green amphibole up to 2cm in diameter (Coleman and Gaskarth, 1970). The belt trends northwards from the, now worked out, Hanson Lake Mine over a strike length in excess of 1km, and contains a number of strong Zn anomalies (Coleman and Gaskarth, 1970; Smith 1970).

The ore horizon at the Hanson Lake Mine is within a unit of recrystallised tuffs, containing layers rich in garnet, biotite, chlorite and green mica, which are chemically similar to rocks mapped as 'metasomatised volcanics' (Smith, 1970).

Parallel to, and overlying, rocks of the Agnew Bay-Bluebird Island zone are a belt of calc-silicate rocks (Gaskarth, 1967; Coleman and Gaskarth, 1970) which, according to Smith (1970), show chemical affinities with the Amisk-type metasediments with which they are interbedded. In the northern part of the area these metasediments contain thin interlayers of iron formation, with up to 2.4% MnO located within unidentified silicate phases (Smith 1970). Descriptions of mineral deposits in the Hanson Lake area (Clark, 1955; Byers, 1957) contain a number of Zn-Cu showings in close association with

garnetiferous units. Clark (1955) describes "1-inch" thick sphalerite veins (from HBM&S prospect number 2) interbedded with basic and siliceous tuffs. The basic rocks are garnet-rich and contain a fibrous green amphibole (interpreted by Clark as tremolite). Refractive index measurements by Clark (1955) indicate that the garnet contains >80% of the spessartine molecule.

The following conclusions are quoted directly from Smith (1970, p127) concerning the association of felsic volcanics, mineralisation and metasomatised rocks in the eastern Hanson Lake area:

(1) Pervasive magnesia metasomatism involving leaching of CaO from volcanic rocks by emanations from intrusive rhyolite porphyry might have caused precipitation of calcite from hot-springs on the overlying sub-aqueous (or sub-aerial) surface.

(2) After subsequent burial of the calciferous rocks, they, in turn, might have been metasomatised by later or continuing emanations from underlying intrusions of rhyolite porphyry, with concomitant deposition of calcite on still higher surfaces.

(3) The latest precipitation by this process formed the Young Peninsula unit of calc silicate rocks. It was not metasomatised because metasomatizing emanations from underlying porphyries had abated or changed in their chemical nature before the burial of the unit under the overlying greywackes.

(4) Zinc-bearing solutions continued to rise, and they locally enriched the Young Peninsula unit of calciferous rock and the contemporaneous Young Peninsula Tuff in Zn.

Smith's conclusions are almost identical to the evolutionary sequence of events suggested above for the Bigstone deposit, and the general model recently proposed for all Mattabi-type deposits by Morton and Franklin, 1987). Thus, the Hanson Lake deposit was of the Mattabi-type, and the Mn-rich rocks containing Mn-garnet along with fibrous green amphiboles (grunerites?), iron-rich calc-silicate strata and garnetiferous 'metasomatised felsic volcanics' are closely analogous to the UIF, LIF, and TIF rocks of the Bigstone sequence.

Further to the west, in the Deschambault Lake area, Padgham (1968) described rocks with "large garnets and radiating tremolite" (his unit 6b)

associated with a Cu-Zn showing on the western shore of the northwest arm of Deschambault Lake. Padgham also describes a "most unusual rock" (his unit 4a) containing "large splotches of tremolite and 1-inch garnets", and narrow staurolite-rich, lenticular bodies of limited aerial extent which occur on the same stratigraphic level as rocks containing red (2mm-3mm) garnets and acicular amphiboles (his unit 4f). These units may have affinities with lower grade chloritoid-, and garnet-bearing rocks described from the Bigstone sequence.

It is concluded that the unusual lithologies associated with mineralisation at Bigstone may also be developed in other parts of the Flin Flon belt, and that the recognition of such rocks may have important exploration potential in the region.

5.4 SUMMARY OF CONCLUSIONS

1) The Bigstone deposit occurs within a sequence of felsic pyroclastic rocks, of presumed shallow water origin, developed in a caldera-type environment. Mafic rocks from the footwall sequence and from the adjacent NLA to the north indicate an overall environment similar to those of present-day primitive island arcs.

2) Geochemical and mineralogical studies point to the presence of a) distinctive iron-rich, and chloritoid-bearing alteration assemblages within chemically zoned altered tuffs of the Mineralised Horizon, and b) mineralogically distinctive chemical sediments of the Uppper and Lower Iron Formations.

3) The deposit has many of the characteristics of Mattabi-type deposits (Morton and Franklin, 1987) hitherto unrecognised within the Flin Flon greenstone belt.

4) An examination of published data from adjacent areas points to a number of localities containing similar assemblages to those of the Bigstone deposit, which are thus worthy of further study.

REFERENCES

- Bachinski, D. J., 1976. Metamorphism of cupriferous iron sulfide deposits, Notre Dame Bay, Newfoundland. *Econ. Geol.*, v. 71, p. 443-452.
- Bailes, A.H. and McRitchie, W.D., 1978. The transition from low to high grade metamorphism in the Kisseynew sedimentary gneiss belt, Manitoba. In *Metamorphism in the Canadian Shield*. Frazer, J.A. and Heywood, W.W. (Eds). *Geol. Surv. Can. Pap.* 78-10, p. 155-177.
- Bokhari, F.Y. and Kramers, J. D., 1981. Island arc character and late Precambrian age of volcanics at Wadi Shwas, Hijaz, Saudi Arabia; geochemical and Sr and Nd isotopic evidence. *Earth Planet. Sci. Lett.* v. 54, p. 409-422.
- Burton, K. W., 1986. Garnet-quartz intergrowths in graphitic pelites: the role of the fluid phase. *Min. Mag.* v. 50, p. 611-620.
- Byers, A.R., 1957. Geology and mineral deposits of the Hanson Lake area, Saskatchewan. Saskatchewan Dept. of Mineral Resources, Report No. 30, 47p.
- Byers, A.R. and Dahlstrom, C.D.A, 1954. Geology and mineral deposits of the Amisk-Wildnest Lakes area, Saskatchewan. Sask. Dep. Mineral Resources report 14, 177p.
- Cas, R.A.F and Wright, J.V., 1987. Volcanic successions ancient and modern. Allen and Unwin, London. 528p.
- Clark, L.A., 1955. Sulphide deposits of the Hanson Lake area. Univ. of Saskatchewan Dept. of Geology. unpub M.Sc. thesis.
- Coleman, L. C. and Gaskarth, J. W., 1970. Geology and geochemistry of the Hanson Lake Area, Saskatchewan. Part I: Geology: Saskatchewan Research Council Rep. No. 10, p. 7-86.

- Deer, W. A., Howie, R. A. and Zussman, J., 1986. Rock Forming Minerals: Volume 1A: Orthosilicates: New York, John Wiley & Sons, 321p.
- Deptuck, R., Squair, H. and Wierzbicki, V., 1982. Geology of the Detour zinc-copper deposits, Brouillan Township, Quebec. In Precambrian massive sulphide deposits: Hutchinson, R. W., Spence, C. D. and Franklin, J. M. (Eds). Geol. Assoc. Can. Spec. Paper. 25.
- Eldridge, S. C., Barton, Jr. P. B. and Ohmoto, H., 1983. Mineral textures and their bearing on the formation of the Kuroko orebodies. Econ. Geol. Monograph 5, p. 241-281.
- Ewart, A., 1979. A review of the mineralogy and chemistry of Tertiary-Recent dacitic, latitic, rhyolitic and related salic rocks. In Trondhjemites, dacites and related rocks., Barker, F. (Ed.). Elsevier, New York, p. 13-122.
- Finlow-Bates, T. and Stumpfl, E.F., 1981. The behaviour of so-called immobile elements in hydrothermally altered rocks associated with volcanogenic submarine-exhalative ore deposits. Mineral. Deposita. v. 16, p. 319-328.
- Floran, R. J. and Papike, J. J., 1978: Mineralogy and petrology of the Gunflint Iron Formation, Minnesota-Ontario: Correlation of compositional and assemblage variations at low to moderate grade. J. Petrol., v. 19, p. 215-288.
- Franklin, J. M., 1986. Volcanic associated massive sulphide deposits-an update. Irish Assoc. Economic Geology Spec. Pub. 4, p. 49-69.
- Franklin, J. M. and Thorpe, R. I., 1982. Comparative metallogeny of the Superior, Slave and Churchill Provinces. In Precambrian massive sulphide deposits. Hutchinson, R. W., Spence, C. D. and Franklin, J. M. (Eds). Geol. Assoc. Can. Spec. Paper. 25.

- Franklin, J. M., Kasarda, J. and Poulsen, K. H., 1975. Petrology and chemistry of the alteration zone of the Mattabi massive sulphide deposit. *Econ. Geol.*, v. 70, p. 63-79.
- Franklin, J. M., Lydon, J. W. and Sangster, D. F., 1981. Volcanic associated massive sulphide deposits. In *Econ. Geol. 75th anniversary volume*, Skinner, B. J. and Sims, P. K. (Eds.), p. 485-627.
- Frater, K. M., 1985. Mineralisation at the Golden Grove Cu-Zn deposit, Western Australia. 1: Premetamorphic textures of the opaque minerals. *Can. J. Earth. Sci.*, v. 22, p. 1-14.
- French, B. M., 1968. Progressive contact metamorphism of the Bibiwak Iron Formation, Mesabi Range, Minnesota. *Minn., Geol. Surv. Bull.*, v. 45, 103pp.
- Froese, E., 1969. General Geology of the Coronation mine area: *Geol. Surv. Can.*, Paper 68-5, p. 7-35.
- Frost, B. R., 1979. Metamorphism of iron formation: Parageneses in the system Fe-Si-C-O-H. *Econ. Geol.*, v. 74, p. 775-785.
- Frost, B. R., 1982. Contact metamorphic effects of the Stillwater Complex, Montana: The concordant iron-formation: A discussion of the role of buffering in metamorphism of iron-formation. *Am. Mineral.*, v. 67, p. 142-148.
- Fox, J.S., 1977. Silica normalisation of drill hole geochemical data from volcanic rocks of the Hanson Lake Mine, Saskatchewan. *Sask. Res. Council. Geol. Div. Circ. No. 10* (unpaginated).
- Gaskarth, J. W., 1967. Petrogenesis of Precambrian rocks in the Hanson lake area, East-Central Saskatchewan. Unpublished Ph.D thesis, University of Saskatchewan, Saskatoon.

- Gaskarth, J.W., and Parslow, G.R.. Proterozoic volcanism in the Flin Flon greenstone belt, east-central Saskatchewan, Canada. In Geochemistry and Mineralisation of Proterozoic Volcanic Suites. Geol. Soc. Spec. Pub. No. 33, pp. 183-200.
- Gibson, H. L., Watkinson, D. H. and Comba, C. D. A., 1983. Silicification: Hydrothermal alteration in an Archean geothermal system within the Amulet Rhyolite Formation, Noranda, Quebec. *Econ. Geol.*, v. 78, p. 954-971.
- Goodwin, A. M., 1964. Geochemical studies at the Helen iron range. *Econ. Geol.*, v. 59, p. 684-718.
- Goodwin, A. M., Thode, H. G., Chou, C. -L. and Karkhansis, S. N., 1985. Chemostratigraphy and origin of the late Archean siderite-pyrite-rich Helen Iron Formation, Michipicoten belt, Canada: *Can. J. Earth Sci.*, v 22, p. 72-84.
- Graham, C.M. and Powell, R., 1984. A garnet-hornblende geothermometer: calibration, testing and application to the Pelona schist, Southern California. *J. Metamorphic Geol.* v.2, p 12-31.
- Gresens, R.L. 1967. Composition-volume relationships of metasomatism. *Chem. Geol.*, v.2., p. 47-65.
- Haase, C.S., 1982a. Phase equilibria in metamorphosed iron-formations: Qualitative T-X(CO₂) petrogenetic grids. *Am. J. Sci.*, v 282, p. 1623-1655.
- Haase, C.S., 1982b. Metamorphic petrology of the Negaunee Iron Formation, Marquette district, northern Michigan: Mineralogy, metamorphic reactions and phase equilibria. *Econ. Geol.*, v. 77, p. 60-81.
- Halferdahl, L. B., 1961. Chloritoid: Its composition, X-ray and optical properties, stability and occurrences. *J. Petrol.*, v. 49, p. 49-135.

- Hallberg, J. A. and Thompson, J. F. H., 1985. Geologic setting of the Teutonic Bore massive sulfide deposit, Archean Yilgarn Block, Western Australia. *Econ. Geol.*, v. 80, p. 1953-1964.
- Hildreth, W., 1981. Gradients in silicic magma chambers: Implications for lithospheric magmatism. *Jour. Geophys. Res.*, v. 86, p. 10153-10192.
- Hoschek, G. 1969. The stability of staurolite and chloritoid and their significance in metamorphism of pelitic rocks. *Contr. Mineral. Petrol.* v.22, p 208-232.
- Hutchinson, R. W., 1973. Volcanogenic sulphides and their metallogenic significance. *Econ. Geol.*, v. 68, p.1223-1246.
- Hutchinson, M. N. and Scott, S. D., 1980. Sphalerite geobarometry applied to metamorphosed sulfide ores of the Swedish Caledonides and U.S. Appalachians. *Geol. Norges. Unders. No. 360*, p. 59-71.
- Immege, I. P. and Klein, C., 1976: Mineralogy and petrology of some Precambrian iron-formations in southwestern Montana. *Am. Mineral.*, v. 61, p. 1117-1144.
- Irvine, T. N. and Baragar, W. R. A., 1971. A guide to the chemical classification of the common volcanic rocks. *Can. J. Earth Sci.*, v. 8, p. 523-548.
- Kelly Vance, R. and Condie, K.C., 1987. Geochemistry of footwall alteration associated with the early Proterozoic United Verde massive sulphide deposit, Jerome, Arizona. *Econ. Geol.* v.82, p 571-586.
- Klein, C., 1966. Mineralogy and petrology of the metamorphosed Wabush Iron Formation, southwestern Labrador. *J. Petrol.*, v.7, p. 240-305.

- Klein, C., 1973. Changes in mineral assemblages with metamorphism of some banded Precambrian iron-formations. *Econ. Geol.*, v. 68, p. 1075-1088.
- Klein, C., 1978. Regional metamorphism of Proterozoic iron-formation, Labrador Trough, Canada. *Am. Mineral.*, v. 63, p. 898-912.
- Klein, C., 1982. Diagenesis and metamorphism of Precambrian iron-formations., p. 417-469. In *Precambrian Iron Formations*, Elsevier, Amsterdam.
- Koo, J. and Mossman, D. J., 1975. Origin and metamorphism of the Flin Flon stratabound Cu-Zn sulfide deposit, Saskatchewan and Manitoba. *Econ. Geol.*, v.70, p. 48-62.
- Laajoki, k. and Saikkonen, R., 1977. On the geology and geochemistry of the Precambrian iron formations in Väyryläänkyä, south Poulanka area, Finland: *Bull. Geol. Surv. Finland.* no. 292, p. 1-137.
- Leake, B.E., 1978. Nomenclature of amphiboles. *Can. Mineral.* v.16, p. 501-520.
- Lewry, J.F., 1981. Lower Proterozoic arc-microcontinent collisional tectonics in the western Churchill Province. *Nature*, v. 294, No. 5836, p. 69-72.
- Lewry, J.F, and Sibbald, 1977. Variation in lithology and tectonometamorphic relationships in the Precambrian basement of Northern Saskatchewan. *Can. J. Earth Sci.* v. 14, p. 1453-1467.
- Lewry, J.F, and Sibbald, 1980. Thermotectonic evolution of the Churchill Province in Saskatchewan. *Tectonophysics*, v. 68, p. 45-82.

- Lewry, J.F., Sibbald, T.I.I. and Schledewitz, 1985. Variation in the character of Archean rocks in the western Churchill Province and its significance. In Evolution of Archean Supracrustal Sequences (Ayres, L.D., Thurston, P.C., Card, K. and Weber, W. (Eds). Geol. Assoc. of Canada. Spec. Pap. 28, p. 239-261.
- Lydon, J. W., 1984. Ore deposits models-8. Volcanogenic sulphide deposits. Part 1: A descriptive model. Geoscience Canada, v. 11, p. 195-202.
- Mahood, G. A., 1981. Chemical evolution of a Pleistocene rhyolitic centre: Sierra La Primavera, Jalisco, México. Contrib. Mineral. Petrol., v. 77, p. 129-149.
- MacGeehan, P. J. and MacLean, W. H., 1980. An Archean sub-seafloor geothermal system, "calc-alkali" trends, and massive sulphide genesis. Science, V. 286, no. 5775, p. 767-771.
- Miyano, T., 1978. Phase relations in the system Fe-Mg-Si-O-H and environments during low-grade metamorphism of some Precambrian iron-formations. J. Geol. Soc. Japan., v 84, p.679-690.
- Morton, R. L. and Nebel, M. L. 1983. Physical character of Archean felsic volcanism in the vicinity of the Helen iron mine, Wawa, Ontario, Canada. Precamb. Res., v. 20, p. 954-971.
- Morton, R. L. and Nebel, M. L. 1984. Hydrothermal alteration of felsic volcanic rocks at the Helen siderite deposit, Wawa, Ontario. Econ. Geol. v. 79, p. 1318-1333.
- Morton, R. L. and Franklin, J. M., 1987. Two-fold classification of Archean volcanic-associated massive sulfide deposits. Econ. Geol., v. 82, p. 1057-1063.

- Nesbitt, B. E., 1982. Metamorphic sulfide-silicate equilibria in the massive sulfide deposits at Ducktown, Tennessee. *Econ. Geol.*, v. 77, p. 364-378.
- Nesbitt, B. E., 1986a. Oxide-sulfide-silicate equilibria associated with metamorphosed ore deposits. Part 1: Theoretical considerations. *Econ. Geol.*, v. 81, p. 831-840.
- Nesbitt, B. E., 1986b. Oxide-sulfide-silicate equilibria associated with metamorphosed ore deposits. Part 2: Pelitic and felsic volcanic terrains. *Econ. Geol.*, v. 81, p. 841-856.
- Nesbitt, B. E. and Kelly, W. C., 1982. Metamorphic zonation of sulfides, oxides, and graphite in and around the orebodies at Ducktown, Tennessee. *Econ. Geol.*, v. 75, p. 1010-1021.
- Nilsen, O., 1978. Caledonian sulphide deposits and minor iron-formations from the southern Trondheim region, Norway. *Norges. geol. Unders.* v. 340, p. 35-85.
- Padgham, W.A., 1968. The Geology of the Deschambault Lake District. Sask. Dep. of Mineral Resources Report 114, 92pp.
- Parslow, G.R. and Gaskarth, J.W., 1984. Geochemistry of the east Amisk area. Saskatchewan Energy and Mines Open File Rep. 84-23, 156p.
- Parslow, G.R. and Gaskarth, J.W., 1986. Geochemistry of the Hanson Lake Area. Saskatchewan Energy and Mines Open File Rep. 86-1, 106p.
- Papike, J.J., Cameron, K. L. and Baldwin, K., 1974. Amphiboles and pyroxenes: characterisation of other than quadrilateral components, and estimates of ferric iron from microprobe data (abstr.). *Geol. Soc. America Abstr. with Prog.* v. 6, p1053.

- Pearce, J.A., 1982. Trace element characteristics of lavas from destructive plate boundaries. In Andesites. Thorpe, R. S. (Ed.). John Wiley & Sons, New York, p. 525-548.
- Pearce, J.A. and Gale G.H., 1977. Identification of ore deposition environment from trace-element geochemistry of associated igneous host rocks. In Volcanic processes in ore genesis. Geol. Soc. Lond. Spec. Pub. No. 10. p14-24.
- Pearce, J. A. and Norry, M. J., 1979. Petrogenetic implications of Ti, Zr, Y and Nb variations in volcanic rocks. *Contr. Mineral. Petrol.* v. 69, p. 33-47.
- Pearce, J.A., 1983. Role of the sub-continental lithosphere in magma genesis at active continental margins. In Continental basalts and mantle xenoliths. Hawkesworth, C.J. and Norry, M.J. (Eds.). Shiva Publishing, Cheshire. p. 230-249.
- Peterson, M.D., 1983. The use of the "immobile" elements Zr and Ti in lithogeochemical exploration for massive sulphide deposits in the Precambrian Pecos greenstone belt of northern New Mexico.
- Popp, R. K., Gilbert, M. C., and Craig, J. R., 1977. Stability of Fe-Mg amphiboles with respect to sulfur fugacity. *Am. Mineral.*, v. 62, p. 13-30.
- Pottorf, R. J. and Barnes, H. L., 1983. Mineralogy, geochemistry and ore genesis of hydrothermal sediments from the Atlantis II Deep, Red Sea. *Econ. Geol. Monograph* 5, p. 198-223.
- Price, D., 1977. Tour guide, Flin Flon-Snow Lake geology. *Can. Inst. Mining and Metall.*, 55pp.

- Robinson, P., Spear, F. S., Schumacher, C., Laird, J., Klein, C., Evans, B. W. and Doolan, B. L., 1982. Phase relations of metamorphic amphiboles. Natural occurrence and theory. *Min. Soc. Am. Reviews in mineralogy*, v. 9B, p. 1-211.
- Robertson, A.H.F, and Hudson J.D., 1973. Cyprus umbers: chemical precipitates on a Tethyan ocean ridge. *Earth. Planet. Sci. Lett.* v 18, p 93-101.
- Rock, N.M.S, 1987. A FORTRAN program for tabulating and naming amphibole analyses according to the International Mineralogical Association scheme. *Mineralogy and Petrology*, v.37, p 79-88.
- Rozendaal, A., 1978. The Gamsberg zinc deposit, Namaqualand. In *Mineralisation in metamorphic terrains*, Verwoerd, W. J. (Ed.): Spec. Pub. Geol. Soc. South Africa., no. 4, p 235-265.
- Sangster, D. F., 1972. Precambrian massive sulphide deposits in Canada. A review: *Geol. Surv. Can. Paper 72-22*, 44pp.
- Sangster, D. F. and Scott, S. D., 1976. Precambrian stratabound massive Cu-Zn-Pb sulfide ores of North America. In *Handbook of strata-bound and stratiform ore deposits.*, Wolf, K. H. (Ed.), Elsevier, Amsterdam, p. 129-222.
- Saunders, A. D., Tarney, J. and Weaver, S. D., 1980. Transverse geochemical variations across the Antarctic Peninsula: Implications for calc-alkaline magma genesis. *Earth planet. Sci. Letters*, v.46, p. 344-360.
- Schermerhorn, L. J. G., 1971. An outline stratigraphy of the Iberian Pyrite Belt. *Spain Inst. Geol. Minero. Bol. Geol. Minero.* v.82, p. 25-52.
- Scott, S.D., 1973. Experimental calibration of the sphalerite geobarometer. *Econ. Geol.*, v. 68, p. 466-474.

- Scott, S.D., 1982. Seafloor polymetallic sulfide deposits: Modern and ancient. *Marine Mining*, v.5, p.191-212.
- Sibbald, T.I.I., 1986. Overview of the Precambrian geology and aspects of the metallogenesis of Northern Saskatchewan. In *Economic Minerals of Saskatchewan*, Gilboy, C. F. and Vigrass, L.W. (Eds.). Saskatchewan Geol. Soc. Spec. Pub. No. 8. p. 1-16.
- Siedel, E. and Okrusch, M., 1975. Chloritoid-bearing metapelites associated with glaucophane rocks in W. Greece. *Contrib. Mineral. Petrol.*, v.49, p105-115.
- Sillitoe, R.H., 1980. Are porphyry copper and Kuroko-type massive sulfide deposits incompatible ? *Geology*, v. 8, p.11-14.
- Slack, J. F., 1982. Tourmaline in Appalachian-Caledonian massive sulphide deposits and its exploration significance. *Trans. Inst. Mining and Metall.*, v. 91, p. B81-B89.
- Smith, J. R., 1970. Geology and geochemistry of the Hanson Lake Area, Saskatchewan: Part II: Geochemistry. Saskatchewan Research Council Rep. no. 10, p. 87.
- Smith, R. L., 1979. Ash-flow magmatism: *Geol. Soc. Am. Sp. Pap.* 180., p. 5-27.
- Smith, R.L. and Bailey, R.A., 1968. Resurgent calderas. In *Studies in volcanology* (Coats R.R, Hay, R.L and Anderson, C.A., eds), *Geol. Soc. Am. Mem.* no. 116., pp. 83-104.
- Spence, C.D. and de Rosen-Spence, A.F., 1975. The place of sulfide mineralisation in the volcanic sequence at Noranda, Quebec. *Econ. Geol.* v. 70, p. 90-101.
- Spry, P. G., 1987. Compositional zoning in zincian spinel. *Can. Mineralogist*, v. 25, p 97-104.

- Spry, P. G. and Scott, S. D., 1986. The stability of zincian spinels in sulfide systems and their potential as exploration guides for metamorphosed massive sulfide deposits. *Econ. Geol.*, v. 81, p. 1446-1463.
- Stanton, R. L., 1976. Petrochemical studies of the ore environment at Broken Hill, New South Wales, parts 1, 2, 3 and 4. *Trans. Instn. Min. Metall.*, v. 85, p B33-B46, B118-B131, B132-B141, B221-B233.
- Stanton, R. L. and Williams, K. L., 1978. Garnet compositions at Broken Hill, New South Wales, as indicators of metamorphic processes: *J. Petrol.* v. 19, p. 514-529.
- Stauffer, M.R., Mukherjee, A.C. and Koo, J., 1975. The Amisk Group: an Aphebian? island arc deposit. *Can. J. Earth. Sci.*, v.12, p. 2021-2035.
- Sweeney, M. A., 1985. Diagenetic processes in ore formation with special reference to the Zambian Copperbelt and Permian Marl Slate. Unpub. Ph.D. Thesis. University of Aston in Birmingham.
- Tarney, J., Weaver, S. D., Saunders, A. D., Pankhurst, R. J. and Barker, P. F., 1982. Volcanic evolution of the northern Antarctic Peninsula and the Scotia arc. *In* Andesites. Thorpe, R. S. (Ed.). John Wiley & Sons, New York., p. 371-400.
- Thompson, J. B. and Norton, S. A., 1968. Paleozoic regional metamorphism in New England and adjacent areas. *In* Studies of Appalachian Geology: E-An Zen et.al. (eds.), John Wiley & Sons, New York.
- Thurlow, J. G., Swanson, E. A. and Strong, D. F., 1975. Geology and lithogeochemistry of the Buchans polymetallic sulphide deposits, Newfoundland. *Econ. Geol.*, v. 70, p. 130-144.
- Tso, J. L., Gilbert, M. C., and Craig, J. R., 1979. Sulfidation of synthetic biotites. *Am. Mineral.*, v. 64, p. 304-316.

- Urabe, T., Scott, S. D. and Hattori, K., 1983. A comparison of footwall-rock alteration and geothermal systems beneath some Japanese and Canadian volcanogenic massive sulphide deposits. In Economic Geology Monograph 5, Ohmoto, H and Skinner, B. J. (Eds.), p. 507-522.
- Vaughan, J. P. and Stanton, R. L., 1986. Sedimentary and metamorphic factors in the development of the Pegmont stratiform Pb-Zn deposit, Queensland, Australia. *Trans. Inst. Mining and Metall.*, v. 95, p. B94-B121.
- Vernon, R. H., 1986. Evaluation of the "quartz-eye" hypothesis. *Econ. Geol.*, v. 81, p. 1520-1527.
- Walford, P. C. and Franklin, J. M., 1982. The Anderson Lake Mine, Snow Lake, Manitoba. In Precambrian massive sulphide deposits, Hutchinson, R. W., Spence, C. D. and Franklin, J. M. (Eds.). *Geol. Assoc. Can. Spec. Paper 25*, p. 481-523.
- Walker, G. P. L., 1972. Crystal concentration in ignimbrites. *Contrib. Mineral. Petrol.*, v. 36, p. 135-146.
- Wall, V.J. and England, R. N., 1979. Zn-Fe spinel-silicate-sulphide reactions as sensors of metamorphic intensive variables and processes (abstr.). *Geol. Soc. America. Prog. with Abstr.* v. 11, p. 354.
- Winkler, H. G. F., 1979. *Petrogenesis of metamorphic rocks*. New York, Springer-Verlag, 334 pp.

Appendix 1

The geology of the North Limestone Area (after Padgham, 1968) is shown in Figure 1.3 (main text). Superimposed on the geology are the positions of various traverse lines along which 1kg rock samples were collected. Samples referred to in the text and/or other appendices are prefixed by their traverse number; eg, D4-1 refers to the first sample taken from traverse number 4. The following samples were collected:

Traverse No. 4 (from north to south) D4-25 through D4-39

Traverse No. 5 (circular, anticlockwise) D5-40 through D5-47

Traverse No. 6 (from south to north) D6-48 through D6-55

Traverse No.7 (from south to north) D7-57 through D7-70

Traverse No. 10 (from west to east) D10-1 through D10-76

Individual samples can be located by referring to the field map, permanently stored in the Dept. of Geological Sciences at Aston University.

The location of various drill holes sampled in the study are shown in Figure 1.2, along with the surface projection of the e.m. anomaly, and the grid system employed by Granges. The location of various samples used in the thesis is tabulated overleaf. Tabulation is carried out according to:

- a) The source diamond drill hole
- b) The depth (in metres from the drill collar), from which the sample was collected.
- c) sample number

Various samples contain either the suffix 'b', or 'w', where 'b' refers to a sample from which both a thin section and a whole rock geochemical analysis were prepared, and 'w' refers to a sample where only whole rock analyses are available. Sample numbers carrying no suffix refer to those for which only thin sections were prepared.

BS30	depth	BS45	depth	BS35	depth	BS42	depth
2	72.5	92b	55.5	200	56.6	274	140.2
3	78.4	94b	57.8	201	58.5	275	142.8
5	86.0	96	60.8	203	61.0	276	144.8
7b	88.0	97b	68.3	205	64.6	277	145.4
8b	97.6	106b	90.2	206	67.1	278	147.4
9b	103.7	108b	95.6	208	69.5	279	149.1
11	109.3	109b	101.5	209	70.9	280	151.2
				210	71.5	281	152.4
BS30	depth	BS45	depth	212	73.8	282	154.9
				213	75.0	283	154.7
13	116.3	110	103.7	214	75.6	284	157.2
15b	118.6	111	104.4	215	77.4	285	155.2
20	134.0	112b	106.1	216	78.0	286	160.2
21	136.7	113	109.5	217	79.0	287	161.3
23	140.0	114b	111.0	219	80.5	288	163.4
24	145.0	117	117.7	221	82.6		
28	152.4	118b	123.9	222	82.8	BS40v1	depth
31	153.7	119b	124.7	223	84.0		
33	155.6	121b	129.9	224	85.7	1400	187.5
34	156.6	122b	134.5	224	85.7	1402	208.8
36	158.5	123b	134.6	225	87.0	1403	227.4
39	162.8	124b	137.2	227	89.6	1404	229.3
41	164.6	126b	148.8	228	90.2	1405	230.6
46	168.4	129b	157	228	90.2	1406	230.8
49	169.6	130b	159.5	230	91.8	1407	233.7
52	172.0	133b	166.2	231b	92.8	1408	232.9
53	172.7	134b	169.4	233b	95.7	1433	267.1
54	173.3	136b	174.2	234	97.3	1434	268.6
57	174.8	138	184.8	235	98.2	1441	280.8
58	175.2	139b	186.7	237	100.0	1449	296.8
60	176.0	144	197.6	238	100.6	1452	301.8
61b	181.9	147	201.4	239	101.8	1453	302.6
62b	183.8	154	216.6	240	103.4	1454	303.0
63b	184.3	164	227.9	242	108.2	1455	304.7
64	188.8	165	230.6	243	109.5	1456	305.8
65b	190.0	167	232.8	244	110.9	1457	306.3
67b	197.0	168	234.8	245	114.0	1458	307.6
69	201.8	169	236.7	246	118.8	1460	309.1
71	207.0	170	235.2	246	118.8	1462	310.4
72	207.9	172	240.2	247	120.6	1463	311.6
75	211.7	173	241.2	249	123.3		
77	214.5	181	274.4	250	125.0	BS120	depth
78	214.6	193	298.9	251Y	126.0		
81b	220.7	196	303.2	252b	127.4	545	170.1
82b	221.2	91Y	235.7	253b	128.8	546	171.6
84b	223.2	98Y	72.7	254	130.6	548	175.0
87b	228.4	105Y	90.9	255	139.0	550	180.6
89b	223.6	115Y	117.1	256b	134.5	563	206.7
90	230.5	116Y	111.4	257	135.2	568	213.7
1Y	72.5	120Y	128.8	258	136.9	588	252.9
6Y	87.0	127Y	154.3	259	141.0		
16Y	123.0	128Y	155.2	260	142.0	BS64	depth
17Y	126.8	131Y	162.7	262	145.7		
18Y	129.1	132Y	164.2	263	146.0	441Y	58.8
19Y	131.6	135Y	173.2	264	147.0	443Y	59.5
25Y	145.9			265	148.0	445Y	60.7
56Y	174.4	BS119	depth	267	153.5	447Y	61.6
59Y	174.0			268	155.0	448	61.9
68Y	201.5	704	152.9	271	163.0	449Y	62.5
74Y	211.3	705	153.0			453Y	63.7
76Y	212.8	711	161.6	BS37	depth	455Y	64.6
79Y	215.2	716	169.1			457	65.8
83Y	222.9	720	175.5	1245	152.1	459Y	66.2

BS30	depth	BS119	depth	BS37	depth	BS64	depth
---	---	---	---	---	---	---	---
85V	224.7	723	180.8	1251	214.2	461V	67.4
86V	226.8	724	182.6	1308	298.8	463V	70.7
88V	228.7	725	183.1	1309	300.3	467V	77.2
---	---	727	186.3	1311	303.2	469V	80.5
BS121	depth	729	189.0	1312	297.4	470	82.9
---	---	730	190.5	1313	306.9	471V	83.5
749	108.5	732	189.2	1315	307.3	473V	86.3
750	118.6	734	199.7	1316	309.1	475	89.9
751	127.0	---	---	1317	311.9	477V	96.2
753	199.5	BS122	depth	1320	316.3	478	97.0
753	199.5	---	---	---	---	479b	100.0
754	183.5	904	100.0	BS54	depth	481V	115.5
757	202.6	905	89.0	---	---	484	124.7
763	210.5	912	98.2	1328	69.0	485V	132.3
764	211.6	922	118.3	---	---	486	134.5
767	213.7	---	---	BS110*	depth	487	136.6
769	217.5	BS120	depth	---	---	488	139.9
770	219.2	---	---	1181	68.8	489b	141.3
---	---	743	221.3	1182	82.3	490	141.8
BS52	depth	---	---	1183	89.5	491	145.6
---	---	BS40	depth	---	---	493b	152.1
1155	48.5	---	---	BS111*	depth	495b	155.5
1158	76.5	927	238.4	---	---	497	157.3
1159	80.2	928	240.0	1185	45.0	499b	159.6
1160	84.3	944	268.9	---	---	500	162.8
---	---	---	---	BS88*	depth	501V	166.3
BS53	depth	BS42	depth	---	---	502	169.2
---	---	---	---	1192	25.8	503V	173.6
1125	?	815	245.0	1193	30.9	528	151.7
---	---	817	248.8	1194	33.1	---	---
BS118	depth	823	259.5	---	---	---	---
---	---	824	260.2	---	---	---	---
1144	71.6	827	264.8	---	---	---	---
---	---	830	267.2	1197	8.8	---	---
BS75	depth	835	273.6	1201	30.3	---	---
---	---	837	275.8	1202	39.3	---	---
1016V	40.2	839	247.6	---	---	---	---
1017	54.6	840	280.0	BS83*	depth	---	---
1018V	64.6	844	285.7	---	---	---	---
1019V	88.6	851	294.2	1211	30.5	---	---
1020V	107.5	857	302.6	---	---	---	---
1021V	125.9	858	304.3	BS84*	depth	---	---
1022	146.9	859	305.8	---	---	---	---
1024	170.4	---	---	1214	18.9	---	---
1026	200.9	---	---	1215	22.6	---	---
1029	223.5	---	---	1216	26.5	---	---
1031	247.9	---	---	1217	31.4	---	---
1032	262.3	---	---	1218	35.1	---	---
1033	267.8	---	---	---	---	---	---
1034	268.4	---	---	BS86*	depth	---	---
1038	299.5	---	---	---	---	---	---
1042	378.7	---	---	1221	10.5	---	---
---	---	---	---	1224	32.3	---	---
---	---	---	---	---	---	---	---

APPENDIX 2.1: XRF ANALYSIS TECHNIQUES

1. Whole Rock analysis using fused discs.

43 samples were analysed for major elements on fused discs (see Appendix 2.2 for lists of analyses). 0.75g of weighed sample (in dried powder form) is combined with 5.3333 times the measured weight of Johnson and Matthey Spectroflux 105. This is then placed in an oven at 1100°C for 20 minutes. Any weight loss upon cooling is made up by adding Spectroflux. The sample is then re-heated under a meker burner, and formed into a disc using a graphite mould.

Analyses were carried out on a Phillips PW1400 X-ray Spectrometer fitted with a rhodium tube, and calibrated using USGS standards.

2. Trace element analysis using pressed powder pellets

225 samples (Appendix 2.2) were analysed for a range of trace elements (Cr, V, Cu, Ni, Zn, Rb, Sr, Y, Zr, Nb, Ba, Pb). Samples were prepared by adding 1.5g of Bakelite binding agent to 8.5g of dried sample powder. The samples were shaken for a period of 10-15 minutes to ensure homogenisation, and then formed into disc-shaped pellets by applying a load pressure of 20 tons. The pellets were then cured overnight in an oven at 120°C.

The samples were then analysed using a Phillips PW1400 X-ray spectrometer.

3. Precision

Precisions for trace elements are reported in Parslow and Gaskarth (1986). Individual samples were analysed up to 11 times in order to determine analytical precision for major elements, reported below:

Oxide	Standard deviation (%)
SiO ₂	0.22
Al ₂ O ₃	0.13
TiO ₂	0.09
Fe ₂ O ₃	0.05
MnO	0.09
MgO	0.13
CaO	0.05
Na ₂ O	0.05
K ₂ O	0.01
P ₂ O ₅	0.01

4. Major element analysis using pressed powder pellets.

Semi-quantitative analysis of major elements on pressed powder pellets was achieved by generating regression data for an appropriate range of USGS standards incorporating line overlap and matrix corrections, using the existing Phillips software. Analyses were recalculated to 100% (ie. anhydrous) to facilitate comparison with a selected subset of fused disc data which served as a 'control group'. It was thought that this procedure may have the effect of compounding errors for some elements. In order to test this, an estimate of the relative accuracy of the analyses was made by comparing the semi-quantitative data with the same samples analysed by the fused disc method. The two data sets (n=30) were regressed against each other, allowing an estimate of the 'error' involved. Reported below, for each element, is the degree of correlation between the quantitative and semi-quantitative data, and an estimated error, based on the equation of the regression line:

	Quantitative value	Semiquantitative value	%error
SiO₂ r=0.94			
	40.0	41.5	3.8
	50.0	50.4	0.8
	60.0	59.4	1.0
	70.0	68.0	2.9
	80.0	77.0	3.8
TiO₂ r=0.98			
	0.3	0.32	6.0
	0.5	0.51	2.0
	1.0	0.93	7.0
CaO r=0.99			
	5.0	4.95	1.0
	10.0	10.8	8.0
	15.0	16.7	11.0
Na₂O r=0.84			
	1.0	1.3	33.0
	2.0	2.2	10.0
	3.0	3.1	3.3
K₂O r=0.96			
	1.0	1.1	10.0
	2.0	2.1	5.0
	3.0	3.1	3.0
P₂O₅ r=0.99			
	0.1	0.09	10.0
	0.2	0.2	0.0
	0.3	0.31	3.0
	1.0	1.1	10.0
Fe₂O₃ r=0.92			
	5.0	6.5	30.0
	10.0	12.2	22.0
	20	23.5	17.0
MnO r=0.91			
	0.2	0.24	20.0
	0.4	0.52	30.0
	5.0	6.7	38.0

Errors involving elements used extensively in the thesis (mainly SiO_2 and TiO_2) are low, which is considered to validate use of this method for comparison of various rocks. It should be noted that elements associated with a large error have not been used in the text except in the case of iron formation analyses, where they should be treated with due caution.

APPENDIX 2.2 WHOLE ROCK ANALYSES

1. Quantitative (fused disc) data.

Key: F= Footwall Mafic Unit

H= Hanging Wall

Q= Footwall Quartz-Feldspar Porphyry

NLA= North Limestone Area

BIGSTONE QUANT. DATA

Sample no.	F112	F114	F115	F116	F118	F119	F120
SiO2	47.68	48.33	49.09	43.96	48.08	50.40	47.00
TiO2	0.64	0.67	0.58	0.58	0.56	0.61	0.59
Al2O3	15.59	15.85	14.16	14.65	14.86	15.01	14.62
Fe2O3	14.89	14.59	12.53	17.09	13.39	11.37	12.41
MnO	0.21	0.20	0.18	0.20	0.23	0.21	0.21
MgO	6.23	5.84	5.62	4.68	5.65	4.77	5.61
CaO	14.50	12.30	14.20	13.50	15.90	15.00	16.80
Na2O	1.40	1.89	1.86	0.73	0.49	1.55	0.77
K2O	0.30	0.37	0.33	0.75	0.17	0.15	0.24
P2O5	0.15	0.13	0.11	0.11	0.13	0.12	0.12
TOTAL	101.59	100.17	98.66	96.25	99.46	99.19	98.37

Sample no.	F121	F122	F124	F433	F1238	F1239	F1241
SiO2	48.00	47.68	49.59	47.32	48.02	47.63	44.60
TiO2	0.63	0.54	0.63	0.56	0.71	0.63	0.59
Al2O3	16.08	14.28	16.03	14.81	14.71	15.07	13.88
Fe2O3	12.33	11.73	11.00	17.04	16.83	12.88	15.63
MnO	0.19	0.20	0.20	0.19	0.20	0.22	0.16
MgO	5.65	4.98	4.95	5.20	5.28	5.58	4.64
CaO	14.70	17.90	13.60	10.40	10.80	15.00	11.00
Na2O	1.29	0.34	1.93	1.42	1.41	1.23	1.69
K2O	0.31	0.16	0.33	1.17	1.17	0.49	0.73
P2O5	0.11	0.12	0.12	0.11	0.13	0.14	0.13
TOTAL	99.29	97.93	98.38	98.22	99.26	98.87	93.05

Sample no.	F1243	F1244	F1245	H1017
SiO2	47.65	47.63	48.09	51.66
TiO2	0.70	0.70	0.61	0.83
Al2O3	16.94	17.04	14.84	16.12
Fe2O3	14.55	14.57	16.48	13.60
MnO	0.20	0.18	0.16	0.19
MgO	5.25	5.25	4.92	3.77
CaO	12.70	12.70	11.40	8.18
Na2O	1.53	1.56	1.71	1.82
K2O	0.44	0.44	0.75	1.67
P2O5	0.11	0.11	0.14	0.23
TOTAL	100.07	100.18	99.10	98.07

QUANT BS BASAN+ANDESITE

Sample no.	F435	F436	F437	F438	F1237	H1019	H1020
SiO2	53.77	54.88	59.60	55.59	53.08	53.71	55.19
TiO2	0.88	0.83	0.70	0.97	1.09	0.78	0.76
Al2O3	16.34	15.73	17.08	14.79	15.38	16.59	16.33
Fe2O3	13.96	10.12	9.32	13.52	15.50	13.46	12.44
MnO	0.17	0.16	0.12	0.12	0.12	0.19	0.15
MgO	3.17	2.18	2.06	3.29	3.64	3.71	3.52
CaO	7.84	9.49	6.79	5.02	5.26	7.52	7.84
Na2O	2.82	2.95	3.67	2.26	0.02	1.97	1.71
K2O	1.19	0.66	1.11	3.02	2.76	1.98	1.80
P2O5	0.28	0.27	0.18	0.42	0.44	0.25	0.22
TOTAL	100.42	97.27	100.63	99.00	97.29	100.16	99.96

BIGSTONE QUANT. DAC+RHY

Sample no.	Q432	Q439	F1246	H1016
SiO2	68.29	66.98	68.81	63.03
TiO2	0.35	0.42	0.30	0.73
Al2O3	15.95	13.71	16.00	15.88
Fe2O3	2.55	6.86	4.54	8.60
MnO	0.04	0.09	0.08	0.10
MgO	0.99	0.82	2.49	2.00
CaO	3.12	3.69	1.86	5.60
Na2O	4.75	3.77	1.20	2.89
K2O	2.14	2.49	4.17	1.45
P2O5	0.16	0.13	0.14	0.28
TOTAL	98.34	98.96	99.59	100.56

NLA QUANT DATA

Sample no.	B4.28	85.42	85.43	B6.48	B6.50	B6.51	B6.52
SiO2	52.60	48.92	47.66	42.10	40.86	40.84	43.60
TiO2	0.72	0.74	0.47	1.08	1.12	1.17	1.03
Al2O3	15.61	13.99	9.50	8.97	8.10	7.97	8.83
Fe2O3	12.05	12.89	13.13	19.82	20.73	21.39	18.81
MnO	0.23	0.17	0.16	0.19	0.17	0.18	0.18
MgO	5.36	8.14	14.50	10.00	10.40	10.60	11.50
CaO	9.01	9.51	10.60	14.10	14.70	14.20	14.70
Na2O	0.03	2.70	1.03	0.59	0.41	0.32	0.47
K2O	1.20	0.48	0.24	0.50	0.56	0.42	0.43
P2O5	0.31	0.20	0.09	0.11	0.07	0.08	0.12
TOTAL	97.12	97.74	97.38	97.46	97.12	97.17	99.67

Sample no.	A4.27	D4.25	D4.35	D4.36	D5.46	D5.47
SiO2	59.28	63.16	66.94	67.24	66.39	67.94
TiO2	0.80	0.75	0.54	0.34	0.31	0.35
Al2O3	14.63	14.63	13.89	15.16	9.50	13.60
Fe2O3	11.35	9.28	8.14	7.24	5.84	6.49
MnO	0.18	0.19	0.16	0.16	0.10	0.11
MgO	2.48	1.68	0.91	1.55	1.45	1.33
CaO	5.96	7.32	4.41	3.97	4.13	2.86
Na2O	3.13	2.99	2.93	3.30	1.03	3.35
K2O	1.52	0.68	2.62	1.79	1.68	1.97
P2O5	0.54	0.50	0.17	0.15	0.08	0.15
TOTAL	99.87	101.18	100.71	100.90	90.51	98.15

2. Analyses for the North Limestone Area.
(Major elements determined from pressed powders)

NLA BASALTS

Sample no.	D10-1	D10-3	D10-4	D10-5	D10-9	D10-10	D10-13
SiO2	47.75	47.50	51.25	45.25	46.50	48.26	47.50
TiO2	0.65	0.61	0.62	0.84	0.58	0.81	0.70
V	379	356	330	406	337	412	386
Cr	266	392	301	172	553	48	276
Ni	91	61	59	58	171	31	75
Cu	106	109	75	55	57	159	106
Zn	112	111	102	95	87	96	97
Rb	2	2	2	7	12	4	2
Sr	178	190	297	237	375	361	243
Y	11	9	8	8	7	11	11
Zr	30	26	27	19	24	33	32
Nb	4	3	3	2	2	4	3
Ba	246	157	121	345	692	135	151

Sample no.	D10-16	D10-22	D10-23	D10-24	D10-27	D10-28	D10-32
SiO2	47.26	45.50	49.04	52.75	49.75	50.12	52.25
TiO2	0.84	0.67	0.56	0.49	0.44	0.95	0.69
V	427	340	317	293	705	274	226
Cr	259	430	625	613	652	224	177
Ni	101	76	127	95	107	94	44
Cu	147	21	102	67	18	128	33
Zn	96	109	112	74	86	97	142
Rb	4	2	4	5	12	9	6
Sr	488	309	196	313	172	471	227
Y	10	10	8	7	8	28	18
Zr	29	27	27	22	21	91	56
Nb	3	4	3	3	3	9	4
Ba	254	107	140	127	753	258	211

Sample no.	D10-35	D10-36	D10-42	D5-42	D5-43	D6-48	D6-49
SiO2	44.75	45.75	48.75	48.25	43.87	41.25	48.31
TiO2	1.00	0.84	0.66	0.76	0.46	1.09	0.49
V	545	414	301	355	277	25	274
Cr	92	90	177	258	1066	764	782
Ni	55	52	57	72	343	166	209
Cu	34	62	81	260	33	45	57
Zn	111	112	110	86	76	105	77
Rb	11	21	18	10	3	8	6
Sr	411	501	296	421	169	359	261
Y	17	16	11	7	6	8	8
Zr	32	31	33	22	18	22	20
Nb	5	4	4	3	2	3	2
Ba	279	606	282	355	138	206	224

Sample no.	D6-50	D6-51	D6-52	D6-53	D6-54	D6-55	D7-67
SiO2	40.55	40.33	42.75	41.85	43.11	49.80	47.32
TiO2	1.12	1.10	0.96	1.02	0.93	0.76	0.68
V	644	890	648	778	585	356	307
Cr	2	2	128	0	0	68	446
Ni	157	167	188	132	44	24	127
Cu	25	24	59	48	520	158	105
Zn	149	111	94	173	91	76	98
Rb	7	7	5	5	15	5	24
Sr	276	258	426	446	759	241	284
Y	9	7	7	8	6	13	10
Zr	22	20	22	23	22	29	40
Nb	3	3	2	3	3	2	3
Ba	191	190	269	290	205	120	583

Sample no.	D7-68
SiO2	52.00
TiO2	0.74
V	239
Cr	99
Ni	36
Cu	144
Zn	107
Rb	22
Sr	324
Y	16
Zr	47
Nb	4
Ba	709

NLA BASALTIC	ANDESITES						
Sample no.	D10-2	D10-21	D10-25	D10-37	D10-51	D10-56	10-58
SiO2	54.25	55.75	53.54	53.50	53.75	55.00	54.35
TiO2	1.38	1.40	1.54	0.73	0.57	0.93	0.73
V	150	90	285	229	222	183	262
Cr	188	0	10	6	174	3	22
Ni	89	15	10	18	49	8	22
Cu	115	215	38	153	17	48	161
Zn	97	103	143	127	88	95	96
Rb	10	20	10	28	11	42	40
Sr	431	436	294	376	504	797	550
Y	25	25	49	18	13	20	22
Zr	202	150	140	55	52	90	55
Nb	13	8	10	6	4	6	4
Ba	301	823	312	1319	247	920	526

Sample no.	D10-59	D10-60	D10-61	D10-62	D5-40	D7-65	D7-66
SiO2	54.62	54.50	55.00	54.75	54.51	54.36	55.11
TiO2	0.73	0.71	0.68	0.67	0.67	1.66	0.77
V	262	254	240	242	244	299	152
Cr	25	22	26	26	113	5	19
Ni	21	20	20	20	32	11	11
Cu	202	186	112	129	128	288	138
Zn	103	119	104	101	91	137	119
Rb	31	31	20	8	39	44	51
Sr	411	341	439	441	338	486	488
Y	20	20	21	19	17	38	19
Zr	56	54	54	53	71	162	65
Nb	5	6	4	5	6	10	5
Ba	539	600	424	413	454	956	1064

NLA ANDESITES

Sample no.	D10-18	D10-26	D10-29	D10-33	D10-43	D10-45	D10-46
SiO ₂	62.75	56.31	58.25	56.50	57.81	56.87	57.86
TiO ₂	0.54	0.86	0.78	0.78	0.70	0.69	0.68
V	47	141	118	122	143	141	138
Cr	23	29	2	3	11	37	10
Ni	6	12	5	5	9	14	10
Cu	94	36	186	92	167	21	291
Zn	69	78	86	133	116	109	124
Rb	54	25	26	39	31	42	35
Sr	337	440	378	511	551	546	461
Y	28	23	21	23	21	20	19
Zr	137	99	69	71	65	61	61
Nb	12	5	6	7	6	6	5
Ba	1129	821	698	1535	773	767	732

Sample no.	D10-49	D10-50	D10-52	D10-53	D10-54	D10-55	D10-57
SiO ₂	57.84	58.25	59.30	60.32	57.25	56.75	57.25
TiO ₂	0.70	0.67	0.82	0.58	0.86	0.64	0.75
V	145	148	67	50	75	222	222
Cr	12	10	0	2	0	25	4
Ni	11	10	4	3	3	10	9
Cu	72	61	164	17	163	92	349
Zn	115	108	124	76	116	98	102
Rb	32	22	42	42	44	30	14
Sr	467	494	542	501	549	599	649
Y	21	19	26	19	27	16	19
Zr	62	60	77	73	77	54	63
Nb	5	5	7	5	8	4	6
Ba	771	375	795	510	679	536	407

Sample no.	D4-25	D4-26	D4-27	D4-39	D7-60	D7-62	D7-63
SiO ₂	62.79	59.25	58.12	57.62	54.25	57.59	56.75
TiO ₂	0.64	0.77	0.80	0.80	0.94	0.71	0.68
V	67	74	68	7	185	151	156
Cr	13	10	0	1	14	11	10
Ni	4	4	5	7	15	9	10
Cu	29	146	83	251	201	129	128
Zn	84	109	132	95	106	125	98
Rb	7	23	37	15	19	26	22
Sr	578	557	439	440	768	537	636
Y	27	27	27	20	24	22	21
Zr	74	76	78	72	99	62	63
Nb	8	7	8	8	7	6	7
Ba	119	449	632	376	471	559	464

Sample no.	D7-64	D7-69	D7-70
SiO ₂	56.50	58.25	58.61
TiO ₂	0.75	0.83	0.62
V	145	75	145
Cr	25	0	17
Ni	11	3	11
Cu	103	174	123
Zn	100	117	89
Rb	25	53	13
Sr	479	536	692
Y	21	23	19
Zr	66	78	62
Nb	6	7	7
Ba	555	835	421

NLA DACITES

Sample no.	D10-15	D10-38	D10-39	D10-41	D10-74	D10-75	D10-76
SiO2	63.78	65.50	65.62	63.35	67.50	67.50	64.12
TiO2	0.58	0.57	0.54	0.59	0.38	0.39	0.52
V	49	10	10	8	21	19	98
Cr	8	10	1	7	1	11	6
Ni	4	1	2	2	3	2	4
Cu	61	48	25	50	7	24	146
Zn	36	93	143	122	91	82	82
Rb	53	28	36	41	26	36	14
Sr	231	425	384	429	317	318	324
Y	29	26	27	28	28	27	21
Zr	129	95	97	99	77	77	73
Nb	9	9	8	8	5	5	6
Ba	304	462	1083	1027	500	645	410

Sample no.	D4-35	D4-36	D4-37	D5-41	D5-46	D5-47	D7-57
SiO2	65.15	65.61	67.11	65.50	67.00	67.50	66.22
TiO2	0.53	0.36	0.32	0.53	0.34	0.37	0.47
V	5	60	53	64	34	33	293
Cr	3	12	16	16	9	17	212
Ni	3	5	3	11	3	2	73
Cu	60	139	36	43	23	1	46
Zn	101	111	91	152	69	56	108
Rb	35	21	26	43	23	25	36
Sr	385	467	447	186	208	365	677
Y	31	26	22	8	27	24	15
Zr	113	95	90	140	112	94	82
Nb	9	7	7	11	6	8	5
Ba	923	504	799	818	484	639	721

Sample no.	D7-59	D7-61
SiO2	64.08	65.50
TiO2	0.57	0.57
V	23	8
Cr	1	2
Ni	3	2
Cu	13	57
Zn	135	109
Rb	28	18
Sr	393	659
Y	27	30
Zr	98	109
Nb	8	10
Ba	723	583

NLA RHYOLITES

Sample no.	D10-67	D10-68	D10-70	D10-71	D10-72	D4-38	D5-45
SiO2	70.06	70.50	71.00	69.50	70.62	70.70	70.50
TiO2	0.29	0.28	0.27	0.41	0.31	0.23	0.29
V	4	5	5	9	4	7	91
Cr	3	4	4	5	0	5	22
Ni	3	2	2	2	1	3	5
Cu	115	7	18	1	5	89	13
Zn	88	66	85	80	96	119	76
Rb	61	36	38	42	38	26	23
Sr	246	248	327	298	295	282	262
Y	32	32	32	27	32	30	37
Zr	123	124	127	85	119	104	119
Nb	11	11	11	6	11	8	7
Ba	995	866	909	305	985	769	449

3. Analyses for the Bigstone deposit sequence.

BIGSTONE LAKE BASALTS

Sample no.	BS91	BS92	BS93	BS105	BS106	BS108	BS109
SiO ₂	50.20	47.50	0.43	48.10	48.20	50.10	51.00
TiO ₂	0.80	0.80	1.10	1.00	0.80	0.90	0.70
U	371	181	407	331	355	308	383
Cr	23	3	30	1	54	4	181
Ni	37	14	58	11	37	11	67
Cu	22	5	12	31	143	38	9
Zn	95	84	129	86	183	63	64
Rb	5	76	28	31	50	25	3
Sr	557	68	424	338	226	374	396
Y	13	16	16	27	29	17	13
Zr	42	83	44	59	49	55	37
Nb	4	8	5	5	5	5	5
Ba	131	459	430	621	900	778	88

Sample no.	BS112	BS114	BS115	BS116	BS118	BS120	BS121
SiO ₂	43.50	48.20	51.10	50.80	52.00	50.90	50.50
TiO ₂	0.60	0.70	0.60	0.60	0.60	0.60	0.60
U	316	378	311	374	322	352	368
Cr	124	287	334	301	291	344	382
Ni	39	54	107	45	59	36	38
Cu	12	11	15	67	12	18	13
Zn	76	77	75	71	78	92	88
Rb	0	2	3	3	3	2	3
Sr	194	373	350	396	365	364	460
Y	12	11	6	10	10	9	7
Zr	31	38	28	35	31	32	32
Nb	3	4	4	5	4	4	3
Ba	182	114	93	89	82	85	95

Sample no.	BS124	BS126	BS127	BS128	BS129	BS274	BS275
SiO ₂	52.40	49.60	51.70	52.00	50.00	49.10	51.50
TiO ₂	0.70	0.70	1.00	1.00	0.60	0.90	0.70
U	355	450	327	303	354	287	272
Cr	164	180	10	10	181	7	20
Ni	26	31	20	16	30	11	18
Cu	7	8	11	6	21	110	106
Zn	84	118	87	75	113	183	111
Rb	3	6	2	1	5	56	46
Sr	553	392	503	510	300	200	247
Y	12	11	16	23	10	16	24
Zr	37	41	58	76	34	45	62
Nb	5	4	8	8	4	4	5
Ba	141	234	122	106	177	583	565

Sample no.	BS522	BS528	BS529	BS530	BS1239	BS1241	BS1242
SiO ₂	45.75	49.25	44.50	48.55	50.25	47.57	45.30
TiO ₂	0.56	0.52	0.80	1.06	0.66	0.63	0.75
U	346	361	422	347	347	365	397
Cr	242	195	186	8	163	249	223
Ni	69	38	50	19	72	57	52
Cu	1	6	4	5	33	120	30
Zn	107	132	91	81	118	67	73
Rb	29	7	77	73	8	10	20
Sr	142	413	259	440	413	310	323
Y	7	8	10	17	11	12	8
Zr	26	28	32	68	35	36	36
Nb	4	4	4	5	5	4	4
Ba	508	188	752	788	110	220	297

Sample no.	BS1243	BS1244
SiO2	44.50	48.00
TiO2	0.63	0.72
V	337	438
Cr	135	257
Ni	46	57
Cu	30	21
Zn	108	104
Rb	19	4
Sr	334	448
Y	12	9
Zr	34	38
Nb	3	4
Ba	478	109

FMU BASALTIC ANDESITES

Sample no.	BS123	BS122	BS119	BS136	BS97
SiO2	55.10	53.10	53.80	53.30	55.30
TiO2	1.00	0.50	0.60	1.10	0.91
V	254	250	347	276	344
Cr	5	293	266	4	6
Ni	10	55	62	16	9
Cu	182	38	80	7	79
Zn	85	70	71	102	65
Rb	2	1	1	66	36
Sr	362	357	345	279	249
Y	23	4	6	26	15
Zr	52	29	31	75	55
Nb	7	4	4	7	5
Ba	148	53	93	1955	626

FMU DACITES

Sample no.	BS94	BS527	BS1016	BS1246
SiO2	62.60	0.68	62.25	65.57
TiO2	0.90	0.43	0.72	0.34
V	319	21	126	9
Cr	7	2	4	7
Ni	11	3	6	5
Cu	164	114	126	2
Zn	53	47	54	52
Rb	11	25	29	64
Sr	622	200	333	105
Y	16	37	21	56
Zr	57	138	87	100
Nb	4	13	6	7
Ba	220	1234	320	821

MINERALISED Sample no.	HORIZON RHYOLITES						
	BS6	BS7	BS9	BS15	BS18	BS25	BS56
SiO2	78.50	75.00	77.00	81.00	74.50	84.23	77.00
TiO2	0.28	0.44	0.33	0.29	0.36	0.24	0.43
CaO	0.84	0.63	2.20	0.22	0.22	0.14	0.28
Na2O	1.27	1.09	2.30	0.56	3.13	1.59	2.12
Al2O3	10.90	14.40	11.50	14.30	16.60	11.90	16.80

V	77	129	64	74	56	56	98
Cr	6	12	4	24	0	12	1
Ni	4	3	4	2	1	2	4
Cu	131	83	114	147	22444	1517	51
Zn	1287	5285	185	72	594	294	27540
Rb	6	26	2	28	7	7	25
Sr	130	122	243	82	109	255	192
Y	10	14	8	8	11	9	5
Zr	51	70	58	53	60	51	55
Nb	4	7	6	5	6	6	8
Ba	126	521	47	381	45	23	221

Sample no.	BS59	BS233	BS251	BS253	BS256	BS445	BS447
SiO2	68.77	79.24	70.35	75.64	71.82	68.86	76.66
TiO2	0.69	0.19	0.57	0.40	0.35	0.54	0.33
CaO	1.80	0.85	0.46	0.11	0.45	0.28	0.12
Na2O	2.50	1.67	0.85	0.50	0.60	1.77	0.32
Al2O3	18.60	7.75	17.80	16.50	13.40	17.40	11.40

V	109	26	127	106	78	118	99
Cr	4	2	32	8	2	3	0
Ni	2	9	3	2	2	4	3
Cu	54	16185	131	51	199	496	1237
Zn	4200	17124	2480	177	328	2858	987
Rb	33	9	40	39	19	21	25
Sr	233	185	108	48	56	203	38
Y	7	45	7	6	9	27	18
Zr	100	43	74	58	56	72	61
Nb	7	4	6	5	5	7	9
Ba	386	142	784	688	320	266	393

Sample no.	BS453	BS455	BS459	BS461	BS467	BS469	BS471
SiO2	81.80	76.21	82.81	77.74	75.44	71.26	73.22
TiO2	0.27	0.25	0.29	0.28	0.26	0.26	0.21
CaO	0.22	0.40	0.02	0.22	0.64	0.21	0.12
Na2O	2.16	3.56	0.43	0.32	0.79	0.15	0.85
Al2O3	13.00	10.90	10.50	11.60	8.41	9.07	9.21

V	81	69	80	89	77	99	64
Cr	27	1	8	23	25	0	0
Ni	3	7	2	3	2	3	7
Cu	86	818	353	269	3785	137	661
Zn	7906	92564	5707	5299	772	284	41414
Rb	7	9	23	19	2	10	14
Sr	131	106	40	28	101	16	20
Y	14	54	12	11	12	14	11
Zr	47	40	56	48	47	50	42
Nb	6	5	7	7	6	6	6
Ba	99	174	331	296	89	155	220

Sample no.	BS493	BS495	BS499	BS501
SiO2	70.54	72.73	88.86	77.67
TiO2	0.33	0.36	0.14	0.39
CaO	0.28	0.26	0.08	0.62
Na2O	5.37	3.30	0.88	0.35
Al2O3	14.50	17.70	8.84	16.00
V	51	79	47	116
Cr	0	34	62	35
Ni	6	5	5	3
Cu	839	12627	37	5
Zn	118507	1150	989	44
Rb	15	7	5	36
Sr	138	158	80	54
Y	8	9	5	21
Zr	56	71	43	73
Nb	8	5	5	5
Ba	233	104	67	1368

IRON FORMATION

Sample No.	BS61	BS62	BS63	BS441	BS443	BS463	BS473	BS475	BS477
SiO2	47.8	51.9	47.8	38.8	31.3	47.8	52.3	53.6	62.4
Al2O3	12.8	13.9	13.7	12.8	14.2	12.8	12.7	7.5	8.1
TiO2	0.56	0.52	0.61	0.46	0.45	0.52	0.59	0.35	0.28
Fe2O3	28.8	13.9	19.6	23.4	25.3	28.8	27.55	33.5	25.8
MnO	1.2	0.46	1.8	0.27	0.46	0.22	0.45	2.8	0.66
P2O5	0.21	0.22	0.25	0.23	0.41	0.85	0.87	0.46	0.2
Cu	61	5	17	383	1358	1542	169	298	3787
Zn	533	542	474	22281	21878	14997	3774	1383	3463
Sr	46	135	47	21	55	15	9	4	13
Y	22	25	28	15	21	23	18	23	19
Zr	73	78	74	59	58	66	72	59	48
Nb	2	3	2	8	4	5	3	5	3

Sample No.	BS479	BS481	BS485	BS489	BS583	BS1*
SiO2	37.6	42.6	33.2	34.5	36.7	35.8
Al2O3	7.2	15.2	13.2	18.3	9.2	18.1
TiO2	0.39	0.72	0.69	0.46	0.44	0.51
Fe2O3	45.7	23.6	36.8	42.2	34.1	27.5
MnO	3.84	0.35	0.25	1.53	1.73	6.13
P2O5	0.15	0.22	0.21	0.23	0.25	0.15
Cu	74	71	15373	37	339	136
Zn	961	786	3259	983	788	3153
Sr	3	142	251	83	23	3
Y	31	33	18	27	38	26
Zr	57	87	86	68	58	65
Nb	7	4	1	5	5	7

MINERALISED Sample no.	HORIZON BASALTS				
	BS16	BS17	BS19	BS449	BS231
SiO ₂	50.75	0.49	50.83	53.24	48.19
TiO ₂	0.84	0.88	0.84	0.81	0.87
U	290	265	299	141	265
Cr	4	1	13	0	136
Ni	10	11	9	5	66
Cu	48	187	30	523	19
Zn	594	2703	2706	4432	723
Rb	4	4	3	17	36
Sr	223	326	255	308	179
Y	16	16	15	31	13
Zr	42	48	42	92	73
Nb	5	6	5	7	6
Ba	85	61	58	219	226

MH DACITES Sample no.	HORIZON BASALTS			
	BS487	BS8	BS252	BS497
SiO ₂	0.65	0.66	0.58	0.78
TiO ₂	0.39	0.31	0.27	0.37
CaO	0.88	0.38	0.28	0.38
Na ₂ O	7.38	0.88	0.28	3.58
Al ₂ O ₃	18.18	9.68	8.48	16.58
U	62	118	87	68
Cr	8	1	3	57
Ni	15	2	6	11
Cu	693	725	1488	6987
Zn	99999	413	15281	35436
Rb	44	5	7	19
Sr	38	8	12	132
Y	11	17	13	15
Zr	58	53	47	66
Nb	7	6	5	5
Ba	576	181	142	169

QFP BASALTS				
Sample no.	BS274	BS275	BS82	BS136
SiO2	49.10	51.50	52.60	53.30
TiO2	0.90	0.70	0.49	1.10
V	287	272	10	276
Cr	7	20	0	4
Ni	11	18	2	16
Cu	110	106	4	7
Zn	103	111	92	102
Rb	56	46	42	66
Sr	288	247	222	279
Y	16	24	33	26
Zr	45	62	123	75
Nb	4	5	8	7
Ba	583	565	422	1955

QFP DACITES							
Sample no.	BS98	BS130	BS133	BS134	BS279	BS285	BS83
SiO2	62.40	67.50	67.70	66.40	66.80	66.90	65.51
TiO2	0.60	0.50	0.40	0.40	0.40	0.20	0.39
CaO	7.30	3.80	4.00	10.00	3.80	0.01	3.60
Na2O	2.97	3.95	4.19	4.25	2.70	0.96	2.78
Al2O3	13.70	13.50	13.90	12.50	16.00	17.60	15.80
V	198	36	18	8	12	5	6
Cr	39	0	11	12	22	24	7
Ni	20	3	2	2	2	1	3
Cu	15	143	111	101	3	0	1
Zn	50	73	48	29	52	48	58
Rb	28	26	26	11	39	39	37
Sr	308	243	200	547	181	66	221
Y	20	27	37	36	23	20	47
Zr	80	136	137	133	112	82	112
Nb	7	11	12	11	7	5	7
Ba	548	1039	1226	372	469	864	360

Sample no.	BS86	BS276	BS65
SiO2	67.75	62.20	67.70
TiO2	0.25	0.50	0.30
CaO	2.00	5.10	2.80
Na2O	0.83	3.13	1.70
Al2O3	12.30	17.30	14.60
V	8	12	7
Cr	5	6	3
Ni	3	2	3
Cu	2	2	5
Zn	71	59	131
Rb	39	42	21
Sr	79	247	127
Y	25	38	44
Zr	80	128	90
Nb	5	7	5
Ba	366	557	288

QFP RHYOLITES

Sample no.	BS67	BS68	BS74	BS75	BS76	BS79	BS81
SiO ₂	73.30	75.60	72.00	70.14	70.00	69.54	73.00
TiO ₂	0.27	0.20	0.26	0.27	0.28	0.29	0.27
CaO	2.20	2.00	3.10	2.70	1.80	2.40	2.80
Na ₂ O	2.30	2.70	2.30	2.14	1.89	1.69	2.11
Al ₂ O ₃	0.13	11.70	13.20	13.30	13.00	14.10	13.00
V	4	8	8	11	6	4	4
Cr	6	3	7	5	6	6	12
Ni	3	3	3	2	3	3	2
Cu	32	999	19	16	8	4	24
Zn	70	91	61	69	63	54	48
Rb	21	10	28	33	43	45	27
Sr	126	181	178	142	140	105	154
Y	31	19	23	21	20	40	21
Zr	83	80	88	86	86	87	86
Nb	6	8	8	7	7	5	6
Ba	234	159	343	430	539	797	274

Sample no.	BS84	BS85	BS87	BS88	BS89	BS131	BS132
SiO ₂	77.50	70.50	73.50	74.57	75.90	69.20	69.08
TiO ₂	0.21	0.25	0.25	0.25	0.22	0.40	0.41
CaO	2.30	4.20	2.60	2.30	1.70	6.50	6.90
Na ₂ O	2.47	1.50	2.27	2.06	2.16	4.30	3.80
Al ₂ O ₃	12.30	12.40	12.80	13.00	11.90	13.20	13.50
V	4	7	6	4	4	10	9
Cr	2	8	12	10	10	3	6
Ni	2	2	3	1	1	1	12
Cu	0	33	999	999	3680	410	74
Zn	30	67	82	85	85	51	36
Rb	17	32	26	26	26	15	14
Sr	127	104	148	125	125	437	495
Y	10	33	49	45	45	35	36
Zr	76	75	87	86	86	138	157
Nb	6	6	6	6	6	11	13
Ba	277	280	287	451	451	554	632

Sample no.	BS135	BS139	BS277	BS278	BS280	BS281	BS282
SiO ₂	70.60	71.50	71.50	80.30	70.60	70.70	72.30
TiO ₂	0.40	0.20	0.30	0.20	0.30	0.30	0.30
CaO	4.90	1.60	2.80	2.30	3.10	2.80	2.30
Na ₂ O	4.60	0.80	2.10	1.60	2.50	2.90	3.10
Al ₂ O ₃	13.80	11.40	13.80	11.30	14.20	14.90	14.70
V	7	7	13	3	18	7	9
Cr	2	5	9	24	8	3	30
Ni	3	1	3	2	5	2	3
Cu	210	3	0	3	2	3	1
Zn	35	70	54	27	44	51	38
Rb	16	31	31	20	37	16	28
Sr	438	89	165	96	211	314	208
Y	40	32	43	16	24	26	30
Zr	141	71	94	65	100	94	98
Nb	13	5	5	5	7	7	6
Ba	572	236	367	273	415	219	311

Sample no.	BS283	BS284	BS286	BS287	BS288
SiO2	72.70	68.40	71.40	70.20	69.20
TiO2	0.30	0.40	0.30	0.30	0.40
CaO	2.40	2.60	1.80	2.20	2.30
Na2O	3.00	3.00	2.30	2.10	3.60
Al2O3	14.80	15.10	14.70	14.50	14.60
V	8	15	7	12	9
Cr	10	7	6	2	8
Ni	2	4	2	2	2
Cu	2	1	1	1	2
Zn	38	50	52	53	61
Rb	26	31	30	36	9
Sr	225	181	150	141	376
Y	32	20	26	24	40
Zr	92	104	91	94	105
Nb	7	6	6	6	7
Ba	317	342	444	516	160

HANGING WALL BASALTS				
Sample no.	BS1021	BS1019	BS1018	BS1017
SiO2	51.75	52.55	51.50	51.80
TiO2	0.78	0.84	0.85	0.92
V	243	309	318	330
Cr	27	3	66	2
Ni	14	11	21	11
Cu	2	7	7	13
Zn	72	92	99	109
Rb	69	38	16	31
Sr	301	496	362	539
Y	17	17	18	16
Zr	71	61	51	62
Nb	4	4	4	5
Ba	615	594	304	547

APPENDIX 2.3 CORRELATIONS AMONGST 'IMMOBILE ELEMENTS'
FOR SELECTED ROCK TYPES.

NLA= NORTH LIMESTONE AREA OUTCROP SAMPLES
FMU=FOOTWALL MAFIC UNIT
QFP= FOOTWALL QUARTZ-FELDSPAR PORPHYRY

NLA SiO₂<56%

	Nb	Y	Zr	TiO ₂
Nb	-	0.56	0.71	0.61
Y		-	0.76	0.56
Zr			-	0.71
TiO ₂				-

FMU SiO₂<56%

	Nb	Y	Zr	TiO ₂
Nb	-	0.85	0.94	0.67
Y		-	0.83	0.63
Zr			-	0.70
TiO ₂				-

QFP SiO₂>68%

	Nb	Y	Zr	TiO ₂
Nb	-	0.13	0.88	0.63
Y		-	0.31	0.25
Zr			-	0.87
TiO ₂				-

Mineralised Horizon SiO₂>60%

	Nb	Y	Zr	TiO ₂
Nb	-	-0.2	0.28	0.35
Y		-	-0.26	-0.20
Zr			-	0.91
TiO ₂				-

APPENDIX 3: MICROPROBE ANALYSES

A3.1 Analytical techniques

Microprobe analyses were carried out on the following machines:

a) On a fully manual Wavelength Dispersive (WD) Cambridge Microscan V, at Aston University. Operating conditions were as follows:

Accelerated voltage: 15Kv

Specimen/beam current: 500 μ A

Data reduction was done using the software package of Micro Analysis Consultants Ltd. Detection limits, and errors, for all major elements are <0.04%, and <0.12% respectively.

b) On a Cambridge Microscan V, fitted with a LINK systems Energy Dispersive (ED) system, at the University of Leicester. Operating conditions were as follows:

Accelerated voltage: 15Kv

*Specimen/beam current: 300 μ A

Detection limits, and errors, for all major elements are in the order of 0.2%, and <0.28%, respectively. data reduction was done using LINK systems software.

c) On a Camica (WD) microprobe, fitted with LINK systems ED analysis system, at the University of Manchester. Operating conditions were as follows:

WD: Accelerated voltage: 15Kv

Take off angle: 40 degrees.

Beam current: 14 μ A

Detection Limits 0.02% for all major elements.

ED: Beam Current 3 μ A.

Detection limits 0.2% for all elements.

APPENDIX 3.2: LISTS OF MICROPROBE ANALYSES.

Structural formulae calculated using the following number of oxygens per unit cell:

Mineral	No. oxygens
Amphibole	23
Garnet	12
Chloritoid	12
Feldspar	10
Tourmaline	29

1. Fe-Mg Amphiboles.

	W2.1	W2.2	W2.3	262-1	262-2	262-3	262-4	262-5
SiO2	49.89	50.36	50.78	51.24	49.57	49.73	50.36	50.78
Al2O3	4.45	1.11	0.29	0.00	0.64	0.25	1.11	0.00
Fe2O3	0.00	0.00	0.00	0.00	0.00	0.00	0.00	0.00
FeO	31.11	33.10	33.49	32.89	30.73	31.38	33.10	33.49
MgO	8.57	9.05	9.16	9.94	10.51	10.32	9.05	9.16
CaO	0.28	0.51	0.24	0.19	1.39	0.44	0.51	0.24
Na2O	0.00	0.00	0.00	0.00	0.00	0.00	0.00	0.00
K2O	0.00	0.00	0.00	0.00	0.00	0.00	0.00	0.00
MnO	1.91	2.12	1.96	1.91	2.01	1.97	2.12	1.96
TOTAL	96.21	96.25	95.92	96.17	94.85	94.89	96.25	95.63

CATIONS PER FORMULA UNIT

O=	23.0	23.0	23.0	23.0	23.0	23.0	23.0	23.0
Si	7.734	7.923	8.019	8.038	7.831	7.952	7.923	8.047
Al	0.814	0.206	0.054	0.000	0.119	0.047	0.206	0.000
Fe	0.000	0.000	0.000	0.000	0.239	0.052	0.000	0.000
Fe	4.031	4.353	4.421	4.313	3.820	4.142	4.353	4.436
Mg	1.981	2.123	2.157	2.325	2.476	2.461	2.123	2.165
Ca	0.047	0.086	0.041	0.032	0.235	0.075	0.086	0.041
Na	0.000	0.000	0.000	0.000	0.000	0.000	0.000	0.000
K	0.000	0.000	0.000	0.000	0.000	0.000	0.000	0.000
Mn	0.251	0.283	0.262	0.254	0.269	0.267	0.283	0.263
TOTAL	14.86	14.97	14.95	14.96	14.99	15.00	14.97	14.95

	723	727-1	727-2	727-3	727	727	727	727
SiO2	46.99	50.89	48.61	49.96	51.37	50.64	49.04	48.77
Al2O3	2.70	0.61	2.92	0.60	1.31	1.56	1.82	2.72
Fe2O3	0.00	0.00	0.00	0.00	0.00	0.00	0.00	0.00
FeO	30.48	34.45	34.74	34.10	36.16	35.87	34.43	34.66
MgO	9.46	9.42	8.28	9.06	8.86	8.68	8.28	8.19
CaO	1.46	0.36	0.66	0.30	0.93	1.00	1.40	1.80
Na2O	0.95	0.00	0.00	0.00	0.00	0.00	0.00	0.00
K2O	0.00	0.00	0.00	0.00	0.00	0.00	0.00	0.00
MnO	1.06	0.89	0.92	1.09	0.89	0.91	0.91	0.85
TOTAL	93.10	96.62	96.13	95.11	99.52	98.72	95.88	96.99

CATIONS PER FORMULA UNIT

O=	23.0	23.0	23.0	23.0	23.0	23.0	23.0	23.0
Si	7.626	7.971	7.679	7.966	7.853	7.883	7.774	7.629
Al	0.517	0.113	0.544	0.113	0.236	0.284	0.340	0.502
Fe	0.000	0.000	0.108	0.000	0.063	0.121	0.122	0.262
Fe	4.135	4.510	4.470	4.545	4.557	4.499	4.441	4.270
Mg	2.289	2.200	1.951	2.154	2.020	1.995	1.958	1.911
Ca	0.254	0.060	0.112	0.051	0.152	0.175	0.238	0.302
Na	0.299	0.000	0.000	0.000	0.000	0.000	0.000	0.000
K	0.000	0.000	0.000	0.000	0.000	0.000	0.000	0.000
Mn	0.146	0.118	0.123	0.147	0.115	0.119	0.122	0.113
TOTAL	15.27	14.97	15.00	14.98	15.00	14.99	14.99	14.99

	727	904-1	904-1A	904-1B	904-2	904-3	904-4	905-1
SiO2	48.93	49.37	49.37	50.39	50.78	48.93	49.00	50.11
Al2O3	3.62	1.80	2.32	1.37	0.44	2.19	2.76	0.40
Fe2O3	0.00	0.00	0.00	0.00	0.00	0.00	0.00	0.00
FeO	33.79	32.45	32.37	32.28	31.50	31.44	31.65	35.45
MgO	7.88	9.86	10.24	10.68	11.15	10.45	10.38	7.59
CaO	2.30	0.54	0.66	0.27	0.32	0.62	1.12	0.28
Na2O	0.00	0.66	0.94	0.66	0.00	0.00	0.58	0.00
K2O	0.00	0.00	0.00	0.00	0.00	0.00	0.00	0.00
MnO	0.93	1.93	1.98	2.28	2.34	2.10	2.07	2.87

TOTAL 97.45 96.61 97.88 97.93 96.53 95.73 97.56 96.70

CATIONS PER FORMULA UNIT

O=	23.0	23.0	23.0	23.0	23.0	23.0	23.0	23.0
Si	7.607	7.745	7.648	7.780	7.883	7.652	7.561	7.970
Al	0.664	0.333	0.424	0.249	0.081	0.404	0.502	0.075
Fe	0.134	0.000	0.000	0.000	0.169	0.319	0.221	0.000
Fe	4.257	4.255	4.192	4.166	3.918	3.791	3.861	4.713
Mg	1.827	2.307	2.366	2.459	2.581	2.437	2.389	1.800
Ca	0.383	0.091	0.110	0.045	0.053	0.104	0.185	0.048
Na	0.000	0.201	0.282	0.198	0.000	0.000	0.174	0.000
K	0.000	0.000	0.000	0.000	0.000	0.000	0.000	0.000
Mn	0.123	0.257	0.260	0.298	0.308	0.278	0.271	0.387

TOTAL 14.99 15.19 15.28 15.19 14.99 14.99 15.16 14.99

	905-1	905-2	905-3	905-4	905-5	905-6	1461-1	1461-2
SiO2	50.11	50.57	50.78	49.28	50.62	49.85	51.20	50.40
Al2O3	0.40	0.00	0.00	1.28	0.41	0.70	0.89	1.95
Fe2O3	0.00	0.00	0.00	0.00	0.00	0.00	0.00	0.00
FeO	35.45	35.82	35.60	35.58	35.57	35.24	31.87	31.09
MgO	7.59	7.39	7.45	6.34	7.55	7.24	10.96	10.30
CaO	0.28	0.19	0.00	1.22	0.40	0.35	0.63	0.69
Na2O	0.00	0.00	0.00	0.00	0.00	0.00	0.00	0.00
K2O	0.00	0.00	0.00	0.00	0.00	0.00	0.00	0.00
MnO	2.87	2.69	2.93	2.52	2.78	3.31	2.22	2.27

TOTAL 96.78 96.66 96.76 96.22 97.33 96.69 97.77 96.78

CATIONS PER FORMULA UNIT

O=	23.0	23.0	23.0	23.0	23.0	23.0	23.0	23.0
Si	7.970	8.044	8.060	7.901	7.988	7.942	7.850	7.887
Al	0.075	0.000	0.000	0.242	0.076	0.132	0.161	0.356
Fe	0.000	0.000	0.000	0.000	0.000	0.000	0.152	0.033
Fe	4.713	4.763	4.723	4.768	4.692	4.693	3.932	3.992
Mg	1.800	1.753	1.763	1.510	1.777	1.720	2.500	2.398
Ca	0.048	0.032	0.000	0.210	0.068	0.060	0.103	0.114
Na	0.000	0.000	0.000	0.000	0.000	0.000	0.000	0.000
K	0.000	0.000	0.000	0.000	0.000	0.000	0.000	0.000
Mn	0.387	0.363	0.394	0.342	0.372	0.447	0.289	0.298

TOTAL 14.99 14.96 14.94 14.98 14.97 14.99 14.99 15.00

	1461-3	1461-4	1461-5	1463-2	1463-3	1463-4	1463-5	1463-6
SiO2	52.15	52.54	50.91	51.69	46.15	52.58	52.10	52.41
Al2O3	0.00	0.00	1.30	1.37	1.20	0.47	0.56	0.00
Fe2O3	0.00	0.00	0.00	0.00	0.00	0.00	0.00	0.00
FeO	31.20	31.77	32.37	31.57	32.53	29.95	30.33	29.48
MgO	11.76	11.28	10.32	10.90	10.56	11.06	12.23	12.79
CaO	0.00	0.29	0.52	0.67	0.72	0.23	0.00	0.25
Na2O	0.00	0.00	0.00	0.61	0.84	0.00	0.00	0.63
K2O	0.00	0.00	0.00	0.00	0.00	0.00	0.00	0.00
MnO	2.28	1.96	1.98	2.40	3.23	2.60	2.40	2.43
TOTAL	97.41	97.84	97.40	99.21	95.23	97.69	97.62	97.99

CATIONS PER FORMULA UNIT

O=	23.0	23.0	23.0	23.0	23.0	23.0	23.0	23.0
Si	0.003	0.033	7.861	7.832	7.344	0.000	7.943	7.958
Al	0.000	0.000	0.237	0.245	0.225	0.004	0.101	0.000
Fe	0.000	0.000	0.044	0.000	0.907	0.000	0.015	0.000
Fe	4.002	4.060	4.134	3.999	3.420	3.009	3.850	3.742
Mg	2.696	2.572	2.377	2.463	2.506	2.691	2.781	2.896
Ca	0.000	0.048	0.086	0.100	0.123	0.037	0.000	0.041
Na	0.000	0.000	0.000	0.179	0.259	0.000	0.000	0.185
K	0.000	0.000	0.000	0.000	0.000	0.000	0.000	0.000
Mn	0.297	0.254	0.259	0.308	0.436	0.335	0.310	0.313
TOTAL	15.00	14.97	15.00	15.13	15.22	14.96	15.00	15.13

	1463-7	1463-8	1463-9
SiO2	52.04	52.73	52.75
Al2O3	0.00	0.52	0.44
Fe2O3	0.00	0.00	0.00
FeO	28.85	29.87	31.09
MgO	9.06	12.00	12.09
CaO	0.25	0.26	0.20
Na2O	0.00	0.00	0.58
K2O	0.00	0.00	0.00
MnO	3.05	2.67	2.26
TOTAL	94.05	98.13	99.41

CATIONS PER FORMULA UNIT

O=	23.0	23.0	23.0
Si	0.212	7.084	7.030
Al	0.000	0.093	0.078
Fe	0.000	0.000	0.000
Fe	3.005	3.700	3.907
Mg	2.320	2.728	2.711
Ca	0.042	0.042	0.032
Na	0.000	0.000	0.169
K	0.000	0.000	0.000
Mn	0.408	0.343	0.288
TOTAL	14.79	14.97	15.12

2. Ca-Amphiboles.

2. Ca-Amphiboles.

	164-1	164-2	227-1	227-2	227-3	228-1	228-2	236-1
SiO2	38.89	38.82	40.47	40.88	40.46	37.52	37.96	37.42
Al2O3	17.93	17.43	17.81	16.83	17.32	17.58	17.81	16.87
Fe2O3	0.00	0.00	0.00	0.00	0.00	0.00	0.00	0.00
FeO	23.48	23.33	24.54	24.40	25.83	24.31	24.58	23.79
MgO	3.86	2.84	2.14	2.20	2.91	2.79	3.88	4.84
CaO	11.66	11.71	11.54	11.65	11.56	11.78	11.58	11.47
Na2O	0.00	0.00	1.41	1.56	2.83	1.64	1.87	1.61
K2O	0.00	0.00	0.65	0.61	0.76	0.69	0.64	0.58
MnO	0.37	0.27	0.29	0.29	0.31	0.32	0.88	0.88
TOTAL	94.59	93.68	98.85	97.62	100.38	96.47	95.76	95.78

CATIONS PER FORMULA UNIT

O=	23.0	23.0	23.0	23.0	23.0	23.0	23.0	23.0
Si	5.913	5.988	6.159	6.214	6.887	5.883	5.947	5.845
Al	3.283	3.238	3.197	3.878	3.873	3.237	3.144	3.188
Fe	1.813	0.835	0.181	0.836	0.289	0.431	0.622	0.761
Fe	2.834	2.236	2.948	3.126	2.858	2.755	2.586	2.345
Mg	0.788	0.667	0.486	0.589	0.653	0.652	0.781	0.941
Ca	1.939	1.976	1.881	1.935	1.863	1.965	1.944	1.919
Na	0.000	0.000	0.416	0.469	0.592	0.499	0.325	0.488
K	0.000	0.000	0.126	0.121	0.146	0.138	0.128	0.116
Mn	0.049	0.036	0.037	0.038	0.048	0.043	0.000	0.000
TOTAL	14.94	14.98	15.42	15.52	15.68	15.68	15.48	15.52

	236-2	236-3	236-4	237-1	237-2	237-3	237-4	484-1
SiO2	37.67	38.33	38.18	38.91	38.67	39.89	38.86	38.71
Al2O3	16.62	18.86	17.73	17.97	17.54	17.59	17.41	17.77
Fe2O3	0.00	0.00	0.00	0.00	0.00	0.00	0.00	0.00
FeO	22.73	22.78	22.78	23.33	23.16	22.51	22.73	23.37
MgO	4.84	3.99	3.72	4.84	3.79	3.84	4.81	3.88
CaO	11.37	11.28	11.48	11.29	11.18	11.44	11.46	11.65
Na2O	1.34	1.71	1.48	1.73	1.75	1.73	1.71	1.88
K2O	0.64	0.61	0.62	0.53	0.63	0.48	0.39	0.68
TiO2	0.34	0.26	0.27	0.88	0.88	0.88	0.88	0.88
MnO	0.55	0.57	0.44	0.42	0.43	0.51	0.39	0.88
TOTAL	95.38	97.51	96.62	98.22	97.13	97.19	96.96	96.26

CATIONS PER FORMULA UNIT

O=	23.0	23.0	23.0	23.0	23.0	23.0	23.0	23.0
Si	5.899	5.846	5.891	5.882	5.933	5.992	5.964	6.814
Al	3.878	3.249	3.227	3.285	3.174	3.188	3.152	3.256
Fe	0.783	0.689	0.596	0.764	0.648	0.471	0.567	0.378
Fe	2.272	2.285	2.342	2.184	2.322	2.413	2.349	2.657
Mg	0.943	0.988	0.856	0.911	0.867	0.878	0.918	0.695
Ca	1.987	1.843	1.884	1.829	1.834	1.879	1.884	1.939
Na	0.487	0.586	0.443	0.587	0.521	0.514	0.589	0.325
K	0.128	0.119	0.122	0.182	0.123	0.894	0.876	0.135
Ti	0.048	0.838	0.831	0.888	0.888	0.888	0.888	0.888
Mn	0.073	0.074	0.858	0.854	0.856	0.866	0.851	0.888
TOTAL	15.44	15.47	15.45	15.44	15.48	15.49	15.47	15.48

	484-2	484-3	928-1	928-2	928-3	724-1	724-2	754-1
SiO2	49.22	38.56	40.54	37.68	38.23	37.83	40.60	38.48
Al2O3	15.50	17.69	15.68	15.75	15.93	17.56	13.94	19.42
Fe2O3	0.00	0.00	0.00	0.00	0.00	0.00	0.00	0.00
FeO	20.00	23.54	23.50	27.06	25.17	24.32	24.69	23.72
MgO	3.35	2.74	4.72	4.60	3.92	3.53	5.10	2.19
CaO	10.02	11.63	11.50	9.48	10.37	11.35	10.58	11.47
Na2O	0.98	0.00	1.64	1.45	1.40	1.89	1.78	1.11
K2O	0.60	0.00	0.54	0.36	0.39	0.61	0.45	0.66
TiO2	0.00	0.00	0.00	0.00	0.00	0.00	0.00	0.26
MnO	0.00	0.00	0.58	0.40	0.59	0.30	0.25	0.31
TOTAL	99.67	94.16	98.70	96.78	96.00	97.39	97.39	97.62

CATIONS PER FORMULA UNIT

O=	23.0	23.0	23.0	23.0	23.0	23.0	23.0	23.0
Si	7.091	6.026	6.113	5.091	5.888	5.828	6.173	5.889
Al	2.634	3.261	2.789	2.806	2.894	3.191	2.500	3.506
Fe	0.000	0.794	0.685	2.251	1.413	0.724	1.095	0.436
Fe	2.408	2.281	2.277	1.165	1.828	2.408	2.043	2.599
Mg	0.720	0.639	1.061	1.036	0.900	0.811	1.156	0.500
Ca	1.546	1.947	1.858	1.534	1.711	1.873	1.723	1.881
Na	0.274	0.000	0.479	0.425	0.418	0.564	0.525	0.329
K	0.110	0.000	0.104	0.069	0.077	0.120	0.087	0.129
Ti	0.000	0.000	0.000	0.000	0.000	0.000	0.000	0.030
Mn	0.000	0.000	0.074	0.051	0.077	0.039	0.032	0.040
TOTAL	14.78	14.95	15.44	15.03	15.21	15.56	15.34	15.34

	724-4	724-6	724-7	724-8	724-9	724-10	724-11	729-1
SiO2	40.92	40.89	50.70	39.40	37.78	40.19	49.72	34.86
Al2O3	14.73	14.65	2.23	15.00	13.78	14.20	2.79	15.48
Fe2O3	0.00	0.00	0.00	0.00	0.00	0.00	0.00	0.00
FeO	25.50	25.41	33.77	25.90	27.17	24.60	33.02	29.50
MgO	4.57	4.63	9.79	3.64	4.86	4.82	9.00	4.70
CaO	11.55	11.21	1.54	11.58	10.29	11.26	2.23	7.65
Na2O	1.65	1.49	0.76	1.94	1.68	1.86	0.61	1.67
K2O	0.50	0.48	0.00	0.44	0.52	0.49	0.00	0.53
MnO	0.00	0.38	0.98	0.35	0.35	0.31	0.76	0.00
TOTAL	99.42	99.14	99.77	98.33	96.43	97.73	98.21	94.39

CATIONS PER FORMULA UNIT

O=	23.0	23.0	23.0	23.0	23.0	23.0	23.0	23.0
Si	6.155	6.136	7.783	6.057	5.827	6.150	7.668	5.345
Al	2.614	2.593	0.400	2.735	2.587	2.563	0.500	2.800
Fe	0.777	1.000	0.000	0.672	1.834	0.797	0.000	3.397
Fe	2.430	2.181	4.288	2.656	1.668	2.349	4.256	0.384
Mg	1.025	1.036	2.218	0.835	1.118	1.100	2.000	1.075
Ca	1.861	1.802	0.251	1.907	1.700	1.846	0.368	1.257
Na	0.481	0.433	0.224	0.578	0.502	0.552	0.182	0.496
K	0.096	0.092	0.000	0.086	0.102	0.096	0.000	0.104
Mn	0.000	0.048	0.126	0.046	0.046	0.040	0.099	0.000
TOTAL	15.44	15.33	15.21	15.57	15.30	15.49	15.17	14.86

	729-2	764-1	764-2	764-3	764-4	764-5	764-6	764-7
SiO2	40.52	40.01	39.59	39.01	39.46	39.48	52.10	40.56
Al2O3	13.86	15.19	15.49	15.67	15.03	16.23	13.00	15.90
Fe2O3	0.00	0.00	0.00	0.00	0.00	0.00	0.00	0.00
FeO	26.37	24.64	23.67	23.45	23.82	24.41	19.80	24.48
MgO	4.69	4.95	4.75	4.56	4.67	3.50	3.39	5.23
CaO	10.85	11.38	11.29	11.48	11.15	11.76	9.31	12.04
Na2O	1.87	2.41	1.94	1.92	1.63	1.82	1.63	2.15
K2O	0.53	0.41	0.35	0.37	0.43	0.39	0.25	0.29
TiO2	0.22	0.00	0.00	0.33	0.00	0.35	0.00	0.28
MnO	0.24	0.00	0.00	0.32	0.41	0.31	0.00	0.29
TOTAL	99.15	98.99	97.88	97.11	96.60	98.25	99.57	101.22

CATIONS PER FORMULA UNIT

O=	23.0	23.0	23.0	23.0	23.0	23.0	23.0	23.0
Si	6.106	6.055	6.074	6.008	6.077	6.054	7.462	5.990
Al	2.464	2.711	2.803	2.847	2.730	2.936	2.196	2.770
Fe	1.124	0.783	0.691	0.628	0.865	0.394	0.000	0.709
Fe	2.197	2.414	2.344	2.391	2.202	2.735	2.381	2.312
Mg	1.854	1.117	1.087	1.047	1.073	0.800	0.724	1.152
Ca	1.751	1.845	1.856	1.894	1.840	1.932	1.428	1.905
Na	0.546	0.707	0.577	0.573	0.487	0.541	0.453	0.616
K	0.102	0.079	0.069	0.073	0.085	0.076	0.046	0.055
Ti	0.025	0.000	0.000	0.038	0.000	0.040	0.000	0.031
Mn	0.031	0.000	0.000	0.042	0.054	0.040	0.000	0.036
TOTAL	15.40	15.63	15.50	15.54	15.41	15.55	14.69	15.57

240

SiO2	36.90
Al2O3	17.17
Fe2O3	0.00
FeO	23.22
MgO	2.97
CaO	10.92
Na2O	1.22
K2O	0.60
TiO2	0.24
MnO	0.45

TOTAL 93.69

CATIONS PER FORMULA UNIT

O=	23.0
Si	5.882
Al	3.228
Fe	0.721
Fe	2.373
Mg	0.706
Ca	1.865
Na	0.377
K	0.122
Ti	0.029
Mn	0.061

TOTAL 15.36

3. LIF Garnets

	209-1	209-2	209-3	209-4	209-5	209-6	209-7	209-8
SiO2	36.90	36.70	37.00	36.60	37.60	37.00	37.20	36.50
Al2O3	21.10	20.40	20.80	20.70	21.30	21.10	21.10	20.20
TiO2	0.00	0.00	0.00	0.00	0.00	0.00	0.00	0.00
FeO	33.60	32.30	31.50	33.50	31.90	34.00	32.70	32.00
MnO	6.00	7.20	7.90	6.50	8.40	6.10	6.50	7.60
MgO	1.20	0.90	0.90	1.00	1.10	1.20	1.40	0.70
CaO	1.60	1.70	1.90	1.70	1.80	1.80	1.90	1.40
Na2O	0.00	0.00	0.00	0.00	0.00	0.00	0.00	0.00
K2O	0.00	0.00	0.00	0.00	0.00	0.00	0.00	0.00
TOTAL	100.40	99.20	100.00	100.00	102.10	101.20	100.80	98.40

Si	5.992	6.043	6.033	5.990	6.007	5.974	6.004	6.054
Al	4.839	3.960	3.998	3.994	4.012	4.017	4.015	3.956
Ti	0.000	0.000	0.000	0.000	0.000	0.000	0.000	0.000
Fe	4.563	4.448	4.295	4.585	4.262	4.591	4.414	4.446
Mn	0.825	1.004	1.091	0.901	1.137	0.834	0.889	1.069
Mg	0.290	0.221	0.219	0.244	0.262	0.289	0.337	0.173
Ca	0.278	0.300	0.332	0.298	0.308	0.311	0.329	0.249
Na	0.000	0.000	0.000	0.000	0.000	0.000	0.000	0.000
K	0.000	0.000	0.000	0.000	0.000	0.000	0.000	0.000

AT%Fe	76.6	74.5	72.3	76.1	71.4	76.2	74.0	74.9
AT%Mn	13.9	16.8	18.4	14.9	19.0	13.8	14.9	18.0
AT%Mg	4.9	3.7	3.7	4.0	4.4	4.8	5.6	2.9
AT%Ca	4.7	5.0	5.6	4.9	5.2	5.2	5.5	4.2

	209-9	209-10	209-11	209-12	209-13	209-14	212-1	212-1A
SiO2	37.30	36.90	37.50	37.00	39.30	37.40	36.50	36.00
Al2O3	21.30	20.80	20.80	20.50	20.40	21.20	20.60	21.00
TiO2	0.00	0.00	0.00	0.00	0.00	0.00	0.00	0.00
FeO	31.70	31.00	34.00	32.30	32.90	33.20	30.70	30.50
MnO	8.40	7.80	5.10	8.20	6.40	6.80	7.70	7.80
MgO	0.80	0.60	1.10	0.50	1.10	1.00	0.70	0.90
CaO	1.50	1.90	1.70	1.90	1.80	1.70	3.20	2.80
Na2O	0.00	0.00	0.00	0.00	0.00	0.00	0.00	0.00
K2O	0.00	0.00	0.00	0.00	0.00	0.00	0.00	0.00
TOTAL	101.00	99.80	101.00	100.40	101.90	101.30	99.40	99.80

Si	6.020	6.030	6.054	6.041	6.239	6.019	5.990	6.000
Al	4.053	4.011	3.959	3.946	3.818	4.022	3.990	4.037
Ti	0.000	0.000	0.000	0.000	0.000	0.000	0.000	0.000
Fe	4.279	4.351	4.698	4.411	4.368	4.469	4.218	4.159
Mn	1.148	1.081	0.697	1.134	0.961	0.927	1.071	1.077
Mg	0.192	0.146	0.265	0.122	0.260	0.240	0.171	0.219
Ca	0.259	0.333	0.294	0.332	0.306	0.293	0.563	0.489
Na	0.000	0.000	0.000	0.000	0.000	0.000	0.000	0.000
K	0.000	0.000	0.000	0.000	0.000	0.000	0.000	0.000

AT%Fe	72.8	73.6	78.9	73.5	75.4	75.4	70.0	70.0
AT%Mn	19.5	18.3	11.7	18.9	14.9	15.6	17.8	18.1
AT%Mg	3.3	2.5	4.4	2.0	4.5	4.0	2.8	3.7
AT%Ca	4.4	5.6	4.9	5.5	5.3	4.9	9.4	8.2

	212-1B	212-1C	212-1D	212-1E	212-1F	212-2A	212-2B	212-3
SiO2	37.20	37.10	37.90	37.40	37.30	37.30	37.10	37.60
Al2O3	20.50	20.40	21.10	20.80	21.00	21.00	21.20	21.10
TiO2	0.00	0.00	0.00	0.00	0.00	0.00	0.00	0.00
FeO	28.90	31.00	30.70	30.70	30.40	33.40	34.80	33.40
MnO	7.30	7.00	7.90	7.50	7.30	4.60	3.60	4.50
MgO	0.60	0.80	0.80	0.70	0.70	1.40	1.70	1.50
CaO	5.00	3.20	3.00	2.60	3.30	2.90	2.40	3.30
Na2O	0.00	0.00	0.00	0.00	0.00	0.00	0.00	0.00
K2O	0.00	0.00	0.00	0.00	0.00	0.00	0.00	0.00
TOTAL	99.50	99.50	101.40	99.70	100.00	100.50	100.80	101.40

Si	6.063	6.067	6.069	6.088	6.052	6.022	5.978	6.015
Al	3.939	3.933	3.983	3.992	4.017	3.997	4.027	3.979
Ti	0.000	0.000	0.000	0.000	0.000	0.000	0.000	0.000
Fe	3.939	4.240	4.111	4.179	4.125	4.510	4.690	4.468
Mn	1.008	0.970	1.071	1.034	1.003	0.629	0.491	0.610
Mg	0.146	0.195	0.191	0.170	0.169	0.337	0.408	0.358
Ca	0.873	0.561	0.515	0.453	0.574	0.484	0.414	0.566
Na	0.000	0.000	0.000	0.000	0.000	0.000	0.000	0.000
K	0.000	0.000	0.000	0.000	0.000	0.000	0.000	0.000

AT%Fe	66.0	71.1	69.8	71.6	70.3	75.7	78.1	74.5
AT%Mn	16.9	16.3	18.2	17.7	17.1	10.6	8.2	10.2
AT%Mg	2.4	3.3	3.2	2.9	2.9	5.7	6.8	6.0
AT%Ca	14.6	9.4	8.7	7.8	9.8	8.1	6.9	9.4

	212-4	212-5	212-6	212-7	212-8	212-9	212-10	212-11
SiO2	37.60	37.00	37.50	36.40	37.30	36.90	36.30	37.00
Al2O3	21.10	20.80	20.80	20.70	21.10	20.90	20.80	21.00
TiO2	0.00	0.00	0.00	0.00	0.00	0.00	0.00	0.00
FeO	33.50	30.70	30.10	28.60	28.90	29.50	28.00	30.00
MnO	4.60	7.70	8.70	9.80	9.60	8.90	10.00	8.00
MgO	1.40	1.10	1.00	0.90	0.80	0.80	0.80	1.00
CaO	3.60	2.90	3.40	2.90	3.60	3.10	2.80	3.30
Na2O	0.00	0.00	0.00	0.00	0.00	0.00	0.00	0.00
K2O	0.00	0.00	0.00	0.00	0.00	0.00	0.00	0.00
TOTAL	101.80	100.20	101.50	99.30	101.30	100.10	98.70	100.30

Si	6.001	6.011	6.022	5.981	5.997	6.005	5.989	5.999
Al	3.978	3.984	3.938	4.010	4.000	4.010	4.046	4.014
Ti	0.000	0.000	0.000	0.000	0.000	0.000	0.000	0.000
Fe	4.472	4.171	4.042	3.930	3.886	4.015	3.864	4.068
Mn	0.622	1.060	1.183	1.364	1.307	1.227	1.398	1.099
Mg	0.333	0.266	0.239	0.220	0.192	0.194	0.197	0.242
Ca	0.616	0.585	0.585	0.511	0.620	0.541	0.495	0.573
Na	0.000	0.000	0.000	0.000	0.000	0.000	0.000	0.000
K	0.000	0.000	0.000	0.000	0.000	0.000	0.000	0.000

AT%Fe	74.0	69.5	66.8	65.2	64.7	67.2	64.9	68.0
AT%Mn	10.3	17.7	19.6	22.6	21.8	20.5	23.5	18.4
AT%Mg	5.5	4.4	4.0	3.7	3.2	3.2	3.3	4.0
AT%Ca	10.2	8.4	9.7	8.5	10.3	9.0	8.3	9.6

	212-12	212-13	213-1	213-1A	213-1B	213-1C	213-1D	213-1E
SiO2	36.88	37.18	37.28	36.68	36.88	37.28	37.68	38.38
Al2O3	21.18	28.98	21.18	28.68	28.88	28.78	21.38	28.48
TiO2	8.88	8.88	8.88	8.88	8.88	8.88	8.88	8.88
FeO	29.98	34.38	33.48	33.78	33.18	38.58	32.78	38.28
MnO	7.38	3.38	4.48	5.28	4.38	7.38	3.98	5.48
MgO	1.28	2.18	1.28	1.88	1.48	8.88	2.38	2.88
CaO	4.88	2.38	3.58	2.98	3.48	3.28	3.58	2.98
Na2O	8.88	8.88	8.88	8.88	8.88	8.88	8.88	8.88
K2O	8.88	8.88	8.88	8.88	8.88	8.88	8.88	8.88
TOTAL	188.38	188.88	188.88	188.88	99.88	99.78	181.38	188.88

Si	5.968	6.887	5.995	5.983	5.998	6.868	5.988	6.137
Al	4.829	3.989	4.889	3.978	3.992	3.976	3.999	3.854
Ti	8.888	8.888	8.888	8.888	8.888	8.888	8.888	8.888
Fe	4.858	4.644	4.582	4.687	4.586	4.156	4.355	4.847
Mn	1.882	8.453	8.681	8.728	8.593	1.887	8.526	8.733
Mg	8.298	8.587	8.288	8.244	8.348	8.194	8.546	8.669
Ca	8.694	8.399	8.684	8.588	8.593	8.559	8.597	8.498
Na	8.888	8.888	8.888	8.888	8.888	8.888	8.888	8.888
K	8.888	8.888	8.888	8.888	8.888	8.888	8.888	8.888

AT%Fe	67.1	77.4	75.1	75.8	74.7	78.2	72.3	68.1
AT%Mn	16.6	7.5	18.8	11.8	9.8	17.8	8.7	12.3
AT%Mg	4.8	8.4	4.8	4.8	5.6	3.3	9.1	11.2
AT%Ca	11.5	6.6	18.1	8.4	9.8	9.4	9.9	8.4

	213-1F	213-1G	213-1H	213-1J	213-1K	213-1L	213-1M	213-1N
SiO2	36.98	37.28	37.58	36.98	36.98	37.48	35.68	37.18
Al2O3	28.68	28.98	21.28	28.78	28.58	28.68	28.88	28.58
TiO2	8.88	8.88	8.88	8.88	8.88	8.88	8.88	8.88
FeO	32.18	38.78	31.98	32.78	31.18	38.38	38.88	38.98
MnO	6.28	5.88	5.88	4.78	6.88	6.38	6.98	5.88
MgO	8.98	1.88	1.68	1.38	1.48	1.88	1.58	1.88
CaO	2.88	4.48	4.88	3.48	3.18	3.98	3.68	3.38
Na2O	8.88	8.88	8.88	8.88	8.88	8.88	8.88	8.88
K2O	8.88	8.88	8.88	8.88	8.88	8.88	8.88	8.88
TOTAL	99.58	188.88	181.28	99.78	99.88	99.58	98.48	98.68

Si	6.838	6.826	5.997	6.812	6.843	6.882	5.892	6.889
Al	3.974	3.992	3.997	3.976	3.958	3.958	4.858	3.966
Ti	8.888	8.888	8.888	8.888	8.888	8.888	8.888	8.888
Fe	4.393	4.159	4.266	4.455	4.259	4.121	4.153	4.241
Mn	8.859	8.796	8.677	8.649	8.832	8.868	8.967	8.886
Mg	8.219	8.241	8.381	8.316	8.342	8.242	8.378	8.245
Ca	8.491	8.764	8.685	8.594	8.544	8.688	8.638	8.588
Na	8.888	8.888	8.888	8.888	8.888	8.888	8.888	8.888
K	8.888	8.888	8.888	8.888	8.888	8.888	8.888	8.888

AT%Fe	73.7	69.8	71.8	74.1	71.3	69.7	67.8	72.2
AT%Mn	14.4	13.4	11.3	18.8	13.9	14.7	15.8	13.7
AT%Mg	3.7	4.1	6.3	5.2	5.7	4.1	6.8	4.2
AT%Ca	8.2	12.8	11.4	9.9	9.1	11.5	18.4	9.9

	213-2	213-3	215-1	215-2	215-3	215-4	215-5	215-6
SiO2	37.50	38.00	36.40	37.60	37.60	37.80	37.20	37.60
Al2O3	21.20	21.40	20.20	20.70	21.10	21.30	21.10	21.30
TiO2	0.00	0.00	0.00	0.00	0.00	0.00	0.00	0.00
FeO	31.60	32.40	30.80	31.00	30.90	29.40	30.40	30.20
MnO	5.20	6.00	5.60	5.50	5.30	8.20	7.20	7.10
MgO	1.90	1.50	1.60	1.60	1.90	1.00	1.40	1.50
CaO	3.50	3.10	3.60	4.00	4.30	3.90	4.00	4.30
Na2O	0.00	0.00	0.00	0.00	0.00	0.00	0.00	0.00
K2O	0.00	0.00	0.00	0.00	0.00	0.00	0.00	0.00
TOTAL	100.90	102.40	96.20	100.40	101.10	101.60	101.30	102.00

Si	6.004	6.017	6.014	6.054	6.005	6.029	5.968	5.977
Al	4.001	3.995	3.934	3.929	3.973	4.005	3.990	3.992
Ti	0.000	0.000	0.000	0.000	0.000	0.000	0.000	0.000
Fe	4.231	4.290	4.256	4.174	4.127	3.922	4.079	4.015
Mn	0.705	0.805	0.784	0.750	0.717	1.108	0.978	0.956
Mg	0.453	0.354	0.394	0.384	0.452	0.238	0.335	0.355
Ca	0.600	0.526	0.637	0.690	0.736	0.667	0.688	0.732
Na	0.000	0.000	0.000	0.000	0.000	0.000	0.000	0.000
K	0.000	0.000	0.000	0.000	0.000	0.000	0.000	0.000

AT%Fe	70.6	71.8	70.1	69.6	68.4	66.1	67.1	66.3
AT%Mn	11.8	13.5	12.9	12.5	11.9	18.7	16.1	15.8
AT%Mg	7.6	5.9	6.5	6.4	7.5	4.0	5.5	5.9
AT%Ca	10.0	8.8	10.5	11.5	12.2	11.2	11.3	12.1

	215-7	215-8	215-9	215-10	216-1	216-1A	216-1B	216-2
SiO2	37.00	37.50	37.80	37.60	37.20	38.20	38.10	37.60
Al2O3	21.10	21.10	21.20	21.00	21.00	21.60	21.00	21.00
TiO2	0.00	0.00	0.00	0.00	0.00	0.00	0.00	0.00
FeO	30.70	30.50	31.00	29.90	29.70	32.20	32.20	31.20
MnO	6.20	7.50	6.60	7.10	8.60	5.40	4.50	4.40
MgO	1.30	1.10	1.40	1.50	1.00	1.90	2.20	2.10
CaO	4.00	3.90	3.90	3.20	3.20	3.50	3.50	3.70
Na2O	0.00	0.00	0.00	0.00	0.00	0.00	0.00	0.00
K2O	0.00	0.00	0.00	0.00	0.00	0.00	0.00	0.00
TOTAL	100.30	101.60	101.90	100.30	100.70	102.80	102.30	100.00

Si	5.981	6.000	6.013	6.056	6.009	6.005	5.995	6.046
Al	4.021	3.980	3.976	3.987	3.999	4.003	4.044	3.981
Ti	0.000	0.000	0.000	0.000	0.000	0.000	0.000	0.000
Fe	4.151	4.081	4.124	4.027	4.012	4.233	4.238	4.196
Mn	0.849	1.017	0.889	0.969	1.177	0.719	0.600	0.599
Mg	0.313	0.262	0.332	0.360	0.241	0.445	0.516	0.503
Ca	0.693	0.669	0.665	0.552	0.554	0.589	0.590	0.638
Na	0.000	0.000	0.000	0.000	0.000	0.000	0.000	0.000
K	0.000	0.000	0.000	0.000	0.000	0.000	0.000	0.000

AT%Fe	69.1	67.7	68.6	68.2	67.1	70.7	71.3	70.7
AT%Mn	14.1	16.9	14.8	16.4	19.7	12.0	10.1	10.1
AT%Mg	5.2	4.4	5.5	6.1	4.0	7.4	8.7	8.5
AT%Ca	11.5	11.1	11.1	9.3	9.3	9.8	9.9	10.7

	216-2A	216-2B	216-2C	216-3A	216-3B	216-4A	216-4B	216-5
SiO2	37.30	37.80	36.90	37.50	37.50	37.40	37.50	37.70
Al2O3	21.30	21.30	21.00	21.20	20.80	21.10	21.20	21.10
TiO2	0.00	0.00	0.00	0.00	0.00	0.00	0.00	0.00
FeO	20.20	31.00	20.90	31.70	31.00	31.60	31.70	31.30
MnO	7.90	4.80	7.20	4.20	4.40	4.50	4.70	4.80
MgO	0.80	2.10	1.30	2.10	2.00	1.80	2.00	1.90
CaO	3.80	3.80	3.70	4.10	4.20	4.20	3.80	4.00
Na2O	0.00	0.00	0.00	0.00	0.00	0.00	0.00	0.00
K2O	0.00	0.00	0.00	0.00	0.00	0.00	0.00	0.00
TOTAL	100.30	100.80	100.00	100.80	99.90	100.60	100.90	100.80

Si	6.822	6.830	5.986	5.997	6.844	6.883	5.999	6.829
Al	4.854	4.866	4.816	3.997	3.952	3.992	3.998	3.978
Ti	0.000	0.000	0.000	0.000	0.000	0.000	0.000	0.000
Fe	3.943	4.135	4.857	4.240	4.178	4.242	4.241	4.186
Mn	1.880	0.649	0.989	0.569	0.601	0.612	0.637	0.650
Mg	0.193	0.499	0.314	0.500	0.480	0.431	0.477	0.453
Ca	0.657	0.649	0.643	0.783	0.725	0.722	0.651	0.685
Na	0.000	0.000	0.000	0.000	0.000	0.000	0.000	0.000
K	0.000	0.000	0.000	0.000	0.000	0.000	0.000	0.000

AT%Fe	67.1	69.7	67.6	70.5	69.8	70.6	70.6	70.1
AT%Mn	18.4	10.9	16.5	9.5	10.0	10.2	10.6	10.9
AT%Mg	3.3	8.4	5.2	8.3	8.0	7.2	7.9	7.6
AT%Ca	11.2	10.9	10.7	11.7	12.1	12.0	10.8	11.5

	216-5A	216-5B	216-5C	216-5D	217-2	217-3	217-4	217-5
SiO2	37.80	37.50	37.00	37.30	37.70	36.90	37.30	37.50
Al2O3	21.40	21.30	20.90	20.90	21.00	20.90	21.10	20.80
TiO2	0.00	0.00	0.00	0.00	0.00	0.00	0.00	0.00
FeO	31.60	32.30	31.60	30.40	29.20	30.00	29.30	29.10
MnO	4.80	4.60	4.90	6.60	6.50	5.50	6.40	6.40
MgO	1.80	1.90	1.60	1.20	2.40	2.10	2.30	2.30
CaO	4.10	3.90	3.50	3.60	2.80	3.40	2.60	3.10
Na2O	0.00	0.00	0.00	0.00	0.00	0.00	0.00	0.00
K2O	0.00	0.00	0.00	0.00	0.00	0.00	0.00	0.00
TOTAL	101.50	101.50	99.50	100.00	99.60	98.00	99.00	99.20

Si	6.887	5.977	6.813	6.848	6.871	6.813	6.847	6.860
Al	4.810	4.882	4.804	3.998	3.987	4.815	4.832	3.969
Ti	0.000	0.000	0.000	0.000	0.000	0.000	0.000	0.000
Fe	4.280	4.385	4.295	4.117	3.932	4.888	3.972	3.939
Mn	0.646	0.621	0.675	0.985	0.887	0.759	0.879	0.877
Mg	0.426	0.451	0.388	0.290	0.576	0.510	0.556	0.555
Ca	0.698	0.666	0.609	0.625	0.483	0.594	0.452	0.538
Na	0.000	0.000	0.000	0.000	0.000	0.000	0.000	0.000
K	0.000	0.000	0.000	0.000	0.000	0.000	0.000	0.000

AT%Fe	70.3	71.2	72.8	69.4	66.9	68.7	67.8	66.7
AT%Mn	10.8	10.3	11.3	15.2	15.1	12.8	15.0	14.8
AT%Mg	7.1	7.5	6.5	4.9	9.8	8.6	9.5	9.4
AT%Ca	11.7	11.0	10.2	10.5	8.2	10.0	7.7	9.1

	217-6	217-7	217-8	221-1	221-2	221-3	221-4	221-5
SiO2	37.88	38.28	37.28	38.88	36.88	37.18	36.88	37.88
Al2O3	21.88	21.48	28.98	21.48	21.18	21.38	28.68	21.48
TiO2	8.88	8.88	8.88	8.88	8.88	8.88	8.88	8.88
FeO	27.98	29.78	31.28	38.98	29.48	38.88	29.58	31.88
MnO	8.88	7.18	6.88	6.58	6.18	6.48	6.68	6.38
MgO	1.38	2.48	8.98	2.88	2.18	2.28	1.58	2.88
CaO	3.98	3.88	3.58	3.88	3.38	2.78	3.68	3.28
Na2O	8.88	8.88	8.88	8.88	8.88	8.88	8.88	8.88
K2O	8.88	8.88	8.88	8.88	8.88	8.88	8.88	8.88
TOTAL	188.78	181.88	188.58	181.88	98.88	188.58	98.68	181.78
Si	6.863	6.836	6.828	6.824	5.995	5.967	6.833	6.883
Al	3.971	3.986	3.987	4.888	4.852	4.839	3.982	4.887
Ti	8.888	8.888	8.888	8.888	8.888	8.888	8.888	8.888
Fe	3.742	3.925	4.223	4.897	4.885	4.143	4.845	4.118
Mn	1.196	8.958	8.932	8.873	8.842	8.872	8.917	8.848
Mg	8.311	8.565	8.217	8.473	8.518	8.527	8.367	8.473
Ca	8.678	8.588	8.687	8.518	8.576	8.465	8.632	8.545
Na	8.888	8.888	8.888	8.888	8.888	8.888	8.888	8.888
K	8.888	8.888	8.888	8.888	8.888	8.888	8.888	8.888
AT%Fe	63.2	66.8	78.6	68.8	67.5	69.8	67.9	68.8
AT%Mn	28.2	16.8	15.6	14.7	14.2	14.5	15.4	14.2
AT%Mg	5.2	9.5	3.6	7.9	8.6	8.8	6.1	7.9
AT%Ca	11.3	8.5	18.2	8.6	9.7	7.7	18.6	9.1
	221-6	221-7	221-8	221-9	221-18	221-11	222-1	222-2
SiO2	37.38	37.68	37.58	37.78	37.38	36.88	37.88	38.88
Al2O3	21.88	21.28	21.28	21.38	21.38	21.88	21.28	21.28
TiO2	8.88	8.88	8.88	8.88	8.88	8.88	8.88	8.88
FeO	38.58	38.18	29.78	38.18	29.78	29.98	28.88	29.48
MnO	6.48	6.38	7.88	7.88	6.28	6.38	8.28	7.98
MgO	2.88	2.18	2.18	1.78	1.98	2.88	1.98	2.28
CaO	3.48	3.48	3.18	3.88	3.78	3.88	3.38	3.38
Na2O	8.88	8.88	8.88	8.88	8.88	8.88	8.88	8.88
K2O	8.88	8.88	8.88	8.88	8.88	8.88	8.88	8.88
TOTAL	188.68	188.78	188.68	181.68	188.18	99.88	181.28	182.88
Si	5.996	6.817	6.812	6.881	6.882	5.962	6.828	6.818
Al	3.988	4.888	4.887	3.997	4.841	4.811	3.986	3.957
Ti	8.888	8.888	8.888	8.888	8.888	8.888	8.888	8.888
Fe	4.181	4.828	3.982	4.887	3.997	4.851	3.841	3.893
Mn	8.872	8.854	8.951	8.944	8.845	8.865	1.188	1.859
Mg	8.479	8.581	8.582	8.483	8.456	8.483	8.452	8.519
Ca	8.586	8.583	8.532	8.648	8.638	8.668	8.564	8.568
Na	8.888	8.888	8.888	8.888	8.888	8.888	8.888	8.888
K	8.888	8.888	8.888	8.888	8.888	8.888	8.888	8.888
AT%Fe	67.9	67.5	66.7	66.8	67.3	66.9	64.4	64.5
AT%Mn	14.4	14.3	15.9	15.7	14.2	14.3	18.6	17.6
AT%Mg	7.9	8.4	8.4	6.7	7.7	8.8	7.6	8.6
AT%Ca	9.7	9.8	8.9	18.8	18.7	18.9	9.5	9.3

	222-3	222-4	222-5	222-6	223-1	223-2	223-2A	223-3
SiO2	37.90	37.70	38.00	37.50	37.30	37.30	37.00	37.40
Al2O3	21.30	21.20	21.10	21.20	21.40	21.20	21.10	21.30
TiO2	0.00	0.00	0.00	0.00	0.00	0.00	0.00	0.00
FeO	28.80	30.20	28.60	30.00	24.70	23.60	21.00	29.20
MnO	8.60	8.40	8.30	8.50	14.10	14.50	17.30	9.60
MgO	1.90	1.30	2.10	0.90	0.00	0.60	0.00	0.90
CaO	3.20	2.80	2.90	2.40	2.80	3.50	3.10	2.30
Na2O	0.00	0.00	0.00	0.00	0.00	0.00	0.00	0.00
K2O	0.00	0.00	0.00	0.00	0.00	0.00	0.00	0.00
TOTAL	101.70	101.60	101.00	100.50	100.30	100.70	99.50	100.70
Si	6.020	6.024	6.060	6.053	6.047	6.010	6.047	6.031
Al	3.909	3.994	3.967	4.034	4.090	4.032	4.065	4.050
Ti	0.000	0.000	0.000	0.000	0.000	0.000	0.000	0.000
Fe	3.826	4.036	3.814	4.050	3.340	3.184	2.870	3.938
Mn	1.157	1.137	1.121	1.162	1.936	1.982	2.395	1.311
Mg	0.450	0.310	0.499	0.216	0.000	0.144	0.000	0.216
Ca	0.545	0.479	0.496	0.415	0.466	0.605	0.543	0.397
Na	0.000	0.000	0.000	0.000	0.000	0.000	0.000	0.000
K	0.000	0.000	0.000	0.000	0.000	0.000	0.000	0.000
AT%Fe	64.0	67.7	64.3	69.3	58.0	53.8	49.4	67.2
AT%Mn	19.4	19.1	18.9	19.9	33.5	33.5	41.2	22.4
AT%Mg	7.5	5.2	8.4	3.7	0.0	2.4	0.0	3.7
AT%Ca	9.1	8.0	8.4	7.1	8.4	10.2	9.3	6.8
	223-3A	223-9B	223-3C	223-4	223-5	224-1	224-2	224-2A
SiO2	37.00	37.10	37.20	37.70	37.30	37.40	37.20	37.20
Al2O3	20.60	21.00	21.10	21.40	21.30	21.20	20.80	21.10
TiO2	0.00	0.00	0.00	0.00	0.00	0.00	0.00	0.00
FeO	27.90	27.10	24.50	31.60	29.70	33.80	32.10	32.10
MnO	9.70	10.40	12.30	5.20	8.30	6.10	8.00	7.50
MgO	1.00	0.70	0.70	2.40	1.00	1.70	0.60	1.10
CaO	2.80	3.40	3.20	3.10	2.70	1.00	2.60	1.60
Na2O	0.00	0.00	0.00	0.00	0.00	0.00	0.00	0.00
K2O	0.00	0.00	0.00	0.00	0.00	0.00	0.00	0.00
TOTAL	99.00	99.70	99.00	101.40	100.30	102.00	101.30	100.60
Si	6.063	6.037	6.070	5.993	6.027	5.977	6.013	6.022
Al	3.979	4.028	4.059	4.011	4.058	3.994	3.964	4.027
Ti	0.000	0.000	0.000	0.000	0.000	0.000	0.000	0.000
Fe	3.823	3.698	3.343	4.201	4.014	4.517	4.339	4.346
Mn	1.346	1.433	1.700	0.700	1.136	0.826	1.095	1.028
Mg	0.244	0.170	0.170	0.569	0.241	0.405	0.145	0.265
Ca	0.492	0.593	0.559	0.528	0.468	0.308	0.450	0.278
Na	0.000	0.000	0.000	0.000	0.000	0.000	0.000	0.000
K	0.000	0.000	0.000	0.000	0.000	0.000	0.000	0.000
AT%Fe	64.7	62.7	57.9	70.0	60.5	74.6	72.0	73.4
AT%Mn	22.0	24.4	29.4	11.7	19.4	13.6	10.2	17.4
AT%Mg	4.1	2.9	2.9	9.5	4.1	6.7	2.4	4.5
AT%Ca	8.3	10.1	9.7	8.8	8.0	5.1	7.5	4.7

	224-3	224-3A	224-3B	224-3C	224-3D	224-3F	224-4	226-1
SiO2	36.90	37.70	37.00	36.20	37.30	36.00	37.20	36.90
Al2O3	21.00	21.20	21.20	20.40	21.20	20.50	21.10	20.50
TiO2	0.00	0.00	0.00	0.00	0.00	0.00	0.00	0.00
FeO	29.00	30.60	32.00	30.50	31.40	30.20	30.70	28.90
MnO	7.00	8.10	7.90	8.70	7.90	8.90	8.10	9.10
MgO	0.60	0.70	0.80	0.40	0.90	0.80	0.80	0.60
CaO	4.50	2.90	2.20	2.80	2.60	2.50	2.40	2.80
Na2O	0.00	0.00	0.00	0.00	0.00	0.00	0.00	0.00
K2O	0.00	0.00	0.00	0.00	0.00	0.00	0.00	0.00
TOTAL	100.60	101.20	101.90	99.00	101.30	99.70	100.30	98.80
Si	5.976	6.052	6.044	5.994	6.001	6.020	6.032	6.073
Al	4.010	4.012	3.995	3.982	4.021	3.959	4.033	3.978
Ti	0.000	0.000	0.000	0.000	0.000	0.000	0.000	0.000
Fe	4.037	4.109	4.279	4.223	4.225	4.137	4.163	3.978
Mn	1.070	1.102	1.070	1.220	1.077	1.235	1.113	1.269
Mg	0.145	0.167	0.191	0.099	0.216	0.195	0.193	0.147
Ca	0.781	0.499	0.377	0.497	0.448	0.439	0.417	0.494
Na	0.000	0.000	0.000	0.000	0.000	0.000	0.000	0.000
K	0.000	0.000	0.000	0.000	0.000	0.000	0.000	0.000
AT#Fe	66.9	69.9	72.3	69.9	70.8	68.9	70.7	67.6
AT#Mn	17.7	18.7	18.1	20.2	18.0	20.6	18.9	21.5
AT#Mg	2.4	2.9	3.2	1.6	3.6	3.3	3.3	2.5
AT#Ca	12.9	8.5	6.4	8.2	7.5	7.3	7.1	8.4
	226-2	226-3	227-1	227-2	227-3	227-4	227-5	227-6
SiO2	37.20	37.10	36.90	37.00	37.30	36.00	37.00	37.20
Al2O3	21.30	21.00	21.00	21.40	20.90	20.30	20.90	20.60
TiO2	0.00	0.00	0.00	0.00	0.00	0.00	0.00	0.00
FeO	34.40	39.10	24.10	29.90	31.00	32.70	31.30	31.20
MnO	6.70	2.50	15.00	9.40	7.60	6.50	8.20	8.30
MgO	0.50	0.00	0.40	1.10	0.00	0.50	0.70	1.00
CaO	1.60	0.90	1.00	1.50	2.10	2.10	1.50	1.70
Na2O	0.00	0.00	0.00	0.00	0.00	0.00	0.00	0.00
K2O	0.00	0.00	0.00	0.00	0.00	0.00	0.00	0.00
TOTAL	101.70	101.40	99.00	101.10	100.50	98.90	99.60	100.00
Si	5.993	6.004	6.001	6.002	6.047	6.076	6.052	6.053
Al	4.045	4.000	4.007	4.045	3.995	3.952	4.030	3.958
Ti	0.000	0.000	0.000	0.000	0.000	0.000	0.000	0.000
Fe	4.035	5.292	3.311	4.010	4.312	4.510	4.282	4.252
Mn	0.914	0.343	2.087	1.277	1.044	0.909	1.135	1.146
Mg	0.120	0.193	0.098	0.263	0.193	0.123	0.171	0.243
Ca	0.276	0.156	0.282	0.258	0.365	0.372	0.263	0.297
Na	0.000	0.000	0.000	0.000	0.000	0.000	0.000	0.000
K	0.000	0.000	0.000	0.000	0.000	0.000	0.000	0.000
AT#Fe	78.0	88.4	57.3	69.0	72.9	76.3	73.2	71.6
AT#Mn	15.4	5.7	30.1	22.0	17.6	15.4	19.4	19.3
AT#Mg	2.0	3.2	1.7	4.5	3.3	2.1	2.9	4.1
AT#Ca	4.6	2.6	4.9	4.4	6.2	6.3	4.5	5.0

	227-7	227-8	227-9	1456-1	1456-2	1456-3	1456-4	1458-1
SiO2	37.00	36.60	36.80	36.90	36.70	37.00	36.80	36.40
Al2O3	20.90	20.70	20.70	20.80	20.40	20.80	20.70	20.30
TiO2	0.00	0.00	0.00	0.00	0.00	0.00	0.00	0.00
FeO	24.90	31.70	33.10	29.10	28.60	27.70	29.60	33.60
MnO	14.70	8.30	6.80	9.50	10.20	11.40	9.10	5.60
MgO	0.60	0.90	0.80	1.30	1.40	1.10	1.40	0.30
CaO	2.20	1.70	1.30	1.90	2.00	1.90	2.40	2.90
Na2O	0.00	0.00	0.00	0.00	0.00	0.00	0.00	0.00
K2O	0.00	0.00	0.00	0.00	0.00	0.00	0.00	0.00
TOTAL	100.30	99.90	99.50	99.50	99.30	99.90	100.00	99.10

Si	6.021	5.995	6.040	6.027	6.022	6.029	5.995	6.021
Al	4.010	3.998	4.005	4.005	3.946	3.996	3.975	3.959
Ti	0.000	0.000	0.000	0.000	0.000	0.000	0.000	0.000
Fe	3.389	4.343	4.543	3.975	3.925	3.775	4.833	4.648
Mn	2.026	1.152	0.945	1.314	1.418	1.574	1.256	0.785
Mg	0.146	0.220	0.196	0.316	0.342	0.267	0.340	0.074
Ca	0.384	0.298	0.229	0.333	0.352	0.332	0.419	0.514
Na	0.000	0.000	0.000	0.000	0.000	0.000	0.000	0.000
K	0.000	0.000	0.000	0.000	0.000	0.000	0.000	0.000

AT#Fe	57.0	72.2	76.8	66.9	65.0	63.5	66.7	77.2
AT#Mn	34.1	19.2	16.0	22.1	23.5	26.5	20.8	13.0
AT#Mg	2.4	3.7	3.3	5.3	5.7	4.5	5.6	1.2
AT#Ca	6.5	5.0	3.9	5.6	5.8	5.6	6.9	8.5

	1458-2	1458-3	1458-4	1458-5	1458-6	1458-7	1458-8	164-1
SiO2	36.70	36.70	36.60	36.10	36.90	37.10	36.20	36.70
Al2O3	21.00	20.60	21.00	20.80	20.90	20.50	20.20	20.60
TiO2	0.00	0.00	0.00	0.00	0.00	0.00	0.00	0.00
FeO	34.00	35.10	34.70	35.20	16.90	28.90	32.50	36.30
MnO	5.30	4.70	4.70	4.90	22.50	11.20	7.20	3.70
MgO	0.50	1.50	1.60	1.00	0.00	0.90	0.70	1.30
CaO	2.90	1.10	1.00	0.90	1.40	1.20	1.00	2.30
Na2O	0.00	0.00	0.00	0.00	0.00	0.00	0.00	0.00
K2O	0.00	0.00	0.00	0.00	0.00	0.00	0.00	0.00
TOTAL	100.40	99.70	99.60	99.70	98.60	99.80	98.60	100.90

Si	5.979	6.009	5.984	5.925	6.009	6.068	6.018	5.962
Al	4.833	3.976	4.048	4.025	4.066	3.953	3.959	3.946
Ti	0.000	0.000	0.000	0.000	0.000	0.000	0.000	0.000
Fe	4.633	4.800	4.745	4.832	2.332	3.953	4.518	4.932
Mn	0.731	0.652	0.651	0.681	3.145	1.552	1.014	0.500
Mg	0.121	0.366	0.390	0.440	0.000	0.219	0.173	0.315
Ca	0.506	0.193	0.175	0.150	0.248	0.210	0.321	0.400
Na	0.000	0.000	0.000	0.000	0.000	0.000	0.000	0.000
K	0.000	0.000	0.000	0.000	0.000	0.000	0.000	0.000

AT#Fe	77.3	79.9	79.6	79.1	40.7	66.6	75.0	80.1
AT#Mn	12.2	10.8	10.9	11.1	54.9	26.1	16.8	8.3
AT#Mg	2.0	6.1	6.5	7.2	0.0	3.7	2.9	5.1
AT#Ca	8.4	3.2	2.9	2.6	4.3	3.5	5.3	6.5

	104-2	104-3	104-4	104-5	104-6	104-7	104-8	104-9
SiO2	37.30	37.40	37.00	36.40	36.00	32.20	37.20	36.60
Al2O3	20.70	21.20	20.00	20.00	20.00	20.00	21.10	20.10
TiO2	0.00	0.00	0.00	0.00	0.00	0.00	0.00	0.00
FeO	32.00	35.10	32.40	31.50	32.90	33.20	31.70	36.00
MnO	6.40	4.60	7.10	7.60	6.70	6.40	7.20	4.00
MgO	1.00	1.10	0.00	0.70	1.00	0.00	0.90	0.00
CaO	2.90	2.20	2.70	2.50	2.50	2.40	2.60	2.10
Na2O	0.00	0.00	0.00	0.00	0.00	0.00	0.00	0.00
K2O	0.00	0.00	0.00	0.00	0.00	0.00	0.00	0.00
TOTAL	101.10	101.60	100.00	98.70	99.90	95.00	100.70	99.60

Si	6.022	6.002	6.001	6.030	5.912	5.505	6.014	6.030
Al	3.940	4.011	3.977	3.912	4.027	4.261	4.022	3.904
Ti	0.000	0.000	0.000	0.000	0.000	0.000	0.000	0.000
Fe	4.420	4.711	4.305	4.370	4.519	4.824	4.286	4.960
Mn	0.875	0.625	0.975	1.000	0.932	0.942	0.986	0.538
Mg	0.241	0.263	0.193	0.173	0.245	0.207	0.217	0.196
Ca	0.502	0.370	0.469	0.444	0.440	0.447	0.450	0.371
Na	0.000	0.000	0.000	0.000	0.000	0.000	0.000	0.000
K	0.000	0.000	0.000	0.000	0.000	0.000	0.000	0.000

AT%Fe	73.2	78.8	72.8	72.2	73.6	75.1	72.2	81.5
AT%Mn	14.5	10.5	16.2	17.6	15.2	14.7	16.6	9.2
AT%Mg	4.0	4.4	3.2	2.9	4.0	3.2	3.7	3.2
AT%Ca	8.3	6.3	7.8	7.3	7.2	7.0	7.6	6.1

	705-1	705-1A	705-1B	705-2	705-2A	705-3	705-4	705-5
SiO2	36.20	39.50	35.20	35.60	36.30	37.40	35.60	36.10
Al2O3	20.00	19.10	19.70	19.60	20.60	19.50	20.20	20.20
TiO2	0.00	0.00	0.00	0.00	0.00	0.00	0.00	0.00
FeO	30.70	30.00	20.40	35.30	34.70	33.30	35.00	34.70
MnO	8.70	7.00	18.30	4.30	5.10	4.70	4.20	4.20
MgO	0.00	2.00	0.50	1.60	2.00	1.00	2.10	1.00
CaO	2.00	1.90	3.00	1.60	1.60	1.70	1.50	1.60
Na2O	0.00	0.00	0.00	0.00	0.00	0.00	0.00	0.00
K2O	0.00	0.00	0.00	0.00	0.00	0.00	0.00	0.00
TOTAL	99.20	99.50	97.10	98.00	100.30	98.40	98.60	98.60

Si	5.992	6.370	5.950	5.970	5.924	6.164	5.913	5.970
Al	3.903	3.632	3.932	3.875	3.963	3.789	3.956	3.945
Ti	0.000	0.000	0.000	0.000	0.000	0.000	0.000	0.000
Fe	4.250	4.046	2.800	4.950	4.736	4.590	4.062	4.007
Mn	1.220	0.950	2.624	0.611	0.705	0.656	0.591	0.589
Mg	0.197	0.481	0.126	0.400	0.486	0.442	0.520	0.444
Ca	0.497	0.320	0.544	0.287	0.280	0.300	0.267	0.284
Na	0.000	0.000	0.000	0.000	0.000	0.000	0.000	0.000
K	0.000	0.000	0.000	0.000	0.000	0.000	0.000	0.000

AT%Fe	69.0	69.6	46.7	79.2	76.3	76.6	77.9	78.5
AT%Mn	19.0	16.5	42.4	9.0	11.4	11.0	9.5	9.6
AT%Mg	3.2	8.3	2.0	6.4	7.8	7.4	8.3	7.3
AT%Ca	8.1	5.6	8.8	4.6	4.5	5.0	4.3	4.6

	722-1	722-2	722-3	722-3A	722-3B	722-4	722-4A	722-4B
SiO2	35.30	36.10	38.10	34.90	35.90	35.30	35.50	35.30
Al2O3	20.00	18.60	19.30	19.30	20.00	19.00	20.00	19.00
TiO2	0.00	0.00	0.00	0.00	0.00	0.00	0.00	0.00
FeO	40.30	36.10	37.40	39.50	37.90	39.00	40.00	39.30
MnO	2.00	3.20	3.70	2.00	4.10	2.90	1.90	3.00
MgO	0.30	0.60	0.00	0.00	0.50	0.50	0.70	0.40
CaO	0.60	2.90	0.50	0.70	0.00	0.60	0.30	0.40
Na2O	0.00	0.00	0.00	0.00	0.00	0.00	0.00	0.00
K2O	0.00	0.00	0.00	0.00	0.00	0.00	0.00	0.00
TOTAL	99.30	97.50	99.00	97.20	99.20	98.90	99.20	98.20
Si	5.919	6.102	6.294	5.979	5.986	5.935	5.939	5.964
Al	3.954	3.706	3.759	3.898	3.931	3.925	3.944	3.944
Ti	0.000	0.000	0.000	0.000	0.000	0.000	0.000	0.000
Fe	5.651	5.103	5.167	5.660	5.285	5.596	5.708	5.553
Mn	0.398	0.458	0.518	0.406	0.579	0.429	0.175	0.101
Mg	0.075	0.151	0.000	0.000	0.124	0.125	0.054	0.072
Ca	0.100	0.525	0.000	0.129	0.143	0.100	0.000	0.000
Na	0.000	0.000	0.000	0.000	0.000	0.000	0.000	0.000
K	0.000	0.000	0.000	0.000	0.000	0.000	0.000	0.000
AT%Fe	90.7	81.8	89.5	91.4	86.2	89.6	92.0	90.2
AT%Mn	6.4	7.3	9.0	6.6	9.4	6.6	4.3	7.0
AT%Mg	1.2	2.4	0.0	0.0	2.0	2.0	2.8	1.6
AT%Ca	1.7	8.4	1.5	2.1	2.3	1.7	0.9	1.2
	722-4C	722-5	722-6	722-7	724-1	724-2	724-3	724-4
SiO2	36.30	35.70	35.60	35.50	37.40	37.30	37.20	0.00
Al2O3	20.10	19.90	19.70	19.60	21.30	20.70	20.00	1.00
TiO2	0.00	0.00	0.00	0.00	0.00	0.00	0.00	1.00
FeO	38.50	36.70	38.00	37.60	32.70	31.50	26.00	1.00
MnO	4.20	4.50	4.10	4.40	4.00	0.70	10.90	1.00
MgO	0.50	0.40	0.40	0.50	1.90	1.10	0.00	1.00
CaO	0.40	1.50	0.00	1.10	3.10	2.00	3.60	1.00
Na2O	0.00	0.00	0.00	0.00	0.00	0.00	0.00	0.00
K2O	0.00	0.00	0.00	0.00	0.00	0.00	0.00	1.00
TOTAL	100.00	98.70	99.60	98.70	100.40	100.10	100.10	7.00
Si	6.005	5.979	5.986	5.968	6.010	6.054	6.037	0.000
Al	3.920	3.929	3.905	3.885	4.035	3.901	3.900	3.459
Ti	0.000	0.000	0.000	0.000	0.000	0.000	0.000	2.213
Fe	5.327	5.141	5.343	5.287	4.395	4.276	3.638	2.461
Mn	0.589	0.638	0.584	0.627	0.544	0.921	1.498	2.493
Mg	0.123	0.100	0.100	0.125	0.455	0.266	0.193	4.386
Ca	0.071	0.269	0.144	0.190	0.534	0.487	0.626	3.153
Na	0.000	0.000	0.000	0.000	0.000	0.000	0.000	0.000
K	0.000	0.000	0.000	0.000	0.000	0.000	0.000	3.754
AT%Fe	87.2	83.6	86.6	84.8	74.1	71.9	61.1	19.7
AT%Mn	9.6	10.4	9.5	10.0	9.2	15.5	25.2	20.0
AT%Mg	2.0	1.5	1.0	2.0	7.7	4.5	3.2	35.1
AT%Ca	1.2	4.4	2.3	3.2	9.0	8.2	10.5	25.2

	724-5	724-6	724-7	724-8	724-9	724-10	724-11	754-1
SiO2	37.38	36.88	37.18	37.78	38.18	38.18	38.18	37.48
Al2O3	28.88	28.38	28.58	21.18	21.38	21.38	28.88	28.88
TiO2	8.88	8.88	8.88	8.88	8.88	8.88	8.88	8.88
FeO	29.78	31.88	32.68	33.28	32.78	32.78	31.48	33.38
MnO	8.48	4.48	4.98	4.48	4.88	4.88	5.18	7.88
MgO	8.98	1.58	1.38	1.58	1.88	1.88	1.38	1.88
CaO	3.88	4.88	3.38	3.88	4.38	4.38	4.68	1.48
Na2O	8.88	8.88	8.88	8.88	8.88	8.88	8.88	8.88
K2O	8.88	8.88	8.88	8.88	8.88	8.88	8.88	8.88
TOTAL	188.18	98.88	99.78	181.88	182.28	182.28	181.38	188.98
Si	6.853	6.835	6.843	6.848	6.848	6.848	6.879	6.858
Al	3.979	3.925	3.937	3.985	3.981	3.981	3.912	3.967
Ti	8.888	8.888	8.888	8.888	8.888	8.888	8.888	8.888
Fe	4.831	4.362	4.441	4.448	4.336	4.336	4.198	4.585
Mn	1.155	8.811	8.876	8.597	8.845	8.845	8.889	8.959
Mg	8.218	8.367	8.316	8.382	8.236	8.236	8.389	8.241
Ca	8.522	8.783	8.576	8.515	8.738	8.738	8.786	8.243
Na	8.888	8.888	8.888	8.888	8.888	8.888	8.888	8.888
K	8.888	8.888	8.888	8.888	8.888	8.888	8.888	8.888
AT%Fe	68.8	72.2	73.9	74.9	72.9	72.9	78.1	75.7
AT%Mn	19.5	18.1	11.3	18.8	18.8	18.8	11.5	16.1
AT%Mg	3.7	6.1	5.3	6.4	4.8	4.8	5.2	4.1
AT%Ca	8.8	11.6	9.6	8.7	12.3	12.3	13.2	4.1
	754-2	754-3	754-4	754-5	754-6	754-7	484-1	484-1R
SiO2	36.98	36.78	37.58	37.18	36.88	37.18	37.88	42.18
Al2O3	28.88	21.28	28.68	28.68	28.88	21.88	21.88	19.88
TiO2	8.88	8.88	8.88	8.88	8.88	8.88	8.88	8.88
FeO	31.68	38.88	32.38	32.48	31.88	29.88	31.98	26.78
MnO	7.78	8.88	7.18	8.28	7.28	7.38	6.78	6.98
MgO	8.78	8.88	1.28	1.38	8.68	8.78	8.98	8.98
CaO	1.88	3.38	2.78	1.88	3.88	3.48	2.68	5.38
Na2O	8.88	8.88	8.88	8.88	8.88	8.88	8.88	8.88
K2O	8.88	8.88	8.88	8.88	8.88	8.88	8.88	8.88
TOTAL	99.58	99.48	181.48	99.48	99.48	99.38	188.18	181.78
Mn	1.868	8.913	8.968	8.858	8.999	1.889	8.923	8.988
Mg	8.171	8.195	8.288	8.317	8.146	8.178	8.218	8.288
Ca	8.316	8.577	8.466	8.315	8.527	8.594	8.453	8.883
Na	8.888	8.888	8.888	8.888	8.888	8.888	8.888	8.888
K	8.888	8.888	8.888	8.888	8.888	8.888	8.888	8.888
AT%Fe	73.6	71.4	71.6	74.8	71.8	69.6	73.1	63.4
AT%Mn	18.2	15.5	15.9	14.5	16.9	17.3	15.6	16.6
AT%Mg	2.9	3.3	4.7	5.3	2.5	2.9	3.7	3.8
AT%Ca	5.4	9.8	7.7	5.3	8.9	18.2	7.6	16.1

	484-1B	484-1C	484-2	489-1	489-2	489-3	489-4	489-5A
SiO2	37.40	38.10	36.70	36.30	35.90	35.80	36.20	36.30
Al2O3	20.00	21.50	20.50	20.20	20.00	20.10	20.70	20.40
TiO2	0.00	0.00	0.00	0.00	0.00	0.00	0.00	0.00
FeO	31.80	35.90	32.70	26.60	34.30	37.60	31.90	28.90
MnO	7.20	3.80	5.20	4.30	5.80	3.30	8.20	8.30
MgO	0.90	1.50	1.20	1.00	0.80	0.90	1.00	0.90
CaO	2.00	1.90	2.00	1.00	0.90	0.70	2.10	3.80
Na2O	0.00	0.00	0.00	0.00	0.00	0.00	0.00	0.00
K2O	0.00	0.00	0.00	0.00	0.00	0.00	0.00	0.00
TOTAL	100.10	102.70	98.30	89.40	97.70	98.40	100.10	98.60

Si	6.075	6.026	6.060	6.370	6.028	5.988	5.936	5.906
Al	3.983	4.009	3.991	4.179	3.959	3.964	4.001	3.973
Ti	0.000	0.000	0.000	0.000	0.000	0.000	0.000	0.000
Fe	4.320	4.749	4.516	3.984	4.817	5.260	4.374	3.903
Mn	0.991	0.509	0.727	0.639	0.825	0.468	1.139	1.161
Mg	0.218	0.354	0.295	0.262	0.200	0.224	0.244	0.222
Ca	0.348	0.322	0.354	0.100	0.162	0.125	0.369	0.673
Na	0.000	0.000	0.000	0.000	0.000	0.000	0.000	0.000
K	0.000	0.000	0.000	0.000	0.000	0.000	0.000	0.000

AT%Fe	73.5	80.0	76.6	78.2	80.2	86.6	71.4	66.0
AT%Mn	16.9	8.6	12.3	12.8	13.7	7.7	18.6	19.2
AT%Mg	3.7	6.0	5.0	5.2	3.3	3.7	4.0	3.7
AT%Ca	5.9	5.4	6.0	3.8	2.7	2.1	6.0	11.1

	489-5B	489-5C	489-5D	489-5E	489-5F	489-5G	489-5H	489-5J
SiO2	37.50	35.40	36.00	35.70	36.00	36.10	37.00	36.30
Al2O3	20.40	20.40	20.60	20.60	20.90	20.80	21.30	21.10
TiO2	0.00	0.00	0.00	0.00	0.00	0.00	0.00	0.00
FeO	30.50	30.90	28.50	28.60	31.90	28.40	27.40	28.40
MnO	8.10	8.80	12.00	13.00	10.30	12.40	14.70	13.60
MgO	1.10	1.00	0.00	0.50	0.90	0.70	0.70	0.60
CaO	3.00	3.10	1.10	0.60	0.90	0.80	0.80	1.00
Na2O	0.00	0.00	0.00	0.00	0.00	0.00	0.00	0.00
K2O	0.00	0.00	0.00	0.00	0.00	0.00	0.00	0.00
TOTAL	100.60	99.60	98.20	99.00	100.90	99.20	101.90	101.00

Si	6.069	5.860	6.016	5.944	5.891	5.969	5.962	5.920
Al	3.892	3.981	4.059	4.044	4.032	4.055	4.047	4.057
Ti	0.000	0.000	0.000	0.000	0.000	0.000	0.000	0.000
Fe	4.120	4.278	3.983	3.982	4.366	3.928	3.693	3.874
Mn	1.110	1.234	1.699	1.833	1.428	1.737	2.087	1.879
Mg	0.265	0.247	0.000	0.124	0.219	0.173	0.168	0.146
Ca	0.520	0.550	0.197	0.107	0.150	0.142	0.130	0.175
Na	0.000	0.000	0.000	0.000	0.000	0.000	0.000	0.000
K	0.000	0.000	0.000	0.000	0.000	0.000	0.000	0.000

AT%Fe	68.5	67.8	67.8	65.9	70.7	65.7	61.5	63.8
AT%Mn	18.4	19.6	20.9	20.3	23.1	29.1	33.4	30.9
AT%Mg	4.4	3.9	0.0	2.1	3.6	2.9	2.8	2.4
AT%Ca	8.6	8.7	3.4	1.8	2.6	2.4	2.3	2.9

	490-1	490-2	490-3	490-4	490-5	490-5b	490-7	490-8
SiO2	36.60	35.80	35.50	36.20	35.70	37.10	36.30	35.50
Al2O3	20.00	22.00	20.90	21.10	20.60	21.30	20.90	20.70
TiO2	0.00	0.00	0.00	0.00	0.00	0.00	0.00	0.00
FeO	37.20	33.90	34.40	26.50	28.00	32.00	32.50	29.50
MnO	3.00	6.10	6.00	15.20	13.50	7.40	9.40	11.70
MgO	1.30	0.90	1.00	0.70	0.70	1.00	0.80	0.40
CaO	1.10	1.40	1.00	0.80	0.80	2.00	1.00	1.00
Na2O	0.00	0.00	0.00	0.00	0.00	0.00	0.00	0.00
K2O	0.00	0.00	0.00	0.00	0.00	0.00	0.00	0.00
TOTAL	100.80	100.10	99.60	100.50	99.30	101.60	100.90	98.00

Si	5.958	5.850	5.874	5.924	5.926	5.968	5.928	5.923
Al	3.992	4.238	4.077	4.071	4.031	4.024	4.071	
Ti	0.000	0.000	0.000	0.000	0.000	0.000	0.000	0.000
Fe	5.065	4.633	4.760	3.627	3.887	4.413	4.439	4.116
Mn	0.524	0.844	0.953	2.107	1.898	1.008	1.300	1.653
Mg	0.315	0.219	0.247	0.171	0.173	0.240	0.195	0.099
Ca	0.192	0.245	0.177	0.140	0.142	0.345	0.175	0.179
Na	0.000	0.000	0.000	0.000	0.000	0.000	0.000	0.000
K	0.000	0.000	0.000	0.000	0.000	0.000	0.000	0.000

AT%Fe	83.1	78.0	77.6	60.0	63.7	73.5	72.7	68.1
AT%Mn	8.6	14.2	15.5	34.9	31.1	16.8	21.3	27.3
AT%Mg	5.2	3.7	4.0	2.8	2.8	4.0	3.2	1.6
AT%Ca	3.1	4.1	2.9	2.3	2.3	5.7	2.9	3.0

	490-9	927-1	927-2	927-3	927-4	927-5	927-6	927-7
SiO2	36.20	36.50	36.50	36.20	36.30	36.90	37.00	37.40
Al2O3	20.50	20.70	20.70	20.90	20.40	20.90	20.60	20.80
TiO2	0.00	0.00	0.00	0.00	0.00	0.00	0.00	0.00
FeO	26.60	33.90	33.20	33.10	33.40	33.60	34.40	33.50
MnO	14.30	2.90	3.00	4.30	3.20	4.40	2.00	4.70
MgO	0.40	1.40	1.40	1.30	1.50	1.00	1.60	1.30
CaO	0.70	3.00	3.90	3.90	3.60	2.70	3.70	2.30
Na2O	0.00	0.00	0.00	0.00	0.00	0.00	0.00	0.00
K2O	0.00	0.00	0.00	0.00	0.00	0.00	0.00	0.00
TOTAL	98.70	99.20	98.70	99.70	98.40	99.50	99.90	100.00

Si	6.018	5.977	5.993	5.918	5.991	6.026	6.010	6.066
Al	4.018	3.996	4.007	4.028	3.969	4.024	3.945	3.977
Ti	0.000	0.000	0.000	0.000	0.000	0.000	0.000	0.000
Fe	3.699	4.642	4.559	4.526	4.610	4.509	4.673	4.544
Mn	2.014	0.402	0.417	0.595	0.447	0.609	0.358	0.646
Mg	0.099	0.342	0.343	0.317	0.360	0.243	0.387	0.314
Ca	0.125	0.667	0.666	0.663	0.637	0.472	0.644	0.400
Na	0.000	0.000	0.000	0.000	0.000	0.000	0.000	0.000
K	0.000	0.000	0.000	0.000	0.000	0.000	0.000	0.000

AT%Fe	62.3	76.7	75.9	73.9	76.0	77.6	77.1	77.0
AT%Mn	33.9	6.6	6.9	9.7	7.4	10.3	5.9	10.9
AT%Mg	1.7	5.6	5.7	5.2	6.1	4.1	6.4	5.3
AT%Ca	2.1	11.0	11.4	11.2	10.5	8.0	10.6	6.8

927-8
SiO2 36.90
Al2O3 20.00
TiO2 0.00
FeO 33.00
MnO 2.90
MgO 1.00
CaO 3.00
Na2O 0.00
K2O 0.00
TOTAL 100.00

Si 5.081
Al 3.975
Mn 0.398
Mg 0.435

AT%Fe 75.4
AT%Mn 6.6
AT%Mg 7.2
AT%Ca 10.9

4. UIF Garnets

	1463-1	1463-2	1463-3	1463-4	1463-5	1463-6	1463-7	1463-8
SiO2	37.50	36.10	36.60	36.40	36.90	37.20	36.90	36.70
Al2O3	20.00	20.50	20.70	20.40	20.70	20.00	20.70	20.50
TiO2	0.00	0.00	0.00	0.00	0.00	0.00	0.00	0.00
FeO	26.10	23.70	24.20	21.50	22.00	26.00	23.00	23.30
MnO	13.50	14.40	13.10	16.60	16.00	13.50	15.90	14.70
MgO	1.00	0.90	0.50	0.50	1.40	1.00	1.10	0.00
CaO	1.70	2.30	4.00	3.30	2.00	1.90	1.60	3.40
Na2O	0.00	0.00	0.00	0.00	0.00	0.00	0.00	0.00
K2O	0.00	0.00	0.00	0.00	0.00	0.00	0.00	0.00
TOTAL	100.60	97.90	99.10	98.70	99.00	100.40	99.20	98.60

Si	6.066	6.005	6.009	6.017	6.014	6.037	6.047	6.065
Al	3.967	4.020	4.007	3.975	3.977	3.979	3.999	3.994
Ti	0.000	0.000	0.000	0.000	0.000	0.000	0.000	0.000
Fe	3.531	3.297	3.323	2.972	2.999	3.529	3.152	3.220
Mn	1.850	2.029	1.822	2.324	2.319	1.856	2.287	2.058
Mg	0.241	0.223	0.122	0.123	0.340	0.242	0.269	0.000
Ca	0.295	0.410	0.704	0.504	0.349	0.330	0.281	0.602
Na	0.000	0.000	0.000	0.000	0.000	0.000	0.000	0.000
K	0.000	0.000	0.000	0.000	0.000	0.000	0.000	0.000

AT%Fe	59.7	55.3	55.7	49.5	49.9	59.2	53.3	54.8
AT%Mn	31.3	34.0	30.5	38.7	38.6	31.2	37.4	35.0
AT%Mg	4.1	3.7	2.0	2.1	5.7	4.1	4.5	0.0
AT%Ca	5.0	6.9	11.8	9.7	5.8	5.5	4.8	10.2

	1463-9	1463-1	1461-1	1461-2	1461-3	1461-4	1461-5	1461-6
SiO2	36.00	36.00	37.50	36.00	36.20	37.30	36.50	36.50
Al2O3	20.60	20.60	20.70	20.40	20.30	19.90	20.10	20.40
TiO2	0.00	0.00	0.00	0.00	0.00	0.00	0.00	0.00
FeO	21.00	21.30	26.00	28.40	30.00	20.50	27.30	20.00
MnO	17.30	17.20	13.00	12.30	9.40	18.00	12.00	10.70
MgO	0.00	0.50	0.70	0.50	0.40	0.00	0.00	0.50
CaO	3.50	3.10	1.70	1.90	2.30	1.00	1.00	2.50
Na2O	0.00	0.00	0.00	0.00	0.00	0.00	0.00	0.00
K2O	0.00	0.00	0.00	0.00	0.00	0.00	0.00	0.00
TOTAL	99.20	99.50	100.40	99.50	99.40	98.10	98.50	91.40

Si	6.049	6.030	6.065	5.958	5.988	6.100	6.077	6.304
Al	3.992	3.979	3.960	3.980	3.959	3.893	3.945	4.154
Ti	0.000	0.000	0.000	0.000	0.000	0.000	0.000	0.000
Fe	2.887	2.919	3.637	3.931	4.261	2.845	3.001	3.004
Mn	2.409	2.387	1.787	1.724	1.317	2.615	1.805	1.565
Mg	0.000	0.122	0.160	0.123	0.000	0.000	0.000	0.120
Ca	0.616	0.544	0.296	0.337	0.400	0.320	0.321	0.463
Na	0.000	0.000	0.000	0.000	0.000	0.000	0.000	0.000
K	0.000	0.000	0.000	0.000	0.000	0.000	0.000	0.000

AT%Fe	48.8	48.9	61.8	64.3	70.0	49.2	64.1	58.2
AT%Mn	40.7	40.0	30.3	28.2	21.6	45.2	30.5	30.3
AT%Mg	0.0	2.0	2.9	2.0	1.6	0.0	0.0	2.5
AT%Ca	10.4	9.1	5.0	5.5	6.7	5.5	5.4	9.0

	1451-7	262-1	262-2	262-3	262-4	262-5	262-6	904-1
SiO2	36.90	37.30	36.80	31.80	37.40	37.50	37.70	34.90
Al2O3	20.50	20.60	20.40	21.10	21.00	21.00	21.30	19.40
TiO2	0.00	0.00	0.00	0.00	0.00	0.00	0.00	0.00
FeO	27.00	27.00	27.10	24.90	25.20	23.70	26.20	29.50
MnO	12.60	11.60	11.60	13.80	13.40	14.90	13.20	11.80
MgO	0.80	0.70	1.30	1.90	1.70	1.00	0.70	1.20
CaO	2.10	2.30	2.70	1.10	1.30	1.70	2.00	1.30
Na2O	0.00	0.00	0.00	0.00	0.00	0.00	0.00	0.00
K2O	0.00	0.00	0.00	0.00	0.00	0.00	0.00	0.00
TOTAL	99.90	99.50	99.90	94.60	100.00	99.60	101.10	98.10

Si	6.835	6.892	6.808	5.553	6.853	6.886	6.858	5.900
Al	3.953	3.967	3.927	4.344	4.007	4.018	4.035	3.867
Ti	0.000	0.000	0.000	0.000	0.000	0.000	0.000	0.000
Fe	3.693	3.688	3.700	3.636	3.411	3.217	3.521	4.171
Mn	1.746	1.685	1.604	2.041	1.837	2.048	1.797	1.690
Mg	0.195	0.170	0.316	0.494	0.410	0.242	0.168	0.302
Ca	0.358	0.483	0.472	0.206	0.225	0.296	0.344	0.236
Na	0.000	0.000	0.000	0.000	0.000	0.000	0.000	0.000
K	0.000	0.000	0.000	0.000	0.000	0.000	0.000	0.000

AT%Fe	61.5	62.9	60.7	57.0	58.0	55.4	60.4	65.2
AT%Mn	29.1	27.4	26.3	32.0	31.2	35.3	30.8	26.4
AT%Mg	3.2	2.9	5.2	7.8	7.0	4.2	2.9	4.7
AT%Ca	6.1	6.9	7.8	3.2	3.8	5.1	5.9	3.7

	904-2	904-3	904-4	904-5	904-6	904-7	904-8	904-9
SiO2	37.20	35.70	35.80	36.20	36.30	36.40	36.30	36.10
Al2O3	20.50	20.00	19.80	20.50	20.50	20.80	20.20	20.30
TiO2	0.00	0.00	0.00	0.00	0.00	0.00	0.00	0.00
FeO	28.50	25.40	27.40	28.70	28.10	28.20	24.80	29.00
MnO	12.70	15.00	13.20	12.70	12.10	12.50	15.20	11.50
MgO	0.90	0.70	0.90	1.00	1.40	1.10	0.90	1.10
CaO	1.40	0.90	0.50	1.00	1.20	1.30	1.20	1.00
Na2O	0.00	0.00	0.00	0.00	0.00	0.00	0.00	0.00
K2O	0.00	0.00	0.00	0.00	0.00	0.00	0.00	0.00
TOTAL	101.20	97.70	97.60	100.10	99.60	100.30	98.60	99.00

Si	6.829	6.883	6.826	5.952	5.968	5.951	6.826	5.983
Al	3.917	3.965	3.929	3.974	3.974	4.009	3.954	3.967
Ti	0.000	0.000	0.000	0.000	0.000	0.000	0.000	0.000
Fe	3.863	3.572	3.857	3.946	3.864	3.856	3.443	4.020
Mn	1.743	2.137	1.882	1.769	1.685	1.731	2.137	1.615
Mg	0.217	0.175	0.226	0.245	0.343	0.268	0.223	0.272
Ca	0.243	0.162	0.090	0.176	0.211	0.228	0.213	0.178
Na	0.000	0.000	0.000	0.000	0.000	0.000	0.000	0.000
K	0.000	0.000	0.000	0.000	0.000	0.000	0.000	0.000

AT%Fe	63.7	59.1	63.7	64.3	63.3	63.4	57.2	66.1
AT%Mn	28.7	35.3	31.1	28.8	27.6	28.5	35.5	26.5
AT%Mg	3.6	2.9	3.7	4.0	5.6	4.4	3.7	4.5
AT%Ca	4.0	2.7	1.5	2.9	3.5	3.7	3.5	2.9

	984-10	984-11	985-1	985-2	985-3	985-4	985-5	264-1
SiO2	36.10	35.40	37.30	37.30	37.30	37.30	36.70	36.80
Al2O3	20.30	19.60	20.60	20.10	20.60	20.20	20.30	19.90
TiO2	0.00	0.00	0.00	0.00	0.00	0.00	0.00	0.00
FeO	28.90	28.00	21.90	22.00	17.90	17.90	15.10	28.80
MnO	11.20	12.00	14.70	17.70	16.40	18.60	20.40	12.00
MgO	1.40	0.00	0.50	0.00	0.40	0.50	0.00	0.80
CaO	1.20	0.70	4.60	2.00	7.40	4.70	5.20	1.70
Na2O	0.00	0.00	0.00	0.00	0.00	0.00	0.00	0.00
K2O	0.00	0.00	0.00	0.00	0.00	0.00	0.00	0.00
TOTAL	99.10	95.70	99.60	99.10	100.00	99.20	97.70	100.00

Si	5.970	6.078	6.070	6.145	6.032	6.097	6.084	6.047
Al	3.958	3.967	3.952	3.904	3.927	3.893	3.967	3.855
Ti	0.000	0.000	0.000	0.000	0.000	0.000	0.000	0.000
Fe	3.997	4.020	2.981	3.031	2.421	2.447	2.093	3.958
Mn	1.569	1.745	2.026	2.470	2.246	2.575	2.804	1.670
Mg	0.345	0.000	0.121	0.000	0.096	0.122	0.000	0.196
Ca	0.213	0.129	0.002	0.353	1.282	0.823	0.924	0.299
Na	0.000	0.000	0.000	0.000	0.000	0.000	0.000	0.000
K	0.000	0.000	0.000	0.000	0.000	0.000	0.000	0.000

AT%Fe	65.3	68.2	50.3	51.8	40.0	41.0	35.6	64.6
AT%Mn	25.6	29.6	34.2	42.2	37.2	43.2	48.7	27.3
AT%Mg	5.6	0.0	2.0	0.0	1.0	2.0	0.0	3.2
AT%Ca	3.5	2.2	13.5	6.0	21.2	13.8	15.7	4.9

	264-2	264-3						
SiO2	35.90	35.40	0.00	0.00	0.00	0.00	0.00	0.00
Al2O3	19.20	19.60	0.00	0.00	0.00	0.00	0.00	0.00
TiO2	0.00	0.00	0.00	0.00	0.00	0.00	0.00	0.00
FeO	28.70	28.90	0.00	0.00	0.00	0.00	0.00	0.00
MnO	11.90	12.50	0.00	0.00	0.00	0.00	0.00	0.00
MgO	1.00	1.00	0.00	0.00	0.00	0.00	0.00	0.00
CaO	1.50	1.20	0.00	0.00	0.00	0.00	0.00	0.00
Na2O	0.00	0.00	0.00	0.00	0.00	0.00	0.00	0.00
K2O	0.00	0.00	0.00	0.00	0.00	0.00	0.00	0.00
TOTAL	98.20	99.60	0.00	0.00	0.00	0.00	0.00	0.00

Si	6.028	6.025	0.000	0.000	0.000	0.000	0.000	0.000
Al	3.801	3.825	0.000	0.000	0.000	0.000	0.000	0.000
Ti	0.000	0.000	0.000	0.000	0.000	0.000	0.000	0.000
Fe	4.030	4.001	0.000	0.000	0.000	0.000	0.000	0.000
Mn	1.693	1.753	0.000	0.000	0.000	0.000	0.000	0.000
Mg	0.250	0.247	0.000	0.000	0.000	0.000	0.000	0.000
Ca	0.270	0.213	0.000	0.000	0.000	0.000	0.000	0.000
Na	0.000	0.000	0.000	0.000	0.000	0.000	0.000	0.000
K	0.000	0.000	0.000	0.000	0.000	0.000	0.000	0.000

AT%Fe	64.6	64.4	0.0	0.0	0.0	0.0	0.0	0.0
AT%Mn	27.1	28.2	0.0	0.0	0.0	0.0	0.0	0.0
AT%Mg	4.0	4.0	0.0	0.0	0.0	0.0	0.0	0.0
AT%Ca	4.3	3.4	0.0	0.0	0.0	0.0	0.0	0.0

5. TIF Garnets

	235-1	235-2	257-1	257-2	257-3	257-4	257-5	268-1
SiO2	38.70	37.70	36.20	36.50	36.90	35.50	36.50	37.30
Al2O3	21.00	21.30	20.20	20.60	20.90	20.30	19.90	21.00
TiO2	0.00	0.00	0.00	0.00	0.00	0.00	0.00	0.00
FeO	24.10	26.40	29.20	30.60	27.00	30.50	27.70	29.50
MnO	11.10	10.70	11.00	9.00	11.00	11.40	13.70	7.90
MgO	0.00	0.50	0.60	0.60	0.50	0.70	0.90	0.00
CaO	6.00	4.00	1.00	3.10	3.70	0.00	1.00	3.90
Na2O	0.00	0.00	0.00	0.00	0.00	0.00	0.00	0.00
K2O	0.00	0.00	0.00	0.00	0.00	0.00	0.00	0.00
TOTAL	101.70	100.60	99.00	101.20	100.00	99.30	99.70	100.40
Si	6.113	6.063	5.977	5.937	5.982	5.914	6.026	6.020
Al	4.060	4.038	3.932	3.951	3.994	3.987	3.873	4.002
Ti	0.000	0.000	0.000	0.000	0.000	0.000	0.000	0.000
Fe	3.184	3.551	4.032	4.163	3.661	4.240	3.825	3.988
Mn	1.485	1.458	1.650	1.350	1.620	1.689	1.916	1.082
Mg	0.000	0.120	0.148	0.145	0.121	0.174	0.221	0.193
Ca	1.016	0.689	0.318	0.540	0.643	0.161	0.177	0.676
Na	0.000	0.000	0.000	0.000	0.000	0.000	0.000	0.000
K	0.000	0.000	0.000	0.000	0.000	0.000	0.000	0.000
AT%Fe	56.0	61.0	65.6	67.2	60.6	68.6	62.3	67.2
AT%Mn	26.1	25.1	26.8	21.8	26.8	26.0	31.2	18.2
AT%Mg	0.0	2.1	2.4	2.3	2.0	2.8	3.6	3.2
AT%Ca	17.9	11.8	5.2	8.7	10.6	2.6	2.9	11.4
	268-2	268-3	268-4	268-5	268-6	268-7	268-8	268-9
SiO2	37.20	37.00	37.30	36.00	36.00	36.00	37.30	37.70
Al2O3	20.50	20.60	20.70	20.90	21.00	20.50	21.00	21.10
TiO2	0.00	0.00	0.00	0.00	0.00	0.00	0.00	0.00
FeO	31.30	32.00	32.00	31.70	31.60	32.70	23.90	33.20
MnO	7.90	7.60	7.20	7.00	8.40	7.80	13.20	6.70
MgO	1.00	0.60	0.00	0.60	0.70	0.50	2.60	1.10
CaO	1.70	1.60	1.90	2.00	1.40	2.20	2.00	1.70
Na2O	0.00	0.00	0.00	0.00	0.00	0.00	0.00	0.00
K2O	0.00	0.00	0.00	0.00	0.00	0.00	0.00	0.00
TOTAL	99.60	99.40	99.90	99.00	99.90	100.50	100.00	101.50
Si	6.000	6.072	6.078	6.020	6.015	6.012	6.011	6.040
Al	3.950	3.986	3.976	4.031	4.047	3.948	3.990	3.990
Ti	0.000	0.000	0.000	0.000	0.000	0.000	0.000	0.000
Fe	4.279	4.392	4.361	4.337	4.320	4.460	3.221	4.454
Mn	1.094	1.057	0.994	1.001	1.163	1.079	1.802	0.910
Mg	0.244	0.147	0.194	0.146	0.171	0.122	0.624	0.263
Ca	0.290	0.281	0.332	0.351	0.245	0.385	0.345	0.292
Na	0.000	0.000	0.000	0.000	0.000	0.000	0.000	0.000
K	0.000	0.000	0.000	0.000	0.000	0.000	0.000	0.000
AT%Fe	72.4	74.7	74.2	73.3	73.2	73.8	53.8	75.2
AT%Mn	10.5	10.0	10.9	10.3	11.7	11.8	18.1	15.4
AT%Mg	4.1	2.5	3.3	2.5	2.9	2.0	10.4	4.4
AT%Ca	5.0	4.8	5.6	5.9	4.2	6.4	5.8	4.9

	260-10	260-11	260-12	260-14	479-1	479-2	479-3	479-4
SiO2	36.00	37.70	37.60	37.60	36.40	35.00	36.20	35.60
Al2O3	21.00	21.00	21.20	21.00	20.00	20.00	20.40	20.70
TiO2	0.00	0.00	0.00	0.00	0.00	0.00	0.00	0.00
FeO	30.20	23.50	33.20	21.70	27.50	26.70	33.00	31.70
MnO	9.00	13.90	6.90	14.00	12.30	13.00	6.40	7.70
MgO	0.00	2.00	1.40	2.60	0.00	0.40	0.50	0.70
CaO	2.10	2.00	1.70	1.70	2.70	2.00	2.40	3.10
Na2O	0.00	0.00	0.00	0.00	0.00	0.00	0.00	0.00
K2O	0.00	0.00	0.00	0.00	0.00	0.00	0.00	0.00
TOTAL	99.90	100.10	102.00	99.40	99.70	99.50	99.70	99.50

Si	6.006	6.069	6.008	6.060	5.908	5.912	5.972	5.884
Al	4.040	3.985	3.993	3.995	4.034	4.050	3.968	4.034
Ti	0.000	0.000	0.000	0.000	0.000	0.000	0.000	0.000
Fe	4.122	3.164	4.436	2.929	3.783	3.688	4.663	4.382
Mn	1.244	1.895	0.934	2.023	1.714	1.819	0.894	1.078
Mg	0.195	0.400	0.333	0.625	0.000	0.098	0.123	0.172
Ca	0.367	0.345	0.291	0.294	0.476	0.495	0.424	0.549
Na	0.000	0.000	0.000	0.000	0.000	0.000	0.000	0.000
K	0.000	0.000	0.000	0.000	0.000	0.000	0.000	0.000

AT%Fe	69.5	53.8	74.0	49.9	63.3	60.5	76.4	70.9
AT%Mn	21.0	32.2	15.6	34.5	28.7	29.8	14.0	17.4
AT%Mg	3.3	8.2	5.6	10.7	0.0	1.6	2.0	2.8
AT%Ca	6.2	5.9	4.9	5.0	0.0	0.1	6.9	8.9

	479-5	479-6	479-7	479-8	479-9	479-10	755-1	755-2
SiO2	36.30	36.10	37.10	37.00	35.50	35.00	37.10	36.90
Al2O3	20.70	20.40	20.00	20.00	20.60	20.20	21.20	20.70
TiO2	0.00	0.00	0.00	0.00	0.00	0.00	0.00	0.00
FeO	27.00	29.70	37.00	36.10	29.50	32.50	36.00	38.30
MnO	11.00	9.90	4.70	5.00	9.20	7.50	4.30	2.50
MgO	0.30	0.00	0.70	0.90	0.60	0.50	1.00	1.00
CaO	2.60	2.70	1.20	1.00	3.10	2.00	1.50	1.30
Na2O	0.00	0.00	0.00	0.00	0.00	0.00	0.00	0.00
K2O	0.00	0.00	0.00	0.00	0.00	0.00	0.00	0.00
TOTAL	98.70	98.00	101.50	101.60	98.50	99.30	101.90	100.70

Si	6.008	6.000	6.007	5.981	5.912	5.942	5.968	6.007
Al	4.039	3.997	3.970	3.964	4.045	3.953	4.020	3.972
Ti	0.000	0.000	0.000	0.000	0.000	0.000	0.000	0.000
Fe	3.737	4.129	5.010	4.800	4.109	4.511	4.950	5.214
Mn	1.654	1.394	0.645	0.685	1.208	1.054	0.586	0.345
Mg	0.074	0.000	0.169	0.217	0.149	0.124	0.240	0.243
Ca	0.461	0.481	0.200	0.312	0.553	0.498	0.259	0.227
Na	0.000	0.000	0.000	0.000	0.000	0.000	0.000	0.000
K	0.000	0.000	0.000	0.000	0.000	0.000	0.000	0.000

AT%Fe	63.1	60.0	83.1	80.1	67.3	72.9	82.0	86.5
AT%Mn	27.9	23.2	10.7	11.2	21.2	17.0	9.7	5.7
AT%Mg	1.2	0.0	2.8	3.6	2.4	2.0	4.0	4.0
AT%Ca	7.0	8.0	3.5	5.1	9.1	6.0	4.3	3.8

	755-3	755-4	755-5	755-6	755-7	755-8
SiO2	37.40	37.20	36.50	40.80	37.00	36.70
Al2O3	20.90	21.40	21.10	19.70	20.60	20.50
TiO2	0.00	0.00	0.00	0.00	0.00	0.00
FeO	36.50	37.30	34.50	33.10	33.30	36.00
MnO	4.40	3.60	5.70	4.80	6.50	4.60
MgO	0.80	0.80	1.10	0.70	0.60	0.70
CaO	1.80	1.80	1.40	1.90	2.10	1.70
Na2O	0.00	0.00	0.00	0.00	0.00	0.00
K2O	0.00	0.00	0.00	0.00	0.00	0.00
TOTAL	101.00	102.10	100.30	101.00	100.10	100.20
Si	6.019	5.968	5.954	6.473	6.044	6.011
Al	3.965	4.047	4.050	3.685	3.967	3.959
Ca	0.310	0.309	0.245	0.323	0.368	0.298
Na	0.000	0.000	0.000	0.000	0.000	0.000
K	0.000	0.000	0.000	0.000	0.000	0.000
AT%Fe	81.7	83.5	78.4	79.5	76.3	81.7
AT%Mn	10.0	8.2	13.1	11.7	15.1	10.6
AT%Mg	3.2	3.2	4.5	3.0	2.4	2.8
AT%Ca	5.2	5.2	4.1	5.8	6.2	4.9

6. Chloritoid Zone Garnets

	243-1	243-2	243-3	243-4	37.55,	243-5A	243-5B	243-6
SiO2	36.30	36.30	36.70	36.10	37.50	37.70	37.20	37.00
Al2O3	20.50	20.40	20.60	20.10	21.30	20.70	21.00	21.00
TiO2	0.00	0.00	0.00	0.00	0.00	0.00	0.00	0.00
FeO	33.90	32.90	33.30	34.70	33.20	29.80	32.70	33.10
MnO	8.00	9.00	8.50	8.90	8.40	7.60	8.00	8.10
MgO	0.30	0.40	0.00	0.50	0.60	0.00	0.60	0.00
CaO	1.90	1.20	1.00	0.60	1.00	4.10	1.00	1.30
Na2O	0.00	0.00	0.00	0.00	0.00	0.00	0.00	0.00
K2O	0.00	0.00	0.00	0.00	0.00	0.00	0.00	0.00
TOTAL	100.90	100.20	101.70	100.90	102.00	99.90	101.30	100.50
Si	5.948	5.900	5.951	5.947	6.020	6.123	6.020	6.038
Al	3.960	3.962	3.938	3.904	4.031	3.964	4.007	4.040
Ti	0.000	0.000	0.000	0.000	0.000	0.000	0.000	0.000
Fe	4.646	4.532	4.516	4.781	4.457	4.048	4.426	4.517
Mn	1.110	1.256	1.168	1.242	1.142	1.046	1.206	1.120
Mg	0.073	0.098	0.193	0.123	0.144	0.000	0.145	0.000
Ca	0.334	0.212	0.313	0.106	0.172	0.714	0.173	0.227
Na	0.000	0.000	0.000	0.000	0.000	0.000	0.000	0.000
K	0.000	0.000	0.000	0.000	0.000	0.000	0.000	0.000
AT%Fe	75.4	74.3	73.0	76.5	75.4	69.7	74.4	77.0
AT%Mn	18.0	20.6	18.9	19.9	19.3	18.0	20.3	19.1
AT%Mg	1.2	1.6	3.1	2.0	2.4	0.0	2.4	0.0
AT%Ca	5.4	3.5	5.1	1.7	2.9	12.3	2.9	3.9
	243-7	243-8	243-9	252-1	252-2	733-1	733-2	733-3
SiO2	37.10	37.40	37.90	34.50	39.00	37.30	37.10	37.10
Al2O3	20.90	21.20	20.90	19.90	19.60	21.00	20.00	20.60
TiO2	0.00	0.00	0.00	0.00	0.00	0.00	0.00	0.00
FeO	32.90	33.20	32.70	37.40	32.20	26.70	32.90	34.30
MnO	10.00	8.70	7.50	4.00	7.50	12.20	4.00	4.90
MgO	0.50	0.50	0.40	0.60	7.50	0.50	1.00	0.00
CaO	0.40	0.60	1.60	0.70	2.30	2.00	3.30	2.60
Na2O	0.00	0.00	0.00	0.00	0.00	0.00	0.00	0.00
K2O	0.00	0.00	0.00	0.00	0.00	0.00	0.00	0.00
TOTAL	101.00	101.60	101.00	97.90	100.10	100.50	99.90	100.30
Si	6.003	6.032	6.114	5.065	5.065	6.043	6.033	6.030
Al	3.987	4.031	3.975	3.908	3.475	4.011	3.908	3.953
Ti	0.000	0.000	0.000	0.000	0.000	0.000	0.000	0.000
Fe	4.452	4.478	4.412	5.317	4.050	3.610	4.474	4.669
Mn	1.371	1.189	1.025	0.691	0.955	1.674	0.661	0.676
Mg	0.121	0.120	0.096	0.152	1.681	0.121	0.242	0.194
Ca	0.069	0.104	0.277	0.120	0.371	0.406	0.575	0.453
Na	0.000	0.000	0.000	0.000	0.000	0.000	0.000	0.000
K	0.000	0.000	0.000	0.000	0.000	0.000	0.000	0.000
AT%Fe	74.0	76.0	75.9	84.6	57.4	61.3	75.2	77.9
AT%Mn	22.8	20.2	17.6	11.0	13.5	28.4	11.1	11.3
AT%Mg	2.0	2.0	1.7	2.4	23.8	2.0	4.1	3.2
AT%Ca	1.2	1.8	4.8	2.0	5.3	8.2	9.7	7.6

	733-4	733-5	733-6	733-7	733-8	733-9	1433-1	1433-2
SiO2	36.48	36.68	37.38	36.98	36.98	36.98	36.28	36.28
Al2O3	28.68	28.98	28.98	28.98	28.78	28.78	28.38	28.78
TiO2	0.88	0.88	0.88	0.88	0.88	0.88	0.88	0.88
FeO	23.98	31.88	34.38	32.48	33.28	27.58	29.18	27.18
MnO	13.98	7.38	4.28	4.88	5.58	11.28	11.68	13.38
MgO	8.58	8.78	1.18	8.98	8.78	8.48	8.88	8.58
CaO	3.18	3.78	2.38	3.98	2.48	3.18	1.58	1.68
Na2O	8.88	8.88	8.88	8.88	8.88	8.88	8.88	8.88
K2O	8.88	8.88	8.88	8.88	8.88	8.88	8.88	8.88
TOTAL	98.48	108.28	108.18	99.78	99.48	99.88	98.78	99.48
Si	6.822	5.964	6.852	6.811	6.847	6.832	6.838	5.975
Al	4.818	4.815	3.998	4.814	3.999	3.989	3.987	4.828
41								
Mn	1.948	1.888	8.577	8.662	8.764	1.551	1.637	1.868
Mg	8.123	8.178	8.266	8897	8.888	8.123		
Ca	8.558	8.646	8.488	8.663	8.421	8.543	8.268	8.283
Na	8.888	8.888	8.888	8.888	8.888	8.888	8.888	8.888
K	8.888	8.888	8.888	8.888	8.888	8.888	8.888	8.888
AT%Fe	55.8	69.8	78.9	74.1	77.8	63.2	68.8	62.3
AT%Mn	32.9	16.7	9.8	11.1	12.9	26.1	27.5	31.8
AT%Mg	2.1	2.8	4.5	3.7	2.9	1.6	8.8	2.8
AT%Ca	9.3	18.7	8.8	11.1	7.1	9.1	4.5	4.7
	1433-3	1433-4	1433-5	1433-6	1433-7	1433-8	1433-9	1444-1
SiO2	37.88	36.98	36.78	36.98	36.38	36.48	36.58	38.78
Al2O3	28.58	28.68	28.78	28.28	19.68	28.88	28.98	28.28
TiO2	8.88	8.88	8.88	8.88	8.88	8.88	8.88	8.88
FeO	35.88	33.78	36.28	32.18	34.28	35.38	36.28	48.58
MnO	5.88	6.58	4.68	7.38	5.78	5.88	5.38	1.58
MgO	8.88	8.88	1.18	8.78	8.58	8.88	8.88	1.18
CaO	2.88	1.98	1.98	2.68	2.88	1.78	1.68	8.48
Na2O	8.88	8.88	8.88	8.88	8.88	8.88	8.88	8.88
K2O	8.88	8.88	8.88	8.88	8.88	8.88	8.88	8.88
TOTAL	188.98	188.28	181.28	99.88	98.38	99.88	181.18	94.48
Si	6.822	6.831	5.957	6.858	6.868	6.848	5.946	5.485
Al	3.933	3.969	3.961	3.985	3.862	3.912	4.814	4.255
Ti	8.888	8.888	8.888	8.888	8.888	8.888	8.888	8.888
Fe	4.873	4.686	4.914	4.482	4.781	4.899	4.932	6.852
Mn	8.689	8.988	8.632	1.814	8.887	8.783	8.731	8.227
Mg	8.146	8.146	8.266	8.171	8.125	8.148	8.146	8.293
Ca	8.349	8.333	8.338	8.457	8.358	8.382	8.279	8.877
Na	8.888	8.888	8.888	8.888	8.888	8.888	8.888	8.888
K	8.888	8.888	8.888	8.888	8.888	8.888	8.888	8.888
AT%Fe	88.5	77.8	88.8	72.8	78.8	88.9	81.8	91.8
AT%Mn	11.4	15.8	18.3	16.8	13.3	11.6	12.8	3.4
AT%Mg	2.4	2.4	4.3	2.8	2.1	2.5	2.4	4.4
AT%Ca	5.8	5.8	5.4	7.6	5.9	5.8	4.6	1.2

	1444-2	1444-3	1444-4	1444-5	1444-6	1444-7	1444-8	1444-9
SiO2	36.60	36.60	36.30	36.80	37.00	36.60	36.50	36.80
Al2O3	20.50	20.70	20.90	20.80	21.10	21.30	21.00	20.90
TiO2	0.00	0.00	0.00	0.00	0.00	0.00	0.00	0.00
FeO	38.00	40.10	39.50	36.90	38.10	39.60	39.00	39.80
MnO	3.90	1.00	3.10	5.70	2.90	2.00	3.00	1.90
MgO	0.80	1.10	0.70	0.80	0.80	1.20	1.10	0.90
CaO	0.30	0.40	0.40	0.20	0.90	0.70	0.70	0.70
Na2O	0.00	0.00	0.00	0.00	0.00	0.00	0.00	0.00
K2O	0.00	0.00	0.00	0.00	0.00	0.00	0.00	0.00
TOTAL	100.10	99.90	100.90	101.20	100.80	101.40	101.30	101.00

Si	6.014	6.006	5.939	5.989	6.009	5.926	5.932	5.986
Al	3.971	4.005	4.031	3.991	4.040	4.066	0.543	0.139
Mg	0.196	0.269	0.171	0.194	0.194	0.290	0.266	0.218
Ca	0.053	0.070	0.070	0.035	0.157	0.121	0.122	0.122
Na	0.000	0.000	0.000	0.000	0.000	0.000	0.000	0.000
K	0.000	0.000	0.000	0.000	0.000	0.000	0.000	0.000

AT%Fe	86.8	92.0	89.0	83.2	87.4	88.7	86.9	90.0
AT%Mn	9.0	2.3	7.1	13.0	6.7	4.5	6.8	4.4
AT%Mg	3.3	4.5	2.8	3.2	3.3	4.8	4.4	3.6
AT%Ca	0.9	1.2	1.2	0.6	2.6	2.0	2.0	2.0

	1449-1	1449-2	1449-3
SiO2	37.60	36.70	37.20
Al2O3	21.20	21.20	21.00
TiO2	0.00	0.00	0.00
FeO	25.90	14.20	22.80
MnO	12.60	14.20	15.40
MgO	0.90	0.60	0.60
CaO	3.40	1.90	3.20
Na2O	0.00	0.00	0.00
K2O	0.00	0.00	0.00
TOTAL	101.60	88.80	100.20

Si	6.016	6.395	6.034
Al	3.999	4.355	4.015
Ti	0.000	0.000	0.000
Fe	3.456	2.070	3.093
Mn	1.708	2.096	2.116
Mg	0.215	0.156	0.145
Ca	0.583	0.355	0.556
Na	0.000	0.000	0.000
K	0.000	0.000	0.000

AT%Fe	58.0	44.3	52.3
AT%Mn	28.6	44.8	35.8
AT%Mg	3.6	3.3	2.5
AT%Ca	9.8	7.6	9.4

7. Chloritoid Analyses

	1433-1	1433-2	1433-3	1433-4	1433-5	143-6	743-1	743-2
SiO2	24.10	24.40	23.90	24.50	24.60	24.40	23.40	23.40
Al2O3	40.00	39.30	39.70	39.60	40.00	39.50	38.70	38.90
TiO2	0.00	0.00	0.00	0.00	0.00	0.00	0.00	0.00
FeO	25.40	25.40	25.80	25.80	26.60	27.30	25.80	26.80
MnO	1.00	1.00	0.90	1.10	0.50	0.50	1.30	1.20
MgO	1.00	1.20	1.50	1.50	1.00	0.90	1.40	1.50
CaO	0.00	0.00	0.00	0.00	0.00	0.00	0.00	0.00
Na2O	0.00	0.00	0.00	0.00	0.00	0.00	0.00	0.00
K2O	0.00	0.00	0.00	0.00	0.00	0.00	0.00	0.00
TOTAL	91.50	91.30	91.80	92.50	92.70	92.60	90.60	91.80
Si	2.029	2.059	2.011	2.045	2.049	2.044	2.006	1.988
Al	3.971	3.911	3.939	3.897	3.927	3.901	3.911	3.896
Ti	0.000	0.000	0.000	0.000	0.000	0.000	0.000	0.000
Fe	1.789	1.793	1.816	1.801	1.853	1.913	1.849	1.904
Mn	0.071	0.071	0.064	0.078	0.035	0.035	0.094	0.086
Mg	0.125	0.151	0.188	0.187	0.124	0.112	0.179	0.190
Ca	0.000	0.000	0.000	0.000	0.000	0.000	0.000	0.000
Na	0.000	0.000	0.000	0.000	0.000	0.000	0.000	0.000
K	0.000	0.000	0.000	0.000	0.000	0.000	0.000	0.000
AT#Fe	90.1	89.0	87.8	87.2	92.1	92.8	87.1	87.3
AT#Mn	3.6	3.5	3.1	3.8	1.8	1.7	4.4	4.0
AT#Mg	6.3	7.5	9.1	9.0	6.2	5.5	8.4	8.7
AT#Ca	0.0	0.0	0.0	0.0	0.0	0.0	0.0	0.0
	743-3	743-4	257-1	257-2	1433	1433	1433	1433
SiO2	23.90	23.90	23.80	23.50	24.10	24.40	23.90	24.50
Al2O3	39.50	38.80	38.50	38.20	40.00	39.30	39.70	39.60
TiO2	0.00	0.00	0.00	0.00	0.00	0.00	0.00	0.00
FeO	25.40	25.20	27.20	27.70	25.40	25.40	25.80	25.80
MnO	1.10	1.20	1.30	1.00	1.00	1.00	0.90	1.10
MgO	1.00	2.00	1.20	0.70	1.00	1.20	1.50	1.50
CaO	0.00	0.00	0.00	0.00	0.00	0.00	0.00	0.00
Na2O	0.00	0.00	0.00	0.00	0.00	0.00	0.00	0.00
K2O	0.00	0.00	0.00	0.00	0.00	0.00	0.00	0.00
TOTAL	91.70	91.10	92.00	91.10	91.50	91.30	91.80	92.50
Si	2.013	2.027	2.021	2.020	2.029	2.059	2.011	2.045
Al	3.921	3.880	3.854	3.871	3.971	3.911	3.939	3.897
Ti	0.000	0.000	0.000	0.000	0.000	0.000	0.000	0.000
Fe	1.789	1.787	1.932	1.991	1.789	1.793	1.816	1.801
Mn	0.078	0.086	0.094	0.073	0.071	0.071	0.064	0.078
Mg	0.226	0.253	0.152	0.090	0.125	0.151	0.188	0.187
Ca	0.000	0.000	0.000	0.000	0.000	0.000	0.000	0.000
Na	0.000	0.000	0.000	0.000	0.000	0.000	0.000	0.000
K	0.000	0.000	0.000	0.000	0.000	0.000	0.000	0.000
AT#Fe	85.5	84.1	88.7	92.5	90.1	89.0	87.8	87.2
AT#Mn	3.7	4.1	4.3	3.4	3.6	3.5	3.1	3.8
AT#Mg	10.8	11.9	7.0	4.2	6.3	7.5	9.1	9.0
AT#Ca	0.0	0.0	0.0	0.0	0.0	0.0	0.0	0.0

	1444	1444	46	46	46
SiO2	24.60	24.40	23.80	23.10	23.30
Al2O3	40.00	39.50	39.60	38.00	38.70
TiO2	0.00	0.00	0.00	0.00	0.00
FeO	26.60	37.30	25.20	24.20	25.40
MnO	0.50	0.50	1.10	1.40	1.10
MgO	1.00	0.90	1.60	1.80	1.60
CaO	0.00	0.00	0.00	0.00	0.00
Na2O	0.00	0.00	0.00	0.00	0.00
K2O	0.00	0.00	0.00	0.00	0.00
TOTAL	92.70	102.60	91.30	88.50	90.10

Si	2.049	1.931	2.011	2.016	2.003
Al	3.927	3.686	3.945	3.910	3.922
Ti	0.000	0.000	0.000	0.000	0.000
Fe	1.853	2.469	1.781	1.766	1.826
Mn	0.035	0.034	0.079	0.103	0.080
Mg	0.124	0.105	0.201	0.234	0.205
Ca	0.000	0.000	0.000	0.000	0.000
Na	0.000	0.000	0.000	0.000	0.000
K	0.000	0.000	0.000	0.000	0.000

AT%Fe	92.1	94.6	86.4	84.0	85.5
AT%Mn	1.8	1.3	3.8	4.9	3.8
AT%Mg	6.2	4.1	9.8	11.1	9.7
AT%Ca	0.0	0.0	0.0	0.0	0.0

8. Feldspar Analyses

	200.1	200.2C	200.2R	200.3C	200.3R	200.4	200.5R	200.6C
SiO2	53.00	60.20	52.20	53.40	56.90	53.40	55.70	52.70
Al2O3	27.10	23.20	26.90	26.40	25.40	26.00	24.50	27.20
TiO2	0.00	0.00	0.00	0.00	0.00	0.00	0.00	0.00
FeO	0.00	0.00	0.00	0.00	0.00	0.00	0.00	0.00
MnO	0.00	0.00	0.00	0.00	0.00	0.00	0.00	0.00
MgO	0.00	0.00	0.00	0.00	0.00	0.00	0.00	0.00
CaO	10.30	5.10	11.00	10.10	8.40	10.40	7.10	10.90
Na2O	4.80	7.80	4.90	5.50	6.50	5.10	3.50	4.50
K2O	0.00	0.10	0.00	0.00	0.00	0.20	5.00	0.00
TOTAL	95.20	96.40	95.00	95.40	97.20	95.90	95.00	95.30
Si	5.000	5.519	4.956	5.037	5.232	5.014	5.276	4.973
Al	3.014	2.508	3.011	2.936	2.753	2.967	2.736	3.026
Ti	0.000	0.000	0.000	0.000	0.000	0.000	0.000	0.000
Fe	0.000	0.000	0.000	0.000	0.000	0.000	0.000	0.000
Mn	0.000	0.000	0.000	0.000	0.000	0.000	0.000	0.000
Mg	0.000	0.000	0.000	0.000	0.000	0.000	0.000	0.000
Ca	1.041	0.501	1.119	1.021	0.828	1.046	0.721	1.102
Na	0.878	1.387	0.902	1.006	1.159	0.928	0.643	0.823
K	0.000	0.012	0.000	0.000	0.000	0.024	0.604	0.000
	200.6R	200.7	200.7R	235.1	756.1	756.2	280.1	280.2
SiO2	54.10	49.60	54.60	54.60	63.00	64.10	56.00	58.30
Al2O3	26.30	30.20	26.10	26.10	22.70	20.60	26.40	26.00
TiO2	0.00	0.00	0.00	0.00	0.00	0.00	0.00	0.00
FeO	0.00	0.00	0.00	0.00	0.00	0.00	0.00	0.00
MnO	0.00	0.00	0.00	0.00	0.00	0.00	0.00	0.00
MgO	0.00	0.00	0.00	0.00	0.00	0.00	0.00	0.00
CaO	9.90	14.00	9.30	5.30	4.10	2.00	8.90	8.10
Na2O	5.80	3.10	5.90	8.50	9.70	5.10	6.20	7.00
K2O	0.00	0.00	0.00	0.00	0.00	7.20	0.00	0.20
TOTAL	96.10	96.90	95.90	94.50	99.50	99.00	98.30	100.20
Si	5.064	4.651	5.108	5.161	5.602	5.817	5.123	5.204
Al	2.902	3.339	2.878	2.908	2.380	2.204	2.847	2.799
Ti	0.000	0.000	0.000	0.000	0.000	0.000	0.000	0.000
Fe	0.000	0.000	0.000	0.000	0.000	0.000	0.000	0.000
Mn	0.000	0.000	0.000	0.000	0.000	0.000	0.000	0.000
Mg	0.000	0.000	0.000	0.000	0.000	0.000	0.000	0.000
Ca	0.993	1.407	0.932	0.537	0.391	0.194	0.872	0.775
Na	1.053	0.564	1.070	1.558	1.672	0.897	1.100	1.212
K	0.000	0.000	0.000	0.000	0.000	0.834	0.000	0.023

	288.3	288.4	288.5	288.6	288.7	46.1	46.2	236.1C
SiO2	58.10	58.30	58.00	58.40	59.00	58.90	58.10	58.90
Al2O3	25.90	27.10	27.00	26.00	25.90	24.30	24.20	24.70
TiO2	0.00	0.00	0.00	0.00	0.00	0.00	0.00	0.00
FeO	0.00	0.00	0.00	0.00	0.00	0.00	0.00	0.00
MnO	0.00	0.00	0.00	0.00	0.00	0.00	0.00	0.00
MgO	0.00	0.00	0.00	0.00	0.00	0.00	0.00	0.00
CaO	7.30	8.60	8.70	8.40	5.30	6.70	6.60	7.10
Na2O	7.20	7.00	6.90	6.90	6.60	7.20	7.30	7.30
K2O	0.40	0.00	0.00	0.00	1.90	0.00	0.00	0.00
TOTAL	98.98	101.00	100.60	100.50	98.70	97.10	96.20	98.00

Si	4.977	5.167	5.162	5.194	5.331	5.387	5.369	5.350
Al	3.833	2.832	2.833	2.810	2.759	2.620	2.636	2.645
Ti	0.000	0.000	0.000	0.000	0.000	0.000	0.000	0.000
Fe	0.000	0.000	0.000	0.000	0.000	0.000	0.000	0.000
Mn	0.000	0.000	0.000	0.000	0.000	0.000	0.000	0.000
Mg	0.000	0.000	0.000	0.000	0.000	0.000	0.000	0.000
Ca	0.777	0.817	0.830	0.801	0.513	0.657	0.654	0.691
Na	1.387	1.283	1.191	1.190	1.156	1.277	1.308	1.286
K	0.051	0.000	0.000	0.000	0.219	0.000	0.000	0.000

	236.1R	236.2C	236.2R	240	240.2	240.3	588.1	588.3
SiO2	59.40	57.30	57.20	59.00	63.30	62.20	59.60	56.30
Al2O3	23.70	25.20	25.50	25.10	23.90	24.20	26.00	27.30
TiO2	0.00	0.00	0.00	0.00	0.00	0.00	0.00	0.00
FeO	0.00	0.00	0.00	0.00	0.00	0.00	0.10	0.20
MnO	0.00	0.00	0.00	0.00	0.00	0.00	0.00	0.00
MgO	0.00	0.00	0.00	0.00	0.00	0.00	0.00	0.00
CaO	6.40	7.80	8.30	7.30	5.00	5.60	7.40	8.70
Na2O	6.90	6.50	6.60	7.00	9.00	8.10	7.70	4.50
K2O	0.00	0.20	0.00	0.00	0.00	0.00	0.00	2.60
TOTAL	96.40	97.00	97.60	99.20	101.20	100.10	100.80	99.60

Si	5.454	5.270	5.236	5.357	5.536	5.497	5.279	5.107
Al	2.505	2.733	2.752	2.651	2.464	2.521	2.715	2.919
Ti	0.000	0.000	0.000	0.000	0.000	0.000	0.000	0.000
Fe	0.000	0.000	0.000	0.000	0.000	0.000	0.007	0.015
Mn	0.000	0.000	0.000	0.000	0.000	0.000	0.000	0.000
Mg	0.000	0.000	0.000	0.000	0.000	0.000	0.000	0.000
Ca	0.630	0.769	0.814	0.701	0.469	0.530	0.702	0.846
Na	1.228	1.159	1.171	1.216	1.526	1.388	1.322	0.791
K	0.000	0.023	0.000	0.000	0.000	0.000	0.000	0.381

	588.4	257.1
SiO2	58.50	59.30
Al2O3	26.20	23.50
TiO2	0.00	0.00
FeO	0.10	0.70
MnO	0.00	0.00
MgO	0.00	0.00
CaO	7.70	5.90
Na2O	7.00	7.50
K2O	0.00	0.00
TOTAL	99.50	96.90

Si	5.245	5.442
Al	2.769	2.543
Ti	0.000	0.000
Fe	0.007	0.054
Mn	0.000	0.000
Mg	0.000	0.000
Ca	0.740	0.500
Na	1.217	1.335
K	0.000	0.000

Sample No.	252-1	252-2	252-3	235-1	235-2	235-3*	235-4*
SiO ₂	-	-	-	-	0.54	0.58	0.44
Al ₂ O ₃	55.78	56.17	57.00	57.35	56.94	56.33	56.12
FeO	8.00	8.14	7.93	7.45	7.26	7.05	7.27
ZnO	35.44	35.7	36.96	35.77	34.41	33.44	36.16
TOTAL	99.22	100.01	101.89	100.57	99.15	100.00	100.00

Sample No.	235-5a	235.5b	235.5c	235.5d	235.5e
SiO ₂	0.63	0.45	-	0.54	0.60
Al ₂ O ₃	57.69	57.52	57.35	56.94	58.18
FeO	7.42	7.45	7.45	7.26	7.97
ZnO	37.19	37.06	35.77	34.41	36.17
TOTAL	102.93	102.48	100.57	99.21	102.92

10. Tourmaline Analyses (29 oxygens)

Sample No.	54-1 Core	54-2 Rim	54-3 Core	857-1	857-2	1449-1	1449-2
SiO ₂	36.22	36.33	36.65	36.4	36.83	35.87	35.54
Al ₂ O ₃	31.64	33.27	31.65	31.85	31.22	38.67	31.84
TiO ₂	0.42	0.25	0.54	0.67	0.74	n.a.	0.36
FeO	8.85	11.89	12.64	6.13	6.36	9.28	10.3
MnO	-	-	-	-	-	-	-
MgO	6.36	4.2	3.13	7.81	7.84	5.88	5.54
CaO	0.93	0.68	0.16	1.58	1.52	0.62	0.62
Na ₂ O	1.83	1.88	2.84	1.82	2.82	1.85	1.94
K ₂ O	-	-	-	0.14	-	-	-
TOTAL	85.45	88.58	86.81	86.32	85.73	84.81	86.14
Si	6.88	7.88	7.28	7.82	7.82	7.38	7.88
Al	7.88	7.55	7.33	7.24	7.17	7.38	7.38
Ti	0.86	0.84	0.88	0.89	0.15	-	0.86
Fe	1.28	1.92	2.88	0.99	1.84	1.56	1.69
Mn	-	-	-	-	-	-	-
Mg	1.88	1.21	0.92	2.25	2.27	1.75	1.63
Ca	0.18	0.14	0.84	0.28	0.32	0.13	0.13
Na	0.67	0.78	0.78	0.68	0.77	0.71	0.75
K	-	-	-	0.84	-	-	-
Fe/Fe+Mg	0.41	0.61	0.69	0.31	0.31	0.47	0.51

(29 oxygens)

Sample No.	858-1	858-2	858-3	588-1 Core	588-2	588-3	588-4
SiO ₂	36.77	38.21	37.57	36.51	36.99	35.98	36.28
Al ₂ O ₃	31.54	33.65	32.39	34.85	32.86	33.39	33.33
TiO ₂	0.49	0.23	0.36	0.38	-	-	-
FeO	5.57	5.48	5.62	13.83	12.55	11.78	12.79
MnO	-	-	-	-	-	-	-
MgO	6.98	6.22	7.89	2.71	3.36	2.34	2.47
CaO	0.96	0.47	0.88	0.65	0.45	0.27	0.28
Na ₂ O	1.58	2.48	1.72	1.58	1.86	1.34	1.61
K ₂ O	-	-	-	-	-	-	-
TOTAL	83.81	86.74	85.63	88.75	88.87	85.82	86.68
Si	7.22	7.24	7.21	7.82	7.14	7.14	7.18
Al	7.38	7.51	7.32	7.71	7.48	7.81	7.69
Ti	-	-	0.85	0.84	-	-	-
Fe	0.91	0.87	0.98	2.89	2.83	1.94	2.18
Mn	-	-	-	-	-	-	-
Mg	2.82	1.76	2.83	0.78	0.97	0.69	0.72
Ca	0.28	0.89	0.18	0.13	0.89	0.86	0.84
Na	0.68	0.91	0.64	0.56	0.69	0.51	0.61
K	-	-	-	-	-	-	-
Fe/Fe+Mg	0.31	0.33	0.28	0.73	0.68	0.74	0.74

(29 oxygens)

Appendix 3.3

Most probed gahnite grains are unzoned with respect to iron and zinc. where zoning is developed (Figure A3.1), iron shows a slight enrichment, from core to rim, consistent with crystallisation during a prograde metamorphic event (Spry, 1987)

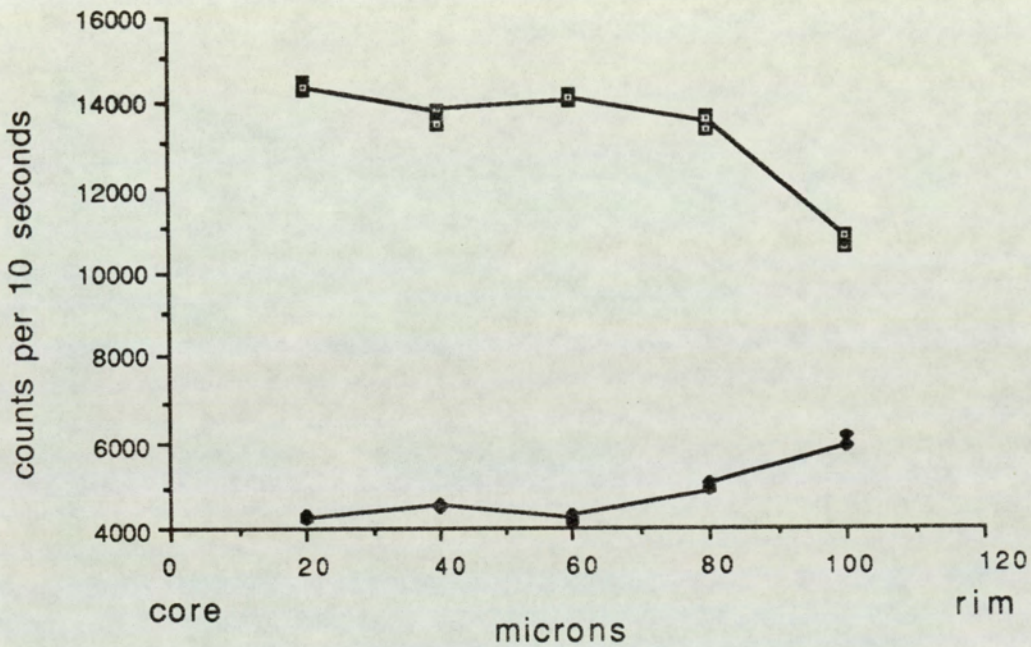


Figure A3.1 Core to rim zoning of Fe and Zn in gahnite.

(filled symbol is Fe, open symbol Zn)

Appedix 3.4 Trace element contents of plagioclase feldspars

Trace elements (Cu, Zn, Fe, Mn) contents of plagioclase feldspars were investigated by WD at Manchester University. Because of the generally low levels of trace elements, long counting times were used (300 seconds on peak, and 150 seconds on background) in order to improve detection limits. Detection limits are reported in the main text. Listed below are representative analyses for mineralised and unmineralised feldspars (values in ppm).

a) Unmineralised Plagioclase (bd= below detection limit)

Cu	Zn	Fe	Mn
bd	bd	7980	bd
bd	bd	bd	bd
bd	bd	bd	bd

b) Mineralised Plagioclase

Cu	Zn	Fe	Mn
400	bd	1450	bd
570	bd	1390	bd
680	bd	1050	bd
1130	550	1390	bd
880	bd	19850	770
1140	bd	1650	bd